

OAK RIDGE NATIONAL LABORATORY LIBRARIES



3 4456 0576299 3

cy. 1
2

FAST BREEDER REACTOR OXIDE FUELS DEVELOPMENT — FINAL REPORT



OAK RIDGE NATIONAL LABORATORY
 CENTRAL RESEARCH LIBRARY
 DOCUMENT COLLECTION
LIBRARY LOAN COPY
 DO NOT TRANSFER TO ANOTHER PERSON
 If you wish someone else to see this
 document, send in name with document
 and the library will arrange a loan.

UCRL-7564
 12 3-6-71



OAK RIDGE NATIONAL LABORATORY
 OPERATED BY UNION CARBIDE CORPORATION • FOR THE U.S. ATOMIC ENERGY COMMISSION

Printed in the United States of America. Available from
the U.S. Atomic Energy Commission, Technical Information Center
P.O. Box 62, Oak Ridge, Tennessee 37830
Price: Printed Copy \$7.60 ; Microfiche \$1.45

This report was prepared as an account of work sponsored by the United States Government. Neither the United States nor the United States Atomic Energy Commission, nor any of their employees, nor any of their contractors, subcontractors, or their employees, makes any warranty, express or implied, or assumes any legal liability or responsibility for the accuracy, completeness or usefulness of any information, apparatus, product or process disclosed, or represents that its use would not infringe privately owned rights.

Contract No. W-7405-eng-26

**METALS AND CERAMICS DIVISION
CHEMICAL TECHNOLOGY DIVISION**

FAST BREEDER REACTOR OXIDE FUELS DEVELOPMENT -- FINAL REPORT

Compiled by

A. L. Lotts

Contributions by

| | | | |
|---------------|-----------------|-----------------|----------------|
| R. A. Bradley | F. J. Homan | E. L. Long, Jr. | W. H. Pechin |
| J. A. Conlin | A. Jostsons | A. L. Lotts | J. D. Sease |
| C. M. Cox | J. Komatsu | E. J. Manthos | R. L. Senn |
| R. B. Fitts | W. J. Lackey | W. T. McDuffee | J. O. Stiegler |
| B. Fleischer | J. M. Leitnaker | F. L. Miller | T. N. Washburn |
| P. A. Haas | T. B. Lindemer | A. R. Olsen | R. G. Wymer |

Edited by

S. Peterson

NOVEMBER 1973

OAK RIDGE NATIONAL LABORATORY
Oak Ridge, Tennessee 37830
operated by
UNION CARBIDE CORPORATION
for the
U.S. ATOMIC ENERGY COMMISSION

Contents

| | |
|---|----|
| Abstract | 1 |
| 1. Introduction | 2 |
| 1.1 Program History | 2 |
| 1.2 Program Organization | 2 |
| 1.3 Content of Report | 3 |
| 2. Fuel Preparation | 4 |
| 2.1 Sol Preparation | 4 |
| 2.1.1 UO_2 Sol Preparation from Natural Uranium | 4 |
| 2.1.2 Plutonia Sol Preparation | 11 |
| 2.1.3 UO_2 Sol Preparation from Enriched Uranium | 11 |
| 2.1.4 Preparation of Mixed (U,Pu) O_2 Sols | 12 |
| 2.2 Microsphere Preparation | 12 |
| 2.2.1 Preparation of UO_2 -Pu O_2 Spheres in Fluidized-Bed Columns | 13 |
| 2.2.2 Nonfluidized Preparation of UO_2 or UO_2 -Pu O_2 Spheres | 14 |
| 2.3 Preparation of (U,Pu) O_2 Sol-Gel Powder | 14 |
| 2.4 Discussion of Status of Technology and Recommendations | 16 |
| 3. Fabrication Development | 17 |
| 3.1 Sphere-Pac Fabrication Techniques | 17 |
| 3.1.1 Sphere-Pac Development | 17 |
| 3.1.2 Sphere-Pac Fabrication of Fuel Rods | 22 |
| 3.1.3 U-Fines Sphere-Pac Process | 23 |
| 3.2 Methods for Pelletizing Fuel | 26 |
| 3.2.1 Fabrication of Low-Density (83--88%) Pellets | 27 |
| 3.2.2 Fabrication of Intermediate-Density (88--92%) Pellets | 28 |
| 3.2.3 Fabrication of High-Density (92--97%) Pellets | 29 |
| 3.2.4 Fabrication of Pellets for Irradiation Tests | 32 |
| 3.3 Preliminary Extrusion Evaluation of Sol-Gel Materials | 36 |
| 3.4 Adjustment of Oxygen-to-Metal Ratio | 37 |
| 3.5 Procedures for Reduction of Sorbed Gases | 38 |
| 3.6 Discussion, Conclusions, and Recommended Future Work | 39 |

| | |
|---|-----|
| 4. Fuel Characterization | 41 |
| 4.1 Analytical Chemistry Techniques | 41 |
| 4.1.1 Determination of Oxygen-to-Metal Ratio | 41 |
| 4.1.2 Moisture Analysis | 42 |
| 4.1.3 Sorbed Gas Content | 43 |
| 4.1.4 Actinide Analysis | 44 |
| 4.2 Microstructure of Microspheres and Pellets | 44 |
| 4.2.1 Coarse Microspheres | 45 |
| 4.2.2 Fine Microspheres | 50 |
| 4.2.3 Pellets | 51 |
| 4.3 Typical Fuel Characterization | 55 |
| 4.4 Discussion, Conclusions, and Recommendations | 56 |
| 5. Irradiation Program | 57 |
| 5.1 ETR Tests – Noninstrumented Series | 58 |
| 5.1.1 Experimental Plan | 58 |
| 5.1.2 Results of Irradiation Tests | 60 |
| 5.2 ORR Thermal Performance Tests | 72 |
| 5.2.1 Experimental Plan | 72 |
| 5.2.2 Design and Operation | 73 |
| 5.2.3 Results | 75 |
| 5.2.4 Discussion | 79 |
| 5.2.5 Conclusions | 85 |
| 5.3 ETR Tests – Instrumented Series | 85 |
| 5.3.1 Experimental Plans | 85 |
| 5.3.2 Design and Construction | 86 |
| 5.3.3 Irradiation History | 89 |
| 5.3.4 Results | 89 |
| 5.4 Mechanical Interaction Test | 101 |
| 5.4.1 Experimental Plan | 101 |
| 5.4.2 Design and Construction | 101 |
| 5.4.3 Results | 102 |
| 5.5 Fast Reactor Tests – EBR-II Encapsulated Pins | 102 |
| 5.5.1 Experimental Plan | 103 |
| 5.5.2 Test Capsule Design and Fabrication | 103 |
| 5.5.3 Test Results | 104 |
| 5.6 Fast Reactor Tests – EBR-II Unencapsulated Pins | 111 |
| 5.6.1 Experimental Plan | 111 |
| 5.6.2 Design and Construction | 113 |
| 5.6.3 Irradiation Results | 113 |
| 5.7 Transient Tests in TREAT | 114 |
| 5.7.1 Experimental Plan | 114 |
| 5.7.2 Design and Construction | 115 |
| 5.7.3 Results | 117 |

| | |
|---|-----|
| 5.8 Discussion of Results of Irradiation Program | 124 |
| 5.8.1 Thermal Performance | 124 |
| 5.8.2 Fuel Restructuring | 126 |
| 5.8.3 Actinide and Fission Product Redistribution | 128 |
| 5.8.4 Electron Microscopy of Irradiated (U,Pu)O ₂ | 128 |
| 5.8.5 Fuel-Cladding Mechanical Interactions | 130 |
| 5.8.6 Fuel-Cladding Chemical Interactions | 130 |
| 5.8.7 Recommendations for Further Work on Irradiation Effects | 136 |
| 6. Fuel Performance, Process, and Economic Evaluations | 137 |
| 6.1 Fuel Performance Modeling | 137 |
| 6.1.1 Integrated Code Description | 137 |
| 6.1.2 Comparison of Code Results with Experimental Results | 139 |
| 6.1.3 Discussion of Individual Models | 146 |
| 6.1.4 Thermodynamic Considerations in Fuel Behavior | 149 |
| 6.2 Process and Economic Evaluations | 158 |
| 6.2.1 Future Industrial Basis for LMFBR Fuel Fabrication | 158 |
| 6.2.2 Projections for the LMFBR Fuel Fabrication Industry | 163 |
| 6.3 Discussion of Current Status of Fuel Performance, Process, and Economic Evaluations | 168 |
| 6.3.1 Relative Fuel Performance | 169 |
| 6.3.2 Process Options | 169 |
| 6.3.3 Fuel Element Hardware | 170 |
| 6.3.4 Recommendations | 170 |
| 7. Summary, Conclusions, and Recommendations | 172 |
| 7.1 Summary and Conclusions of Research and Development | 172 |
| 7.1.1 Fuel Preparation | 172 |
| 7.1.2 Fabrication Development | 173 |
| 7.1.3 Fuel Characterization | 173 |
| 7.1.4 Irradiation Program | 174 |
| 7.1.5 Fuel Performance, Process, and Economic Evaluations | 175 |
| 7.2 Recommendations for Future Work | 175 |
| 7.2.1 Fuel Preparation | 176 |
| 7.2.2 Fuel Fabrication | 176 |
| 7.2.3 Fuel Characterization | 176 |
| 7.2.4 Irradiation Program | 176 |
| 7.2.5 Fuel Performance, Process, and Economic Evaluations | 177 |
| 8. Publications and Documents | 178 |
| 8.1 Topical Reports and Papers | 178 |
| 8.2 Progress Reports | 181 |
| 8.2.1 Metals and Ceramics Division Annual Reports | 182 |
| 8.2.2 Fuels and Materials Development Program Quarterly Progress Reports | 182 |
| 8.2.3 LMFBR Fuel Cycle Studies Progress Reports | 182 |

| | |
|---|-----|
| 8.3 Quality Assurance Documents | 183 |
| 8.3.1 General Operating and Quality Assurance Plans | 183 |
| 8.3.2 Experimental Plans | 183 |
| 8.3.3 Preirradiation Data Summary | 183 |
| 8.3.4 Fabrication and Quality Assurance Plan | 183 |
| 8.3.5 Process Procedures | 184 |
| 8.3.6 Operator Procedures | 185 |
| 8.3.7 Material Specifications | 185 |
| 8.3.8 Test Specifications | 186 |
| 8.3.9 Fabrication and Quality Assurance Networks | 186 |

Abstract

Preparation, fabrication, irradiation, and evaluation of fast breeder oxide fuels are reported for a five-year development program. Emphasis is on irradiation testing of sol-gel uranium-plutonium, particularly fabricated by the Sphere-Pac loading of coarse and fine

microspheres into the cladding. The scope of the program is outlined in Chap. 1, and Chap. 7 presents a summary, conclusions, and recommendations. Publications and other documents of the program are listed.

1. Introduction

A. L. Lotts

To advance the technology of (U,Pu)O₂ as a fuel for the Liquid-Metal Fast Breeder Reactor (LMFBR), the oxide fuels development program was conducted for a period of five years. Funding for the program was terminated June 30, 1972. The main objectives of the oxide fuels development program were:

1. to establish the performance characteristics and limitations of (U,Pu)O₂ fuels fabricated by different processes,
2. to obtain a fundamental understanding of the mechanisms involved in the irradiation behavior of fuel elements incorporating these fuels,
3. to develop fabrication techniques that provide both economy and a fuel with optimized performance,
4. to develop analytical models adequate to optimize experimental design and to predict fuel element response to LMFBR conditions.

The program emphasized determination of the properties and performance of sol-gel-derived oxide fuels fabricated by the Sphere-Pac and pelletizing techniques. The performance of these fuels was compared with that of other fuels such as pellets from mechanically blended or coprecipitated oxide.

The purpose of this terminal report is to summarize the accomplishments of the program for development of LMFBR oxide fuels, to set forth the status of the program at the terminal date, and to suggest work that may be required in the future.

1.1 PROGRAM HISTORY

The program was initiated late in fiscal year 1967 with the irradiation of fuels intended primarily for chemical reprocessing studies. Substantial progress was made toward the objectives outlined previously through a program that included fabrication of fuel with different structures, characterization of these structures by out-of-reactor methods, and irradiation under a

variety of conditions. The program emphasized irradiation testing, postirradiation examination of various fuel structures, and evaluation of the results in terms of performance models. A number of irradiation tests were still in progress when the program was terminated, and responsibility for these tests was turned over to other USAEC contractors. Accordingly, all documentation, quality assurance work, and archive specimens have been transferred.

1.2 PROGRAM ORGANIZATION

The program was organized into four specific tasks: (1) fabrication of (U,Pu)O₂ fuels, (2) characterization of fuel, (3) irradiation testing of oxide fuels, and (4) analysis of fuel element performance. In addition to these functional tasks, a comprehensive effort was made to develop and apply quality assurance procedures to the development work and to the irradiation tests. Facilities and equipment were designed and constructed at the beginning of the program. The critical-path method (CPM) was used to schedule and coordinate all aspects of the program. The method proved to be very useful, even for meeting research and development goals.

Concerning the task of fabricating (U,Pu)O₂ fuels, the objective was to provide experimental quantities of well-characterized (U,Pu)O₂ fuels for the irradiation tests. Fabrication development required to prepare mixed oxide fuel of controlled density and stoichiometry was accomplished. Commercially available UO₂ and PuO₂ powders were used in preparing mechanically mixed (U,Pu)O₂ pellets for irradiation tests. Sol-gel technology was used to prepare small quantities of (U,Pu)O₂ microspheres and powder for fabrication of pellets. These materials were prepared, fabricated into fuel pins as required for the irradiation tests, and also provided to other sites—for example, Argonne National Laboratory and the Hanford Engineering Development Laboratory (HEDL).

The second task area, characterization of fuel, was an important part of the program, since a thorough understanding of the chemical, thermophysical, mechanical, and structural properties of the $(U,Pu)O_2$ products and the effects of processing and fabrication procedures on these properties was deemed essential to the evaluation of their performance. Each fuel form to be irradiation tested was fully characterized with complete microstructural, x-ray diffraction, and chemical analyses to assure a better understanding of its irradiation performance. Substantial effort was made to improve fuel characterization procedures and methods. The underlying philosophy of the program was that, since chemical contaminants such as carbon and absorbed gas and the ratio of oxygen to metal affect the compatibility of fuel and cladding, these must be thoroughly understood and accurately analyzed. Another underlying philosophy was that, since porosity distribution, particle size, and in-reactor sintering kinetics all have a marked effect on thermal conductivity and thus the temperature distribution in the fuel, it was essential that these variables be understood. Therefore, the program placed a large amount of emphasis on out-of-reactor characterization of each fuel form to establish basic information for correlation with irradiation tests.

In the third task area, irradiation testing of oxide fuels, the purpose was to compare the irradiation performance of the various fuel forms and obtain basic information on the effects of irradiation on $(U,Pu)O_2$ fuels and fuel-cladding interactions. The principal test facility utilized in the program was the EBR-II, the test data from which were used to develop and refine models of fuel and fuel element performance. The variables in the program included burnup, stoichiometry, smear density, void deployment, and cladding temperature. The irradiations in the EBR-II were augmented by thermal flux tests in the Engineering Test

Reactor (ETR) to obtain high levels of burnup in a relatively short time. In addition, the Oak Ridge Research Reactor (ORR) was utilized to permit highly instrumented tests in which detailed measurement and adjustment of in-reactor test conditions could be accomplished. Screening tests were also done under transient conditions in the transient test facility in the TREAT reactor.

In the fourth task area, analysis of fuel element performance, the objective was to integrate mathematically the other aspects of the FBR Oxide Fuels Development Program in such a way that fundamental understanding of the behavior of LMFBR fuel elements could be obtained. The final output of this task was an analytical model that describes the performance and possibility of failure of the fuel pins under operating conditions. The fuel element performance modeling effort was used in essentially two ways: (1) to obtain an analytical understanding of the behavior sufficient for fuel element design, and (2) to assist in directing other task areas of the program in proper channels to answer pertinent and high-priority questions. The attainment of the model as a tool for design was considered a longer-range objective. The model in its various stages was quite useful in the design and interpretation of irradiation experiments.

1.3 CONTENT OF REPORT

This report is organized to set forth specific technology in the various technical areas in which development was accomplished. These include fuel preparation, fabrication development, fuel characterization, fuels irradiation, and fuel performance and economic evaluation. In addition, it includes sections that discuss the work, present conclusions from it, and give recommendations for future work. A section on publications and documentation of the program is also included.

2. Fuel Preparation

R. G. Wymer¹ A. L. Lotts

Fuel material for the fast breeder reactor oxide fuel program was prepared by mixing UO_2 sols with PuO_2 sols to give the uranium-to-plutonium ratio sought. The mixed sol was then either formed into microspheres for use in Sphere-Pac fuel studies or dried to form shards from which powder was prepared for use in pellet fuel studies. In this chapter the processes used to prepare sols, microspheres, and ceramic-grade powder for pellets are discussed.

2.1 SOL PREPARATION

W. T. McDuffee¹

2.1.1 UO_2 Sol Preparation from Natural Uranium

2.1.1.1 Process Description

The 1 M natural urania sols used to mix with plutonia sols were prepared by the Concentrated Urania Sol Preparation (CUSP) process.²⁻⁴ It is a batch process for preparing a 1 to 1.4 M crystalline urania sol directly by solvent extraction. This process avoids the handling of solids, as required in some earlier urania sol processes, while eliminating or minimizing the sol concentration step inherent in the earlier solvent extraction process for the preparation of dilute sols.⁵ Further, it lends itself to closer control than can be imposed easily on the previous processes. In general, the

sols prepared by the CUSP process have better reproducibility and longer shelf life than urania sols prepared previously by solvent extraction.

In the CUSP process, a 1 M urania sol is prepared by continuously extracting nitrate at a controlled rate from a U(IV) nitrate-formate solution into an organic solvent of 0.25 M Amberlite LA-2,⁶ a secondary amine, in a mixed diluent of 75 vol % diethyl benzene and 25 vol % $n\text{-C}_{12}$ paraffin.⁷ Following a prescribed conductivity-temperature-time path produces stable $\sim 1 M$ urania sol containing highly crystalline colloidal particles with a high U(IV) content. The operating curve or path followed in preparing the sol is shown in Fig. 2.1; a typical chemical flowsheet is presented in Fig. 2.2.

Nitrate extractions are carried out at three different temperatures. An extraction is initiated by starting solvent flow and ended by stopping solvent flow. The first extraction is at 35 to 40°C; as the feed solution is heated from room temperature there is a slight increase in conductivity. Conductivity increases with both temperature and free nitrate concentration. The first extraction is continued until the conductivity is reduced to about 25,000 micromhos/cm; then the solvent flow is turned off. The solution is heated to 57 to 58°C, and crystallization of the UO_2 to form colloiddally suspended crystallites begins. The solvent flow is turned on and heating is continued until 60 to 62°C is attained, and the second extraction is performed at this temperature. Crystallization is accompanied by a change in solution color from dark green to black, evolution of gas that is ~ 85 vol % NO , and a conductivity increase. In 15 to 30 min the gassing abates, indicating that crystallization is essentially complete, and the extraction is continued until the conductivity decreases to about 20,000 micromhos/cm.

1. Chemical Technology Division.

2. J. P. McBride, K. H. McCorkle, Jr., W. L. Pattison, and B. C. Finney, "The CUSP Process for Preparing Concentrated, Crystalline Urania Sols by Solvent Extraction," *Nucl. Technol.* **13**(2), 148-58 (February 1972).

3. B. C. Finney and P. A. Haas, *Sol-Gel Process -- Engineering-Scale Demonstration of High-Density UO_2 Microsphere Preparation*, ORNL-4802 (in preparation).

4. J. P. McBride (compiler), *Preparation of UO_2 Microspheres by Sol-Gel Technique*, ORNL-3874 (February 1966).

5. J. P. McBride, K. H. McCorkle, and W. L. Pattison, *Production of Predominantly Crystalline Sols of Urania*. U.S. Patent 3,629,133 (Dec. 21, 1971).

6. Rohm and Haas Company.

7. South Hampton Company. The C_{12} represents an average molecular size of a mixture.

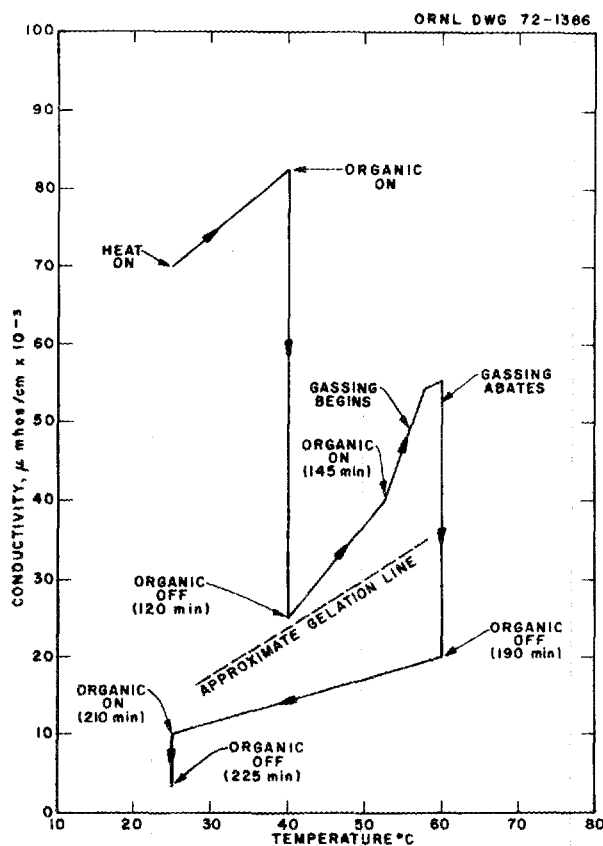


Fig. 2.1. Engineering-scale CUSP operating curve.

Solvent flow is then turned off. The second extraction takes 45 to 60 min to assure that the crystallization is complete. The solution, which is a sol at this point, is cooled to about 25°C , and there is an accompanying decrease in conductivity to about 10,000 micromhos/cm. Additional nitrate is extracted until the conductivity is in the range 3000 to 4500 micromhos/cm, which corresponds to a nitrate-to-uranium mole ratio of 0.11 ± 0.02 .

It requires 3.5 to 4 hr to prepare a sol, and since nitrate is extracted for prescribed periods of time, the preparation time is independent of batch size. Certain precautions must be taken in preparing the sol. The first nitrate extraction should take at least 90 min to allow time for the proper release of nitrate; otherwise, the nitrate-to-uranium mole ratio of the sol product will be too high, even though the conductivity is in the proper range. There are conditions under which gelation occurs, as shown on Fig. 2.1, and care must be taken during the first nitrate extraction not to overextract in order to prevent thickening or possibly gelling the solution. During the second extraction, good oxidizing

conditions are present (elevated temperature and NO being released); consequently, the time of the second extraction, while long enough to assure complete crystallization, should be no longer than necessary so that the oxidation of U(IV) to U(VI) is minimized.

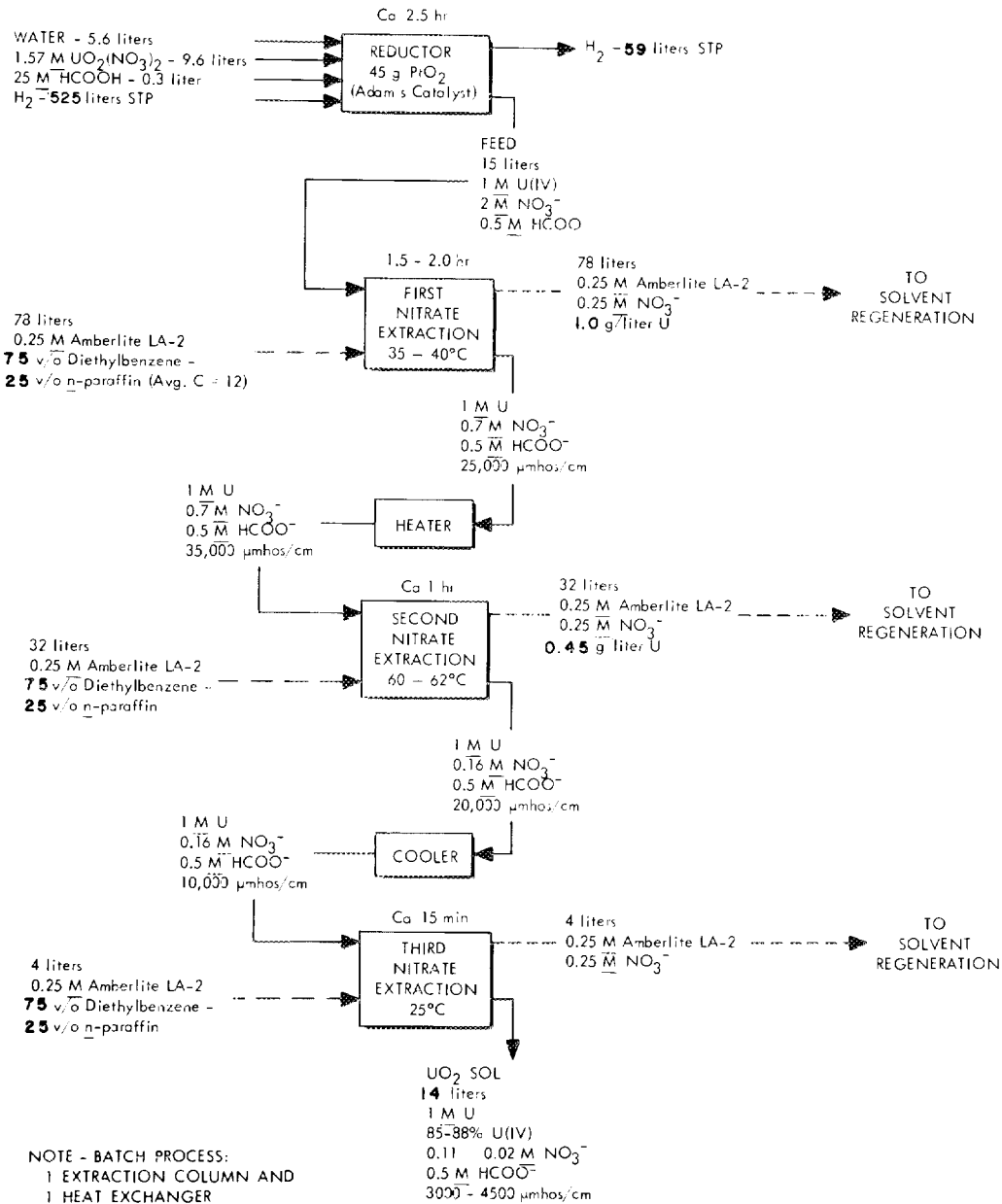
To prepare the feed solution for the sol preparation steps, water, concentrated uranyl nitrate solution that is stoichiometric in nitrate (NO_3^-/U mole ratio = 2), and formic acid are mixed in the proper proportions to give a solution that is 1 M UO_2^{2+} , 2 M NO_3^- , and 0.5 M HCOOH (Fig. 2.2) and reduced with H_2 . From 1.3 to 1.4 moles of H_2 is consumed per mole of uranium reduced, and the feed to the sol preparation equipment is 1 M U(IV) , 2 M NO_3^- , and 0.5 M HCOOH . The first, second, and third extractions remove approximately 65, 25, and 5%, respectively, of the original nitrate, and the extraction times are controlled by regulating the solvent flow rate. The sol product is about 1 M U that is 85 to 88% U(IV), $0.11 \pm 0.02\text{ M NO}_3^-$, 0.5 M COOH^- , and 3000 to 4500 micromhos/cm in conductivity.

2.1.1.2 Equipment and Procedures

An equipment flowsheet for the preparation of UO_2 sol by the CUSP process is presented in Fig. 2.3. The order in which the equipment is discussed corresponds to the sequence of process steps.

Feed preparation. The U(IV) feed is prepared in the batch slurry uranium reductor shown in Fig. 2.4. The uranyl nitrate solution (1 M UO_2^{2+} , 2 M NO_3^- , and 0.5 M HCOOH) is reduced with hydrogen at atmospheric pressure, using a commercially available platinum catalyst (PtO_2 , "Adams Catalyst"). The extent of reduction is monitored by measuring the U(IV)/U(VI) redox potential, using platinum and glass electrodes. When the uranium reduction is nearing completion, the slope of the graph of time against potential decreases rapidly and abruptly approaches zero. Then the hydrogen flow is turned off (Fig. 2.5). Vigorous agitation is required to assure uniform reduction. Continuing hydrogen flow in the absence of uranyl ions produces ammonia. More than about 0.01 mole of ammonia per mole of uranium promotes early gelation and falsifies the conductivity, which is the major process control variable in the extraction steps. To reduce 15 liters of 1 M uranyl nitrate solution ($\sim 4\text{ kg}$ of UO_2) requires 2 to 2.5 hr.

After the reduction, the U(IV) feed solution is drained from the reductor, and the catalyst, which has been reduced to metallic platinum, is caught on the $10\text{-}\mu\text{m}$ -pore stainless steel filter. The catalyst is washed with water and 5 M HNO_3 . The acid wash maintains catalytic activity.

Fig. 2.2. Chemical flowsheet for preparing UO_2 sol by the CUSP process.

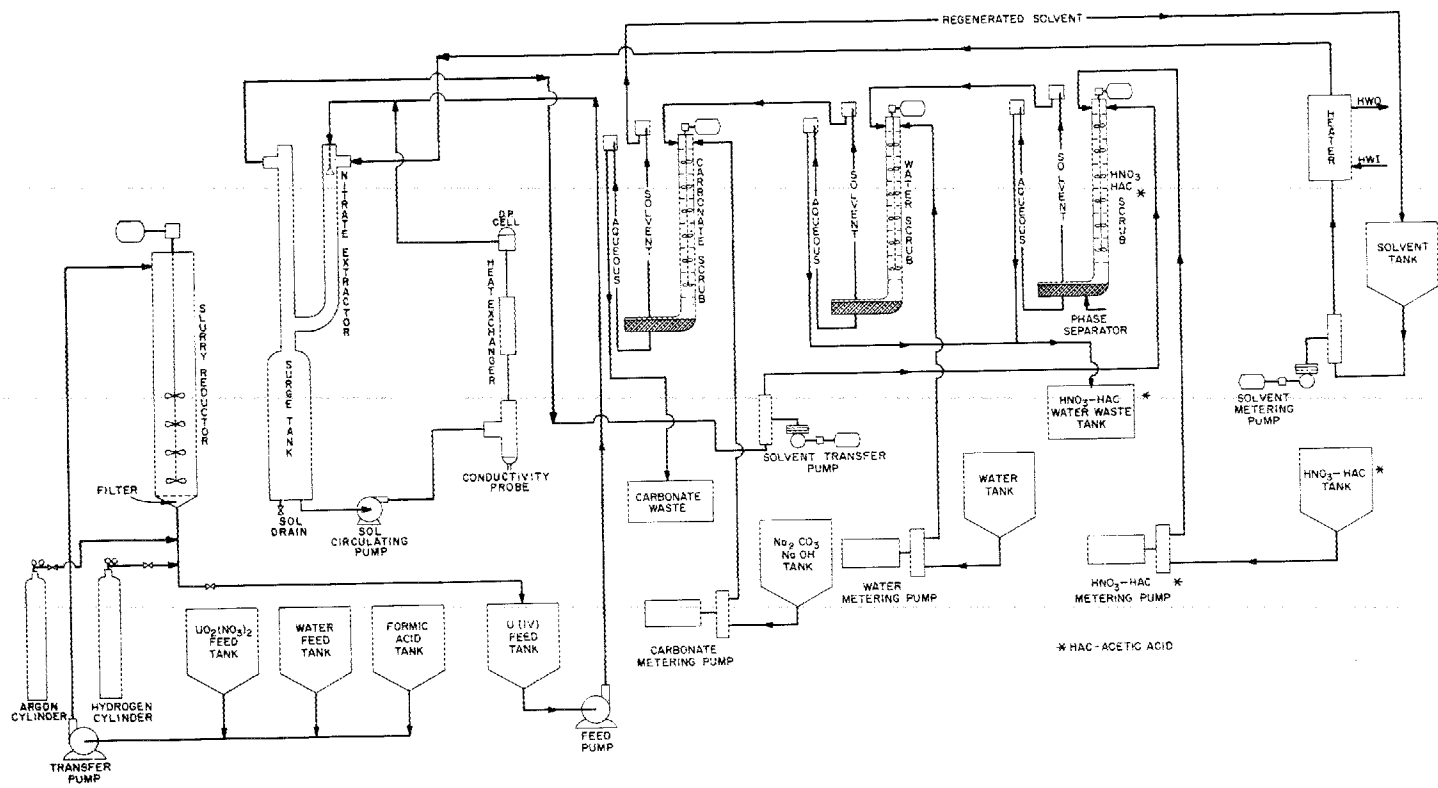


Fig. 2.3. Equipment flowsheet for the preparation of UO_2 sol by the CUSP process.

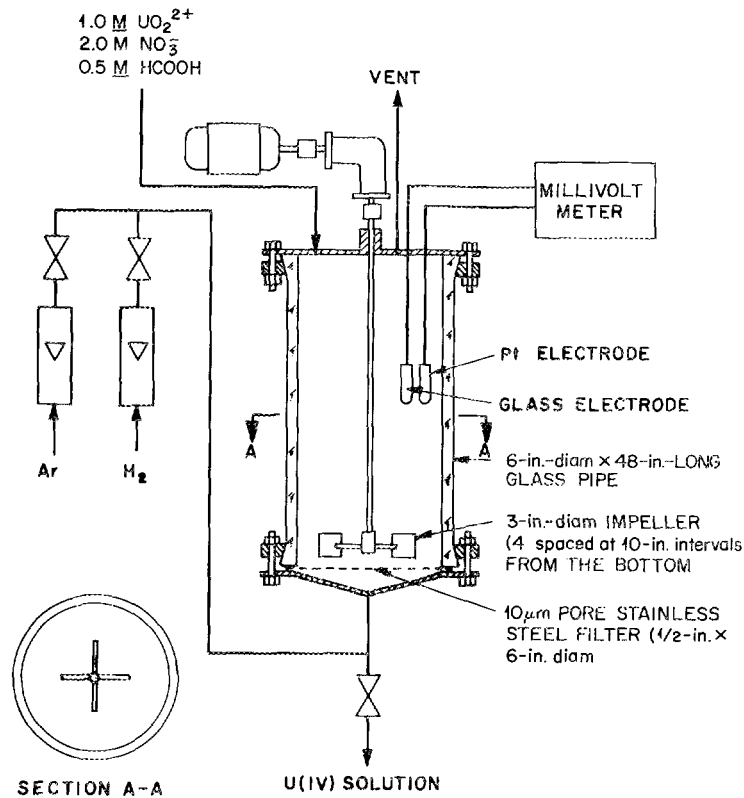
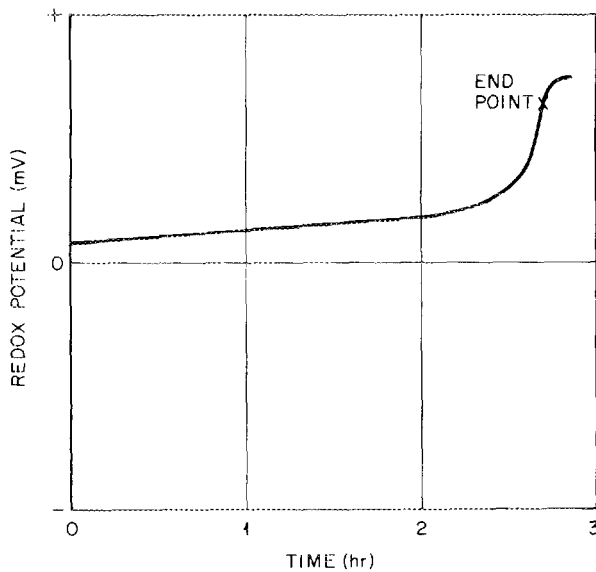


Fig. 2.4. Batch slurry uranium reductor.

ORNL-DWG 73-7875A

Fig. 2.5. Plot of redox potential against time for the reduction of a 1 M $UO_2(NO_3)_2$ -0.5 M $HCOOH$ solution.

Sol preparation by solvent extraction. The sol preparation equipment (Fig. 2.6) has a 15-liter aqueous phase capacity (~ 4 kg of UO_2) and consists of a spray column nitrate extraction contactor, solvent reservoir, aqueous phase surge tank, centrifugal pump, conductivity probe, heat exchanger, differential pressure cell, and spray header to disperse the aqueous phase into drops. The aqueous phase is circulated at 3 to 4 liters/min cocurrent with the solvent down the contactor. During the extraction periods, the solvent flows continuously to the nitrate extraction contactor, and the spent solvent is sent to the solvent cleanup and regeneration system.

After the sol preparation, the sol and solvent are drained separately and the equipment is washed out with about 3 M HNO_3 and then with water. Some solids accumulate at the solvent-sol interface, primarily during the crystallization phase. These solids tend to cling to the equipment during draining. As a result, 2 to 4% of the uranium in the feed solution is lost to the equipment wash solution and about 0.5% to the solvent

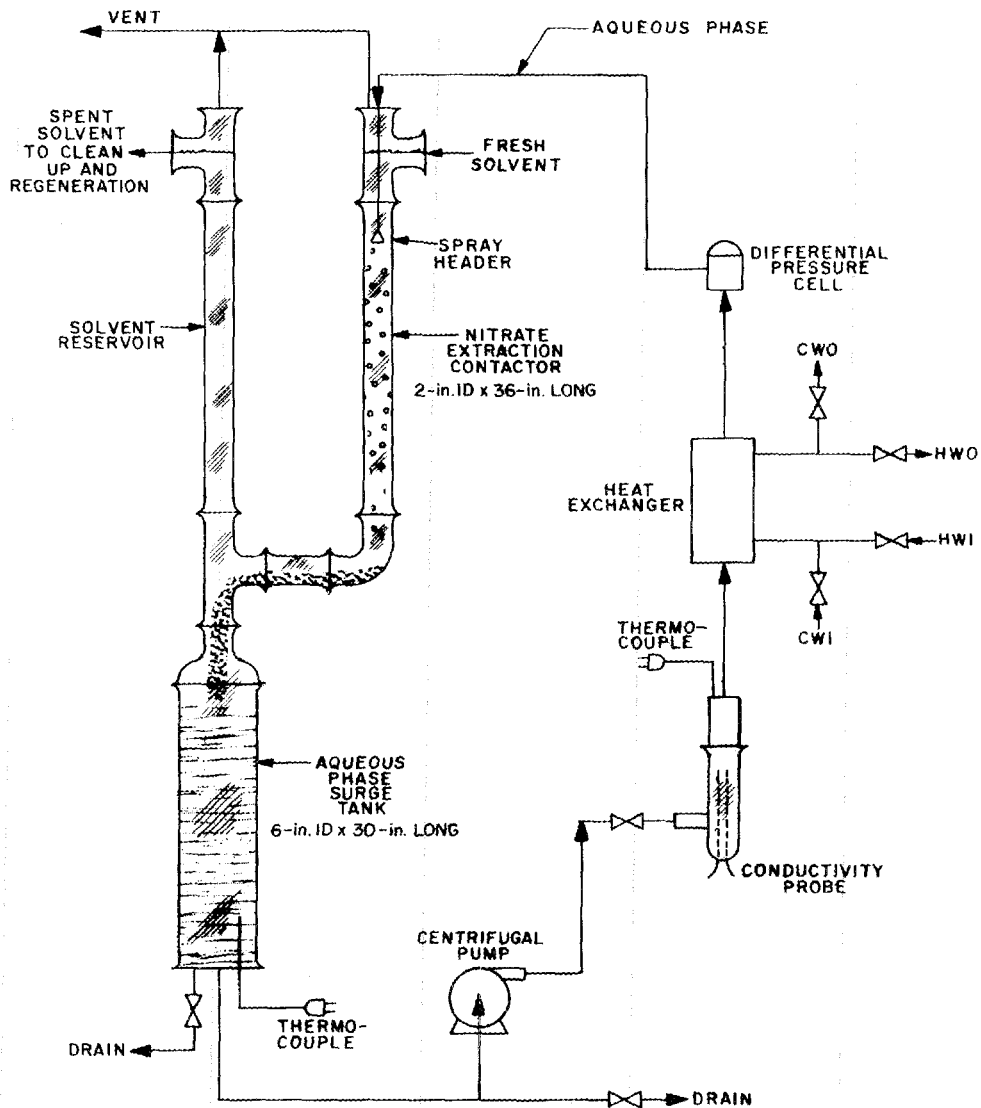


Fig. 2.6. CUSP UO_2 sol preparation equipment (15-liter aqueous phase, 4 kg of UO_2).

wash (dilute HNO_3). The uranium can be recovered from these acidic wash solutions.

Solvent cleanup and regeneration. Some uranium is picked up by the solvent, primarily during the first and second nitrate extractions. This pickup is about 0.5% of the uranium in the feed. The uranium is in the form of entrained sol and a colloidal suspension. These particles are well dispersed, carry a slight negative charge, and cannot be removed by filtration or adsorption on silica gel or activated carbon. There is also a slight loss of amine (approximately 0.06 to 0.10 mole/kg of UO_2 prepared as a 1 M sol) during the sol preparation. The

amine can be satisfactorily maintained at an essentially constant concentration by periodic additions of Amberlite LA-2 to the solvent storage tank. A three-stage solvent treatment system consisting of two cleanup stages and a regeneration stage was found to be satisfactory (see Fig. 2.7). The solvent cleanup is a 1 M HNO_3 , 0.4 M $HC_2H_3O_2$ scrub and water wash, and the regeneration is a 1 M Na_2CO_3 , 1 M $NaOH$ scrub. Essentially all the uranium in the solvent is removed in the cleanup acidic effluent, from which it can be recovered.

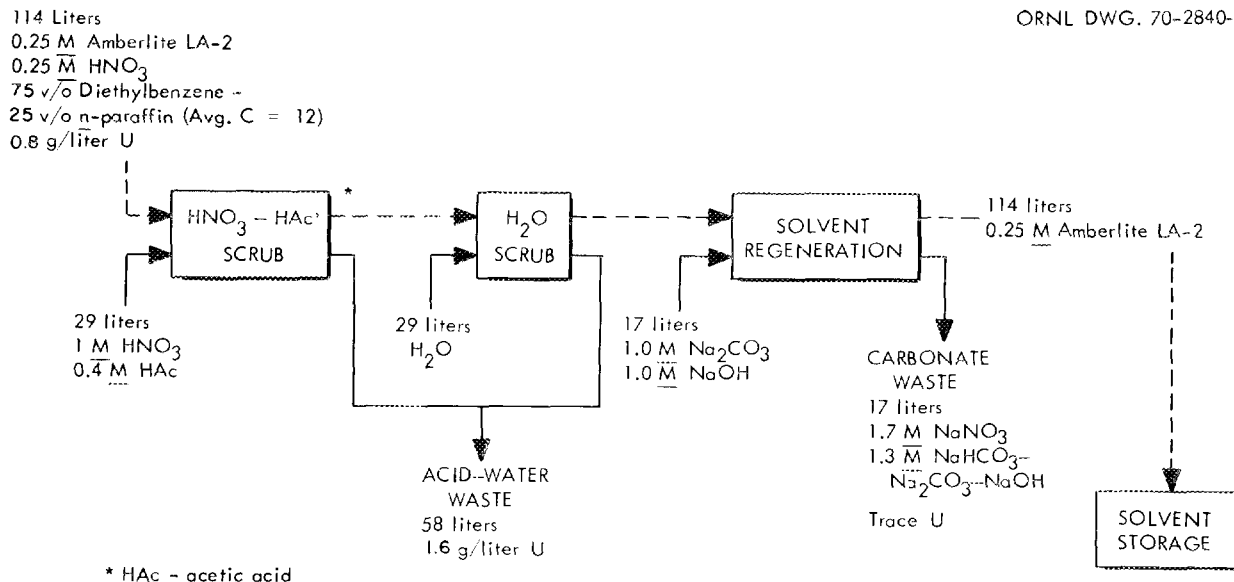


Fig. 2.7. Chemical flowsheet for solvent cleanup and regeneration in the CUSP process.

The solvent extraction contactors used⁸ in the solvent treatment system are mixer-settlers of the type shown in Fig. 2.8. Each mixer-settler is made of 3-in.-diam glass pipe to permit observation of the process streams and the operating characteristics. It is divided into six compartments, each of which has a mixing impeller; the six impellers are mounted on a common shaft with a variable-speed drive. The aqueous and organic phases enter at the top and flow cocurrently down through the six compartments to give the effect of mixing vessels in series. This arrangement ensures good stage efficiency. The mixer is designed in such a manner that the aqueous phase is dispersed into the organic phase (the organic phase is maintained continuous to minimize emulsification). At shutdown, the aqueous phase drains out of the vessel; consequently, only the organic phase is present at start-up, and the aqueous stream is easily dispersed as it enters. Each mixer is equipped with two U-shaped sections of stainless steel tubing through which hot water can be circulated.

Phase separation occurs in the section located below the mixer. The position of the interface is controlled by adjustable weirs on both the aqueous and the organic overflow lines. The nominal volumetric capacity of the mixing section is 2.0 liters; that of the settler is 2.8 liters of organic phase and 1.5 liters of aqueous phase.

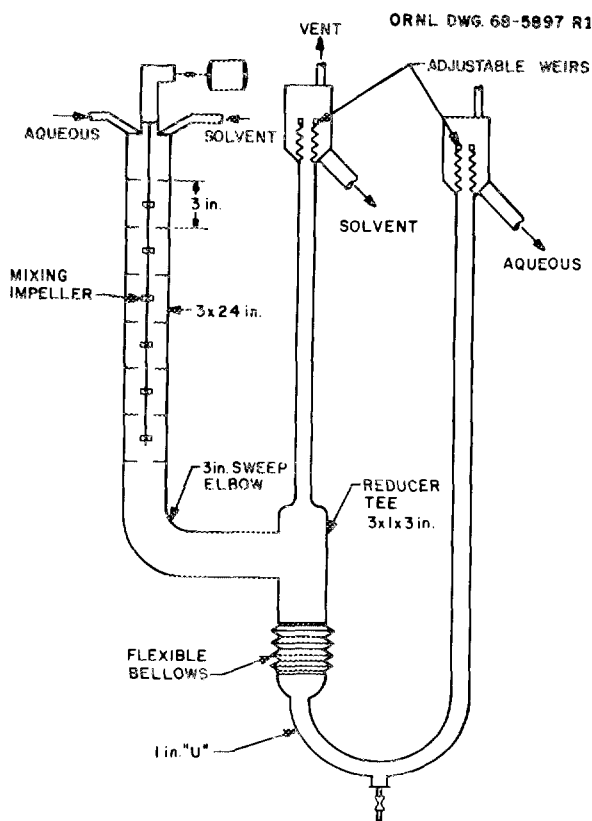


Fig. 2.8. Mixer-settler stage.

8. J. W. Snider, *The Design of Engineering-Scale Soxhlet Equipment*, ORNL-4256 (April 1969).

2.1.1.3 Discussion of Results

Properties of typical 1 M UO_2 sols prepared by the CUSP process are presented in Table 2.1. The reproducibility of the sols is very good: 253 to 255 mg/ml U, 85 to 87% U(IV), 0.09 to 0.11 nitrate-to-uranium mole ratio, and conductivity of 2910 to 3500 micromhos/cm.

From experience and number of material balances, we estimate that the sol recovery for a large number of repetitive batches would be 92 to 95%. The largest uranium losses are to the solvent acid and water scrubs and to the extraction equipment and solvent acid washes. These are acidic solutions from which the uranium can be recovered easily.

2.1.2 Plutonia Sol Preparation

Plutonia sols equivalent to 5 kg of Pu were prepared from aqueous $\text{Pu}(\text{NO}_3)_4$ according to the standard

ORNL precipitation peptization flowsheet⁹ shown in Fig. 2.9. Sols prepared in this manner were typically stable over long periods of time. The composition of a typical PuO_2 sol is as follows:

| | |
|--|-------|
| Pu, g/liter | 300 |
| NO_3^-/Pu (mole ratio) | 0.12 |
| NH_3/Pu (mole ratio) | <0.01 |

2.1.3 UO_2 Sol Preparation from Enriched Uranium

Urania sols equivalent to 17.5 kg of U were prepared from enriched uranium by an adaptation of the

9. M. H. Lloyd and R. G. Haire, "A Sol-Gel Process for Preparing Dense Forms of PuO_2 ," *Nucl. Appl.* 5, 114-22 (1968).

Table 2.1. Properties of typical 1 M UO_2 sols prepared by the CUSP process

| Run | U (mg/ml) | U(IV) content (%) | Mole Ratios | | | | Conductivity at 25°C (micromhos/cm) | pH |
|-----|-----------|-------------------|--------------------------|--------------------------|--------------------------|------------------------|-------------------------------------|------|
| | | | NO_3^-/U | HCOO^-/U | NH_4^+/U | Na^+/U | | |
| 1 | 253 | 86 | 0.10 | 0.40 | 0.0021 | 0.0053 | 3078 | 2.44 |
| 2 | 254 | 87 | 0.11 | 0.40 | 0.0017 | 0.0023 | 2884 | 2.53 |
| 3 | 253 | 85 | 0.09 | 0.47 | | 0.0040 | 3010 | 2.53 |
| 4 | 255 | 87 | 0.11 | 0.40 | 0.0025 | 0.0033 | 3477 | 2.57 |

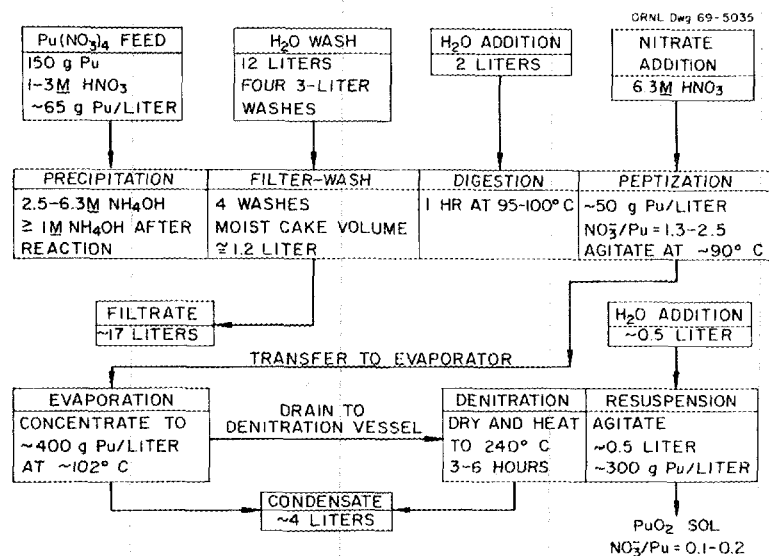


Fig. 2.9. Flowsheet for plutonia sol preparation.

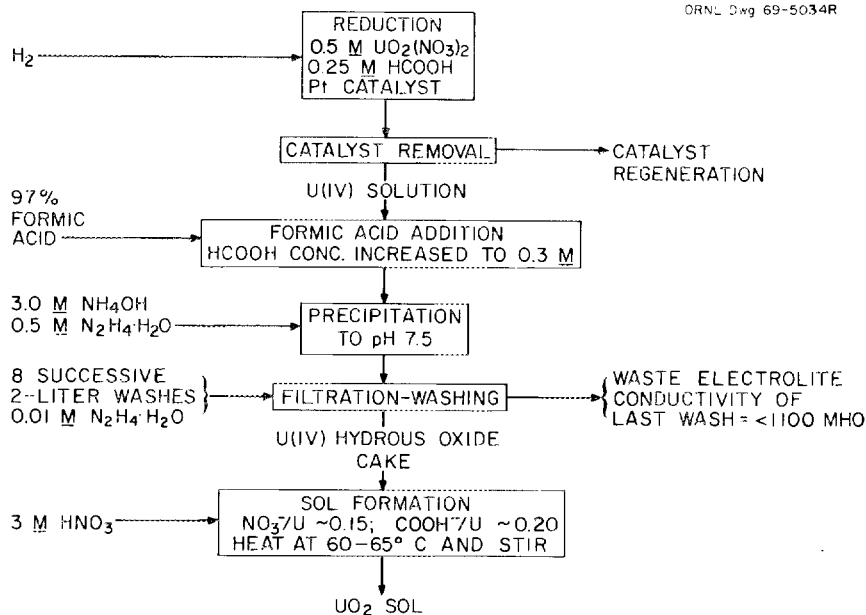


Fig. 2.10. Flowsheet for laboratory-scale preparation of urania sol.

standard ORNL precipitation-peptization flowsheet¹⁰ shown in Fig. 2.10. This process was chosen because batch sizes were limited to about 325 g of U for safety considerations. These sols as prepared were stable for about two weeks and deposited little if any solids when standing.

2.1.4 Preparation of Mixed (U,Pu)O₂ Sols

In the preparation of powders, UO₂ sols prepared as described in Sects. 2.1.1 and 2.1.3 were either dried as prepared or blended with the appropriate quantity of PuO₂ sol to achieve the desired plutonium-to-uranium ratio, and the mixture was dried. However, if the UO₂ sol was to be blended with PuO₂ sol and the mixed sol converted into dense microspheres, the UO₂ sols were allowed to stand for about 16 hr and then decanted from any solids that had settled; the supernatant sol was then extracted several times with *n*-hexanol to reduce the formic acid concentration before blending with the PuO₂ sol. The composition of a typical UO₂ sol as prepared and after extraction twice with an equal volume of dry *n*-hexanol is given in Table 2.2.

10. J. P. McBride, K. H. McCorkel, and W. L. Pattison, "Urania Sol-Gel Process," pp. 25-29 in *Laboratory Studies of Sol-Gel Processes at the Oak Ridge National Laboratory*, J. P. McBride (compiler), ORNL-TM-1980 (September 1967).

Table 2.2. Typical UO₂ sols

| Type of UO ₂ sol | U (g/liter) | U ^{IV} /U | NO ₃ ⁻ /U (mole ratio) | HCO ₂ ⁻ /U (mole ratio) |
|-----------------------------|-------------|--------------------|--|---|
| As prepared | 220 | 0.88 | 0.17 | 0.28 |
| Extracted ^a | 260 | 0.88 | 0.17 | 0.08 |

^aExtracted successively with two equal volumes of *n*-hexanol.

2.2 MICROSPHERE PREPARATION

P. A. Haas¹¹ W. T. McDuffee¹¹

The ORNL sol-gel process for the preparation of microspheres from oxide sols and information on the design and operation of the equipment have been previously reported.¹²⁻¹⁴ In general terms, conversion

11. Chemical Technology Division.

12. C. C. Haws, B. C. Finney, and W. D. Bond, *Engineering-Scale Demonstration of the Sol-Gel Process: Preparation of 100 kg of ThO₂-UO₂ Microspheres at the Rate of 10 kg/Day*, ORNL-4544 (May 1971).

13. P. A. Haas, *Sol-Gel Preparation of Spheres: Design and Operation of Fluidized Bed Columns*, ORNL-4398 (September 1969).

14. P. A. Haas, "Preparation of Sol-Gel Spheres Smaller than 200 Microns without Fluidization," *Nucl. Technol.* 10, 283-92 (March 1971).

of a sol into dense spheres requires six principal process operations:

1. dispersion of the sol into drops, each of which contains the amount of oxide that will be in a fired sphere;
2. suspension of the sol drop in an organic liquid, usually 2-ethyl-1-hexanol (2EH), while water is extracted to cause gelation;
3. separation of gel microspheres from the organic liquid;
4. recovery of the organic liquid for reuse;
5. drying of the gel spheres;
6. firing the dried spheres at controlled conditions to remove volatiles, to sinter to a high density, and to reduce or chemically convert.

The first four operations are usually carried out in continuous systems, while the last two are batch operations.

The optimum conditions for forming a sol into gel microspheres vary in a complex manner with the properties of the sol. When a sol with specified properties is formed into gel spheres, the composition of the organic drying medium is the principal operating variable. The successful continuous operation of a sphere-forming system requires that the alcohol composition be controlled within satisfactory ranges. This is largely empirical and requires demonstration in three stages: (1) satisfactory initial operation, (2) control of surfactant depletion, and (3) control of excessive accumulations of surfactant degradation products or impurities.

The formation of a good sphere requires that the sol drop be suspended until enough water is extracted to cause gelation. Nearly all of our successful operation with CUSP UO_2 sols has been with 2EH containing Span 80 and Ethomeen S/15 as surfactants. The times required for gelation can be calculated from mass transfer considerations. For CUSP sols, from 4 to 40 min is required to form gel spheres that will calcine to high-density UO_2 spheres 200 μm in diameter, and from 10 to 100 min is required to form gel spheres that will calcine to 500- μm -diam UO_2 spheres. The principal variables affecting the gelation time for a given sol are the sphere diameter, temperature of the 2EH, and water content of the 2EH. Higher 2EH temperatures greatly reduce the gelation times and often improve the surface appearance of the gel spheres but may increase the amount of clustering or cracking.

The two most troublesome operating problems for preparation of UO_2 spheres from CUSP sols are:

1. increasing amounts of sticking, clustering, or coalescence as column operation is continued because of a combination of loss of Span 80, extraction of formic acid from the UO_2 sol into the 2EH, and accumulation of surfactant degradation products;
2. excessive cracking during drying and firing even though the cracking is not noticeable in the gel. This cracking depends very much upon the size of the microspheres produced. High surfactant concentrations in the 2EH, impurities in the 2EH, inferior sol properties, and oxidation of the UO_2 all tend to increase the amount of cracking.

2.2.1 Preparation of UO_2 - PuO_2 Spheres in Fluidized-Bed Columns

Plutonia sol, urania sol, and mixtures of the two were formed into droplets of the desired size by use of a two-fluid nozzle in which the sol was forced as a jet stream into an annulus of 2EH, which was used as a drying (gelling) solvent. The stream of droplets was introduced at the top of a tapered column through which a second stream of 2EH passed up. The second stream maintained the droplets in a fluidized bed, the depth of which depended on the density of the droplet, the sol feed rate, and the flow of the fluidizing stream. As water was extracted from the droplets, the sol gelled; continued extraction of water from the gelled droplet shrank it, hardened it, and increased its density. By careful adjustment of the fluidizing stream flow, the sol droplets and gelled microspheres were retained in the column until the gel microspheres were rigid enough to be handled before being allowed to fall out of the column. Continuous operation (with feed and the 2EH fluidizing stream balanced) could be obtained with 95 to 98% of the microspheres being sufficiently dry to support 2- to 3-in. beds without noticeable distortion.

To promote droplet formation, to prevent droplet coalescence, and to prevent sticking to the walls of the column, surfactants are added in small concentration to the 2EH drying solvent. The water content of the 2EH also exerts an effect. For the most part, to control these effects Ethomeen S/15 (a condensed ethylene oxide amine) and Span 80 (sorbitan monooleate) have been used. Ethomeen S/15 reduces coalescence; however, it tends to promote clustering of partially dried droplets as well as sticking to the column walls. Also, the effects

Table 2.3. Properties of typical dense microspheres

| Type | Diameter (μm) | | Pu (U + Pu) | Density (g/cm^3) | | Porosity (%) | O/M | Carbon (ppm) |
|---|-------------------------------|-----|----------------|------------------------------------|-----|-----------------|-------|-----------------|
| | | | | Microsphere | Tap | | | |
| PuO_2 | 100 | 250 | 1 | 11.4 | | <1 | 2.00 | <50 |
| $^{235}\text{U}_{0.8}\text{Pu}_{0.2}\text{O}_2$ | 350 | 595 | 0.202 | 11.03 | 6.7 | 0.44 | 2.001 | 40 |

of Ethomeen S/15 and Span 80 are somewhat antagonistic to each other; that is, the effects of one can be offset by the other. Too much of either is harmful: Ethomeen S/15 may lead to pitting, while excess Span 80 used to control clustering promotes malformation and surface wrinkling. Recently, Pluronic L-92 (a polyoxy propylene ethylene glycol manufactured by Wyandotte Chemical) has been used instead of Ethomeen S/15 and has been very successful in permitting use of low surfactant concentrations. The water content of the 2EH controls the drying rate — high removal rates associated with low water concentration tend to promote malformation and cracked microspheres, while low rates promote sticking to the walls.

Generally, much less trouble is encountered in the formation of droplets and gel microspheres from PuO_2 sols than from PuO_2 - UO_2 sol mixtures. As a rule, only 0.2 to 0.3 vol % Ethomeen S/15 (no Span 80) is required to form stable PuO_2 sol droplets and gel microspheres, contrasted with ~ 0.2 vol % Ethomeen S/15 and up to 2% Span 80 being required to form UO_2 or PuO_2 - UO_2 mixtures without severe clustering and sticking.

In addition to the problems of sticking and clustering in the column during forming, a common difficulty encountered with PuO_2 - UO_2 mixtures but rarely with PuO_2 alone has been cracking of the microspheres; this sometimes occurs in the column during the forming and drying, but usually appears in later steps. This results in a reduced product yield as well as in an inferior product. The tendency of microspheres to crack depends principally on the nature of the sol and to a lesser extent on other conditions. Fast drying and gelation in the forming column, because of the low water content of the 2EH as well as high surfactant concentrations, both favor cracking to some extent, but final drying and firing conditions exert a greater effect.

The properties of typical dense microspheres prepared by the methods described above are shown in Table 2.3.

2.2.2 Nonfluidized Preparation of UO_2 or UO_2 - PuO_2 Spheres

Fewer problems are usually encountered if gel spheres are not fluidized during formation. Coalescence, sticking, and clustering are much less troublesome because of the much lower particle concentrations and the absence of particle-to-particle interactions. However, the nonfluidized operation is only practical for smaller spheres. Spheres of UO_2 up to 200 μ in diameter after firing were prepared during demonstration runs in a 28-ft-high nonfluidized column.¹⁵ Spheres of UO_2 smaller than 100 μ in diameter were made in nonfluidized systems using turbulent operation of a two-fluid nozzle for sol dispersion.¹⁴ The UO_2 spheres of 25 μm mean diameter for "U-fines" type of Sphere-Pac fabrication require average sol drop diameters of about 80 μm for 1 M CUSP sols. Spheres of UO_2 - PuO_2 smaller than 44 μm were formed by use of the same 2EH compositions as for larger spheres, but the 2EH was usually 10 to 20°C warmer.

2.3 PREPARATION OF (U,Pu) O_2 SOL-GEL POWDER

R. A. Bradley

Sol-gel (U,Pu) O_2 powder was prepared for use in making the mixed oxide pellets described in Sect. 3.2. This powder was required to have the ratio $\text{Pu}/(\text{U} + \text{Pu})$ controlled to within ± 0.005 , to be homogeneous with respect to uranium and plutonium distribution, and to be suitable for fabricating 83- to 93%-dense pellets by the cold press and sintering technique.

The sol-gel process for making (U,Pu) O_2 powder is illustrated in Fig. 2.11. Sols of UO_2 and PuO_2 were blended, dried to gel shards at about 100°C, and then

15. B. C. Finney and P. A. Haas, *Sol-Gel Process: Engineering-Scale Demonstration of High-Density UO_2 Microsphere Preparation*. ORNL-4802 (in preparation).

ORNL-DWG 68-10791R

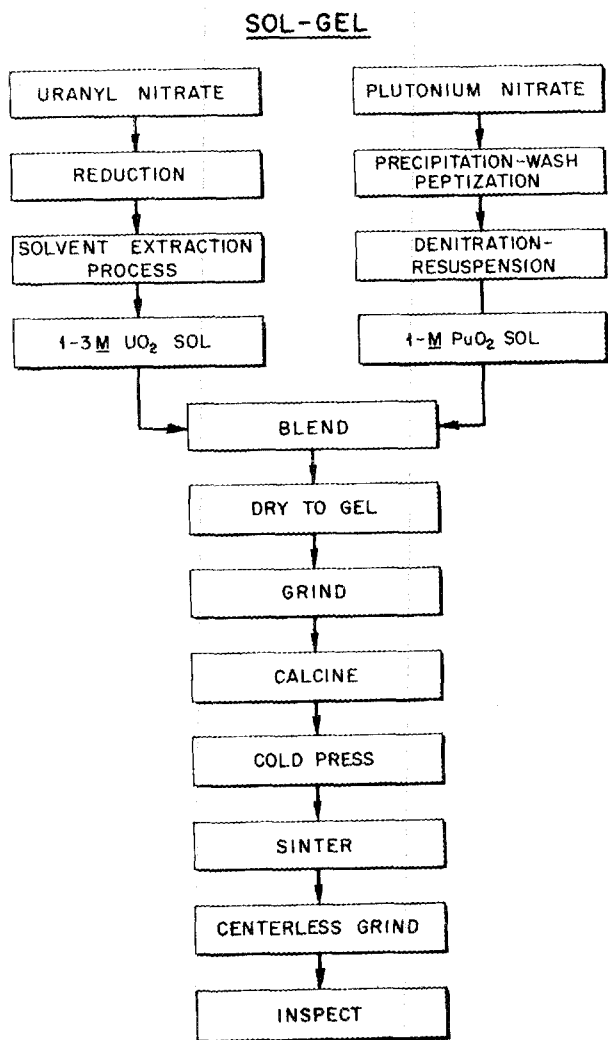


Fig. 2.11. Flowsheet for the preparation of (U,Pu)O₂ powder and pellets by the sol-gel process.

ground to ~ 325 mesh in a fluid energy mill. Since the sols consist of 50- to 200-Å crystallites of UO₂ or PuO₂ dispersed in an aqueous medium, an intimate mixture of the UO₂ and PuO₂ was easily obtained. Alpha autoradiography and electron microprobe analysis of sintered pellets, discussed in Sect. 4.2.3, showed the distribution of uranium and plutonium to be uniform.

Mercury porosimetry analyses of individual gel shards showed them to have bulk densities 45 to 50% of theoretical with only 1 to 2% of the porosity penetrable by mercury at 10,000 psi. The BET surface area of gel shards was 55 to 60 m²/g. From these analyses we conclude that the gel shards are porous agglomerates of 50- to 200-Å UO₂ and PuO₂ crystallites and that the interconnected porosity has openings smaller than 170 Å. Grinding the gel shards to ~ 325 -mesh powder in a fluid energy mill did not change the surface area significantly. This indicates that the porous agglomerates of crystallites are not destroyed during grinding; they are only reduced in size.

The ~ 325 -mesh powder was calcined at about 500°C to remove residual H₂O and other volatiles, to reduce its surface area to about 10 m²/g, and to stabilize its oxygen-to-metal ratio at about 2.1. The atmosphere used during calcination was selected to yield powder suitable for fabricating the particular type of pellets required. For making low-density pellets (83 to 87% of theoretical), the powder was calcined in Ar-4% H₂ to preserve the agglomerated nature of the sol-gel particles. For intermediate- or high-density pellets, the powder was given an oxidation-reduction treatment and sometimes ball-milled to destroy the agglomerates of crystallites. The role played by these agglomerates in producing low-density pellets is discussed in Sect. 3.2.

The ability to control the ratio Pu/(U + Pu) in sol-gel (U,Pu)O₂ is illustrated by the data in Table 2.4. Two samples of each of six batches of blended (U,Pu)O₂ sol

Table 2.4. Ratio of Pu/(U + Pu) in six batches of sol-gel (U,Pu)O₂ powder for GCFR F1 replacement rod fuel pellets

| Analysis | Ratio for various batches | | | | | |
|------------------------------------|---------------------------|--------|--------|--------|--------|--------|
| | GA2A | GA2B | GA2C | GA2D | GA2E | GA2F |
| Sample 1 | 0.1518 | 0.1495 | 0.1504 | 0.1518 | 0.1516 | 0.1516 |
| Sample 2 | 0.1516 | 0.1499 | 0.1504 | 0.1522 | 0.1512 | 0.1517 |
| Average ^a (\bar{x}) | 0.1517 | 0.1497 | 0.1504 | 0.1520 | 0.1514 | 0.1516 |

^aBased on an analysis of variance of these data, the 95% confidence interval about the average is ± 0.0004 .

were analyzed for uranium and plutonium. The ratios of Pu/(U + Pu) for all six batches were within the range 0.150 to 0.152, compared with a specified value of 0.150 ± 0.005 . These results are typical of all the mixed oxide powder prepared by the sol-gel process.

2.4 DISCUSSION OF STATUS OF TECHNOLOGY AND RECOMMENDATIONS

R. G. Wymer¹⁶

All work directly aimed at the development of sol-gel processes for preparing FBR fuels was terminated when support in this area was withdrawn. Related work has continued in support of HTGR fuel preparation. The need for urania sol is common to both HTGR and FBR fuel preparation by sol-gel processes, and the recent engineering demonstration¹⁵ of UO₂ sol preparation made under the HTGR fuel program is potentially of as much use in FBR as in HTGR fuel preparation.

Research and development has been carried out on sol-gel processes by ORNL scientists on assignment at

the Swiss Federal Research Institute near Zurich, Switzerland, and supported by the Swiss. This work is on FBR fuel preparation by the Sphere-Pac technique. Significant progress in plutonia sol preparation has been made, such that if either FBR or HTGR fuel requirements in the future include PuO₂, either alone or in admixture with UO₂ or ThO₂, the PuO₂ sol preparation process can be readily adapted to a useful engineering scale.

Many of the same techniques, people, and pieces of equipment are used for HTGR fuel preparation¹⁷ by sol-gel processes as for FBR fuel preparation. Thus, as work progresses on HTGR fuels, it is in effect progressing on the FBR fuels, though with some significant exceptions, most importantly in the area of engineering development and scale-up for preparation of fuel containing plutonium. This HTGR fuel work continues, though at a reduced level, since the short-term goals have nearly been reached, and work is not yet really started toward the next goals.

16. Chemical Technology Division.

17. A. L. Lotts, *National HTGR Fuel Recycle Development Program Plan*, ORNL-4702 (August 1971).

3. Fabrication Development

J. D. Sease R. A. Bradley

3.1 SPHERE-PAC FABRICATION TECHNIQUES

R. B. Fitts A. R. Olsen
R. A. Bradley J. Komatsu¹

The high-density spheres produced in the sol-gel process are ideally suited for fabrication into reactor fuel rods by a low-energy vibratory loading process. In the Sphere-Pac process, illustrated in Fig. 3.1, low-energy vibration of the cladding tube is employed to impart energy to the microspheres; this allows them to assume the preferred closely packed, high-density configuration. The purpose of our work on the Sphere-Pac process was to establish the feasibility of loading fuel rods by this technique, to define the variables that must be controlled to yield rods with reproducible densities, and to develop the technology required to fabricate

rods for irradiation tests. The use of this process with sol-gel microspheres offers a fabrication technique employing a minimum number of operations and items of equipment. The elimination of powder processes and their attendant dust problems would appear to be beneficial with regard to both equipment maintenance and inventory control. These factors are particularly important for remote fabrication.

3.1.1 Sphere-Pac Development

Using sol-gel ThO₂ microspheres, we have investigated loading procedures, equipment requirements, time cycles, and attainable packing densities. This investigation was based on the reported work of others^{2,3} and was

1. Visiting scientist from Japan Power Reactor and Nuclear Fuel Development Corporation.

2. R. K. McGeary, *J. Am. Ceram. Soc.* **44**(10), 513--22 (1961).

3. J. E. Ayre and F. E. Soppet, *J. Am. Ceram. Soc.* **48**(4), 180--83 (1965).

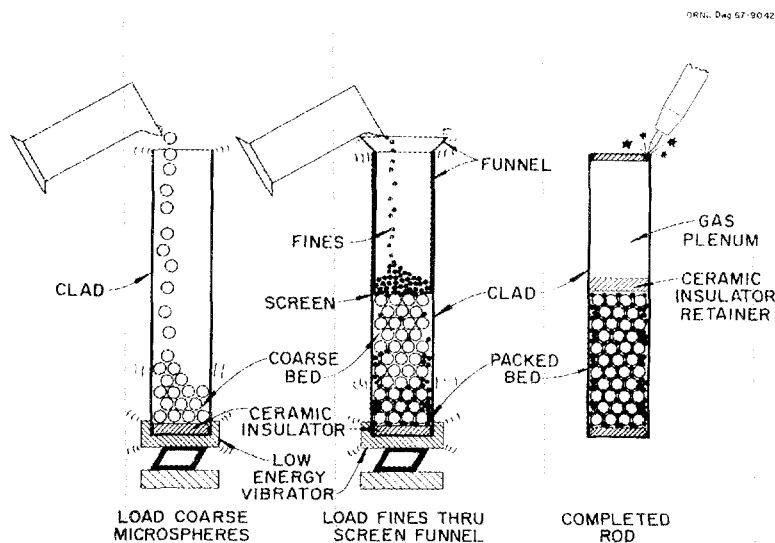


Fig. 3.1. The Sphere-Pac process.

directed toward providing practical experience with the technique and ultimately toward producing fuel rods for irradiation testing.

To determine general trends in the packing of spheres, we investigated mechanical blending of mixtures composed of 50% coarse and 50% medium spheres; Fig. 3.2 presents these data. A definite increase in bed density is obtained with increasing sphere diameter ratios; however, an unrestrained bed will begin to segregate during vibration when the size ratio exceeds about 3.5. The blended bed density lacks reproducibility at higher diameter ratios. This effect is due to segregation during blending.

Figure 3.3 illustrates our results on blended bed volume packing (P_V) as a function of the volume percentage coarse and medium spheres for three sphere diameter ratios. These results agree well with those obtained by McGeary² and extend them to lower diameter ratios and smaller size spheres. The data obtained from the maximum density point (~65% coarse and 35% medium) on these curves may be used to calculate the efficiency (P_E) of the medium size

ORNL-DWG 68-2259R

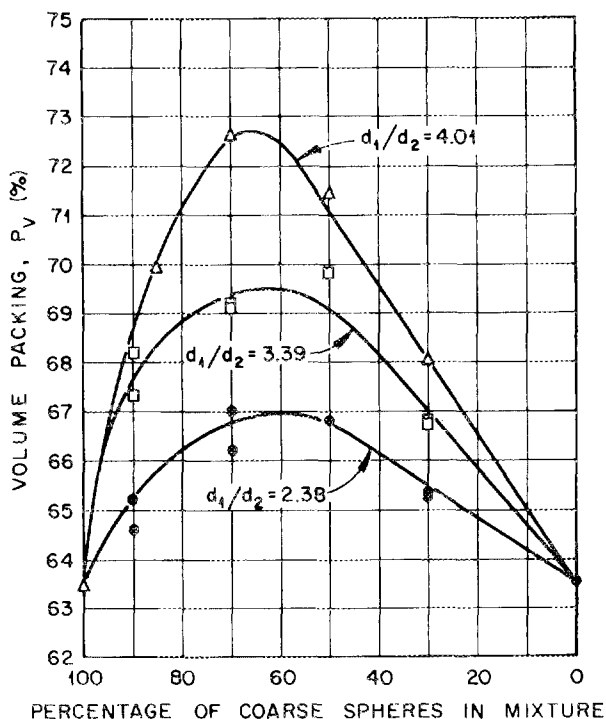


Fig. 3.3. Volume packing of blended spheres of two sizes for various diameter ratios.

ORNL-DWG 68-2260

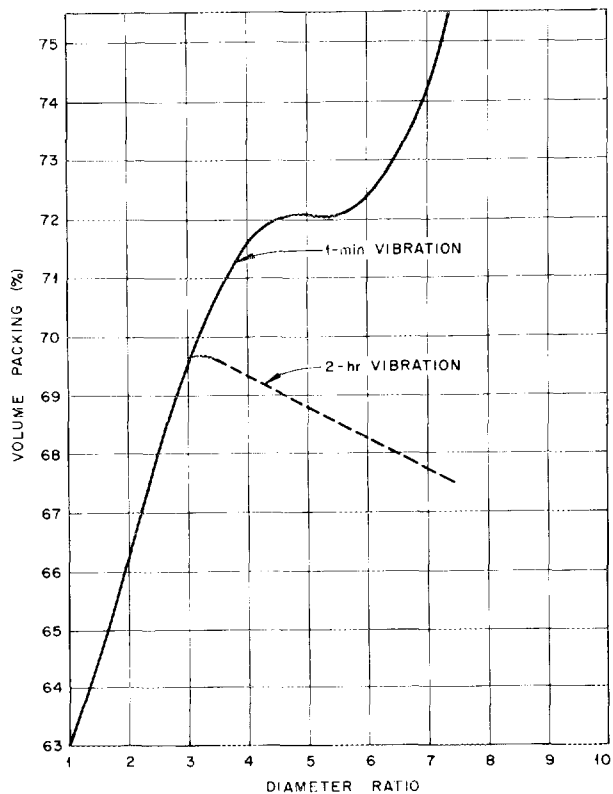


Fig. 3.2. Volume packing for 50:50 mixture of two sizes of spheres and effect of vibration after mixing.

spheres in filling the void available to them around the coarse spheres. To calculate this efficiency on a uniform basis we assume an artificial packing efficiency for the coarse spheres of 63.5%. This is the limit for packing efficiency of a single size sphere in a large tube as presented by Ayre.³ Using this basis for the packing efficiency of smaller spheres in a packed bed of large spheres, the data in Fig. 3.4 were obtained. Some data from the work of McGeary and Ayre are also shown in this figure. The agreement is excellent for diameter ratios up to 8 or 10. Above this range Ayre's work deviates significantly from our findings and those of McGeary.

Using this information on blended bed densities and packing efficiencies we developed a graphical construction that may be used to correlate and generalize all our information relating to the Sphere-Pac fabrication procedure. This is shown in Fig. 3.5, where the horizontal axis represents the volume packing of spheres in a container or bed (packing efficiency), and the vertical axis represents the void volume associated with this volume packing. If a 45° operating line is established between the two zero points of the axes, then the void volume associated with any packed

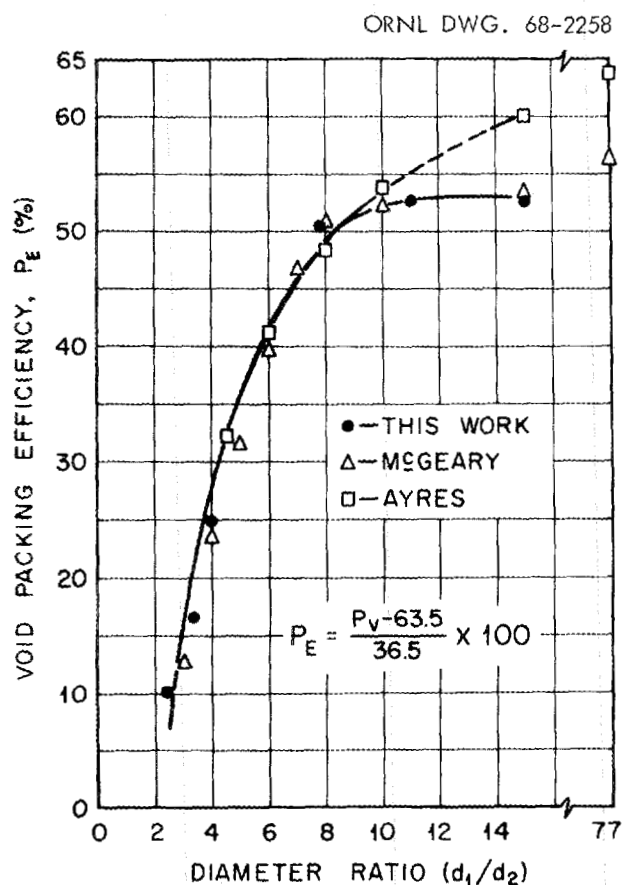


Fig. 3.4. Packing efficiency of small spheres in a packed bed of large spheres.

volume may be determined by reading up and then across (line A-B-C). If we now construct a line joining the volume packing efficiency of a given size sphere (% of available void volume filled by spheres) to the void volume zero point, the horizontal distance between this line and the operating line is always proportional to the packing efficiency multiplied by the void volume associated with that packed bed density. Thus the line A-D represents the packing of a single size sphere in a large tube or in a packed bed (according to Ayre) where the diameter of the sphere is less than approximately $1/25$ that of the smallest sphere already in the packed bed. This curve may be used to illustrate the effect of serial infiltrations with spheres having d_1/d_2 greater than 25. We obtain 63.5% packing with the coarse spheres. If we then infiltrate a small sphere at this same efficiency we would obtain, from point E, an 87%-dense bed, and a second infiltration produces a 95%-dense bed. This type of line must also be plotted separately for the packing of spheres of different

diameter ratios with respect to the bed. Such lines are shown dashed for spheres of $1/4$, $1/7$, and $1/10$ the size of the spheres in the bed, and are obtained from the plot of P_E vs d_1/d_2 (Fig. 3.6), determined as described later.

We may now see the effects of using a blended bed, or the effect of infiltration at less than the optimum 63.5% packing efficiency. If a d_1/d_2 ratio of 4.0 is used for a blended bed, the bed density (volume packing) is increased to 72%, point F. Infiltration with spheres $1/10$ the size of the medium fraction produces an 88%-dense bed, point G. This is exactly the density that we have obtained and reproduced by this technique. We have also produced 86.5%-dense beds by infiltration of a blended bed ($d_1/d_2 = 3.4$) with the 10/1 size ratio of medium to small. This is the density predicted by the graphical correlation for these conditions.

The above discussion shows that to produce a 90%-dense fuel we must use either a double infiltration with very carefully controlled sphere sizes or a blended bed at d_1/d_2 of about 5.8/1, followed by a single infiltration. This requires investigation of the behavior of beds blended at this diameter ratio. They tend to segregate, as was shown in Fig. 3.2.

We tested a variety of vibration frequencies and modes of energy input. Frequency had little effect on final packing density, but 60 Hz provided the best loading rate. The most rapid and dense packing was obtained when a lateral component accompanied the axial vibration. We have obtained 84%-dense packings in 9 min using 0.230-in.-ID tubing with a 2-ft fuel column height. The effect of sphere size variations within a given screen size range appeared to be minimal, since we found no variation in loading characteristics of 14 different batches of microspheres with similar densities but different particle size distributions. The optimum coarse-to-fine particle volume ratio is approximately 2.7 for these microspheres.

We determined the effect of the average coarse particle size on the coarse bed density. Coarse particles with normal size distributions and average sizes ranging from 250 to 535 μm were vibrated into a 0.245-in.-ID tube. Figure 3.6 represents the coarse bed density as a function of the ratio of tube diameter to average sphere diameter (D/d). Ayre and Soppet³ had shown that the packing efficiency of spheres of one size reached a maximum and then flattened at D/d greater than 10. However, as seen in Fig. 3.6, the packing of microspheres with a fairly wide size distribution continues to increase; no maximum was experienced for D/d up to 40.

To economically employ the Sphere-Pac process in a fuel production line, the pin loading time must be kept

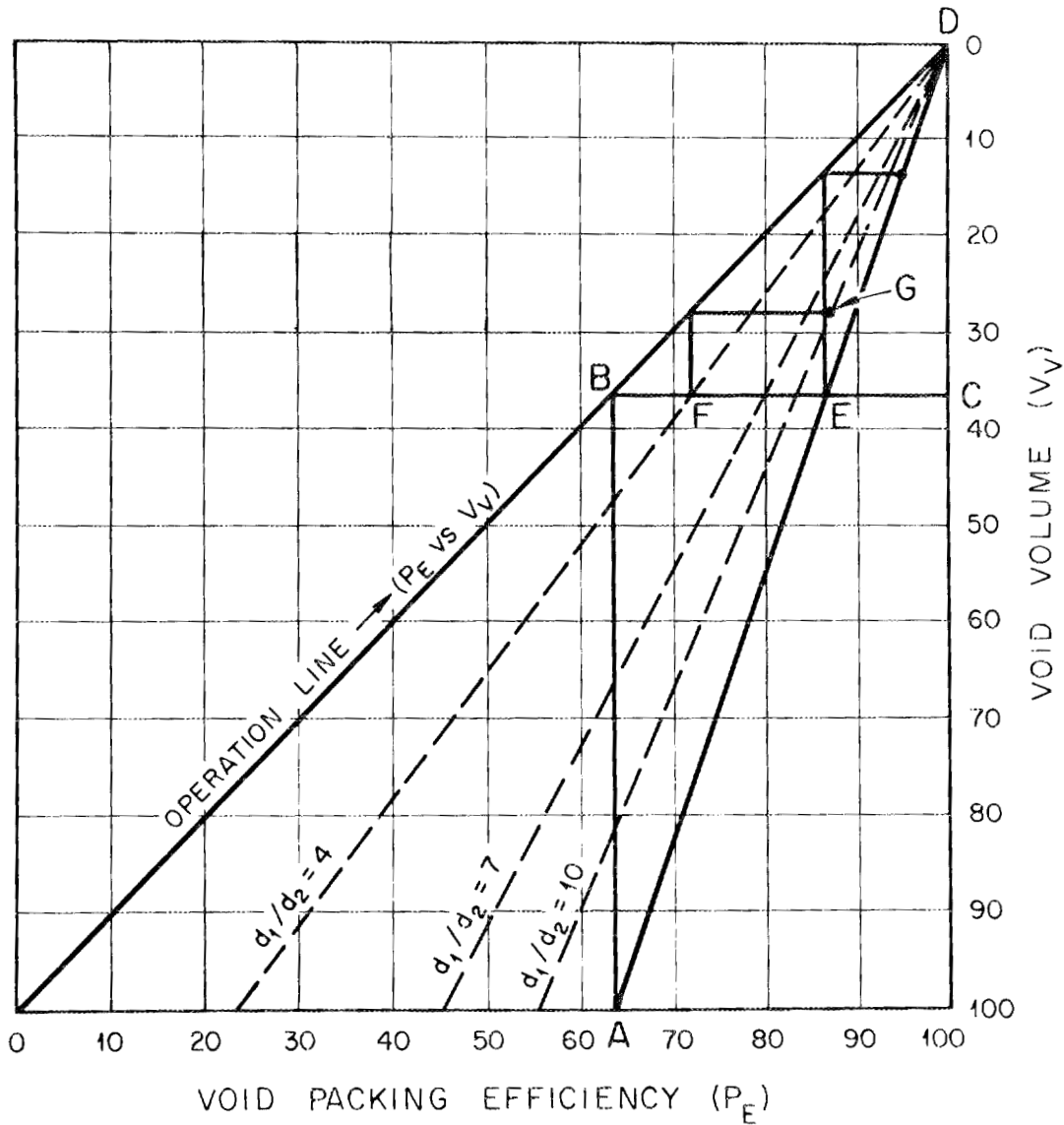


Fig. 3.5. Analysis of Sphere-Pac beds.

reasonable. Although the conditions affecting the coarse bed loading will influence the overall loading procedure, we felt that the infiltration of the fine fraction would be the time-controlling factor in the Sphere-Pac process, so we studied the factors that affect it. During initial infiltrations of fine microspheres with a size range of 25 to 44 μm , addition of all of the fines to the screen funnel at once caused nonreproducible packing and loading times. When loaded in this manner

the small microspheres bridge, preventing penetration into all the voids. The bridging effect was minimized by loading the fine fraction in 2- to 4-g increments.

The influence of tube diameter and bed height upon the fine fraction loading time was studied. Four pins with diameters ranging from 0.186 to 0.370 in. were loaded to three different bed heights. The rate was normalized by dividing by the bed volume to account for the difference in tube sizes. Figure 3.7 shows that

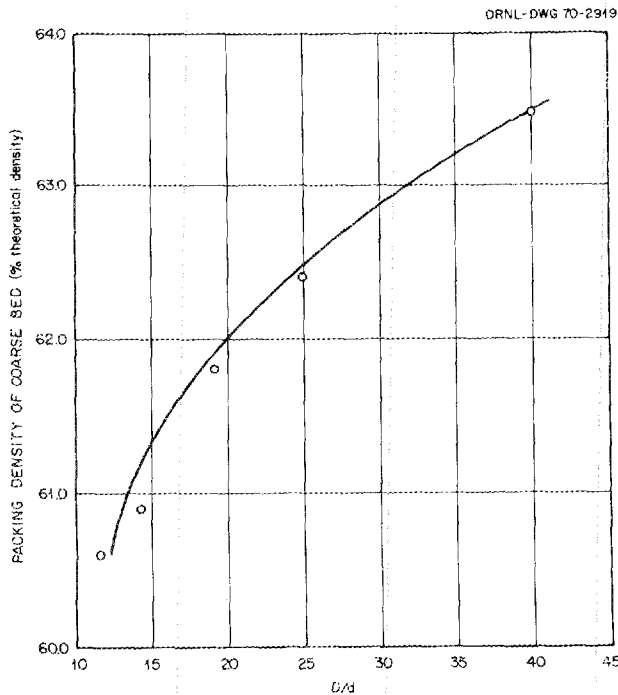


Fig. 3.6. Influence of ratio of fuel pin diameter to average sphere diameter (D/d) on the packing density of the coarse bed.

the rate of fill decreased as the fuel length increased. However, the slope decreased as the bed length continued to increase. Therefore, there is no loading rate penalty for increasing the tube length beyond about 16 in. No appreciable effect of bed diameter was seen. The loading rates of short columns were more difficult to reproduce, probably because of the influence of stacking fault variations in short columns.

A lightweight follower rod on top of the fine-particle bed prevented the expansion of the coarse-particle bed during infiltration and increased the packing density. For fabrication involving plutonia, where low contamination of the upper part of the tube is desirable, we have used a funnel with a screen in the bottom, as suggested by Ayre and Soppet,³ to hold down the coarse bed during the infiltration of the fine fraction.

We did not attempt to optimize all the variables in the Sphere-Pac process. Densities of 82 to 84% are readily attained with two size fractions of spheres, and this is approximately the density range required for high-burnup LMFBR fuel, which was our main concern.

These studies of binary packing generally verified the results of earlier workers,^{2,3} provided practical evidence of the simplicity and reproducibility of the binary Sphere-Pac beds, and yielded samples at around 85% volume packing density for characterization and irradiation testing.

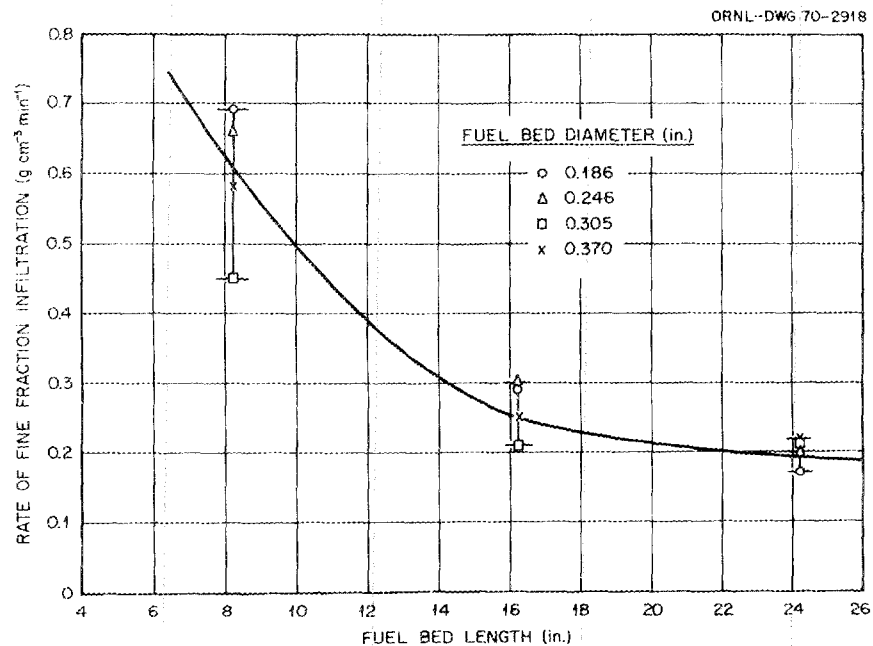


Fig. 3.7. Effect of fuel bed length on rate of infiltration of the fine fraction.

We also investigated the formation of Sphere-Pac fuel beds in the higher density range (88% and higher), using more than two sizes of spheres. With the currently available sol-gel products, the use of three sizes of particles and sequential infiltration steps appears impractical, because the ratio of tube diameter to the diameter of the large size fraction and the subsequent size fraction ratios for each fraction must be about 10 for optimal packing in the beds of spheres. For the practical minimum size of about 20 μm , the large microspheres would have to be 2000 μm in diameter, which is about four times our current maximum size.

We examined the effectiveness of blending two sizes of large spheres to form the initial poured bed before infiltration. The blending studies were carried out by placing about 60 g of coarse and medium spheres in a 3.5-cm-diam 120-cm³ bottle, rolling the bottle at 275 rpm for times up to 5 min, pouring the blended spheres into a 1.07-cm-ID graduated tube, and packing the unrestrained bed by vibrating for from 1 to 120 min. Blending was complete after about 1 min, and the poured bed was fully settled after about 1 min of vibration on a Syntron vibrator. The conditions of vibration were 60 Hz with about 7g acceleration of the bed.

The process development work has shown the Sphere-Pac process to be a viable technique for bulk oxide fuel fabrication to obtain fuel loadings occupying at least 80% of the volume. The use of blended beds to raise the fuel column to the 90%-dense range is an attractive approach, since it would eliminate the need for more than one infiltration step and be quicker and easier to control than a double infiltration approach.

In fabricating Sphere-Pac fuel pins for irradiation tests, we found that the smear density of the pin was a linear function of the coarse bed density, which varied as much as 5% between pins. We conducted a statistically designed experiment to determine the source and magnitude of the variation in coarse bed densities. The experiment covered a coarse bed density range from 57.6 to 61.3% of theoretical. An analysis of variance on the data led to the following conclusions:

1. We were more than 99% sure that there was a variation between batches of microspheres.
2. There was not sufficient evidence to indicate a difference between operators nor between two samples from a particular batch.
3. The standard deviation describing a single operator's ability to reproduce his work with the same sample of microspheres was 0.40%.
4. The feed rate and the time and amplitude of vibration had no significant effect on the density of the coarse bed.

We believe that most of the observed variation in coarse bed densities was caused by differences in the densities of the microspheres in different batches. This experiment showed that the density of the coarse bed from a given batch of microspheres can be reproduced within 1% if the loading conditions are properly controlled.

Since the density of the microspheres has the greatest effect on the density of the coarse bed and thus on the final smear density, we conclude that altering the density of the microspheres is the most practical way of controlling the density of Sphere-Pac fuel pins. When we loaded 13 Sphere-Pac pins for the EBR-II series II irradiation experiment, we attempted to vary the smear density from 80 to 85% of theoretical. However, since all the pins were loaded with microspheres with similar densities, all 13 fuel pins had smear densities between 81.6 and 83.8% of theoretical.⁴

3.1.2 Sphere-Pac Fabrication of Fuel Rods

We have fabricated about 60 plutonium-bearing fuel rods by the Sphere-Pac process. They consist of fuel columns up to 13½ in. long in 0.250-in.-OD × 0.015-in.-wall stainless steel or 0.5-in.-OD × 0.035-in.-wall Zircaloy-2 tubes. Most of these rods have been irradiated in the ETR, the ORR, and the EBR-II.

The principal items of equipment used to fabricate these rods were a Syntron vibratory feeder tilted at a 45° angle to provide lateral and axial vibration and a C-clamp modified to hold the tube and funnel, as shown in Fig. 3.8. These were housed in a glove box along with the equipment for welding the fuel pin end plugs under a helium atmosphere.

The cladding tube — with bottom end plug and thoria insulator in place and protected by a plastic bag — was put into the loading box, the large microspheres were poured into the tube, the screen-end funnel was inserted, and the tube was clamped into the vibrator fixture. The tube was vibrated for about 20 sec to settle the large fraction before the fine fraction was introduced through the funnel. The follower rod was then inserted, and the assembly was vibrated for 2 min. The follower rod and funnel were replaced with the top thoria spacer, and a piece of outgassed Fiberfrax was inserted to prevent fuel movement during subsequent

4. F. G. Kitts, R. B. Fitts, and A. R. Olsen. "Sol-Gel Urania-Plutonia Microsphere Preparation and Fabrication into Fuel Rods," pp. 195–210 in *Intern. Symp. Plutonium Fuels, Technol.*, Scottsdale, Ariz., 1967, *Nucl. Met.* **13**, ed. by K. E. Horton, R. E. Macherey, and R. J. Allio, American Institute of Mining, Metallurgical, and Petroleum Engineers, New York, 1968.

handling. The assembly was transferred to the welding box, where the top end plug was TIG welded in place.

The completed rods were inspected, and the density variations were measured by a gamma-scanning tech-

nique, which detects variations of $\pm 1\%$ of the average density. The results of these test rod loadings in Table 3.1 show that, for the variety of fuels used and the different microsphere densities, the fuel column heights, densities, and density variations are quite consistent.

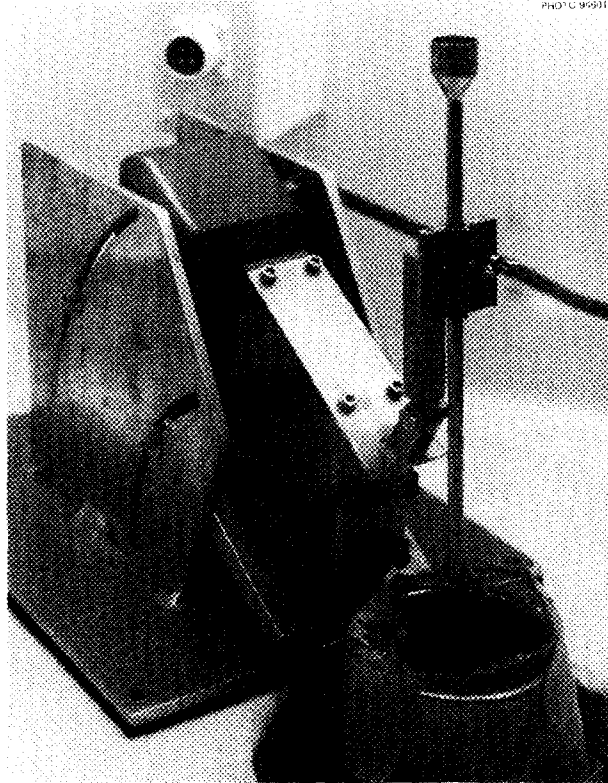


Fig. 3.8. Sphere-Pac loading apparatus.

3.1.3 U-Fines Sphere-Pac Process

U-Fines is a form of Sphere-Pac loading in which all the plutonium is contained in the coarse microspheres; the fine fraction consists of pure UO_2 . To illustrate the advantage of this process, a typical fuel pin design is shown in Fig. 3.9. As shown, the pin consists of a fueled core with upper and lower blanket regions and a long plenum. Any process for loading these long tubes will have a number of difficulties. Adjustment of the core lengths requires the use of shim pellets in pellet-loaded pins or very careful control of quantity of the fine fraction in the conventional Sphere-Pac process. Damage to the interior surface of the cladding by sliding into it close-fitting pellets and screen funnels or seating pins that may be up to 8 ft long is certainly possible, and great care must be taken during these operations. Weld zone contamination resulting from these operations will be a major problem. The U-Fines process is compared with the conventional Sphere-Pac process in Fig. 3.10. In the conventional Sphere-Pac process, use of pellets in the blanket regions would require a means to ensure that the plutonium fine fraction would not sift down into the blanket region.

Table 3.1. Sphere-Pac fuel rods

| Irradiation test | Rod | Fuel Material | Density | | Fuel column height ^c (in.) |
|---------------------|----------|---|---|-----------------------------------|---------------------------------------|
| | | | Fuel smear (% theoretical oxide density) ^a | Variation (% \pm) ^b | |
| Process development | ETR IV-1 | $\text{Th}_{0.95}\text{Pu}_{0.05}\text{O}_2$ | 84.8 | 2 | 6.67 |
| | ETR IV-2 | | 84.7 | 1.5 | 6.70 |
| | ETR IV-3 | | 83.5 | 2 | 6.69 |
| | ETR IV-4 | | 84.0 | 1 | 6.74 |
| | ETR IV-5 | | 83.3 | 1 | 6.69 |
| | ETR IV-7 | | 83.3 | 1 | 6.73 |
| | 2 | | 84.0 | 2 | 3.15 |
| | 3 | | 83.8 | 1 | 3.16 |
| | 4 | | 84.5 | 1 | 3.13 |
| | 5 | | 83.9 | 1.5 | 3.15 |
| EBR-II series I | S-1-A | $\text{U}_{0.80}\text{Pu}_{0.20}\text{O}_2^d$ | 83.3 | 8.6 | 13.4 |
| | S-1-B | | 86.1 | 6.1 | 13.0 |
| | S-1-C | | 82.7 | 2.3 | 13.5 |
| | S-1-D | | 79.7 | 5.8 | 13.1 |
| | S-1-E | | 82.0 | 8.1 | 13.5 |

Table 3.1 (continued)

| Irradiation test | Rod | Fuel Material | Density | | Fuel column height ^c (in.) |
|------------------|--------|---|---|---|--|
| | | | Fuel smear (% theoretical oxide density) ^a | Variation (%, ±) ^b | |
| FBR-II series II | OS-1 | U _{0.80} Pu _{0.20} O ₂ ^d | 81.9 | | 13.3 |
| | OS-2 | | 82.4 | | 13.4 |
| | OS-3 | | 83.2 | | 13.3 |
| | OS-4 | | 81.6 | | 13.5 |
| | OS-5 | | 83.6 | | 13.5 |
| | OS-6 | | 83.1 | | 13.6 |
| | OS-7 | | 82.4 | | 13.5 |
| | OS-8 | | 81.7 | | 13.2 |
| | OS-9 | | 83.2 | | 13.4 |
| | OS-10 | | 82.8 | | 13.3 |
| | OS-11 | | 81.9 | | 13.6 |
| | OS-12 | | 83.1 | | 13.4 |
| | OS-13 | | 82.0 | | 13.3 |
| ETR 43-99 | 7 | U _{0.80} Pu _{0.20} O ₂ ^d | 76.0 ^e | | 3.1 |
| | 8 | | 75.8 ^e | | 3.1 |
| 43-100 | 9 | U _{0.80} Pu _{0.20} O ₂ ^d | 75.9 ^e | | 3.1 |
| | 10 | | 75.9 ^e | | 3.1 |
| 43-103 | 14 | UO _{2.02} ^f | 74.0 ^e | 1.0 | 3.1 |
| | 12 | | 73.0 ^e | 1.0 | 3.1 |
| | 13 | | 74.0 ^e | 1.5 | 3.1 |
| 43-112 | 41 | U _{0.85} Pu _{0.15} O _{1.97} ^g | 78.9 ^e | 1.3 | 3.0 |
| | 25 | | 81.2 | 1.6 | 3.0 |
| | 22 | | 80.3 | 1.5 | 3.1 |
| | 26 | | 73.8 ^e | 1.2 | 3.0 |
| 43-113 | 27 | U _{0.85} Pu _{0.15} O _{1.97} ^g | 82.1 | 1.3 | 3.0 |
| | 38 | | 80.1 | 1.1 | 3.0 |
| | 40 | | 79.9 | 1.2 | 3.0 |
| | 28 | | 73.2 ^e | 1.2 | 3.0 |
| 43-115 | 23 | U _{0.85} Pu _{0.15} O _{1.97} ^g | 80.3 | 1.5 | 3.1 |
| | 32 | | 81.5 | 1.5 | 3.0 |
| | 39 | | 80.8 | 2.5 | 3.0 |
| | 16 | | 74.6 ^e | 1.0 | 3.0 |
| 43-116 | 46 | U _{0.85} Pu _{0.15} O ₂ ^g | 76.2 ^h | +4 | 3.3 |
| | 51 | | 76.3 ^h | ±5 | 3.2 |
| | 49 | | 76.8 ^h | ±4 | 3.2 |
| | 50 | | 76.0 ^h | ±3 | 3.1 |
| | 43-120 | | 19-4-C | U _{0.83} Pu _{0.17} O _{1.98} ^g | 84.8 |
| 19-4-F | 84.6 | | 3.0 | | |
| 43-121 | 19-4-B | U _{0.83} Pu _{0.17} O _{1.99} ^g | 83.9 | | 3.0 |
| | 19-4-E | | 85.5 | | 3.0 |
| ORR SG-1 | SG-1T | U _{0.85} Pu _{0.15} O _{1.99} ^g | 81.0 | | 3.0 |
| | SG-1B | | 81.0 | | 3.0 |
| SG-2 | SG-2T | U _{0.80} Pu _{0.20} O _{1.99} ^g | 81.0 | | 3.0 |
| | SG-2B | | 82.0 | | 3.0 |
| SG-3 | A-3 | U _{0.80} Pu _{0.20} O _{1.98} ^g | 82.5 | | 3.1 |

^aCalculated from height, weight, and inside diameter.

^bDetermined by transmission gamma scan along rod.

^cETR IV group rods were 1/2 in. in diameter, all others, 1/4 in.

^d93%-enriched uranium.

^eLow density due to low-density microspheres.

^f20%-enriched uranium.

^gNormal uranium.

^hLow density due to incorrect operator technique.

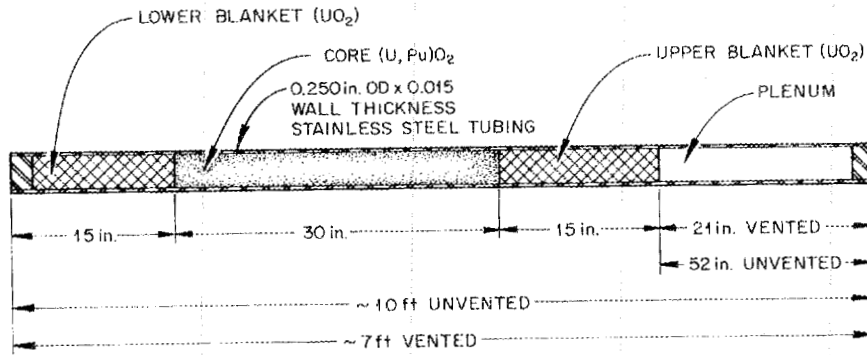


Fig. 3.9. Typical fuel pin design for 1000-MW(e) LMFBR.

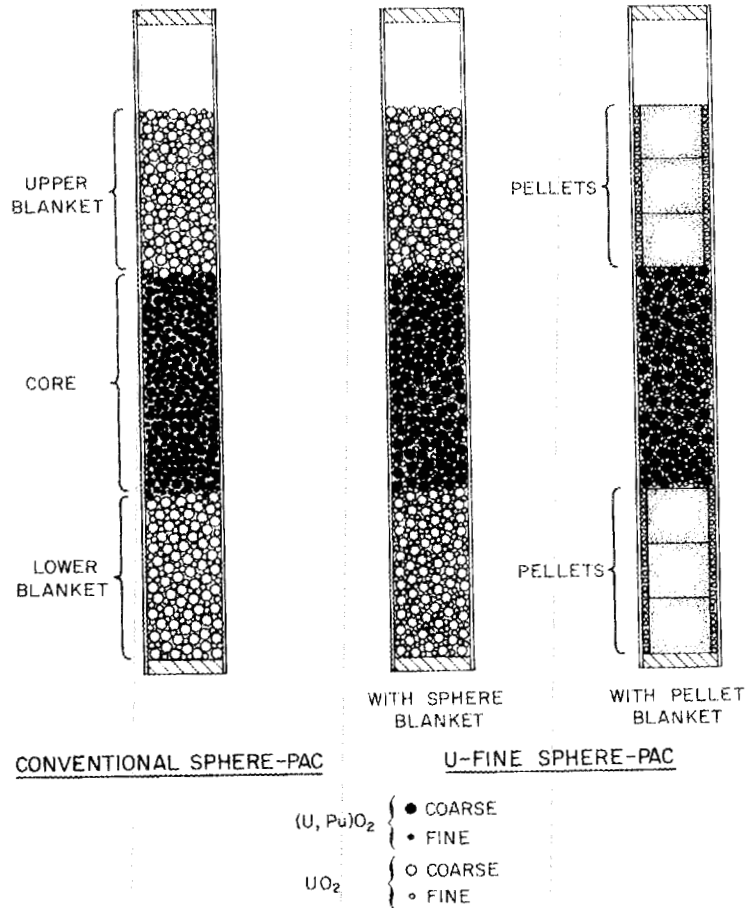


Fig. 3.10. Comparison of conventional and U-Fines Sphere-Pac processes.

The advantages of the U-Fines process are as follows:

1. Weld contamination is minimized. The loading of coarse microspheres is quite simple and should produce a minimum of contamination.

2. One infiltration is required for the core and the blankets. The UO_2 fine fraction can be loaded by infiltrating through the upper blanket to the core and lower blanket.

3. Loosely fitting UO_2 pellets can be used for the blanket regions. By infiltrating UO_2 fines around the blanket pellets, blankets denser than 90% of theoretical can be easily obtained. When the UO_2 fines are infiltrated around pellets, they center the pellets in the cladding; thus mechanical interaction during operation between the cladding and the pellets is minimized. Use of loosely fitting UO_2 pellets will also simplify loading problems and reduce blanket pellet fabrication cost by requiring lower tolerance of the pellets.

4. Controlled sharp cutoffs between the core and blanket regions are readily obtained. Coarse microspheres can easily be poured reproducibly to within 0.03 in. of the desired depth. In the conventional Sphere-Pac process, reproducible coincidence with the fine fraction is more difficult. Pellet loadings require the use of shim pellets.

5. The UO_2 can be made in a cold facility, thus simplifying control of the fine fraction. In the conventional Sphere-Pac process, the fine fraction is dusty and contributes heavily to plutonium losses.

For the U-Fines process, the plutonium content of the coarse microspheres for a (U-20% Pu) O_2 core is less than 27% of the heavy metal. Fuel pin ETR-43-126 fabricated for thermal reactor irradiation testing was

loaded by the U-Fines process. This pin has a 20-in.-long fuel column composed of $\text{Pu}_{0.27}\text{U}_{0.73}\text{O}_{1.97}$ coarse microspheres and $\text{UO}_{2.00}$ fine microspheres with a smear density 81% of theoretical.

3.2 METHODS FOR PELLETIZING FUEL

R. A. Bradley

The purpose of our pelletization studies was to develop techniques for fabricating fuel pellets of controlled density and stoichiometry from sol-gel-derived (U,Pu) O_2 . The irradiation experiments in which these pellets were to be used required pellet densities ranging from 83 to 95% of theoretical and oxygen-to-metal ratios of 1.94 to 1.98. The ratio of Pu/(U + Pu) and the uranium enrichment were varied to obtain the desired heat rating, so a different batch of sol-gel (U,Pu) O_2 powder was usually required for each irradiation experiment. The powder composition, pellet density, and oxygen-to-metal ratio of pellets fabricated for irradiation tests on this program are summarized in Table 3.2. Fabricating pellets with such a wide range of densities from many batches of powder with their inherent differences in sintering behavior required an understanding of the densification behavior of sol-gel mixed oxide.

In describing the techniques used to fabricate sol-gel (U,Pu) O_2 pellets, it will be helpful to classify them as low density (83–88%), intermediate density (88–92%), or high density (92–97%). In some cases, as in the pellets for the EBR-II series II irradiation test, it was necessary to make low-, intermediate-, and high-density pellets from a single blended batch of powder

Table 3.2. Summary of powder composition, pellet density, and oxygen-to-metal ratio of pellets fabricated for irradiation tests

| Irradiation test | Pu/(U + Pu) | Uranium enrichment (%) | Nominal pellet density (% of theoretical) | Oxygen-to-metal ratio | Configuration |
|-------------------------------|-------------|------------------------|---|-----------------------|--|
| TREAT | 0.20 | Normal | 84, 91 | 1.98 | Solid |
| ORR-SG-3 | 0.20 | Normal | 83 | 1.98 | Annular |
| GGA P-9 ^a | 0.12 | 9 | 89 | 1.98 | Annular, dished ends |
| GGA GB-10 ^a | 0.12 | 9 | 87 | 1.97 | Solid, dished ends |
| ETR 43-120, 121 | 0.20 | Normal | 84 | 1.98 | Solid |
| EBR-II series II | 0.20 | 93 | 84, 89, 95 | 1.94 1.98 | Solid |
| GGA F-1 (G1-G8) ^a | 0.15 | 93 | 91 | 1.98 | Annular, dished ends |
| GGA F-1 (G9-G13) ^a | 0.15 | 93 | 88 92 | 1.97 1.94 | Solid, dished ends Annular, dished ends |
| | | | | 1.97 | |

^aFabricated for the Gas-Cooled Fast Breeder Reactor Program.

to eliminate as many sources of variation as possible. We will describe here the techniques developed to achieve each of these ranges in density. The adjustment of the oxygen-to-metal ratio will be discussed in more detail in Sect. 3.4.

The (U,Pu)O₂ powder was prepared by the sol-gel process described in Sect. 2.3. All pellets were formed by uniaxially pressing calcined (U,Pu)O₂ powder without binder. It is necessary to calcine the sol-gel (U,Pu)O₂ powder to remove residual volatiles, reduce its surface area to about 10 m²/g, and to stabilize its oxygen-to-metal ratio. The conditions under which the powder was calcined and the sintering schedule were varied to achieve the required pellet densities.

3.2.1 Fabrication of Low-Density (83--88%) Pellets

The agglomerated nature of the (U,Pu)O₂ powder prepared by the sol-gel process is ideally suited for fabricating pellets with stable densities in the range 83 to 88% of theoretical. For use in making low-density

pellets, therefore, the powder was calcined in such a manner as to preserve the agglomerated sol-gel particles (aggregates). This was accomplished by calcining in a reducing atmosphere (Ar-4% H₂) at about 525°C for 4 hr. The atmosphere was changed to CO₂ during cooling to ambient temperature to stabilize the oxygen-to-metal ratio of the powder at about 2.1. When a pellet made from this powder is sintered, the porous sol-gel aggregates shrink individually, creating macroporosity between adjacent particles. The microstructure of the resulting pellet consists of very dense regions formed by the densification of individual aggregates, surrounded by an extremely porous matrix created as adjacent aggregates shrink away from one another. This type microstructure is shown in Fig. 3.11(a) and has been described elsewhere in more detail.⁵ Although most of the densification occurs within the individual aggregates, there is sufficient sintering between adjacent

5. W. J. Lackey and R. A. Bradley, "Microstructure of Sol-Gel-Derived (U,Pu)O₂ Microspheres and Pellets," *Nucl. Technol.* 14, 257-68 (1972).

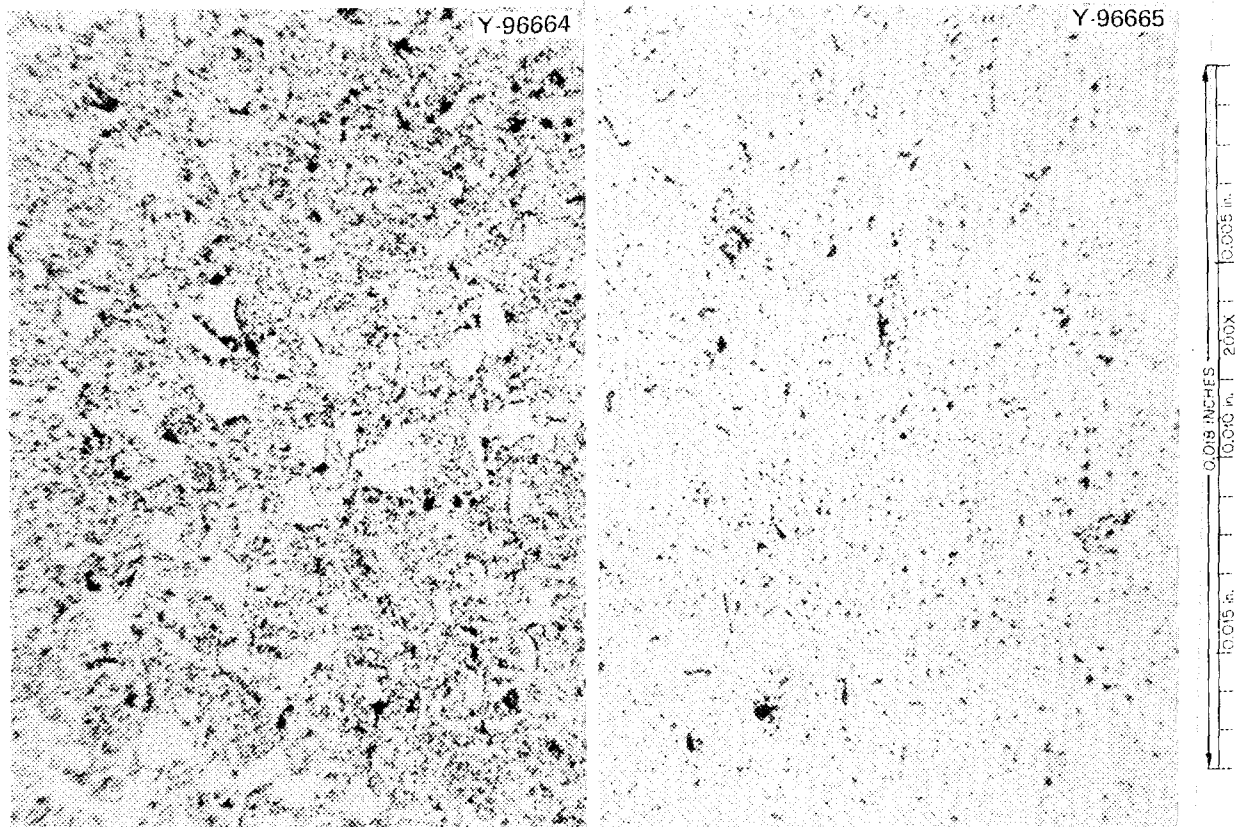


Fig. 3.11. Microstructure of sol-gel (U,Pu)O₂ pellets. As polished. (a) 84%-dense pellet made from powder calcined in Ar-4% H₂. (b) 91%-dense pellet made from powder given an oxidation-reduction treatment.

aggregates to yield a mechanically strong pellet. The macroporosity between the dense areas is sufficiently large to be thermally stable at 1550°C for 24 hr, even with pellet densities as low as 83% of theoretical. We believe that pellets with this type of microstructure would also have stable densities during irradiation.

3.2.2 Fabrication of Intermediate-Density (88–92%) Pellets

To render the sol-gel (U,Pu)O₂ powder suitable for fabricating pellets with densities greater than about 88% of theoretical, it is necessary to destroy the aggregates of crystallites that form the characteristic sol-gel particle. Bard et al.⁶ reported that ADU-derived UO₂ composed of aggregates of crystallites could be activated by an oxidation-reduction treatment. They found that activation resulted from the separation, but not the reduction in size, of primary crystallites by the transformation from the cubic UO₂ to the orthorhombic U₃O₈ phase. An oxidation-reduction treatment similar to that described by Fuhrman et al.⁷ for the activation of UO₂ was used to break up the aggregates of crystallites in the

sol-gel (U,Pu)O₂. The effect of such a treatment on the density of sol-gel (U,Pu)O₂ pellets is illustrated in Fig. 3.12. Two sub-batches of powder from the same parent batch were calcined two different ways. Powder calcined in Ar-4% H₂ to preserve the sol-gel aggregates yielded pellets with densities ranging from 80 to 88% of theoretical, depending on the forming pressure, which ranged from 25,000 to 50,000 psi. Pellets prepared from oxidized and reduced powder and sintered under identical conditions as for the lower-density pellets obtained from powder aggregates had a density about 91% of theoretical regardless of the forming pressure. The comparison of the microstructures of the 84- and 91%-dense pellets in Fig. 3.11 shows that the oxidation-reduction treatment was successful in destroying the sol-gel aggregates.

By controlling the oxidation-reduction treatment so that the sol-gel aggregates are only partially destroyed, one can make pellets of any density in the intermediate range. For example, the sol-gel (U,Pu)O₂ powder that was used to make pellets for the GGA F-1 experiment (G9-G13 in Table 3.2) was calcined by heating in air for 2 hr at 450°C, then in Ar-4% H₂ for 4 hr at 550°C, and then cooled to ambient in CO₂. As illustrated in Fig. 3.13, this powder yielded pellets with densities ranging from 84 to 91% of theoretical, depending on the forming pressure. Figure 3.14(a) shows the microstructure of the 88%-dense pellets fabricated for the F-1

6. R. J. Bard, J. P. Bertino, and D. L. Bunker, "Activating Uranium Dioxide," *Ind. Eng. Chem.* **53**, 1003-6 (1961).

7. N. Fuhrman, L. D. Hower, Jr., and R. B. Holden, "Low-Temperature Sintering of Uranium Dioxide," *J. Am. Ceram. Soc.* **46**, 114-21 (1963).

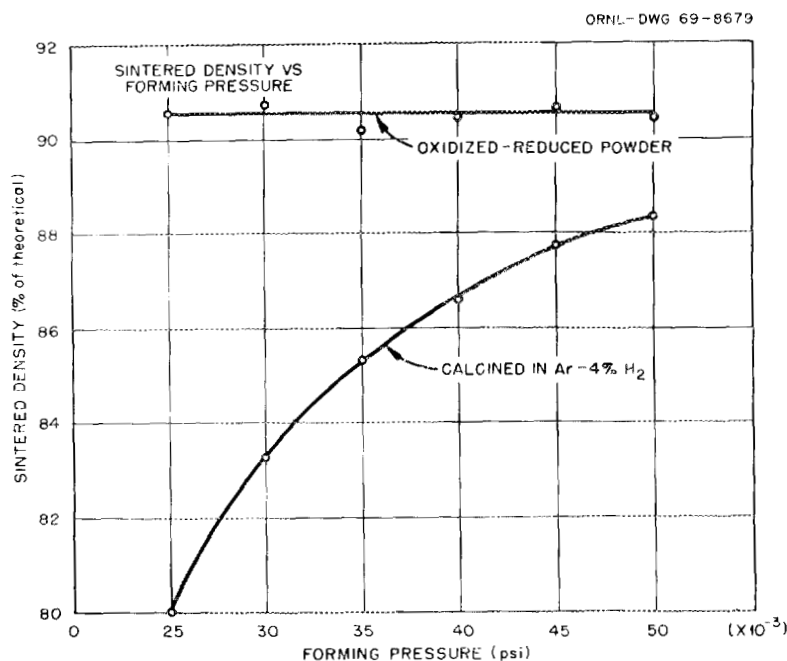


Fig. 3.12. Effect of calcining atmosphere on the forming pressure-density relationship of sol-gel (U,Pu)O₂.

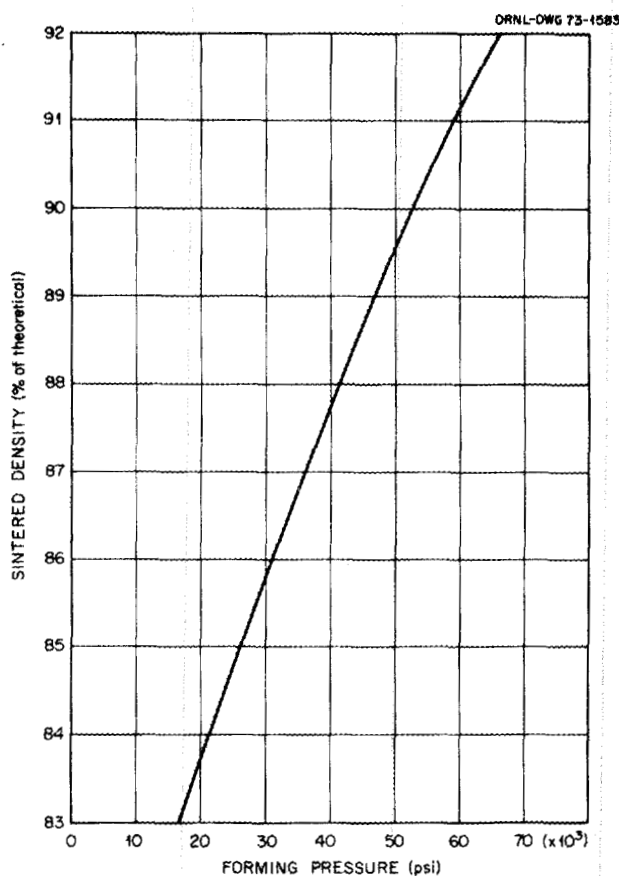


Fig. 3.13. Relationship between forming pressure and sintered density of pellets made from powder given an oxidation-reduction treatment to partially destroy sol-gel aggregates.

replacement pins. Some of the sol-gel aggregates are still visible, but most of them have been destroyed. Compare the microstructure with that of the 84%-dense pellet in Fig. 3.11(a) and the 91%-dense pellet in Fig. 3.11(b).

Another technique successfully employed in making intermediate-density pellets was to completely destroy the sol-gel aggregates by ball-milling the calcined powder and then to intentionally incorporate porosity in the pellet during sintering. Pellets made from powder that has been calcined and then ball-milled to completely destroy the sol-gel aggregates sinter similarly to pellets made from ADU-derived UO_2 or from coprecipitated $(\text{U,Pu})\text{O}_2$; that is, densities 93 to 97% of theoretical can be achieved by sintering in a reducing atmosphere such as $\text{Ar}-4\% \text{H}_2$ at 1550 to 1600°C. To make intermediate-density pellets from such a powder, some means is needed to retain porosity within the microstructure of the pellet. We accomplished this with ball-milled sol-gel $(\text{U,Pu})\text{O}_2$ by sintering in a slightly

oxidizing atmosphere. An oxidizing atmosphere promotes rapid grain growth, which causes pores to be trapped within grains. These trapped pores are more difficult to remove during sintering, so a lower-density pellet results. This is an application of "rate-controlled sintering" as described by Palmour and co-workers,⁸⁻¹⁰ although heretofore rate-controlled sintering has been used to increase density rather than to decrease it. Figure 3.14(b) shows the microstructure of an 89.5%-dense pellet made from ball-milled $(\text{U,Pu})\text{O}_2$ and sintered in an oxidizing atmosphere ($\text{Ar}-10\% \text{CO}_2$). Note that the pore size and distribution are much different from those of the pellet with nearly the same density shown in Fig. 3.14(a), in which a different technique was used to achieve the desired density.

3.2.3 Fabrication of High-Density (92--97%) Pellets

Pellets with densities in the range 92 to 97% of theoretical can be fabricated from calcined sol-gel $(\text{U,Pu})\text{O}_2$ by ball-milling the powder or by using some other method of comminution to completely destroy the sol-gel aggregates. When powder was to be used for high-density pellets, it was given an oxidation-reduction calcination to assist in breaking up the aggregates before ball-milling. Pellets were pressed at 20,000 to 60,000 psi and sintered in $\text{Ar}-4\% \text{H}_2$ at 1550°C for 4 to 8 hr. The density can be varied over the range 92 to 97% of theoretical by varying the forming pressure and the heating rate. The microstructure of a 97%-dense pellet fabricated from ball-milled sol-gel $(\text{U,Pu})\text{O}_2$ powder is shown in Fig. 3.15(c). This pellet was fabricated from the same powder as the 89.5%-dense pellet shown in Fig. 3.15(b).

The 89.5%-dense pellet has porosity trapped within the large grains as a result of sintering in an oxidizing atmosphere, whereas the 97%-dense pellet sintered in a reducing atmosphere has very small pores evident only on the grain boundaries.

8. H. Palmour III and D. R. Johnson, "Phenomenological Model for Rate-Controlled Sintering," pp. 779-91 in *Sintering and Related Phenomena*, ed. by G. C. Kuczynski, N. A. Hooton, and C. F. Gibbon, Gordon and Breach, New York, 1967.

9. H. Palmour III, R. A. Bradley, and D. R. Johnson, "A Reconsideration of Stress and Other Factors in the Kinetics of Densification," pp. 392-407 in *Kinetics of Reactions in Ionic Systems*, ed. by T. J. Gray and V. D. Frechetti, Plenum Press, New York, 1969.

10. M. L. Huckabee and H. Palmour III, "Rate Controlled Sintering of Fine-Grained Al_2O_3 ," *Am. Ceram. Soc. Bull.* 51, 574-76 (1972).

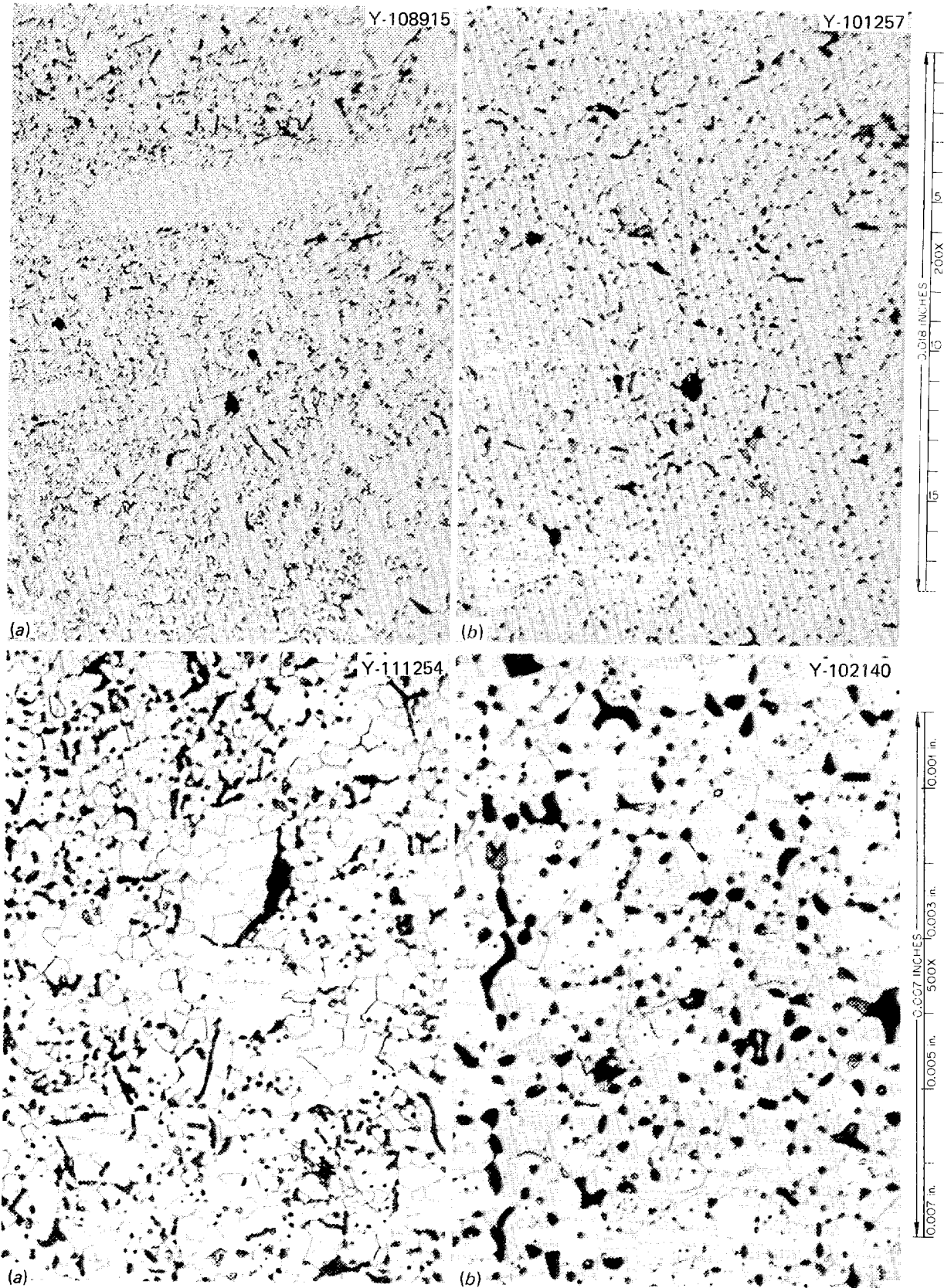


Fig. 3.14. Microstructures of intermediate-density pellets. Top, as polished, 200X. Bottom, etched, 500X. (a) Prepared from powder given an oxidation-reduction treatment to partially destroy sol-gel aggregates (88% dense). (b) Prepared from ball-milled powder and sintered in oxidizing atmosphere to trap pores during rapid densification and grain growth (89.5% dense).

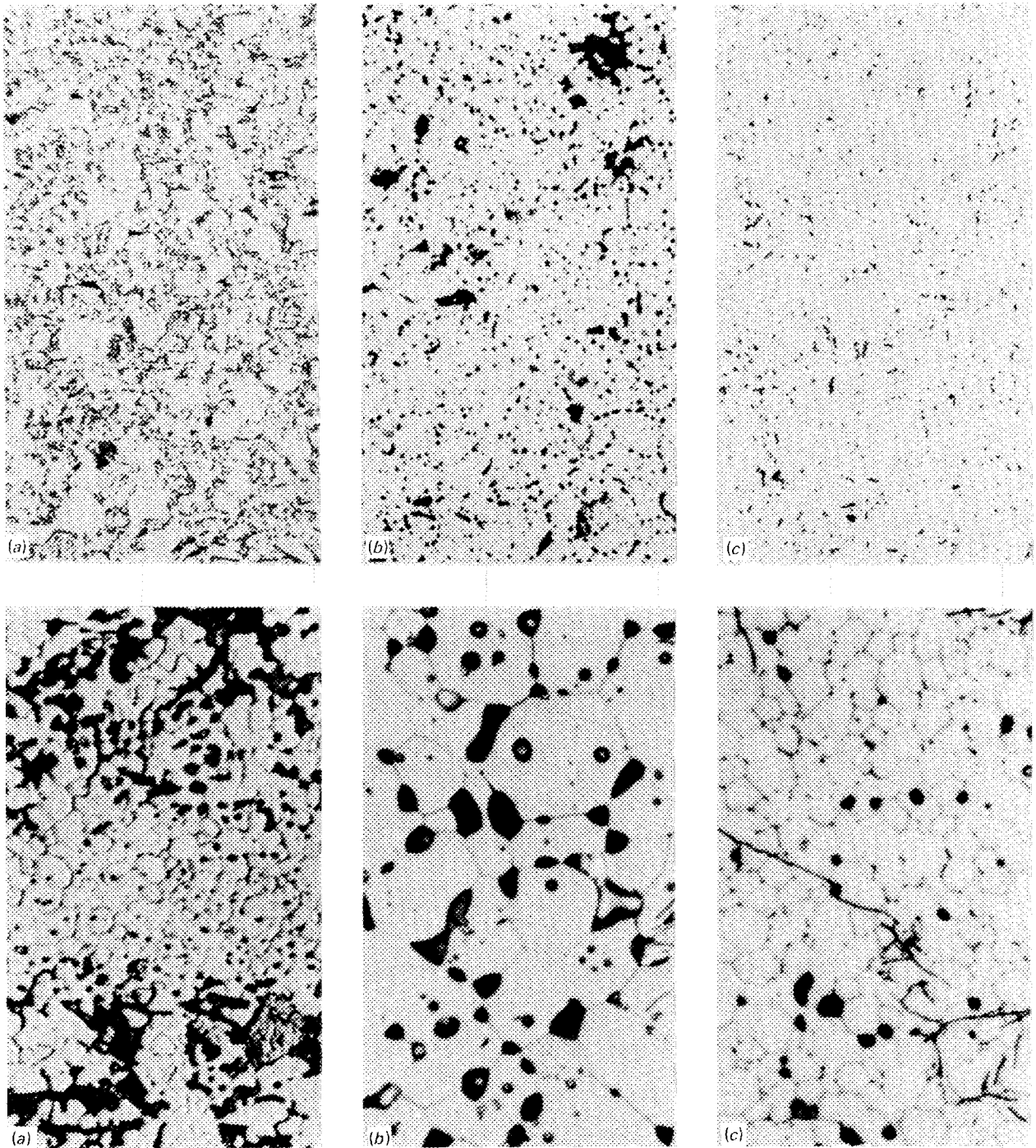


Fig. 3.15. Microstructure of sol-gel $(U,Pu)O_2$ pellets for EBR-II series II irradiation experiment. (a) 84% dense, calcined in argon and sintered in Ar-4% H_2 , 3- μm grain size. (b) 89.5% dense, calcined by oxidation-reduction and sintered in Ar-10% CO_2 , 16- μm grain size. (c) 97% dense, calcined by oxidation-reduction, sintered in Ar-4% H_2 , 4- μm grain size. Upper photos, 200 \times ; lower, 1000 \times . Reduced 12%.

3.2.4 Fabrication of Pellets for Irradiation Tests

The techniques described above were used to fabricate pellets for all the irradiation tests listed in Table 3.2. The following examples will show the specific conditions used to achieve the required pellet densities for two of these experiments.

The EBR-II series II irradiation test, described in Sect. 5.6, required pellets with densities 84, 89, 95% of

theoretical from a single blended batch of powder. The flowsheet in Fig. 3.16 shows the conditions used to calcine the powder and the sintering conditions used to fabricate pellets of each of these densities. In this case the method of "rate-controlled sintering" or "porosity entrapment" was used to produce the intermediate-density pellets. The microstructures of all these types of pellets are shown in Fig. 3.15.

The replacement fuel pins (G9-G13) for the GGA F-1 irradiation experiment required both 88- and 92%-dense

ORNL-DWG 71-4593R

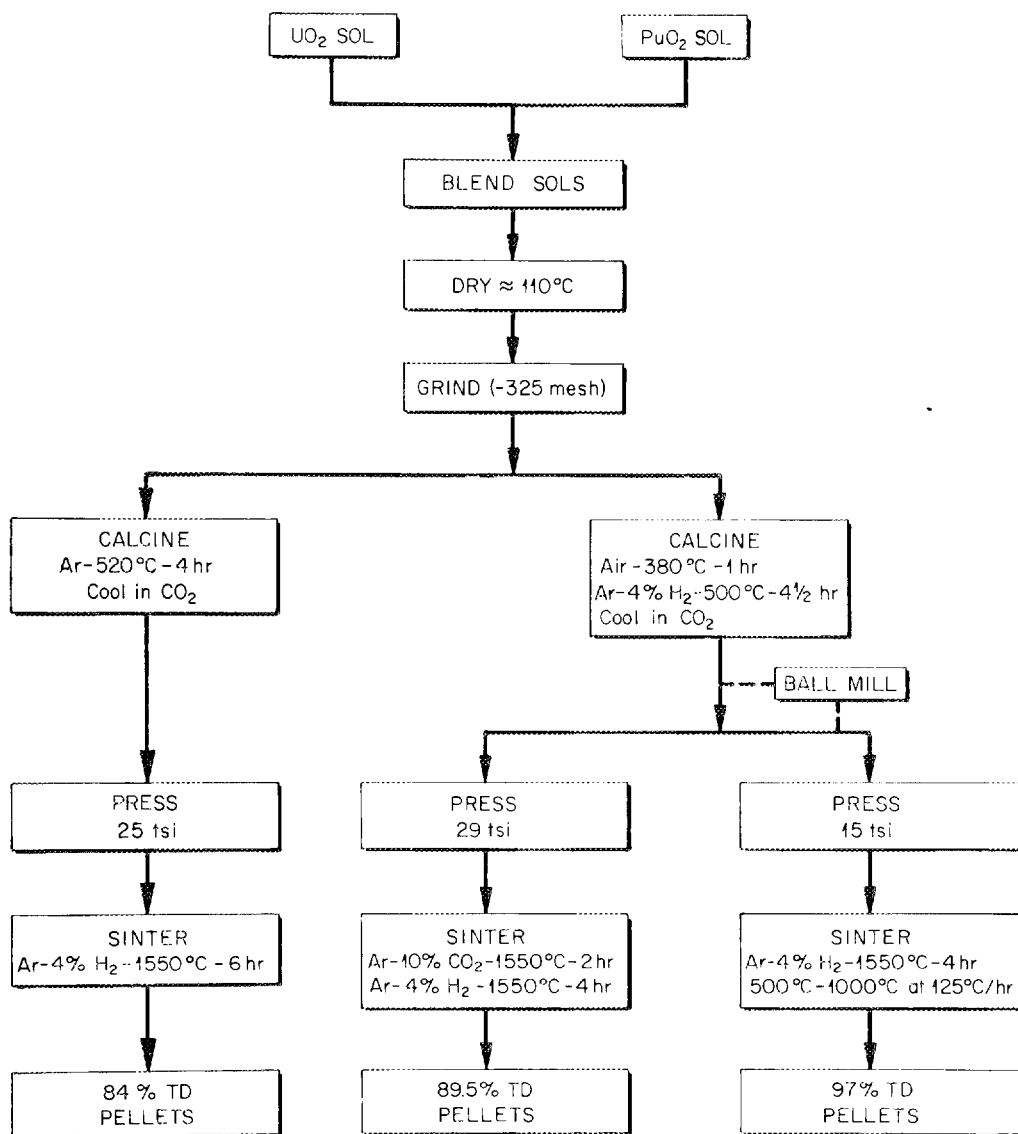


Fig. 3.16. Flowsheet for fabrication of pellets for EBR-II series II irradiation test.

pellets. The flowsheet shown in Fig. 3.17 describes the calcination and sintering conditions used to fabricate these pellets. In this case the intermediate-density pellets were fabricated from powder that had been given an oxidation-reduction treatment to partially

destroy the sol-gel aggregates. The microstructures of these pellets are shown in Fig. 3.18.

Powder calcination conditions and sintering schedules for pellets fabricated for other irradiation tests are summarized in Table 3.3.

ORNL-DWG 73-1584

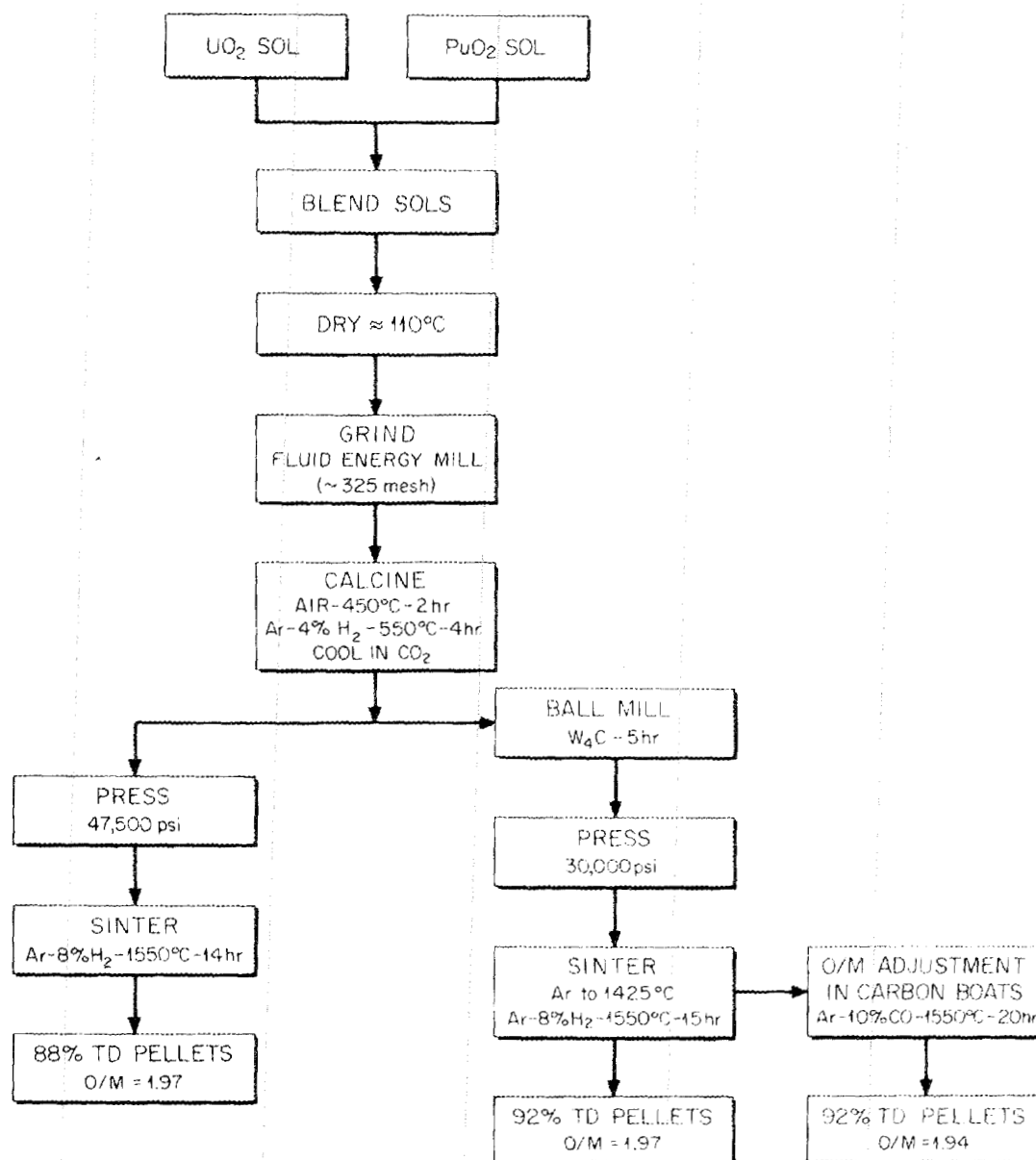


Fig. 3.17. Pellet fabrication for GGA F-1 experiment replacement pins.

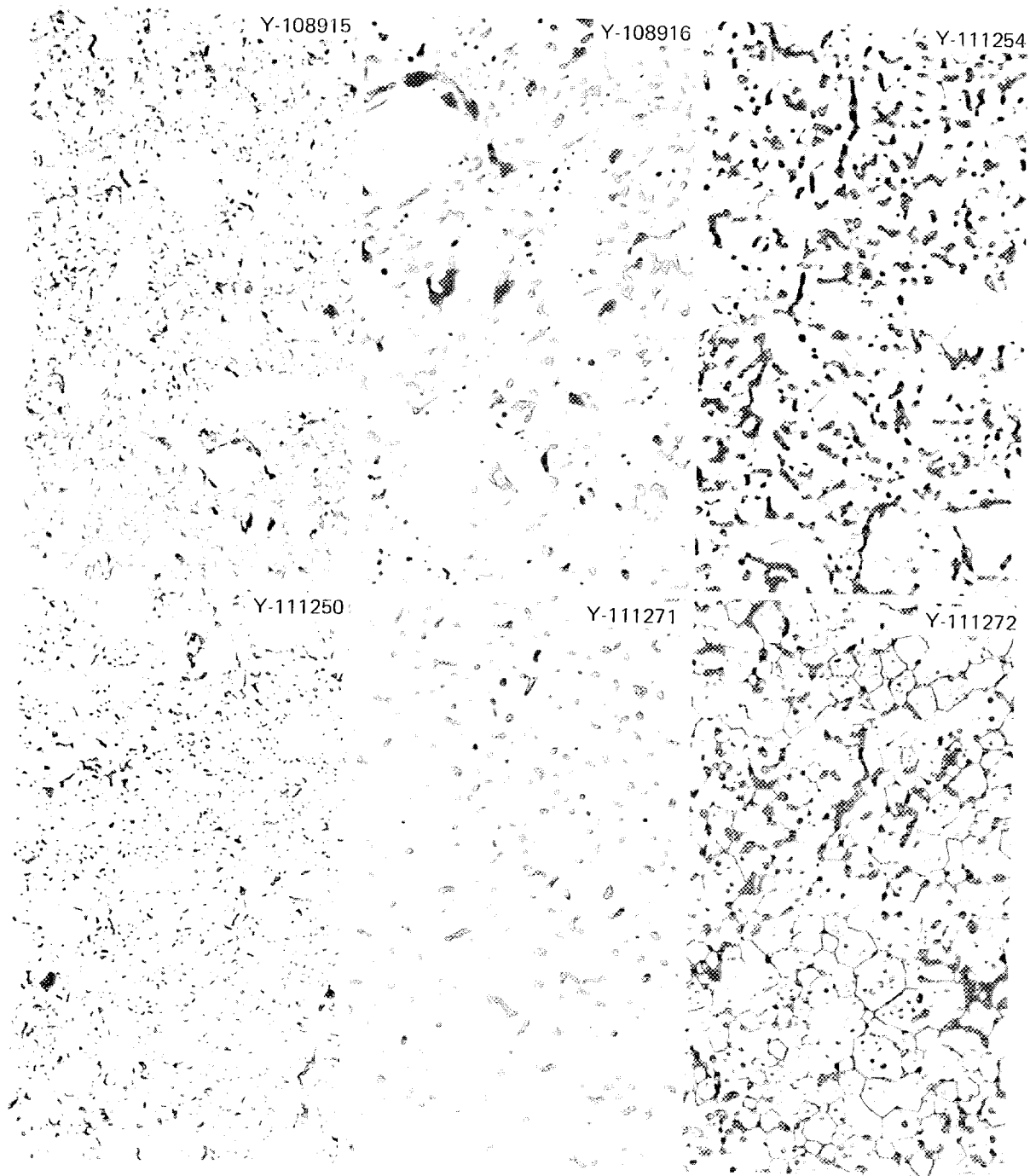


Fig. 3.18. Microstructure of pellets fabricated for replacement fuel pins for GGA F-1 irradiation test. Top: 88%-dense pellet fabricated from powder given an oxidation-reduction treatment to partially destroy sol-gel aggregate. Bottom: 92%-dense pellet fabricated from powder given an oxidation-reduction treatment and then ball-milled to completely destroy sol-gel aggregates. Left: as polished, 200X. Center: as polished, 500X. Right: etched, 500X.

Table 3.3. Summary of powder calcination conditions and pellet sintering conditions for pellets fabricated for irradiation tests

| Irradiation test | Powder calcination conditions ^a | | | | Ball milling time (hr) | Pellet forming pressure (psi) | Pellet sintering conditions ^b | | | | Average pellet density (% of theoretical) | Oxygen-to-metal ratio |
|------------------|--|----------------------|-------------------|--------------------|------------------------|-------------------------------|--|----------------------|----------------------|--------------------|---|-------------------------------|
| | Atmosphere | Heating rate (°C/hr) | Temp. (°C) | Time at temp. (hr) | | | Atmosphere | Heating rate (°C/hr) | Temp. (°C) | Time at temp. (hr) | | |
| TREAT | { Ar-4% H ₂ CO ₂ | 250 | 520 520 | { 4 1 } | 0 | 35,000 | Ar-4% H ₂ | 300 | 1450 | 10 | 84 | 1.99 |
| | { Air Ar-4% H ₂ CO ₂ | 300 | 520 520 520 | { 0 4 1 } | 0 | 50,000 | { Ar Ar-4% H ₂ | 300 | 1450 1450 | { 6 4 } | 93 | 1.98 |
| ORR-SG3 | Ar | 300 | 520 | 4 | 0 | 30,000 | Ar-4% H ₂ | 300 | 1450 | 10 | 83 | 1.99 |
| GGA P-9 | { Air Ar-4% H ₂ | 300 300 | 400 500 | { 0.5 4 } | 0 | 50,000 | { Ar Ar-4% H ₂ | 125 | 1550 1550 | { 2 2 } | 90 | 1.98 |
| GGA GB-10 | Ar-4% H ₂ | 300 | 540 | 4 | 0 | 25,000 | Ar-8% H ₂ | 300 | 1550 | 6 | 87.5 | 1.97 |
| ETR 43-120, 121 | Ar-4% H ₂ | 300 | 520 | 4 | 0 | 41,000 | Ar-4% H ₂ | 300 | 1450 | 10 | 84 | 1.99 |
| EBR-II series II | Ar | 300 | 520 | 4 | 0 | 50,000 | Ar-4% H ₂ | 300 | 1550 | 6 | 84 | 1.96 ^c |
| | { Air Ar-4% H ₂ | 300 300 | 380 500 | { 1 4.5 } | 117 | 30,000 | { Ar-4% H ₂ Ar-4% H ₂ Ar-4% H ₂ | 300 125 300 | 500 1000 1550 | { 0 0 4 } | 95 | 1.97 |
| | { Air Ar-4% H ₂ | 300 300 | 380 500 | { 1 4.5 } | 117 | 57,500 | { Ar-10% CO ₂ Ar Ar-4% H ₂ | 300 | 1550 1550 1550 | { 2 2 2 } | 89.5 | { 1.98 1.96 ^d } |
| GGA F-1 (G1-G8) | Ar-4% H ₂ | 300 | 500 | 5 | 104 | 30,000 | Ar-4% H ₂ | 300 | 1550 | 10 | 92 | 1.98 |
| GGA F-1 (G9-G13) | { Air Ar-4% H ₂ | 300 300 | 450 550 | { 2 4 } | 0 | 47,500 | Ar-8% H ₂ | 300 | 1550 | 14 | 88 | 1.97 |
| | { Air Ar-4% H ₂ | 300 300 | 450 550 | { 2 4 } | 5 | 30,000 | { Ar Ar-8% H ₂ | 300 300 | 1425 1550 | { 0 15 } | 92 | { 1.97 1.94 ^e } |

^aIn all cases the powder was cooled to ambient in CO₂ to stabilize its oxygen-to-metal ratio.

^bAfter being sintered the pellets were cooled from 850°C to ambient in argon to eliminate hydrogen retention.

^cPellets heat treated after sintering (1450°C for 4.5 hr in Ar-4% H₂ in presence of titanium getter) to reduce oxygen-to-metal ratio.

^dPellets heat treated after sintering (1400°C for 4.5 hr in Ar-4% H₂ in presence of titanium getter) to reduce oxygen-to-metal ratio.

^ePellets heat treated after sintering (1550°C for 20 hr in carbon boat in Ar-10% CO) to reduce oxygen-to-metal ratio.

3.3 PRELIMINARY EXTRUSION EVALUATION OF SOL-GEL MATERIALS

R. B. Fitts

The extrusion of ceramic bodies is common industrial practice, but little information is in the literature on extruding pure oxides.¹¹ The fact that extrusion is generally adapted to producing ceramic bodies with large length-to-diameter ratios led to investigations^{12,13} of standard ceramic extrusion techniques for producing oxide nuclear fuels and to recommendations that commercial production facilities be developed. These recommendations were not followed, probably because the apparent economic advantage did not offset the capital investment needed to replace existing equipment for large-scale pelletization. The recent rapid growth of the nuclear power industry and the coming need for processing recycle fuels mean that new facilities will be needed, and such new facilities could be designed to take advantage of the high production rates of extrusion if a reliable process were to be developed.

The sol-gel process developed at Oak Ridge National Laboratory produces high-purity oxides of various nuclear fuel materials.¹⁴⁻¹⁷ One product of this process can be a highly concentrated gel that has many characteristics of a natural clay and is therefore ideally suited to extrusion. We have developed a technique for extruding such a material¹⁸ into variously shaped ceramic bodies with controllable densities.^{19,20} This particular technique was pursued because of the prospect for economic advantage from applying sol-gel extrusion to fabricating small-diameter fast-reactor fuels.^{19,21}

The initial development work²⁰ showing the feasibility of sol-gel extrusion was carried out with sol-gel thorium and ThO_2 -8% UO_2 . Thorium-base materials were used because they were the best developed and understood sol-gel materials at that time, and the initial technique for production of the "sol-gel clay" was developed for that system. The sol-gel clay is formed through concentration of the sols of the desired oxide material by evaporation, precipitation, and filtration. The utilization of this material as the principal ingredient in the extrusions permits the formation of an essentially pure oxide ceramic.

The flowsheet in Fig. 3.19 illustrates the general process for forming ceramic bodies by sol-gel extrusion. The plain clay or clay mixed with powder may be extruded. The plain clay extrusions, when dried at room temperature and sintered at 1150°C in air, yield a

nearly theoretically dense ceramic body. Of more interest for nuclear fuel fabrication is the process in which grog — that is, crushed (–325 mesh) and fired powder — is mixed with the clay before extrusion. This powder may be either recycled scrap, as shown in the figure, or powders produced by the sol-gel process for this purpose. Bodies were obtained by this technique with good green densities and final densities in the range 70 to 98% of theoretical, controlled to $\pm 2\%$. The final density is a function of the amount of grog added to the clay before extrusion. An advantage of the process is that no other means of density control need be employed. A stable density was obtained by firing the ThO_2 1150°C for 1 hr in air, as subsequent firing of the extrusions at temperatures up to 2000°C causes no significant changes in density or structure.

The extension of the sol-gel extrusion process to the uranium and uranium-plutonium systems, which are the systems of interest for fast reactors, has only reached the preliminary stage. Greater problems are associated with the production of sol-gel clay in the uranium system than in the thorium system. When a thorium sol is heated to remove moisture, it goes from a very liquid state, through a jelly-like state, to a clay, and finally to a hydrated crystalline solid. The uranium sols tend to form

11. C. Hyde, "Vertical Extrusion of Nonclay Compositions," pp. 107-11 in *Ceramic Fabrication Processes*, ed. by W. D. Kingery, Wiley, New York, 1958.

12. W. E. Bailey, *UO₂ Fabrication by Extrusion*, CVNA-42 (February 1960).

13. *Final Report, Phase III, Extruded Ceramic Nuclear Fuel Development Programs*, ACNP-62550 (June 15, 1962).

14. O. C. Dean et al., "The Sol-Gel Process for Preparation of Thorium-Base Fuels," pp. 519-42 in *Proceedings of the Thorium Fuel Cycle Symposium, Gatlinburg, Tennessee, December 5-7, 1962*, TID-7650 (July 1963).

15. J. P. McBride, *Preparation of UO₂ Microspheres by a Sol-Gel Technique*, ORNL-3874 (February 1966).

16. J. P. McBride (compiler), *Laboratory Studies of Sol-Gel Processes at the Oak Ridge National Laboratory*, ORNL-TM-1980 (September 1967).

17. P. A. Haas, C. C. Haws, Jr., F. G. Kitts, and A. D. Ryon, *Engineering Development of Sol-Gel Processes at the Oak Ridge National Laboratory*, ORNL-TM-1978 (January 1968).

18. A. B. Meservey, J. D. Sease, and R. B. Fitts, *Method of Fabricating Ceramic Nuclear Fuel Product*, (to U.S. Atomic Energy Commission), U.S. Patent 3,356,776 (Dec. 5, 1967).

19. R. B. Fitts, J. D. Sease, and A. L. Lotts, "Preparation of Ceramic Nuclear Fuels by Sol-Gel Extrusion," *Chem. Eng. Progr. Symp. Ser.* **80**, 28-33 (1967).

20. R. B. Fitts, H. G. Moore, A. R. Olsen, and J. D. Sease, *Sol-Gel Thorium Extrusion*, ORNL-4311 (September 1968).

21. T. N. Washburn, A. L. Lotts, and F. E. Harrington, *Comparative Evaluation of Sol-Gel Fuel Fabrication Costs*, ORNL-TM-1979 (September 1967).

ORNL-DWG 67-5317

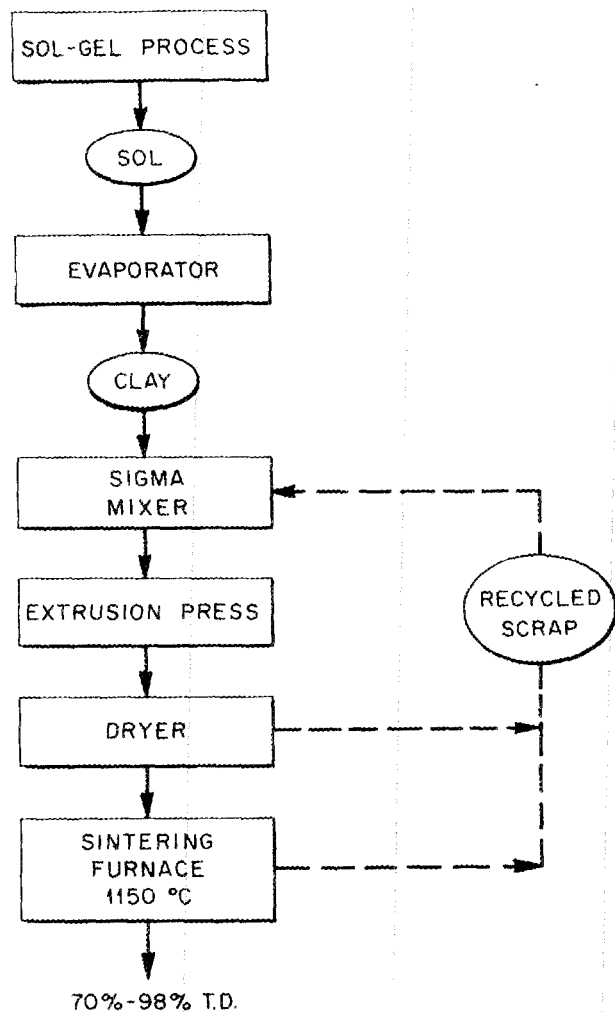


Fig. 3.19. Flowsheet for sol-gel extrusion process.

these various stages at higher water content, and crystalline pieces begin to precipitate while the urania is still too wet for extrusion. Thus, the urania-base materials require modification of the techniques suitable for thorium clay formation. Work with the urania system is also complicated by the possible necessity for use of an inert atmosphere to prevent the oxidation of U(IV) to U(VI).

Our initial work²² on sol-gel clay preparation in the urania system showed that, unlike nitrate-prepared thorium sols, nitrate-prepared urania sols of low molarity (0.7 M) could not be concentrated by evaporation of

liquid to the required 10 M without gelling. However, urania sols were concentrated satisfactorily by freezing with liquid nitrogen and subliming the moisture. The fine sol-gel powders (-325 mesh) added to the clays to adjust properties can also be prepared by completely freeze-drying the sols. During these initial studies we also made clays from chloride-prepared sols, which do not gel during concentration as readily as do nitrate-prepared sols.

Urania extrusions have been prepared in exploratory studies²² using both nitrate- and chloride-prepared materials. Using a 30 wt % powder addition, we obtained bulk densities of 68 and 72% of theoretical on extrusions from the nitrate- and chloride-prepared clays, respectively, after firing for 1 hr at 1600°C in hydrogen. Presintering the chloride-prepared extrusions in steam-Ar-4% H₂ at 1000°C for 1 hr reduced the chloride content to less than 1 ppm.

Despite initial experimental difficulties, experience with thorium-base sol-gel extrusions, the knowledge of sol technology in other systems, and our initial extrusion work in the uranium system^{22,23} itself indicate that this process can be made applicable to the fabrication of urania-base reactor fuels. The results of our investigation show that the sol-gel extrusion technique offers a combination of advantages available in none of the other existing techniques for ceramic nuclear fuel production. These include: (1) elimination of organic binders and plasticizers with their associated impurities, (2) potentially low sintering temperatures, (3) possible reduction or elimination of grinding for diameter control, (4) reduction in handling and inspection costs due to increased length of the pieces formed in the extrusion process, and (5) assurance of angstrom-scale fuel homogeneity.

3.4 ADJUSTMENT OF OXYGEN-TO-METAL RATIO

T. B. Lindemer²⁴ R. A. Bradley

Uranium-plutonium dioxide fuel for LMFBR applications is required to have an oxygen-to-metal ratio near 1.97. For some of our irradiation experiments ratios as low as 1.94 are required. It is not always easy to achieve these oxygen-to-metal ratios; therefore, we

22. J. G. Stradley, R. L. Hamner, and J. M. Robbins, *Metals and Ceramics Div. Annu. Progr. Rep. June 30, 1967*, ORNL-4170, p. 125.

23. C. R. Reese and R. A. Bradley, *Fuels and Materials Development Program Quart. Progr. Rep. June 30, 1968*, ORNL-4330, pp. 10-11.

24. Now in Reactor Chemistry Division.

investigated the reduction of mixed oxide to the hypostoichiometric state.

We theoretically analyzed the reduction of $(U,Pu)O_2$ in flowing hydrogen. The reduction process is kinetically controlled and limited by the rate at which water vapor can be removed from the furnace. Using Markin's²⁵ thermodynamic data, the following equation was developed to predict the time required for reduction to any oxygen-to-metal ratio.

$$t = \frac{11.208Nx}{f} \int_4^{V_{Pu}} H dV_{Pu},$$

where

t = time required to reduce $U_{1-x}Pu_xO_2$ to desired V_{Pu} ,

V_{Pu} = valence of plutonium,

N = moles of mixed oxide,

f = flow rate of H_2 in liters per unit time at STP, and

H = the average H_2/H_2O during an increment of reduction.

The integral $\int_4^{V_{Pu}} H dV_{Pu}$ has been evaluated as a function of V_{Pu} and reduction temperature and is given in Fig. 3.20. The details of the kinetic analysis are described elsewhere.^{26,27} Using the knowledge gained in this study we have consistently obtained the oxygen-to-metal ratio required for various irradiation experiments.

We also investigated the reduction of $(U,Pu)O_2$ by the C-CO-CO₂ system. In this system it is important that the carbon be in close proximity to the mixed oxides; for example, less than 0.025 in. The reduction is then controlled by the rate of the reaction $C + CO_2 \rightleftharpoons 2 CO$.

The kinetic analysis and experimental data show that reduction by the C-CO-CO₂ system is much quicker than by flowing hydrogen.^{26,27} Also, much lower oxygen-to-metal ratios can be achieved than is practical by hydrogen reduction. For example, when we fabricated the pellets for the GGA F-1 replacement pin (see Table 3.3), we achieved an oxygen-to-metal ratio of

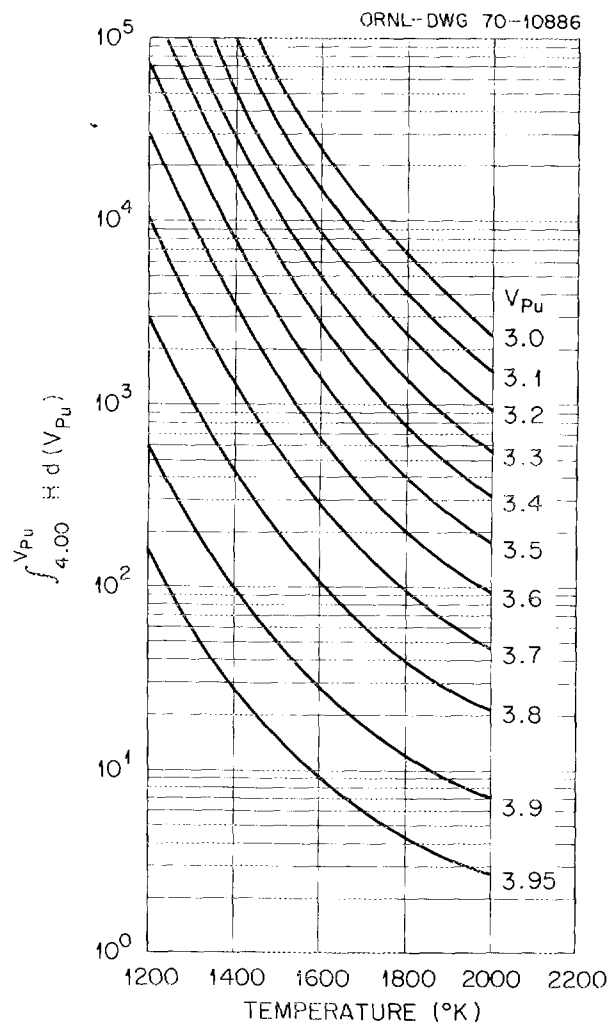


Fig. 3.20. Value of integral as a function of temperature for constant valence of $(U,Pu)O_{2-y}$

1.94 with no difficulty by using the C-CO-CO₂ system. On the other hand, the lowest oxygen-to-metal ratio we were able to achieve by hydrogen reduction was 1.96, even in the presence of titanium getter.

3.5 PROCEDURES FOR REDUCTION OF SORBED GASES

W. H. Pechin R. A. Bradley

Specifications for nuclear fuels normally include an upper limit for the volume of gas evolved by the fuel at elevated temperature. The current specification for $(U,Pu)O_2$ fuel for use in the Fast Test Reactor allows not more than 0.09 cm³ of gas (STP) per gram of fuel;

25. T. L. Markin, *Chem. Eng. Progr. Symp. Ser.* **80**, 43 (1967).

26. T. B. Lindemer and R. A. Bradley, *Kinetic Models for the Synthesis of $(U,Pu)O_{2-y}$ by Hydrogen-Reduction and Carbothermic Techniques*, ORNL-TM-3358 (April 1971).

27. T. B. Lindemer and R. A. Bradley, "Kinetic Models for the Synthesis of $(U,Pu)O_{2-y}$ by Hydrogen-Reduction and Carbothermic Techniques," *J. Nucl. Mater.* **41**, 293-302 (1971).

however, the upper limit was $0.05 \text{ cm}^3/\text{g}$ at the time most of our fuel was fabricated.²⁸ Using a vacuum-extraction gas release technique²⁹ at 1650°C on hypostoichiometric mixed oxide fuel, we have often observed values in excess of 20 times the specified limit. The excessive gas content was observed in both low-density pellets and high-density microspheres and depended on the gas in which the fuel was cooled after reduction, the surface-to-volume ratio, and the oxygen-to-metal ratio.

Hypostoichiometric fuel cooled in Ar-4% H_2 released relatively large quantities of hydrogen on reheating. This evolution began at about 380°C and peaked at about 450°C , then gradually decreased. When similar fuel was cooled in argon from 800°C , it retained considerably less hydrogen. The average gas release of approximately 25 batches of $(\text{U,Pu})\text{O}_{2-x}$ microspheres and pellets fabricated and cooled in Ar-4% H_2 was $0.32 \pm 0.10 \text{ cm}^3/\text{g}$.³⁰ After changing the process so that the fuel was cooled from 850°C in argon, the average gas release of more than 30 batches of similar microspheres and pellets was 0.043 ± 0.010 .³⁰ The gas released from fuel cooled in Ar-4% H_2 contained 95 to 99% H_2 , but that cooled in argon had 60 to 70% H_2 , with the balance $\text{N}_2 + \text{CO}$; thus, cooling in argon reduced the hydrogen content by about 97%, although the content of the other gases was probably unchanged.

Gas release by $(\text{U,Pu})\text{O}_2$ is quite different from that by UO_2 , which is routinely sintered in dry hydrogen without difficulty. The mechanism is probably associated with the plutonium and the hypostoichiometric composition of the fuel. Metallic plutonium combines with hydrogen to form PuH_2 , which has the same CaF_2 -type crystal structure³¹ as PuO_2 , UO_2 , and $(\text{U,Pu})\text{O}_2$. The lattice parameter of PuH_2 differs from that of PuO_2 by only 0.7%, indicating that hydrogen in association with plutonium fills about the same space as oxygen. The reduction of $(\text{U,Pu})\text{O}_2$ to hypostoichiometric oxygen content has been shown to proceed by the formation of oxygen vacancies.³² We believe that when this fuel is cooled in the presence of hydrogen,

28. J. E. Rein et al., *LMFBR/FFTF Fuel Development Analytical Chemistry Program (Phase II)*, LA-4407 (March 1970).

29. W. H. Pechin, *Fuels and Materials Development Program Quart. Progr. Rep. June 30, 1969*, ORNL-4440, p. 12.

30. 95% confidence interval on the mean.

31. O. J. Wick, *The Plutonium Handbook, a Guide to the Technology, Vol. I*, Gordon and Breach, New York, 1967, p. 208.

32. L. E. J. Roberts and T. L. Markin, "Thermodynamics of Non Stoichiometric Oxide Systems," *Proc. Brit. Ceram. Soc.* **6**, 201 (June 1967).

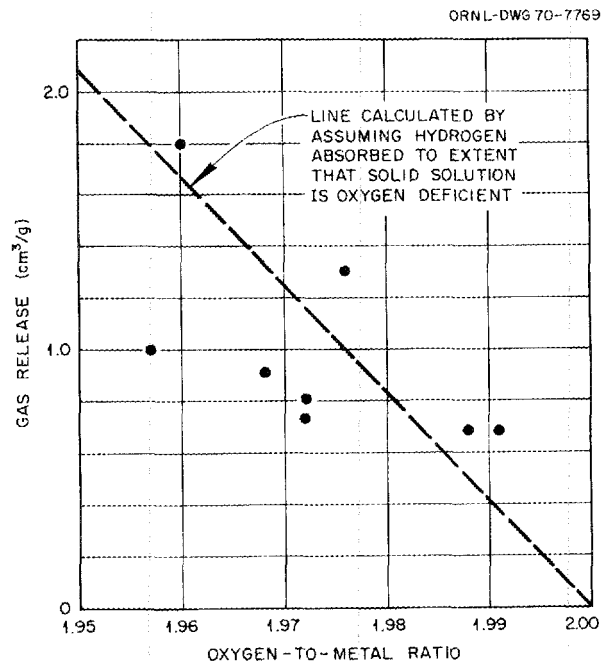


Fig. 3.21. Effect of oxygen-to-metal ratio on gas release in low-density pellets cooled under Ar-4% H_2 .

the hydrogen tends to fill these vacancies, forming a U-Pu-O-H solid solution. The extent to which this process approaches completion would depend on the time in a favorable temperature range, the hydrogen pressure, and the relative surface area of the material. Figure 3.21 shows gas release as a function of oxygen-to-metal ratio. The line indicates the volume of hydrogen corresponding to complete filling of oxygen vacancies. The data indicate that the magnitude of gas sorption is certainly comparable to the volume predicted by the mechanism described above.

3.6 DISCUSSION, CONCLUSIONS, AND RECOMMENDED FUTURE WORK

R. A. Bradley J. D. Sease

The Sphere-Pac process was shown to be suitable for loading microspheres into fuel rods to achieve a fuel column smear density comparable to that required for the FFTF pellets. Smear densities 82 to 84% of theoretical can be achieved by a single infiltration of fine ($<44\text{-}\mu\text{m}$) microspheres into a bed of coarse ($420\text{--}600\text{-}\mu\text{m}$) microspheres. About 60 Sphere-Pac fuel rods with densities in the range 80 to 86% of theoretical were fabricated for irradiation tests on this program. Although higher densities are not expected to be required for fast-reactor applications, our development

work has shown that smear densities up to 88% of theoretical can be achieved by using a blend of two sizes of microspheres for the coarse bed. With recent developments in the fabrication of sol-gel microspheres of closely controlled size and narrow size distribution, the blended bed approach is certainly practical.

The rod-to-rod variation in smear density of the fuel rods listed in Table 3.1 was primarily due to three sources: (1) batch-to-batch variations in the density of the coarse microspheres, (2) batch-to-batch variations in the size distribution and shape of the coarse microspheres, and (3) operator errors in loading the Sphere-Pac pins. With high-density spherical microspheres of controlled size, such as the ThO_2 microspheres being made by the sol-gel process, the smear density of Sphere-Pac rods could be controlled to about $\pm 1\%$.

The biggest objection we found to the Sphere-Pac process was the spread of contamination due to the handling of plutonium-bearing fine microspheres. The U-Fines Sphere-Pac process eliminates this problem by incorporating all the plutonium in the coarse fraction and using fine microspheres containing only UO_2 . This approach is particularly attractive in remote reprocessing of fuel, where many of the dusty operations associated with pellet fabrication would be objectionable.

Methods were developed for fabricating pellets of controlled density in the range 83 to 97% of theoretical from sol-gel-derived $(\text{U,Pu})\text{O}_2$. Sol-gel $(\text{U,Pu})\text{O}_2$ powder, being composed of aggregates of crystallites, is suitable for fabricating 83- to 88%-dense pellets. The microstructure of these pellets consists of a very porous matrix with open, surface-connected porosity and regions of very dense material dispersed throughout the matrix.

Pellets of higher densities (88–97% of theoretical) can be made from sol-gel powder whose properties have been altered by an oxidation-reduction treatment. These pellets contain a more uniform distribution of porosity typical of that obtained in coprecipitated or mechanically mixed powder.

The sol-gel process permits the fabrication of $(\text{U,Pu})\text{O}_2$ pellets with lower densities than can be achieved with coprecipitated or mechanically mixed powders. In addition, it permits one to obtain pellet microstructures with a high percentage of large open porosity. This type of microstructure might be beneficial in solving the fuel densification problem presently being experienced in LWR's.

An analysis of the reduction of mixed oxide fuel to the substoichiometric state led to the conclusion that the process was kinetically controlled. An expression

was derived to predict the time required to reduce a batch of fuel of known weight to the desired oxygen-to-metal ratio. After this model was developed, we were able to achieve the desired oxygen-to-metal ratio in fuel for irradiation tests with no difficulty. For oxygen-to-metal ratios of less than 1.96, reduction by the C-CO- CO_2 system was used because times required to accomplish the reduction with the H_2 - H_2O system were impractical.

We found that substoichiometric $(\text{U,Pu})\text{O}_2$ retained hydrogen when cooled in an atmosphere containing hydrogen. This hydrogen was released on reheating and contributed significantly to the gas released in vacuum at 1600°C , thus causing the gas release values to exceed the maximum permitted for fast-reactor fuels. Cooling from about 850°C to ambient in argon decreased the total gas release by an order of magnitude to an average value of about $0.04 \text{ cm}^3/\text{g}$.

Conduct of additional fabrication work based on sol-gel-derived $(\text{U,Pu})\text{O}_2$ materials depends on the outcome of the in-progress irradiation program and the comparison of these results with more conventional fuels. Should it develop that the performance of sol-gel fuels indicates additional interest in the future, it will be necessary to conduct work in additional areas to place the fabrication development in a proper condition for pilot-plant-scale work or for commercial application. For loading Sphere-Pac fuels it would be necessary to further optimize the particle distributions to accelerate the rate of loading individual fuel pins. In addition, for semiremote or remote application, it would be necessary to design and develop suitable devices for handling and accurately dispensing fuel microspheres. It is notable that a great amount of the technology being developed in the National HTGR Recycle Development Program would be applicable to this particular need, since in both cases the problems are handling, dispensing, and control of a microsphere product.

Should an interest develop in sol-gel-derived pellets, it will be necessary to conduct additional studies of pressing and sintering phenomena in order to determine the optimum procedure for fabricating $(\text{U,Pu})\text{O}_2$ pellets. The object of this work would be to optimize such a process from the standpoint of economics and to obtain a microstructure that is stable under normal conditions.

It is highly recommended that when low oxygen-to-metal ratios are required ($\text{O/M} \leq 1.96$) attention be given to the use of the C-CO- CO_2 system for adjusting the oxygen-to-metal ratios and that an inert atmosphere be used for cooling substoichiometric fuel to ambient temperature.

4. Fuel Characterization

J. D. Sease W. H. Pechin R. A. Bradley

4.1 ANALYTICAL CHEMISTRY TECHNIQUES

W. H. Pechin W. R. Laing¹

Several of the analyses and characterization techniques were developed concurrently with the process development because of requirements peculiar to either the product or the application. For instance, a precision of ± 0.005 for the oxygen-to-metal ratio corresponds to measuring the oxygen content with a precision of 0.25% of the amount present. Early in the program we found that such precision could not be easily achieved and maintained with the techniques available to us for determining total oxygen. At the start of the program, the relationship between moisture analysis and sorbed gas content was not suspected. In general, as the program progressed our knowledge of applicable techniques increased along with ability to correlate the analytical results to the process parameters.

4.1.1 Determination of Oxygen-to-Metal Ratio

We used an adaptation of a method suggested by Lyons² for the determination of oxygen-to-metal ratio (O/M). The pellets or microspheres were weighed and then heated to 500°C in air. At 500°C the atmosphere was changed to Ar-4% H₂, the heating was continued to 850°C, and the furnace was held at that temperature for 13 hr. The samples were then cooled to room temperature in the flowing Ar-4% H₂ atmosphere and reweighed. The assumption is that the heat treatment will adjust the O/M to 2.000 and that the weight change of the sample is due entirely to the addition or removal of oxygen to reach this stoichiometric value.

We did not crush pellet samples, because Bradley and Lindemer³ have shown that the rate of reduction of the mixed oxide by hydrogen is controlled by the removal of water vapor from the furnace by the gas stream and not by diffusion through the solid. We did not dry the samples, since we found that at 100°C there can be a

significant change in O/M during such treatment, as shown by a weight gain in hypostoichiometric oxide samples. Typical moisture values were insignificant compared with O/M change. On 12 pellet samples from a single batch, we calculated the O/M from both the weight before a drying step and on the weight after drying. The drying step consisted of a 1-hr treatment at 100°C in Ar-4% H₂. The gas stream was dried with anhydrous CaSO₄. The average O/M based on "dried" weight was 1.997, but that based on "undried" weight was 1.980 for the same pellets.

This problem could perhaps be lessened by using a more efficient drying agent for the gas stream and removing oxygen from the stream, but our experience with the ceramic tube sintering furnaces, where we continuously monitor the moisture in the effluent gas, has convinced us that the moisture content of the furnace atmosphere is often controlled by the previous history of the furnace and not by the incoming gas. The analytical furnace also has a ceramic tube.

Six samples are analyzed simultaneously. These are arranged in a line in the analytical furnace so that most samples are subjected to a gas whose composition may have been altered by the samples upstream. This fact concerned us as did the question of whether the position of a pellet in the production sintering furnace had an effect on its O/M. Therefore, we performed a statistically designed experiment⁴ to determine the effect of all of these factors and to determine the consistency of the analysis from day to day.

1. Analytical Chemistry Division.

2. W. L. Lyon, *The Measurement of Oxygen-to-Metal Ratio in Solid Solutions of Uranium and Plutonium Dioxides*, GEAP-4271 (May 1963).

3. R. A. Bradley and T. B. Lindemer, *LMFBR Fuel Cycle Studies Progress Rept. January 1971*, ORNL-TM-3312, p. 64.

4. W. J. Lackey, R. A. Bradley, W. H. Pechin, and T. L. Hebble, "Precision and Source of Variation of Oxygen-to-Metal Determinations for (U,Pu)O₂," *Nucl. Technol.* 13(4), 105-7 (April 1972).

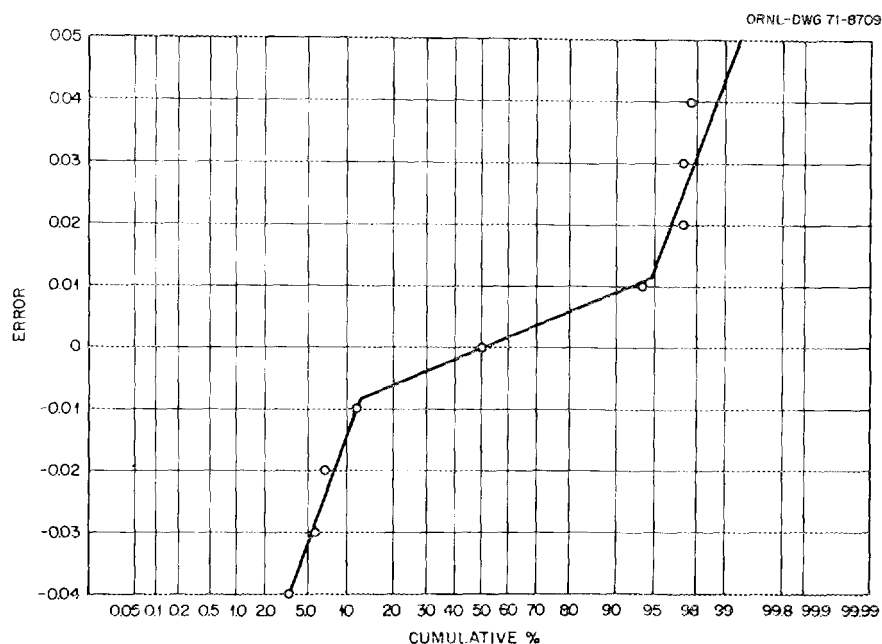


Fig. 4.1. Probability distribution of error in the analysis of oxygen-to-metal ratio of $(U,Pu)O_{2-x}$.

The experiment demonstrated that position in the analytical furnace and position in the production furnace had no effect on the results. However, on one of the six days involved in the experiment the results were significantly lower than average. As we could not isolate the reason for the day-to-day variation, we adopted a strategy in which three samples are analyzed from each sintering batch. Each sample is analyzed on a different day, and any individual result that deviates from the average for the three by more than ± 0.01 O/M unit is discarded.

The data on 175 samples representing about 50 batches of pellets confirmed the results of the experiment described above. Figure 4.1 shows the distribution of the error for these 175 samples. The error was estimated from the difference of each sample result from its batch mean. About 80% of the samples followed a normal distribution whose standard deviation was about 0.003 O/M unit, while the remainder of the samples deviated significantly from this distribution.

4.1.2 Moisture Analysis

Our moisture analyses were performed with a commercial instrument,⁵ which utilized a current integrator

5. *Operation and Maintenance Manual 992212-0010 for Type 26-321A Moisture Analyzer*, Bell and Howell, CEC/Analytical Instruments Division, 1500 S. Shamrock Avenue, Monrovia, Calif. 91016.

on a P_2O_5 electrolytic cell. Moisture was carried to the cell by dry nitrogen sweep gas, which passed over the sample in the furnace. The instrument can be operated from room temperature to $1000^\circ C$. The normal sample weight is 1 g. We found that when the instrument was loaded in air the scatter in the results was quite large. The standard deviation was 12.6 ppm for samples averaging 33 ppm. By enclosing the instrument and sample bottle in a plastic bag purged with argon, we reduced the standard deviation to 3.2 ppm on samples averaging 18 ppm moisture. We have now equipped the moisture analyzer with an air lock, which is purged with dry nitrogen and prevents the entrance of air as the sample is loaded.

A more basic problem with the moisture analysis was concerned with the condition of the mixed oxide being analyzed. If $(U,Pu)O_{2-x}$ is cooled from a temperature of $850^\circ C$ in an atmosphere containing hydrogen, it will form⁶ the compound $(U,Pu)O_{2-x}H_x$. This hydrogen from this compound will be evolved at about $380^\circ C$ if the fuel is reheated in a hydrogen-free atmosphere. With the type of moisture analyzer used, the presence of hydrogen in the gas stream causes an erroneously high moisture value. Figure 4.2 compares the results obtained on samples cooled in $Ar-4\% H_2$ with those ob-

6. W. H. Pechin and R. A. Bradley, *Fuels and Materials Development Program Quart. Progr. Rept. Dec. 31, 1969*, ORNL-4520, pp. 20-27.

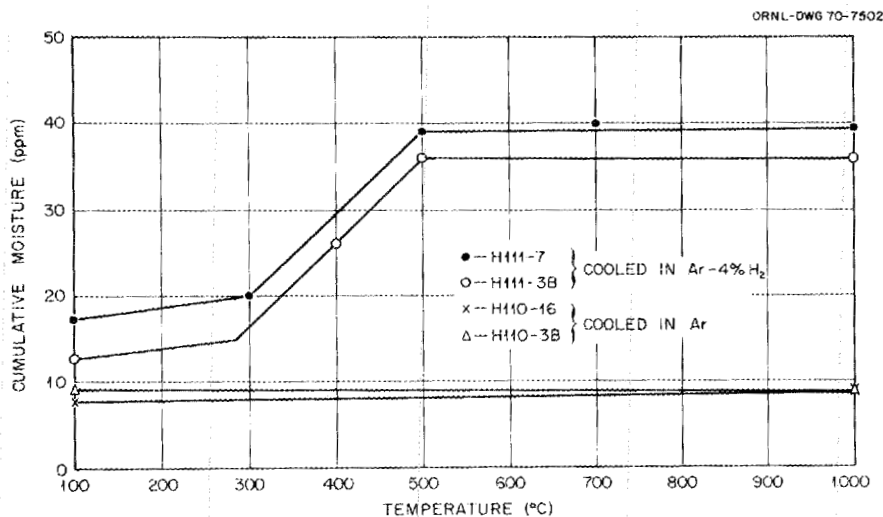


Fig. 4.2. Effect of cooling atmosphere and temperature on moisture evolution.

tained on samples cooled in argon. The samples labeled H111 in Fig. 4.2 were prepared from the same powder as those labeled H110, the two batches of pellets had the same density and O/M, but H110 had a measured gas content of $0.03 \text{ cm}^3/\text{g}$, while H111 contained $0.49 \text{ cm}^3/\text{g}$.

4.1.3 Sorbed Gas Content

Our original system for measuring sorbed gas content of $(\text{U,Pu})\text{O}_2$ fuels consisted of a tungsten crucible suspended in a quartz tube and heated by induction. This system had poor temperature control and a severe disadvantage in that it had to be opened to add the sample after the background was measured. This procedure resulted in high background values and poor reproducibility between samples from the same batch of material.

For these reasons the quartz sample chamber and tungsten crucible were replaced with a small Al_2O_3 tube. As shown in Fig. 4.3 the heat was then supplied from a carbon susceptor outside the sample chamber. The new equipment includes a device for adding samples after the system is brought to temperature and after the background level is measured. The apparatus includes two sample arms, which allow four samples to be measured during each heating cycle. The pressure in the system is recorded at intervals for about 20 min. The evolved gas is pumped out of the evolution section and sampled for mass spectrographic analysis. The present system has a background equivalent to 0.001 to $0.005 \text{ cm}^3/\text{g}$, compared with 0.20 to $0.30 \text{ cm}^3/\text{g}$ with the former design.

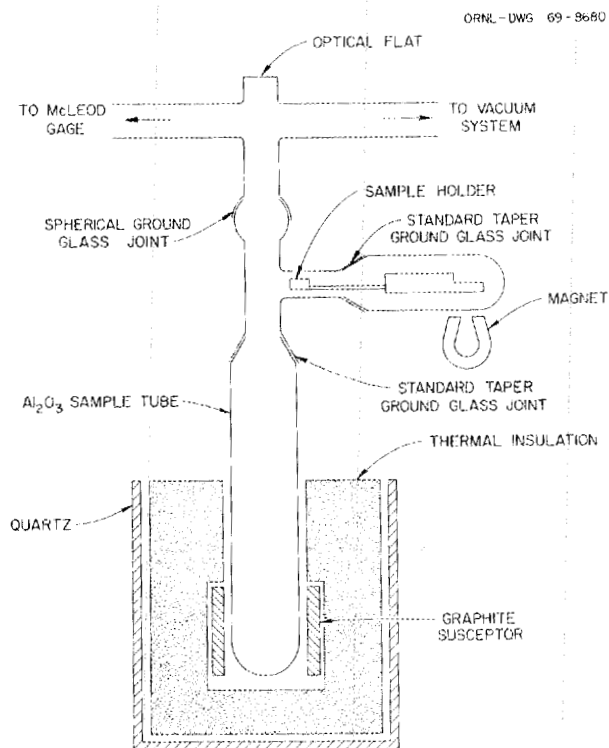


Fig. 4.3. Apparatus with small Al_2O_3 tube for sample chamber for measuring gas release from $(\text{U,Pu})\text{O}_2$ fuel.

Typical $(\text{U,Pu})\text{O}_{2-x}$ samples analyzed with this apparatus evolve 0.5 to over $1.0 \text{ cm}^3/\text{g}$ if cooled in $\text{Ar}-4\% \text{ H}_2$ after sintering and from 0.001 to $0.004 \text{ cm}^3/\text{g}$ if cooled in a hydrogen-free atmosphere. The mass spectrographic analysis indicates that the evolved gas is over

90% H₂ for samples cooled in the presence of hydrogen and about 60 to 70% H₂ for samples cooled in the absence of hydrogen.

4.1.4 Actinide Analysis

Most of the fuel prepared in this program had a nominal plutonium content of 20% by weight of the total actinides. Both the uranium and plutonium contents were determined by controlled-potential coulometric titration.⁷ This method appears to be completely acceptable. Data from duplicate determinations of uranium and plutonium indicated a standard deviation of 0.1% for the ratio of plutonium to total actinides. These were complete duplications made on separate samples from a single batch.

The isotopic composition was determined by mass spectrography -- in most cases from a sample prepared from the same dissolution made for the uranium and plutonium determinations. The results of multiple determinations of uranium and plutonium isotopic compositions indicate standard deviations as listed in Table 4.1 for the major uranium and plutonium isotopes. Again this represents separate samples and dissolutions. For the determination of actinide homogeneity we made a detailed comparison of results from alpha autoradiography, gamma spectroscopy, and the electron microprobe.

7. ORNL Master Analytical Manual, TID-7015, Method 1-219225.

Table 4.1. Precision of mass spectrographic isotopic analysis

| Element | Isotope | Standard deviation (% of amount present) |
|-----------------------|---------|---|
| Plutonium | 239 | 0.06 |
| | 240 | 0.52 |
| | 241 | 0.90 |
| | 242 | 2.12 |
| Uranium (enriched) | 234 | 1.6 |
| | 235 | 0.18 |
| | 236 | 0.62 |
| | 238 | 3.0 |
| Uranium (natural) | 234 | 3.22 |
| | 235 | 0.24 |
| | 236 | 9.09 |
| | 238 | 0 |

4.2 MICROSTRUCTURE OF MICROSPHERES AND PELLETS

W. J. Lackey R. A. Bradley

The anticipated importance of fuel microstructure to such properties as creep, fission gas release, swelling, thermal conductivity, and extent of restructuring led to the extensive microstructural characterization of sol-gel (U,Pu)O₂ microspheres and pellets described in this section. Knowledge of the fuel microstructure serves three purposes: (1) it helps ensure that high-quality fuel is being fabricated, (2) it reveals information concerning the effect of fabrication variables on pore morphology and grain size, and (3) it aids in the interpretation of irradiation tests by providing a comparison between the unirradiated and the irradiated fuel. Although the microstructure of any particular batch of material will depend on the exact conditions of its preparation and thermal treatment, most sol-gel (U,Pu)O₂ can be characterized by the following typical microstructures. Fabrication and characterization data for the fuels shown are summarized in Table 4.2.

Optical microscopy, replica electron microscopy, electron microprobe analysis, and alpha autoradiography were used to characterize the microstructure of the sol-gel (U,Pu)O₂ specimens. Each specimen was mounted in epoxy,⁸ polished, and photographed in a previously described metallographic facility for plutonium-bearing materials.^{9,10} The etched structures were obtained by immersion at room temperature for 60 min in a (U,Pu)O₂ etchant.¹¹ We used the two-stage carbon replica electron microscopy technique developed by Padden.¹² To investigate plutonium and uranium homogeneity, the Pu M β and U M α x-ray intensities were simultaneously measured, and alpha autoradiographs

8. Araldite, CIBA Products Company, Summit, New Jersey.

9. R. J. Gray and B. C. Leslie, "An Alpha Metallography Laboratory at Oak Ridge National Laboratory," pp. 226-57 in *Technical Papers of the 22nd Metallographic Group Meeting, Held June 19-21, 1968, Gulf General Atomic, Inc., San Diego, California*, CONF-680614 (December 1971).

10. R. J. Gray and B. C. Leslie, "A Metallograph for Glove Box Operations," pp. 119-25 in *Proceedings, First Annual Technical Meeting, International Metallographic Society, Inc., November 11, 12, and 13, 1968 - Denver, Colorado, U.S.A.*, ed. by K. A. Johnson and J. H. Bender, International Metallographic Society, Inc., Los Alamos, N.M., 1969.

11. F. M. Smith, S. J. Mayhan, and R. V. Olson, *Metallography* 2, 179-89 (1969).

12. T. R. Padden, *Polyvinyl Chloride Replica Technique for High Burnup Reactor Fuels*, WAPD-T-1595 (August 1963).

Table 4.2. Sintering conditions, grain size, and oxygen-to-metal ratio for sol-gel (U,Pu)O₂ microspheres and pellets

| Batch | Fuel form ^a | Pu U+Pu (%) | Sintering conditions | | | Grain size (μm) | Oxygen-to-metal ratio | Irradiation experiments in which used |
|-----------|------------------------|-------------------|---------------------------------------|------------------------|-------------------------------------|---------------------------------|--------------------------|---|
| | | | Temperature ($^{\circ}\text{C}$) | Time (hr) | Atmosphere | | | |
| PM-11C | C | 20 | 1450 | 9 | Dry Ar-4% H ₂ | 2-3 | 1.97 | ETR 43-120 43-121 |
| PM-5C | C | 20 | 1450 | 9 | Dry Ar-4% H ₂ | 20-60 | 1.99 | EBR-II series I |
| PM-6C | C | 20 | 1450 | 9 | Dry Ar-4% H ₂ | 5-10 | 1.98 | EBR-II series I |
| SPL-80/85 | C | 20 | 1400 1480 | 100 ^b 48 | Dry Ar-4% H ₂ | 2-6 | 1.96 | EBR-II series II |
| M-3785 | C | 15 | 1100 | 2 | Wet Ar-4% H ₂ | 1-3 | 2.00 | None |
| 99C | C | 15 | 1100 | 2 | Wet Ar-4% H ₂ | 1-1.4 | 2.00 | ETR 43-112 43-113 43-115 |
| PM-11F | F | 20 | 1450 | 6 | Dry Ar-4% H ₂ | 1-1.4 | 1.98 | ETR 43-120 43-121 |
| DS 13, 16 | F | 15 | 1100 | 2 | Wet Ar-4% H ₂ | 2-20 | 2.00 | None |
| ET3N | P | 20 | 1450 | 4 | Dry Ar-4% H ₂ | 1-2 | 1.98 | ETR 43-120 43-121 |
| PELL 80 | P | 20 | 1550 | 6 | Dry Ar-4% H ₂ | 3 | 1.96 | EBR-II series II |
| PEL 85 | P | 20 | 1550 | 2 | Ar-10% CO ₂ ^c | 16 | 1.98 | EBR-II series II |
| PEL 90 | P | 20 | 1550 | 4 | Dry Ar-4% H ₂ | 4 | 1.97 | EBR-II series II |

^aC = coarse microspheres; F = fine microspheres; P = pellets.

^bTwo batches were combined after heat treatment to form Batch SPL-80/85.

^cSubsequently heated 4 hr at 1550 $^{\circ}\text{C}$ in dry Ar-4% H₂ for adjustment of oxygen-to-metal ratio.

were prepared by placing cellulose nitrate film¹³ in direct contact with the polished specimen for approximately 5 sec and then developing in 6 N NaOH at 50 to 55 $^{\circ}\text{C}$ for 3 min.

4.2.1 Coarse Microspheres

The coarse microspheres used in fuel pins fabricated by the Sphere-Pack process were shape-separated and screened so that they were very nearly spherical with diameters in the range 420 to 597 μm . Good-quality coarse microspheres are shown in Fig. 4.4. At magnifications below about 100 X, these spheres appear almost fully dense, but numerous small sintering pores are apparent at higher magnifications. The quantity of porosity frequently varies from sphere to sphere, as illustrated in Fig. 4.4. As determined with a Quantimet¹⁴ image analyzing computer, the density of

the most porous sphere observed was 95.4% of theoretical, and that of the most dense sphere was 99.1%. The average density was 96 to 97% for this batch of microspheres. Nearly all of the porosity in the most porous spheres was located at grain boundaries; but that in the dense spheres was trapped within the grains.

In each batch of microspheres that we examined, the grains were equiaxed and their size was relatively uniform within a sphere; however, the grain size often varied from sphere to sphere, depending on porosity. This is apparent in Fig. 4.4, where the average grain diameter of the more porous sphere was $1.7 \pm 0.2 \mu\text{m}$ and that of the most dense sphere was $3.2 \pm 0.4 \mu\text{m}$. These grain sizes are typical for sol-gel material, but microspheres with an average grain size as large as 40 μm have been prepared by variation of the sintering conditions.

Optical and electron micrographs of (U,Pu)O₂ coarse microspheres made during the past several years for irradiation tests are shown in Figs. 4.5 and 4.6. The quality of the microspheres, in terms of roundness and the number of cracks or large voids, for these six

13. Kodak special film type 106-01-A, Eastman Kodak Company, Rochester, N.Y.

14. Quantimet model B, Image Analyzing Computers, 40 Robert Pitt Drive, Monsey, N.Y.

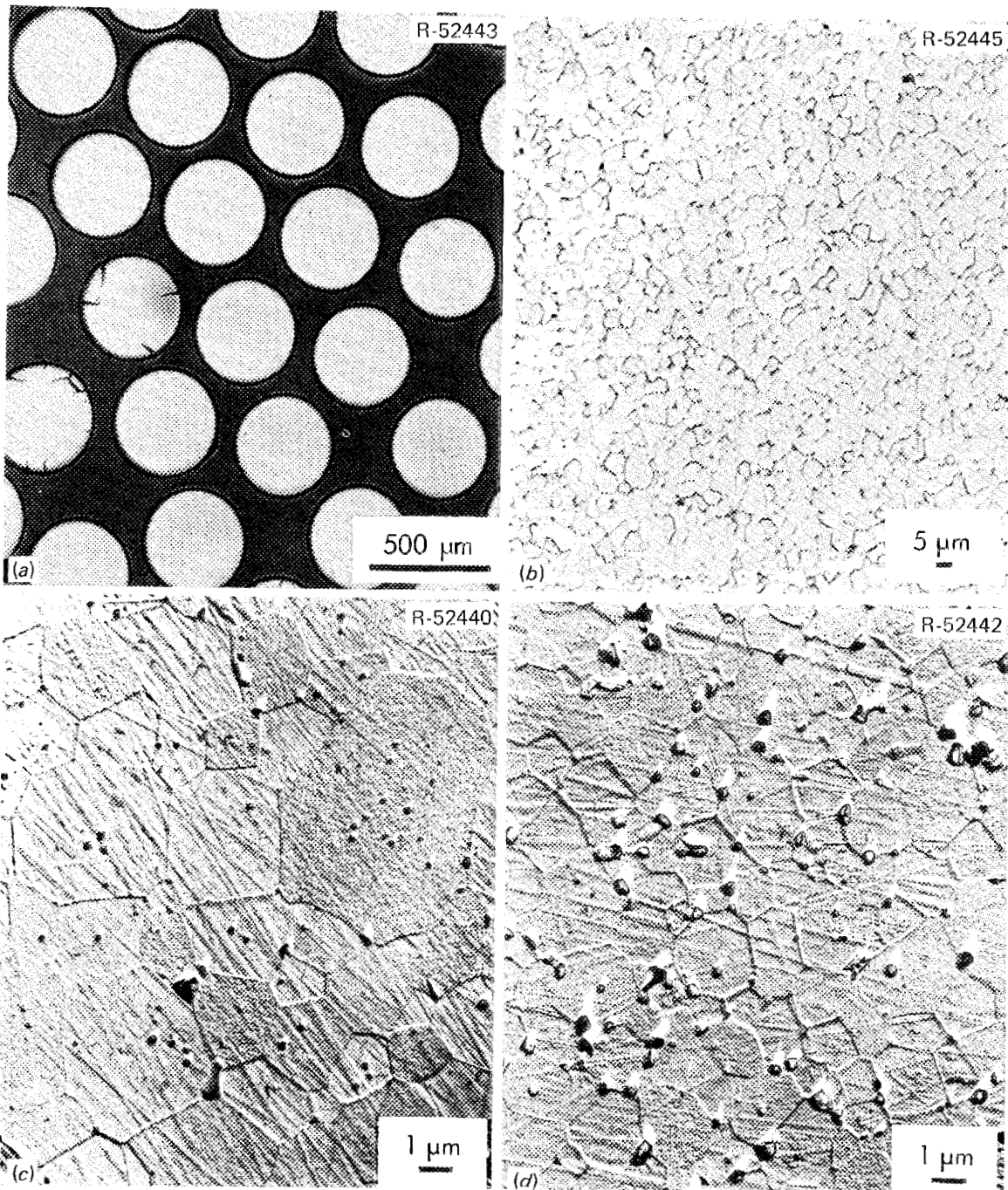


Fig. 4.4. Coarse $U_{0.8}Pu_{0.2}O_2$ microspheres. Batch PM-11C, (a) Optical micrograph. (b) Optical micrograph of a dense sphere. (c) Electron micrograph of a dense sphere. (d) Electron micrograph of a porous sphere. In the electron micrographs, pores appear as dark areas and cast a light shadow.

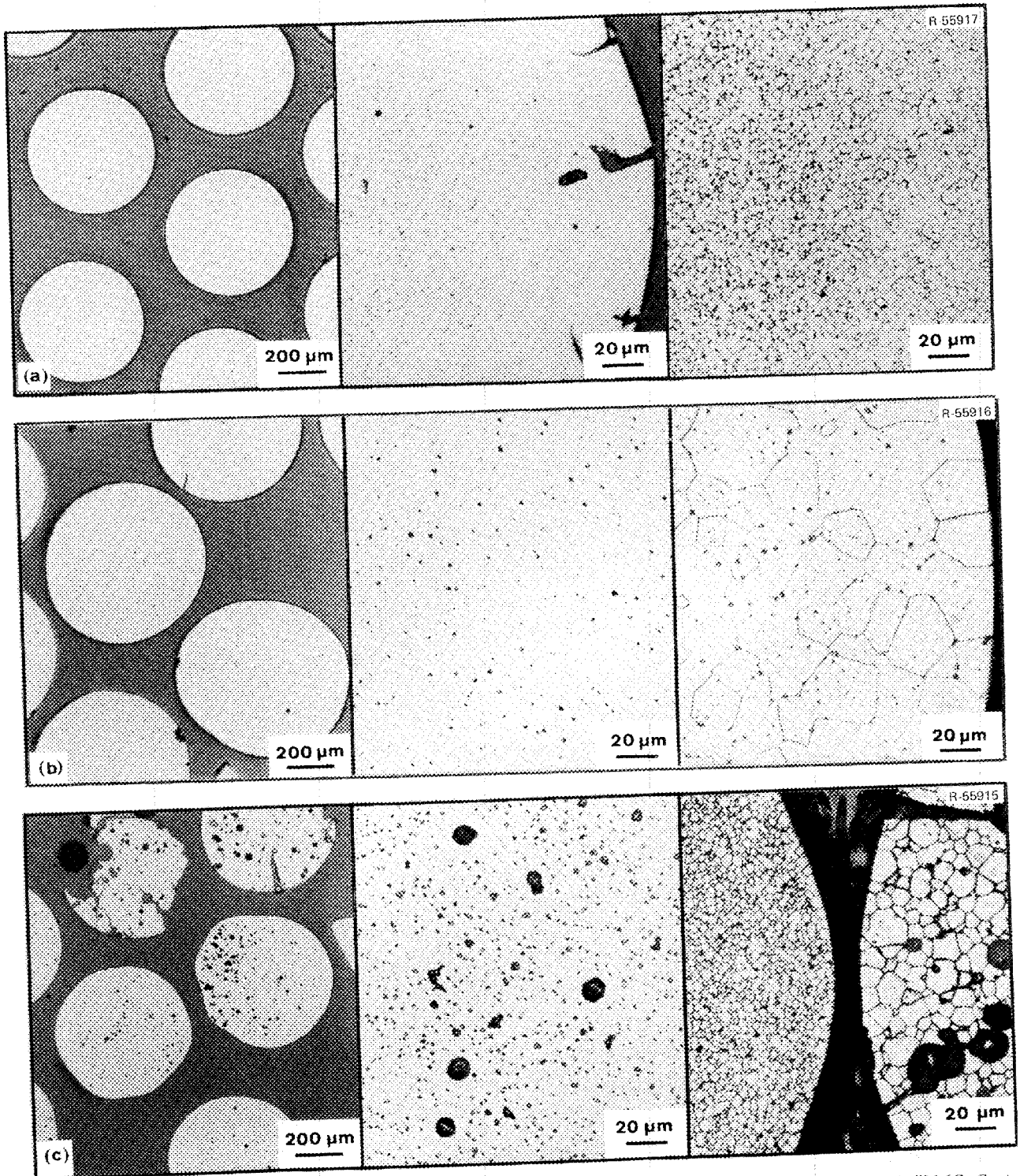


Fig. 4.5. Microstructures of $(U,Pu)O_2$ coarse microspheres. (a) Batch PM-11C. (b) Batch PM-5C. (c) Batch PM-6C. Center micrographs unetched to show porosity. Right etched to show grain size.

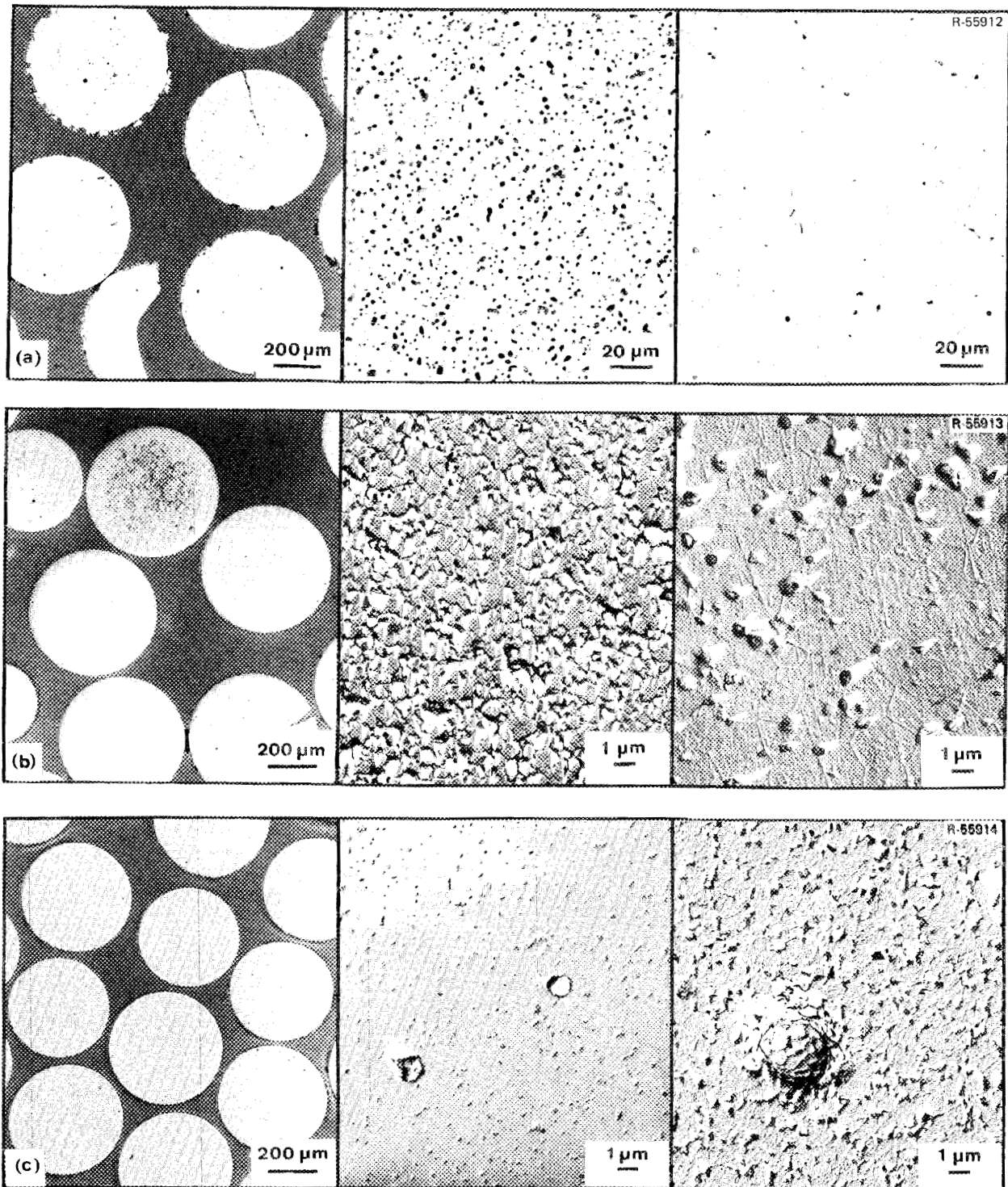


Fig. 4.6. Microstructures of $(U,Pu)O_2$ coarse microspheres. (a) Batch SPL-80/35. (b) Batch M-3785. (c) Batch 99C. The high-magnification views show microstructural extremes in (a) and (b) and compare as-polished and etched microstructures in (c).

batches, ranges from the best to the worst that has been observed for microspheres made by the sol-gel process.

Frequently, on coarse microspheres we observed a surface layer approximately $50\ \mu\text{m}$ thick with a higher density and larger grain size than for the interior of the sphere. An exaggerated example of this structure, which is apparently related to the rate of drying during microsphere formation, is shown in Fig. 4.5(a). Spheres in which this structure is exaggerated frequently contain radial cracks in the high-density layer.

Occasionally, as shown in Fig. 4.5(c), a batch of microspheres containing large pores is produced. Such pores are apparently created during formation of the microsphere in the sol-gel sphere-forming column, since it is doubtful that pores this large result from the sintering process.

The batches of spheres in Figs. 4.5(c), 4.6(a), and 4.6(b) showed the largest within-batch variation in porosity and grain size that we have observed. The high-magnification micrographs shown for these three batches are illustrative of the most porous and most dense spheres in these batches. In contrast, the batch of spheres shown in Fig. 4.5(c) was very uniform in grain size, pore size, and total porosity.

The very small grain size and large number of small intergranular pores for the materials shown in Figs. 4.5(b) and 4.6(c) are the result of sintering at 1100°C , which is lower than our normal sintering temperature. Had these spheres been sintered to 1450°C , additional densification would probably have resulted, since most of the pores were located on grain boundaries and not trapped inside grains.

Alpha autoradiography and electron microprobe analyses typically show the plutonium content to be uniform both within and between spheres to within the limits of detection, which are estimated as $\pm 4\%$ Pu for autoradiography and $\pm 0.5\%$ Pu for microprobe analysis. Homogeneous microspheres are shown in Fig. 4.7. As shown in Fig. 4.8, in some instances variations in the plutonium-to-uranium ratio from sphere to sphere have been observed by alpha autoradiography and electron microprobe analysis. Such inhomogeneity is thought to be caused by failure to properly mix the UO_2 and PuO_2 sols. Subsequent batches of $\text{U}_{0.8}\text{Pu}_{0.2}\text{O}_2$ coarse microspheres were prepared with proper attention given to the mixing step; and each of the resulting batches was homogeneous.

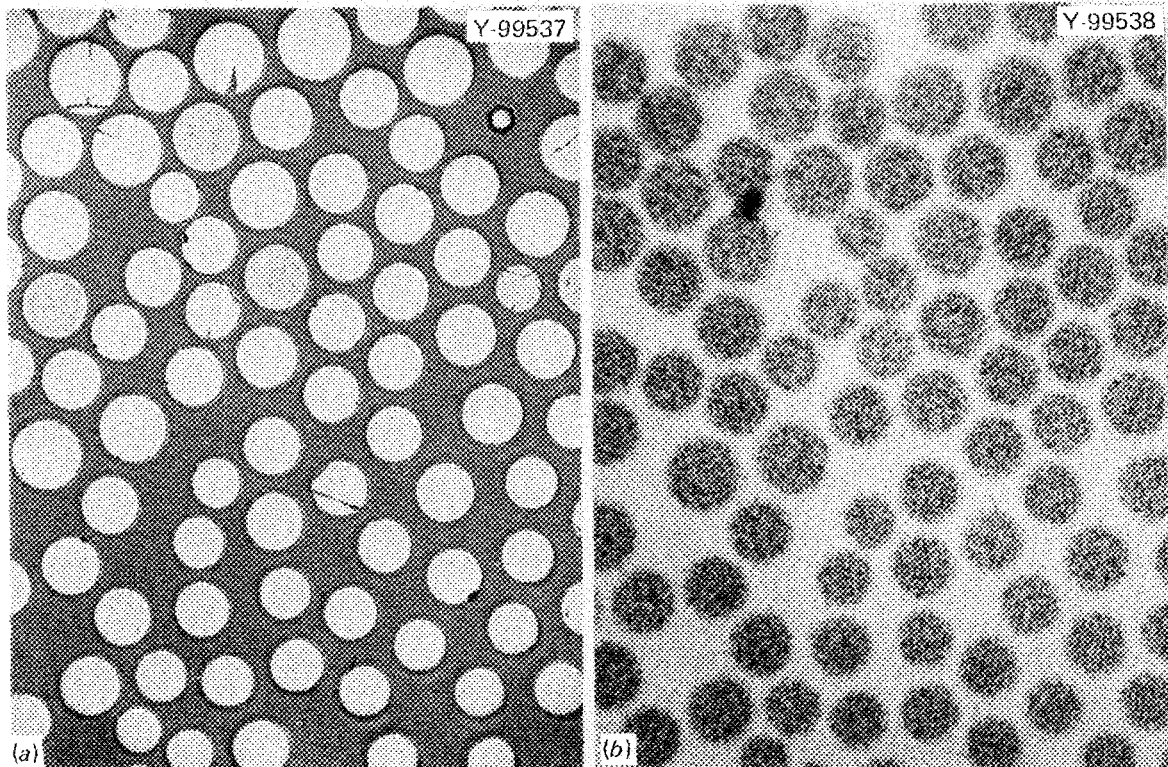


Fig. 4.7. Homogeneous microspheres of $\text{U}_{0.8}\text{Pu}_{0.2}\text{O}_2$. $17\times$. (a) Photomicrograph. (b) Alpha autoradiograph of same field.

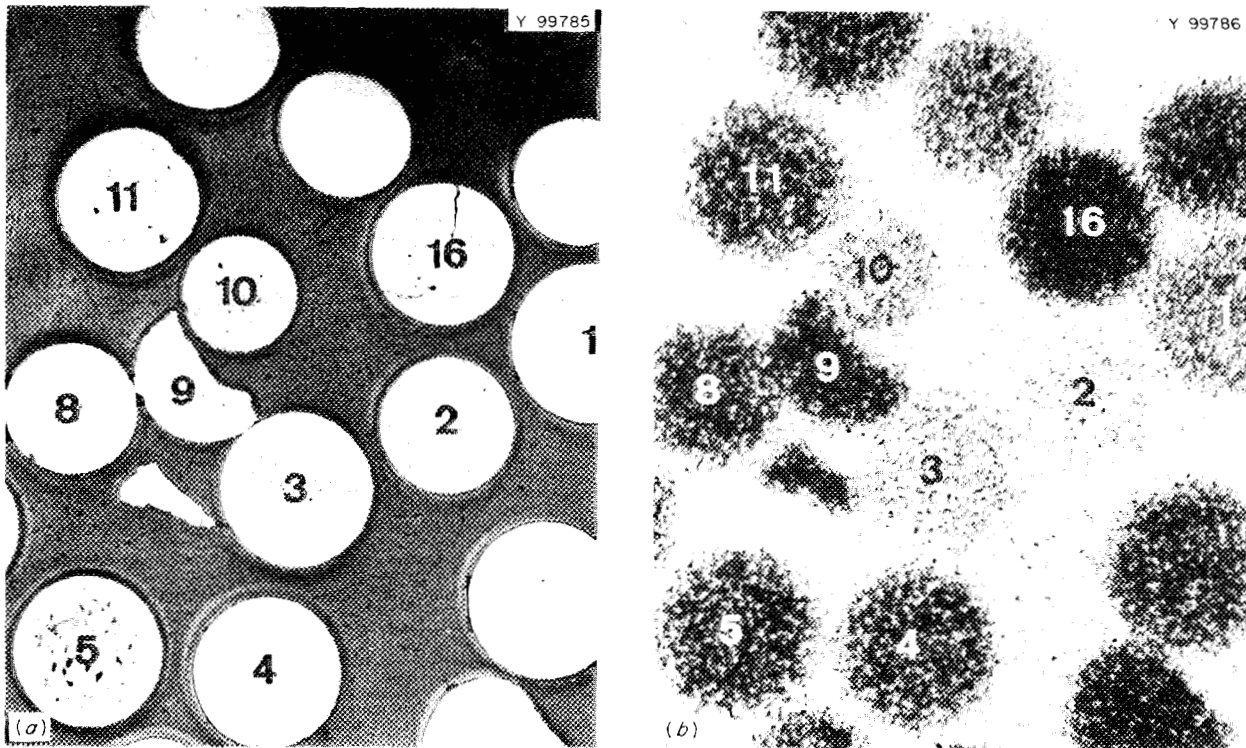


Fig. 4.8. Inhomogeneous microspheres of $U_{0.8}Pu_{0.2}O_2$. 29X. (a) Photomicrograph. (b) Alpha autoradiograph of same field. Electron-probe results:

| Sphere | 1 | 2 | 3 | 4 | 5 | 8 | 9 | 10 | 11 | 16 |
|-------------|------|-----|-----|------|------|------|------|------|------|------|
| Pu/(U + Pu) | 15.0 | 4.7 | 7.3 | 19.3 | 20.3 | 22.6 | 29.5 | 10.7 | 22.7 | 33.9 |

4.2.2 Fine Microspheres

Photomicrographs of representative fine microspheres are shown in Fig. 4.9. The fine microspheres are screened to less than $44 \mu\text{m}$ in diameter. Because of our inability to separate the shapes of the fine microspheres, this material typically contains some aspherical particles. Approximately 2 to 4% of the spheres shown in Fig. 4.9 were hollow. Except for the hollow spheres, electron microscopy showed the spheres to be very dense, perhaps exceeding 99.5% of theoretical. The grain size for this batch of microspheres was uniform within a given sphere and varied only slightly from sphere to sphere; the range was 1.0 to $1.4 \mu\text{m}$.

Material as dense as the microspheres shown in Fig. 4.9 is unusual for single-phase, high-purity sintered ceramics, but is typical of the fine (U,Pu) O_2 microspheres. Even denser material is shown in Fig. 4.10 for a

second batch of fine microspheres. For this batch the grain size varied from sphere to sphere over the range 2 to $20 \mu\text{m}$. For the coarser-grained spheres only two to four grains were intersected by the polishing plane, as shown in Fig. 4.10(d).

Frequently, replication of the void created when a microsphere is pulled out of the mount during metallographic preparation reveals details of the microsphere surface. Examples of this are growth spirals, such as the one shown in Fig. 4.10(d) and the "orange peel" texture shown in Fig. 4.11. Growth spirals were observed only for one batch of microspheres, but the "orange peel" texture is typical. The similarity in size of the surface features in Fig. 4.11 with the grains visible in the intergranularly fractured region shows that the "orange peel" texture results from grooving along the grain boundaries caused by thermal etching during sintering.

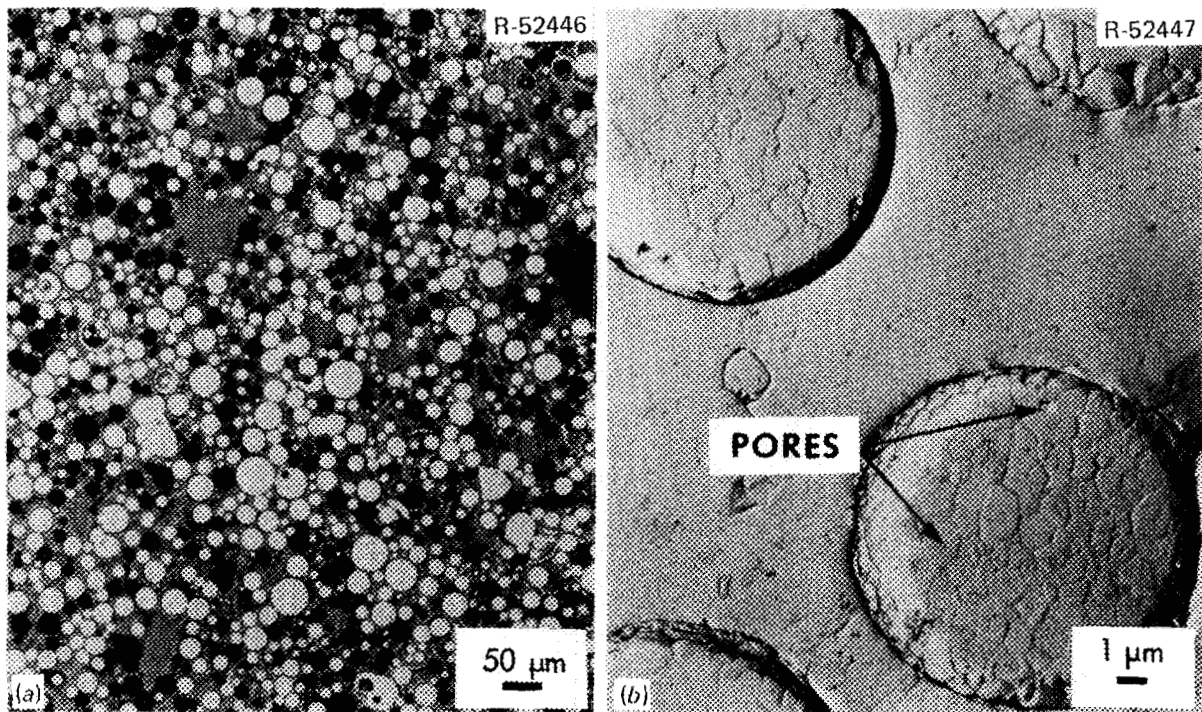


Fig. 4.9. Fine $U_{0.8}Pu_{0.2}O_2$ microspheres. Batch PM-11F. (a) Optical micrograph of typical spheres. (b) Electron micrograph of typical spheres showing high density and small grain size.

4.2.3 Pellets

Optical and electron micrographs of a cold-pressed and sintered pellet $84 \pm 1\%$ of theoretical density are shown in Fig. 4.12. On the basis of the amount and morphology of the porosity, three different types of microstructure are seen in the pellets. First is a very porous matrix containing elongated, irregularly shaped pores interconnected with the surface of the pellet. Dispersed throughout the matrix are very dense areas as large as about $40 \mu\text{m}$ in diameter. Finally, about 5% of the pellet consists of areas, frequently as large as $75 \mu\text{m}$ in diameter and occasionally larger, with an intermediate amount of generally spherical porosity, which is probably not interconnected with the surface of the pellet. These observations agree with results of analysis by mercury porosimetry, which show that nearly all the porosity is open.

This triplex microstructure results from the process used to prepare powder for pelletizing. The sol-gel-derived $(U,Pu)O_2$ shard is a 50%-dense agglomerate of 50- to 100-\AA UO_2 and PuO_2 crystallites. Grinding to -325 mesh powder in a fluid energy mill does not destroy the porous shard particle; it only reduces its size. A dense area in the pellet results from the sintering

of a single piece of -325 mesh shard. Most of the matrix porosity surrounding the dense areas results from the shrinkage necessary for the porous shard to become fully dense. The electron micrographs in Fig. 4.12(b) and (c) show that the dense areas are very nearly theoretically dense and are surrounded by a network of pores. Mounting material in the pores in Fig. 4.12(b) shows that these pores are surface connected. During the grinding process the extremely fine fraction of the powder is separated by the collection system from the bulk of -325 mesh material. After grinding, the fines are combined with the bulk of the material. The large areas with intermediate porosity shown in Fig. 4.12(d) result from agglomeration of the fines before they are recombined with the bulk of the material.

The grains in the dense areas varied from 1 to $2 \mu\text{m}$ in diameter, with $1.7 \mu\text{m}$ being typical. The grain size of the matrix was difficult to measure because of the shadows cast by the numerous pores, but it was slightly less than that of the dense areas. The grains in the areas formed by agglomeration of the fines were about $0.8 \mu\text{m}$ in diameter.

The microstructure of the 84-, 89-, and 97%-dense sol-gel $(U,Pu)O_2$ pellets prepared according to the flow

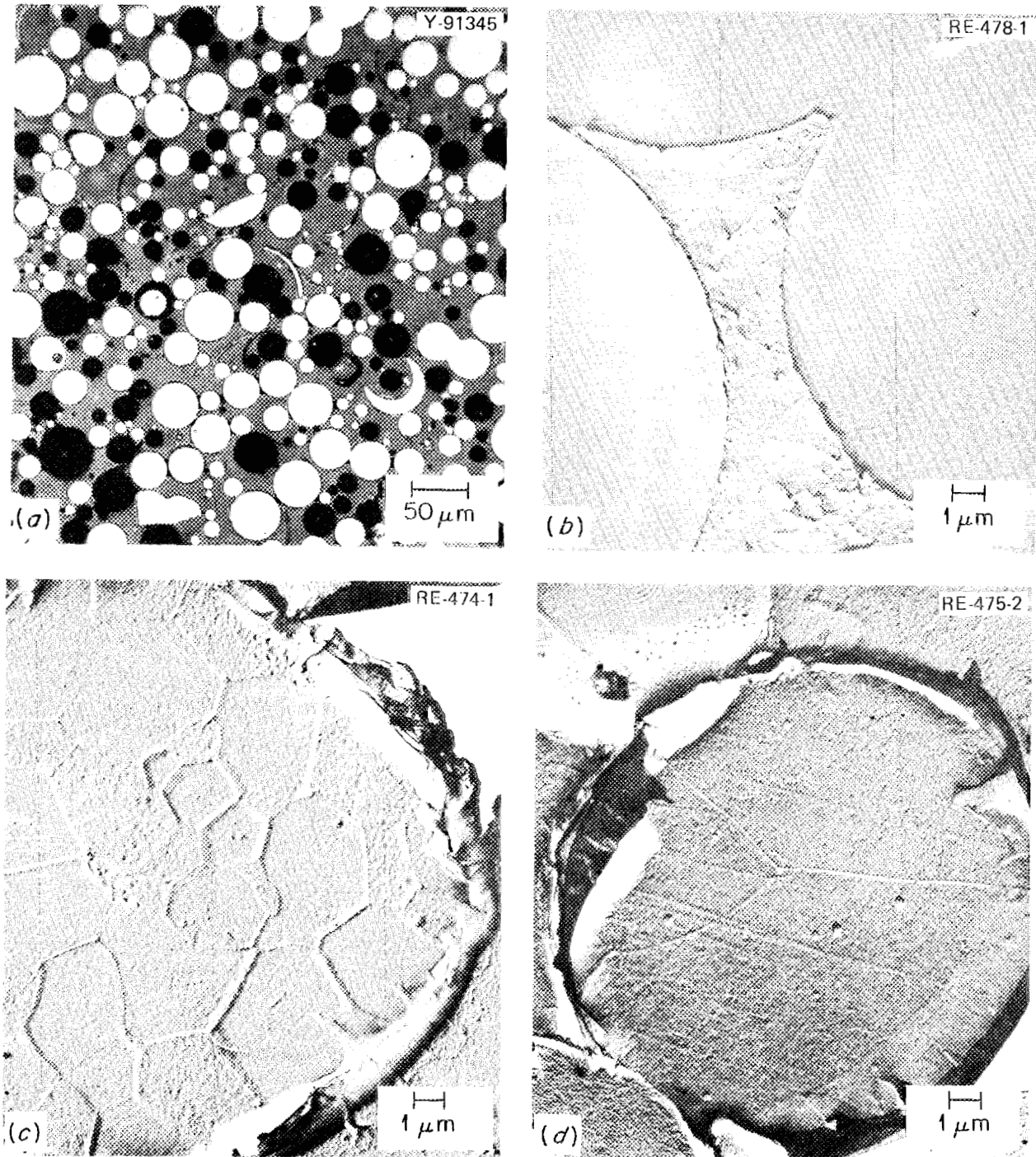


Fig. 4.10. Fine $U_{0.85}Pu_{0.15}O_{2.00}$ microspheres of essentially theoretical density. Batch DS 13, 16. The grain size varied from sphere to sphere. (a) Typical spheres, unetched, 200X. (b) Typical spheres, unetched. (c) Finer grained spheres, etched. (d) Coarser grained spheres, etched.

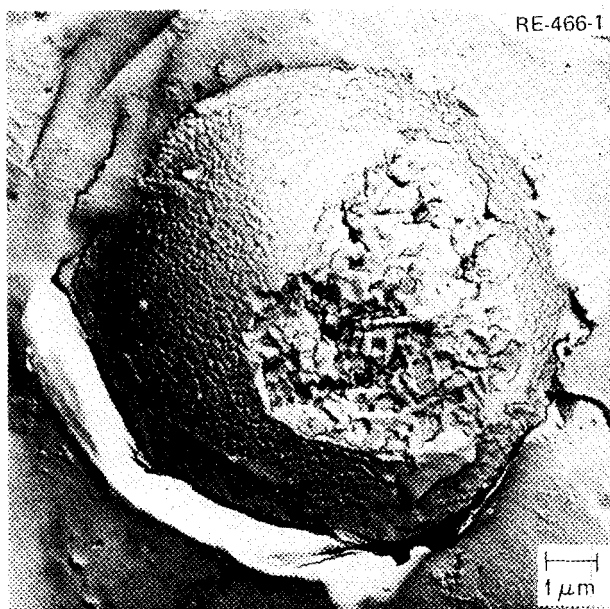


Fig. 4.11. Typical "orange peel" texture of the spherical surface of $(U,Pu)O_2$ microspheres. Note that the size of the surface features corresponds to the size of the grains visible in the intergranular fractured region. Unetched, 750 \times .

diagram of Fig. 3.16 is shown in Fig. 3.15. This fuel was used in the EBR-II series II fuel pins. The microstructure of the 84%-dense pellets consisted of a very porous matrix with open, surface-connected porosity regions of almost theoretically dense material dispersed through the matrix, and regions with an intermediate amount of closed porosity. This structure is typical of low-density pellets produced from sol-gel $(U,Pu)O_2$. The average grain size of these pellets was about 3 μm .

The 89- and 97%-dense pellets, which were made from powder whose properties had been altered by an oxidation-reduction treatment, contained a more uniform distribution of porosity. The 89%-dense pellets contained considerable closed porosity trapped inside grains in addition to porosity on the grain boundaries. The trapped porosity was a result of rapid grain growth during sintering in an oxidizing atmosphere. The 97%-dense pellets, which were made from the same powder as the 89%-dense ones but sintered in a reducing atmosphere, had very fine porosity on the grain boundaries and a relatively small number of larger pores scattered uniformly throughout the pellet. The small

grain size, about 4 μm , and lack of trapped porosity are attributed to the reducing atmosphere.

This work has shown that sintered $(U,Pu)O_2$ microspheres and pellets prepared by the sol-gel technique are typically single phase and of homogeneous composition. The grain size is usually in the range 1 to 5 μm . Typically, the coarse microspheres have densities greater than 95% of theoretical. The fine microspheres are essentially theoretically dense. Low-density cold-pressed-and-sintered pellets have a triplex microstructure consisting of high-density and medium-density islands in a porous matrix. High-density pellets have a more uniform pore distribution. Relation of microstructure to the powder preparation process allows control of the pellet microstructures by variation of the extent to which the shards are ground before pressing and sintering. This work has been reported.¹⁵

15. W. J. Lackey and R. A. Bradley, "Microstructure of Sol-Gel-Derived $(U,Pu)O_2$ Microspheres and Pellets," *Nucl. Technol.* 14, 257-68 (June 1972).

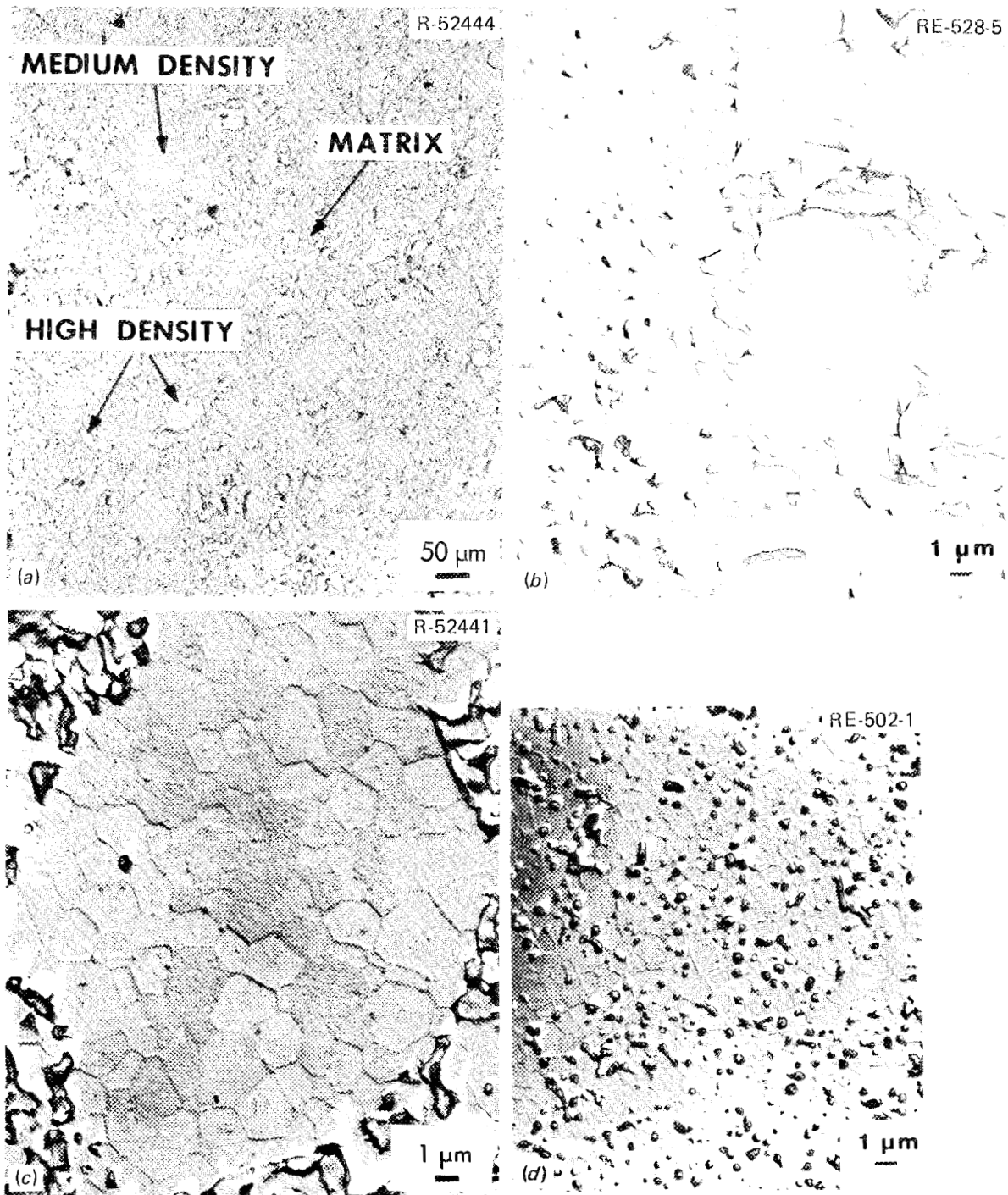


Fig. 4.12. Cold-pressed and sintered $U_{0.8}Pu_{0.2}O_2$ pellet. Batch ET3N. (a) Unetched. (b) Mounting material is apparent in the elongated pores surrounding the high-density regions, 3320X. Unetched. (c) High-density region surrounded by porous matrix. Etched. (d) Medium-density region. Etched.

4.3 TYPICAL FUEL CHARACTERIZATION

W. H. Pechin

The analyses used are summarized in Table 4.3 along with the material types employed as fuel and insulators. Examples of typical results for (U,Pu)O₂ materials are shown in Table 4.4. The table does not show the results for moisture and gas release. The gas release was

invariably less than 0.05 cm³/g for coarse microspheres and pellets and less than 0.10 cm³/g for fine microspheres, once the control of this property was properly understood, as described in Sect. 3.5. Moisture was also 10 ppm or less, once the analysis was altered as described in Sect. 4.1.2 and the interaction between sorbed gas content and moisture analysis became understood.

Table 4.3. Analyses currently in use for characterization of fuel, blank, and insulator materials

| Analysis | ThO ₂ pellets | UO ₂ pellets | UO ₂ fine microspheres | (U,Pu)O ₂ pellets | (U,Pu)O ₂ coarse microspheres | (U,Pu)O ₂ fine microspheres |
|---------------------------------------|-----------------------------|----------------------------|--------------------------------------|---------------------------------|--|--|
| Uranium ^a | | x | x | x | x | x |
| Plutonium ^a | | | | x | x | x |
| Uranium isotopic | | x | x | x | x | x |
| Plutonium isotopic | | | | x | x | x |
| Thorium ^a | x | | | | | |
| Oxygen-to-metal ratio | | x | x | x | x | x |
| Nitrogen | x | x | x | x | x | x |
| Carbon | x | x | x | x | x | x |
| Chloride | x | x | x | x | x | x |
| Fluoride | x | x | x | x | x | x |
| Mass spectrographic for impurities | x | x | x | x | x | x |
| Gas release | | | | | | |
| at 1200°C | x | x | x | | | |
| at 1600°C | | | | x | x | x |
| Metallography | x | x | x | x | x | x |
| Alpha autoradiography ^b | | | | x | x | |
| Gamma spectroscopy ^c | | | | | x | |
| Moisture to 1000°C | x | x | x | x | x | x |

^aHeavy metals present as major constituents; if present as impurities they will be indicated by the mass spectrographic analysis for impurities.

^bResolution currently obtained with alpha autoradiography is not sufficient for examination of fine microspheres.

^cGamma spectroscopy for U/Pu ratio currently applicable only to coarse microspheres containing enriched uranium.

Table 4.4. Typical fuel analyses

| Analysis | Coarse microspheres | Fine microspheres | Pellets |
|-------------------|------------------------|------------------------|------------------------|
| Uranium | 69.91% | 68.26% | 70.24% |
| U isotopic | | | |
| ²³⁴ U | 0.064% | 0.0097% | 0.0054% |
| ²³⁵ U | 0.809% | 1.096% | 0.736% |
| ²³⁶ U | 0.0017% | 0.0034% | 0.0014% |
| ²³⁸ U | 99.18% | 98.89% | 99.26% |
| Plutonium | 16.89% | 16.70% | 16.67% |
| Pu isotopic | | | |
| ²³⁸ Pu | <0.06% | <0.08% | 0.037% |
| ²³⁹ Pu | 88.83% | 88.77% | 88.78% |
| ²⁴⁰ Pu | 9.89% | 9.93% | 9.933% |
| ²⁴¹ Pu | 1.178% | 1.193% | 1.188% |
| ²⁴² Pu | 0.099% | 0.103% | 0.101% |
| O/M ratio | 1.975 | 1.980 | 1.986 |
| Carbon | 40 ppm | <20 ppm | 57 ppm |
| Nitrogen | 23 ppm | 72 ppm | 53 ppm |
| Surface area | <0.1 m ² /g | 0.14 m ² /g | 0.17 m ² /g |
| Al | SNF ^a | SNF | SNF |
| B | SNF | SNF | SNF |
| Cr | SNF | 0.001% | 0.004% |
| Fe | SNF | SNF | 0.019% |
| Mn | SNF | SNF | SNF |
| Mo | SNF | SNF | SNF |
| Ni | SNF | SNF | 0.006% |
| Pb | SNF | SNF | SNF |
| Si | SNF | SNF | SNF |
| Sn | SNF | SNF | SNF |
| Ti | SNF | SNF | SNF |
| V | SNF | SNF | SNF |
| Zr | SNF | SNF | SNF |

^aSought, not found.

4.4 DISCUSSION, CONCLUSIONS, AND RECOMMENDATIONS

J. D. Sease

In the oxygen-to-metal ratio determination, we were never completely satisfied with the gravimetric technique. Submitting duplicate samples in a statistically designed manner to eliminate random day-to-day errors in the results was always a source of concern. The gravimetric analysis can be made to give acceptable results; however, the gravimetric process is not a direct measure of the oxygen potential in the fuel; it is subject to error caused by furnace leaks and weighing errors, and it is extremely time consuming. We would recommend that a galvanic cell-type oxygen determination be pursued, because this determination will measure the

actual oxygen potential in the fuel and should be fast and relatively cheap.

We have developed equipment and techniques for accurately determining both water content and other sorbed gases. In developing the equipment for measuring both of these, we showed that an airlock system was needed to obtain an adequately low background level in the measuring apparatus. The specification of sorbed gas and moisture levels for mixed-oxide fuels must take into account the fact that any moisture present will unavoidably contribute to the sorbed gases in a high-temperature gas release test. In sorbed gas determination, any water that is present in the fuel will react with the substoichiometric fuel to form hydrogen, which will not be removed by a water trap in the gas analysis train. Conversely, in moisture analysis the presence of hydrogen as a sorbed gas can contribute very substantially to the indicated moisture content.

Trace element analysis is an area that can be very difficult. Because of the danger of cross contamination from other samples, the halide analysis needs to be performed in an area completely isolated from other analyses. In determining metallic impurities the sample preparation is extremely important. Although a spark-excited mass spectrograph is a rapid and convenient means for determining many trace element impurities, the results from a direct analysis of small solid samples are not satisfactory, because metallic impurities can form inclusions in the oxide solid solution, causing both high and low results. We feel that mass spectrographic analysis should be run on a solution of the sample rather than on a solid fragment. The solution sample, however, must be prepared extremely carefully to preclude any contamination that may be introduced by the crushing, grinding, and dissolution steps.

A gamma-ray spectroscopic method was developed to determine the variation of uranium-to-plutonium ratio from microsphere to microsphere. The method was as precise as microprobe analysis. With microspheres 500 μm in diameter, it could detect variations in the ratio Pu/(U+Pu) with a standard deviation of $\pm 2\%$.

Metallographic facilities and techniques were developed for the examination of (U,Pu)O₂ by light, scanning, and transmission electron microscopy and by the electron microprobe. By these analytical techniques the pore size, pore morphology, and grain size of the sol-gel fuel were correlated with powder handling and pellet forming and sintering procedures. Typically the sol-gel material is homogeneous in composition, and the grain size is usually between 1 and 5 μm . Coarse microspheres have densities greater than 95% of theoretical, and the fine microspheres approach 100% of theoretical density.

5. Irradiation Program

F. J. Homan A. R. Olsen T. N. Washburn

The irradiation testing phase of the oxide fuels development program involved a limited number of tests designed to investigate particular performance characteristics. Specifically, the areas of thermal performance, fuel restructuring, transient performance of Sphere-Pac fuels, and fuel-cladding mechanical and chemical interaction have been investigated. The initial tests in the program were designed to establish the basic performance of the sol-gel-derived Sphere-Pac fuels in the noninstrumented thermal flux tests, the transient tests, and the encapsulated pin tests in the EBR-II.

Subsequent tests have included other fuel forms. Sol-gel-derived pellet fuels were incorporated in the thermal performance series conducted in the ORR and in the swelling and compatibility tests irradiated in the ETR. Mechanically mixed pellets fabricated by the Hanford Engineering Development Laboratory have been included in the fuel recycle test series, in the fuel-cladding mechanical interaction test, and in the in situ gas release pins. The unencapsulated pins in the EBR-II included Sphere-Pac, pellets from sol-gel and coprecipitated oxide, and Vi-Pac fuel forms.

Table 5.1. Summary of ORNL LMFBR oxide irradiation program

| Fuel | Task | Number of fuel pins | | |
|---|--|---------------------|-----------------|------------|
| | | Irradiated | In-reactor | Fabricated |
| Noninstrumented thermal flux tests | | | | |
| (U,Pu)O ₂ | Basic performance | 13 | | |
| UO ₂ | Basic performance | 7 | | |
| (U,Pu)O ₂ | Fuel recycle | 12 | 8 | |
| Instrumented thermal flux tests | | | | |
| (U,Pu)O ₂ | Thermal performance | 6 | | |
| (U,Pu)O ₂ | Swelling and compatibility | 8 | | |
| (U,Pu)O ₂ | Fuel-cladding mechanical interaction and fission gas release | 1 | | |
| (U,Pu)O ₂ | In situ gas release | | | 2 |
| Transient tests | | | | |
| (U,Pu)O ₂ | Unirradiated fuel | 6 | | |
| Fast flux tests | | | | |
| (U,Pu)O ₂ | Encapsulated pins | 2 | 3 | |
| (U,Pu)O ₂ | Bare pins | 2 | 18 ^a | |
| Summary | | | | |
| (U,Pu)O ₂ | | 50 | 29 | 2 |
| UO ₂ | | 7 | | |
| Total | | 57 | 29 | 2 |

^aWith 19 pins fabricated by B & W to fill a 37-pin subassembly.

The test pins in these irradiations and their status as of July 1, 1972, when ORNL work was phased out, are presented in Table 5.1. The results of these tests are discussed in the following sections, which have been grouped into thermal and fast flux tests and those of similar design. Each section includes a summary of the objectives, design, and principal results together with some discussion of the evaluation of these results. The final section recapitulates the principal findings of these tests and correlates the various observations and conclusions as they apply to the specific areas of fuel pin performance.

5.1 ETR TESTS – NONINSTRUMENTED SERIES

A. R. Olsen

5.1.1 Experimental Plan

The noninstrumented thermal flux series of irradiation tests was initiated in 1966 before any irradiation experience on sol-gel-derived (U,Pu)O₂ fuels was available. The initial plan included a series of irradiation capsules to investigate the effects of fuel form (pellet, Sphere-Pac, Vi-Pac, and extrusion) and processing variables on fuel rod performance as a function of linear heat rate and burnup. The extrusion process was never fully developed, and irradiation tests of pellet and Vi-Pac fuel forms were being conducted by other sites, so the scope was reduced to limited comparison of pellet and Sphere-Pac forms, with emphasis on the Sphere-Pac performance characteristics. The primary performance characteristics determined as a function of linear heat rate and burnup were:

1. fuel restructuring,
2. fuel swelling,
3. fission gas release,
4. actinide redistribution,
5. fission product migration,
6. fuel-cladding mechanical interaction,
7. fuel-cladding chemical interaction.

The use of a thermal flux test reactor for these irradiations resulted in both advantages and disadvantages. The validity of tests in all the available test reactors was evaluated and discussed in a previous report.¹ The principal disadvantages of the thermal flux

tests are the lack of concurrent irradiation damage and swelling of the cladding and, because of self-shielding, radial fission rate distributions unlike those in a fast reactor. These drawbacks are offset by the advantages of available test space and the fact that depleted uranium can be used in the fuel at all linear heat rates of interest. The use of depleted uranium, so that all fissions occur in plutonium, is of particular importance because the fission product yields are typical of commercial LMFBR fuels. Thus, the redistribution of these fission products and their influence on fuel compositions and oxygen potentials as a function of burnup, together with the effects of these changes on fuel swelling, thermal conductivity, and fuel-cladding chemical interaction can be tested without bias. With the exception of the first four pins irradiated, only depleted uranium was used in these tests.

The total group of 11 uninstrumented capsules tested in the ETR is listed in Table 5.2 together with the peak operating conditions in each capsule. Experiments 43-99 through 43-115 were irradiated primarily for performance analysis. Experiments 43-116 through 43-123 were, and are being, irradiated to provide short-cooled irradiated fuel for reprocessing studies. We will discuss only the six capsules irradiated for performance analysis.

The capsules were designed to be irradiated in X-baskets in the ETR. A number of locations in this reactor will accommodate such X-baskets, each with a different peak flux and all with cosine axial flux distribution. A typical flux distribution and pin arrangement are shown in Fig. 5.1. Thus a single design would permit tests over a range of peak linear heat rates, with two positions (2 and 3) being comparable. Specific capsules were relocated to higher flux positions to maintain specified heat rates despite fissile depletion.

The capsule and pin designs are shown schematically in Fig. 5.2. Each capsule contained four pins mounted in tandem and immersed in NaK-44. The fuel pin cladding was annealed type 304 stainless steel tubing 0.252 in. OD with a 0.010-in. wall thickness for experiments 43-99 through 43-116 and type 316 (20% cold worked) 0.230 in. OD with a 0.015-in. wall thickness for experiments 43-117 through 43-123. Each 7.5-in.-long pin contained a 3.1-in. fuel column with ThO₂ or UO₂ insulator pellets at each end and a 3-in.-long gas plenum filled with SiO₂-Al₂O₃ fiber.

For the performance analysis tests, 20 pins were loaded by the Sphere-Pac technique to 84 ± 0.5% volume fraction. Each bed was made up of two sizes of microspheres – a coarse bed of 300 to 600 μm diam and fines below 44 μm diam. The three Sphere-Pac

1. A. R. Olsen, R. B. Fitts, and C. M. Cox, "Analysis of the Validity of Fast Reactor Fuel Tests in Existing Test Reactors," pp. 127-50 in *National Symposium on Developments in Irradiation Testing Technology Held at Sandusky, Ohio, September 9-11, 1969*, CONF-690910.

Table 5.2. Noninstrumented thermal flux tests of (U,Pu)O₂ fuels

| Experiment | Fuel | | Number of rods | Peak burnup (% FIMA) ^a | Peak linear heat rate (W/cm) | Peak cladding inner surface temperature (°C) |
|------------|-------------|---|----------------|-----------------------------------|------------------------------|--|
| | Form | Composition | | | | |
| 43-99 | Sphere-Pac | ²³⁵ U _{0.80} Pu _{0.20} O _{2.00} | 2 | 1.5 ^b | 1640 ^b | 1000 |
| 43-100 | Sphere-Pac | ²³⁵ U _{0.80} Pu _{0.20} O _{2.00} | 2 | 1.4 ^b | 1470 ^b | 900 |
| 43-103 | Sphere-Pac | UO _{2.02} (20% ²³⁵ U) | 3 | 5 | 690 | 530 |
| | Pellet | UO _{2.00} (20% ²³⁵ U) | 1 | | | |
| 43-112 | Sphere-Pac | ²³⁸ U _{0.85} Pu _{0.15} O _{1.97} | 3 | 0.7 | 500 | 360 |
| | | UO _{2.02} (20% ²³⁵ U) | 1 | | | |
| 43-115 | Sphere-Pac | ²³⁸ U _{0.85} Pu _{0.15} O _{1.97} | 3 | 11.3 | 480 | 390 |
| | | UO _{2.02} (20% ²³⁵ U) | 1 | 13.8 | | |
| 43-115 | Sphere-Pac | ²³⁸ U _{0.85} Pu _{0.15} O _{1.97} | 3 | 6.5 | 600 | 460 |
| | | UO _{2.02} (20% ²³⁵ U) | 1 | | | |
| 43-116 | Sphere-Pac | ²³⁸ U _{0.85} Pu _{0.15} O _{1.97} | 4 | 1.5 ^c | 600 ^c | 460 ^c |
| 43-117 | FTR pellets | ²³⁸ U _{0.75} Pu _{0.25} O _{1.98} | 4 | 2.5 ^c | 430 ^c | 360 ^c |
| 43-118 | FTR pellets | ²³⁸ U _{0.75} Pu _{0.25} O _{1.98} | 4 | 8.0 ^c | 430 ^c | 360 ^c |
| 43-119 | FTR pellets | ²³⁸ U _{0.75} Pu _{0.25} O _{1.98} | 4 | 10.0 ^c | 430 ^c | 360 ^c |
| 43-123 | FTR pellets | ²³⁸ U _{0.75} Pu _{0.25} O _{1.98} | 4 | 4.0 ^c | 430 ^c | 360 ^c |

^aFissions per initial actinide metal atom.

^bRods failed in reactor from overpowering.

^cTarget design values.

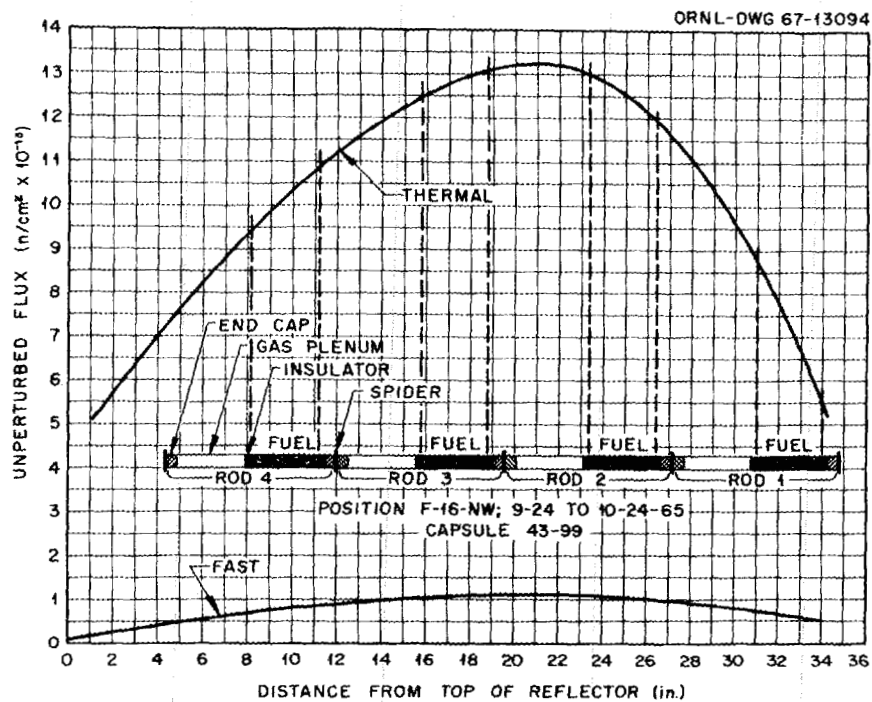


Fig. 5.1. Typical flux distribution for X-basket irradiation.

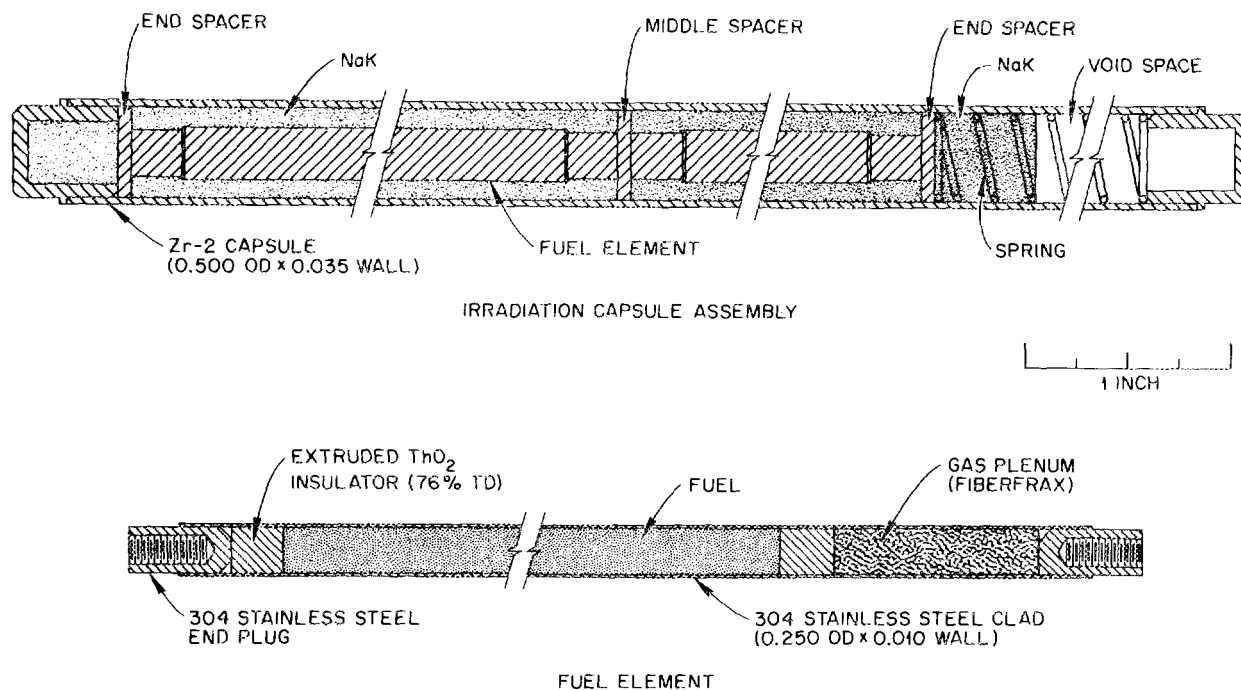


Fig. 5.2. Capsule for ETR tests.

fuel compositions were UO_2 (20% ^{235}U), $^{235}\text{U}_{0.8}\text{Pu}_{0.2}\text{O}_2$, and $^{238}\text{U}_{0.85}\text{Pu}_{0.15}\text{O}_2$. Details of the Sphere-Pac fuel preparation and pin fabrication are reported elsewhere.² In addition, one capsule contained one pin with pelletized UO_2 (20% ^{235}U) made from ADU powder.

All fuel pins were made with tight quality control procedures to assure both pin and capsule integrity and good postirradiation characterization of the components, particularly the fuel material.

5.1.2 Results of Irradiation Tests

The results of these tests have been reported as they became available both in progress reports and at various meetings.³⁻⁷ Detailed summary reports are in preparation. However, the tests can be briefly summarized by breaking them into three categories: low burnup, 43-99, 43-100, and 43-112; intermediate burnup 43-103 and 43-115; and high burnup, 43-113. The fabrication, operating data, and some postirradiation results for all pins are given in Table 5.3. It should be noted that the operating data reflect the actual operating conditions as determined from the history and postirradiation analy-

ses. Thus they include any variations in reactor flux environment.

2. F. G. Kitts, R. B. Fitts, and A. R. Olsen, "Sol-Gel Urania-Plutonia Microsphere Preparation and Fabrication into Fuel Rods," pp. 195-210 in *Intern. Symp. Plutonium Fuels Technol.*, Scottsdale, Ariz., 1967, *Nucl. Met.* 13, ed. by K. E. Horton, R. E. Macherey, and R. J. Allio, American Institute of Mining, Metallurgical, and Petroleum Engineers, New York, 1968.

3. A. R. Olsen, J. D. Sease, R. B. Fitts, and A. L. Lotts, *Fabrication and Irradiation Testing of Sol-Gel Fuels at Oak Ridge National Laboratory*. ORNL-TM-1971 (September 1967); also pp. 321-67 in *Sol-Gel Processes for the Production of Ceramic Nuclear Fuels*, Comitato Nazionale Energia Nucleare, Rome, 1968.

4. A. R. Olsen, C. M. Cox, and R. B. Fitts, "Low Burnup Irradiation Tests of Sphere-Pac Sol-Gel (U,Pu) O_2 Fuels" (summary), *Trans. Amer. Nucl. Soc.* 12(2), 605-6 (1969).

5. A. R. Olsen, "Intermediate Burnup Irradiation Tests of Sphere-Pac Sol-Gel Fuels" (summary), *Trans. Amer. Nucl. Soc.* 13(1), 32-33 (1970).

6. C. M. Cox, R. B. Fitts, A. R. Olsen, and A. L. Lotts, "Irradiation Performance of Sol-Gel (U,Pu) O_2 Fuels for Breeder Reactors," pp. 359-73 in *Symposium on Sol-Gel Processes and Reactor Fuel Cycles*, Gatlinburg, Tennessee, May 4-7, 1970, CONF-700502.

7. A. R. Olsen, "High-Burnup Irradiation Tests of Sphere-Pac Sol-Gel Fuels" (summary), *Trans. Amer. Nucl. Soc.* 15(1), 181-82 (June 1972).

Table 5.3. Fabrication and operating data for thermal flux prototype tests

| Fuel pin | Smear density (% of theoretical) | Fuel form ^a | Fuel composition | ²³⁵ U/U (%) | Peak linear heat rate ^c (kW/ft) | Peak cladding inner temperature (°C) | Fuel center $\int_{400^{\circ}\text{C}} \text{kdT}$ (W/cm) | Burnup (% FIMA) | | Equivalent full power days | Power cycles ^d | Fission gas release (% ⁸⁵ Kr) |
|----------|----------------------------------|------------------------|--|------------------------|--|--------------------------------------|--|-----------------|---------|----------------------------|---------------------------|--|
| | | | | | | | | Peak | Average | | | |
| 99-1 | 76 | SP | U _{0.80} Pu _{0.20} O _{2.00} | 93 | 34.6 | 730 | 56 | 1.4 | 1.2 | 18.9 | 11 | 24 |
| 99-3 | 76 | SP | U _{0.80} Pu _{0.20} O _{2.00} | 93 | 49.9 | 1000 | 84 | 2.8 | | 18.9 | 11 | |
| 100-1 | 76 | SP | U _{0.80} Pu _{0.20} O _{2.00} | 93 | 29.3 | 650 | 48 | 1.2 | 1.1 | 18.9 | 11 | |
| 100-3 | 76 | SP | U _{0.80} Pu _{0.20} O _{2.00} | 93 | 44.9 | 900 | 75 | 2.5 | 2.3 | 18.9 | 11 | |
| 112-1 | 79 | SP | U _{0.85} Pu _{0.15} O _{1.97} | 0.6 | 8.4 | 220 | 18 | 0.5 | 0.45 | 27.8 | 11 | 2 |
| 112-2 | 74 | SP | UO _{2.02} | 20.2 | 11.9 | 260 | 28 | 0.68 | 0.64 | 27.8 | 11 | 34 |
| 112-3 | 81 | SP | U _{0.85} Pu _{0.15} O _{1.97} | 0.6 | 13.6 | 320 | 31 | 0.68 | 0.67 | 27.8 | 11 | 27 |
| 112-4 | 80 | SP | U _{0.85} Pu _{0.15} O _{1.97} | 0.6 | 10.5 | 260 | 24 | 0.55 | 0.52 | 27.8 | 11 | 4 |
| 103-1 | 74 | SP | UO _{2.02} | 20.2 | 16.4 | 380 | 32 | 4.2 | 3.8 | 126.3 | 73 | 30 |
| 103-2 | 84 | P ^b | UO _{2.00} | 19.8 | 25.9 | 540 | 60 | 4.9 | 4.4 | 126.3 | 73 | 47 |
| 103-3 | 73 | SP | UO _{2.02} | 20.2 | 21.6 | 470 | 42 | 5.5 | 4.9 | 126.3 | 73 | 44 |
| 103-4 | 74 | SP | UO _{2.02} | 20.2 | 17.9 | 400 | 35 | 4.5 | 4.0 | 126.3 | 73 | 41 |
| 115-1 | 80 | SP | U _{0.85} Pu _{0.15} O _{1.97} | 0.6 | 18 | 400 | 40 | 6.7 | 6.2 | 174.2 | 97 | 31 |
| 115-2 | 74 | SP | UO _{2.02} | 20.2 | 17.0 | 390 | 31 | 5.9 | 5.8 | 174.2 | 97 | 47 |
| 115-3 | 82 | SP | U _{0.85} Pu _{0.15} O _{1.97} | 0.6 | 20.6 | 460 | 46 | 6.4 | 5.0 | 174.2 | 97 | 44 |
| 115-4 | 81 | SP | U _{0.85} Pu _{0.15} O _{1.97} | 0.6 | 13.4 | 370 | 32 | 4.2 | 4.1 | 174.2 | 97 | 38 |
| 113-1 | 82 | SP | U _{0.85} Pu _{0.15} O _{1.97} | 0.6 | 8.8 | 320 | 24 | 8.6 | 8.2 | 611 | 288 | 89 |
| 113-2 | 73 | SP | UO _{2.02} | 20.2 | 11.2 | 385 | 37 | 13.8 | 12.9 | 611 | 288 | 96 |
| 113-3 | 81 | SP | U _{0.85} Pu _{0.15} O _{1.97} | 0.6 | 10.1 | 370 | 32 | 11.3 | 11.2 | 611 | 288 | 61 |
| 113-4 | 80 | SP | U _{0.85} Pu _{0.15} O _{1.97} | 0.6 | 9.6 | 360 | 29 | 9.7 | 9.6 | 611 | 288 | 65 |

^aSP = Sphere-Pac, P = solid pellet.

^bThese pellets were prepared from ADU fuel and had a 4-mil average cold diametral gap between fuel and cladding.

^cTime-averaged values based on the total exposure in equivalent full power days.

^dCycles from greater than 50% full power to less than 50% full power.

5.1.2.1 Low-Burnup Test Results

The first two capsules irradiated, ORNL 43-99 and ORNL 43-100, contained two elements each of $^{235}\text{U}_{0.8}\text{Pu}_{0.2}\text{O}_2$ fuel at 76% smear density (weight of fuel divided by volume as determined from the inside diameter of the tube) and of $\text{Th}_{0.95}\text{Pu}_{0.05}\text{O}_2$ fuel (also Sphere-Pac) at 84% smear density. The (Th,Pu) O_2 pins will not be discussed here. These tests were intended to operate at a calculated maximum cladding surface temperature of 475°C and linear heat rating of 650 W/cm. These tests were to be compared with fast reactor irradiations of the same (U,Pu) O_2 fuels to be conducted by Argonne National Laboratory.

The (U,Pu) O_2 pins were inadvertently operated at excessively high powers. The hottest pin (approx 50 kW/ft) in each capsule failed during a return to power following a reactor shutdown after 16.5 days of continuous operation at the peak heat rates. Subsequent examination revealed that molten fuel had penetrated the center of the upper ThO_2 insulator pellet and that the cladding failed in the plenum region.

There was some evidence of a fuel-cladding reaction in these high-heat-rate pins, which had calculated cladding temperatures as high as 1000°C, but no gross incompatibility was observed. Transverse microstructures of one pin that operated at 35 kW/ft and did not fail can be seen in Fig. 5.3(a). The fuel has restructured so that only the smallest microspheres around the periphery can be identified.

The next experiment, 43-112, operated at moderate heat rates (8 to 14 kW/ft) to low burnup to verify the

revised power analyses. Postirradiation examinations showed no change in fuel column heights, no cladding deformation, and no fuel-cladding reactions. In Fig. 5.3(b) and (c), typical restructuring of the Sphere-Pac fuel is shown. These low-burnup tests showed no macroscopic evidence of fuel sintering for heat rates below 9 kW/ft. However, at the higher heat rates we saw definite evidence of columnar grain growth, and the unique structure gave clear evidence of the vaporization-condensation mode of restructuring. This can be seen in Fig. 5.4. The test results confirmed our methods of design and provided confirmation of our temperature calculations as well as information on grain growth, all of which indicated that Sphere-Pac performance was similar to that of pellet fuels. Microprobe analyses of actinide distributions in Fig. 5.5 showed that uranium moved preferentially down the temperature gradient in the columnar grain region.

5.1.2.2 Intermediate-Burnup Test Results

The two capsules, 43-103 and 43-115, irradiated to moderate burnup (4 to 6% FIMA) contained five UO_2 -fueled pins and three (U,Pu) O_2 pins. Seven pins were fabricated by the Sphere-Pac process and one pin contained pellets made from ADU powder. The irradiation conditions for both capsules were more stringent than expected in that both the fuel burnup analysis and the fluence measurements by cobalt activation in the stainless steel components indicated that the actual flux was 15 to 30% greater than anticipated from previous ETR flux measurements. This resulted in high linear

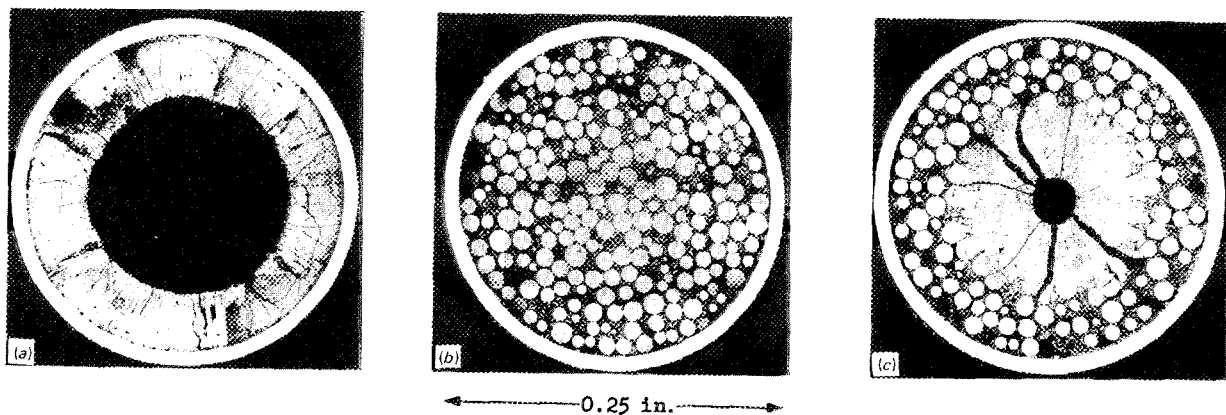


Fig. 5.3. Transverse cross sections of Sphere-Pac fuel pins after irradiation to low burnup. (a) $\text{U}_{0.80}\text{Pu}_{0.20}\text{O}_{2.00}$; 35 kW/ft to 1.4% FIMA; 76% smear density. (b) $\text{U}_{0.85}\text{Pu}_{0.15}\text{O}_{1.97}$; 10.5 kW/ft to 0.6% FIMA; 80% smear density. (c) $\text{U}_{0.85}\text{Pu}_{0.15}\text{O}_{1.97}$; 13.6 kW/ft to 0.7% FIMA; 81% smear density.

R-51301

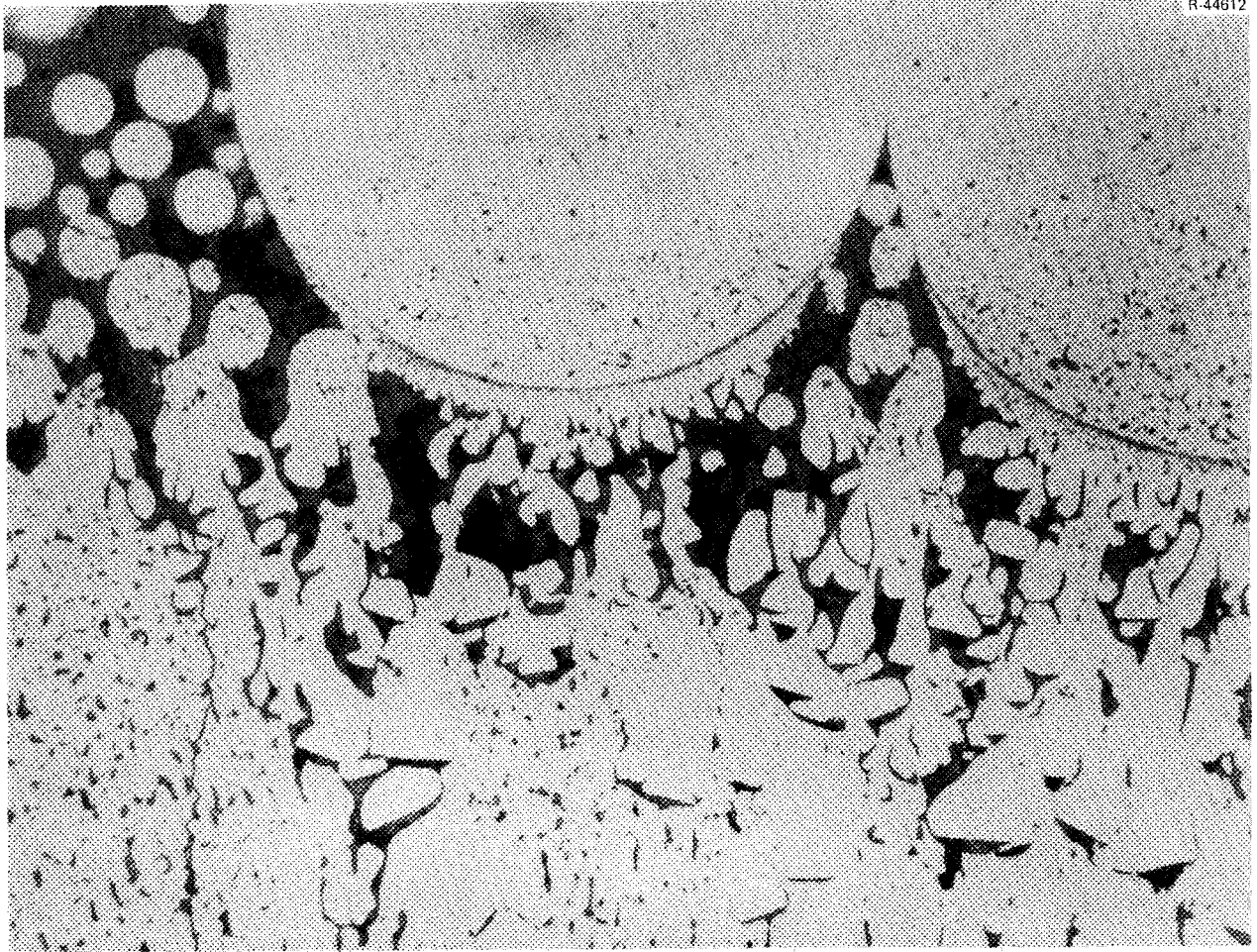


Fig. 5.4. Fuel deposits on the inner surface of microspheres located at the periphery of the columnar grain-growth region. 200 \times . Reduced 37%.

heat rates, particularly for the two central pin positions (2 and 3). The highest time-averaged heat rate of 25.9 kW/ft was developed in the pellet pin 103-2. A comparable heat rate would have been achieved in the adjacent Sphere-Pac pin 103-3 except for the lower smear density. This low smear density is the result of low sphere density in these early production materials, not low volume packing of the spheres. The tabulated time-averaged linear heat rates are less than the peak heat rates at start of irradiation, so some melting occurred in the central pins of both capsules, at least early in the irradiation history. The measured fission gas release rates are typical for oxide fuel irradiated in a thermal flux to 5 to 6 at. % burnup. The cladding diameter measurements after irradiation showed no significant changes from preirradiation measurements.

The fuel central melting and the use of low-density ThO₂ insulators produced some interesting fuel move-

ment phenomena. The postirradiation gamma scans of the two capsules are shown in Fig. 5.6. The axial flux distribution is highest in the center and drops off at each end. Fuel slumping is apparent in three of the pins — the UO₂ pellet pin (103-2) in one capsule and both the UO₂ (115-2) and (U,Pu)O₂ (115-3) pins in the second capsule. Normal burnup distributions are shown for the top and bottom pins in both capsules. For all four of the hottest pins, there is also evidence of fuel above the upper ThO₂ insulator, with gamma activity depressions at the insulator locations, indicating that at least some of the ThO₂ is still present. Fuel penetration through these insulators and into the Fiberfrax-filled gas plenum is more clearly shown in Fig. 5.7 in the neutron radiographs of capsule 43-115. A central void is shown in all four fuel pins, and fuel is above the upper insulator in the two center pins. In addition, it is interesting to note that flux peaking at the fuel column

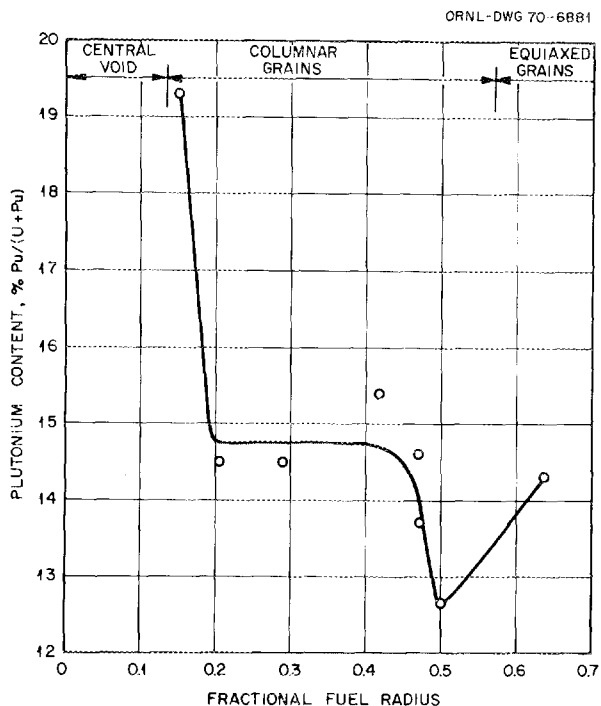


Fig. 5.5. Variation in plutonium content with radial position for $U_{0.85}Pu_{0.15}O_2$ after irradiation at a linear heat rate of 13.6 kW/ft to a burnup of 0.7% FIMA.

ends has resulted in greater fuel restructuring with consequently larger diameter central voids.

Figure 5.8 shows typical transverse sections for the three pins with the highest heat rates. The central void diameter is inversely proportional to the original fuel smear density, and the extent of columnar grain growth is proportional to the linear heat rate. The only significant difference between the Sphere-Pac and pellet fuels is the fact that some spheres remain at the fuel-cladding interface, even at 5% burnup and the high linear heat rate of 22 kW/ft. Analysis of the extent of restructuring in the rods with lower heat rate indicated that the effective thermal conductance of the Sphere-Pac beds is equivalent to that of pellet fuels with similar density.

The unique structure of the Sphere-Pac beds provided clear evidence of the fact that uranium-rich vapors migrated down the temperature gradient in the $(U,Pu)O_2$ pins in these tests. This is shown in Fig. 5.9. This figure shows the microstructure, alpha autoradiograph, and beta-gamma autoradiograph of pin 115-4. The absence of a ring structure in the beta-gamma autoradiograph clearly indicates that there was no fuel melting in this pin. The most interesting features are in the alpha autoradiograph. The typical increase in plutonium activity near the central void, usually seen in

pellet fuel irradiations, is apparent. What is unique is the appearance of spherical islands of higher plutonium concentration in the cooler regions of the columnar grain growth structure. Migration of UO_2 -enriched vapor from the higher temperature center resulted in the apparent plutonium enrichment in the highest temperature region. The UO_2 -rich vapors condensed in the cooler regions and filled the voids around the larger microspheres. At intermediate temperatures, diffusion can provide homogenization, but at the lower temperatures near the periphery of the columnar grains, even 3000 hr was insufficient for homogenization. This was later confirmed by microprobe analysis of these regions, which showed the distinct changes in plutonium content at sphere surfaces.

No evidence of fuel-cladding chemical interaction was seen in any of these pins. However, some evidence of microstructural changes in the cladding of the pellet pin 103-2 is shown in Fig. 5.10. Comparison of the two cladding structures shows that significant carbide precipitation has occurred at grain boundaries where the cladding temperature was above $500^\circ C$. This precipitation under irradiation occurred at a temperature approximately $80^\circ C$ below the out-of-reactor precipitation temperature range. At the time, we suggested that such precipitates might provide the paths for fission product migration and the type of intergranular attack reported by other experimenters. Some out-of-reactor tests to investigate this proposed mechanism were initiated.⁸

5.1.2.3 High-Burnup Test Results

Only one capsule in this series was taken to a high burnup level. Capsule 43-113 was irradiated for 611 effective full-power days of reactor operation. The capsule was moved twice to higher flux positions in the reactor to compensate for the decrease in the linear heat rate with burnup.

The greater fissile content of the UO_2 (20% ^{235}U) tended to maintain a more constant heat rate. This pin started at a linear heat rate of 14.3 kW/ft and was operating at approximately 8 kW/ft at the end of the irradiation. The $(U,Pu)O_2$ pin in position 1 started at 10.6 kW/ft and ended at approximately 7 kW/ft, while both pins 3 and 4 ended irradiation at approximately 6

8. R. B. Fitts, E. L. Long, Jr., and J. M. Leitaker, "Observations of Fuel-Cladding Chemical Interactions as Applied to GCBR Fuel Rods," pp. 431-58 in *Proc. Conf. Fast Reactor Fuel Element Technology*, ed. by Ruth Farmakes, American Nuclear Society, Hinsdale, Illinois, 1971.

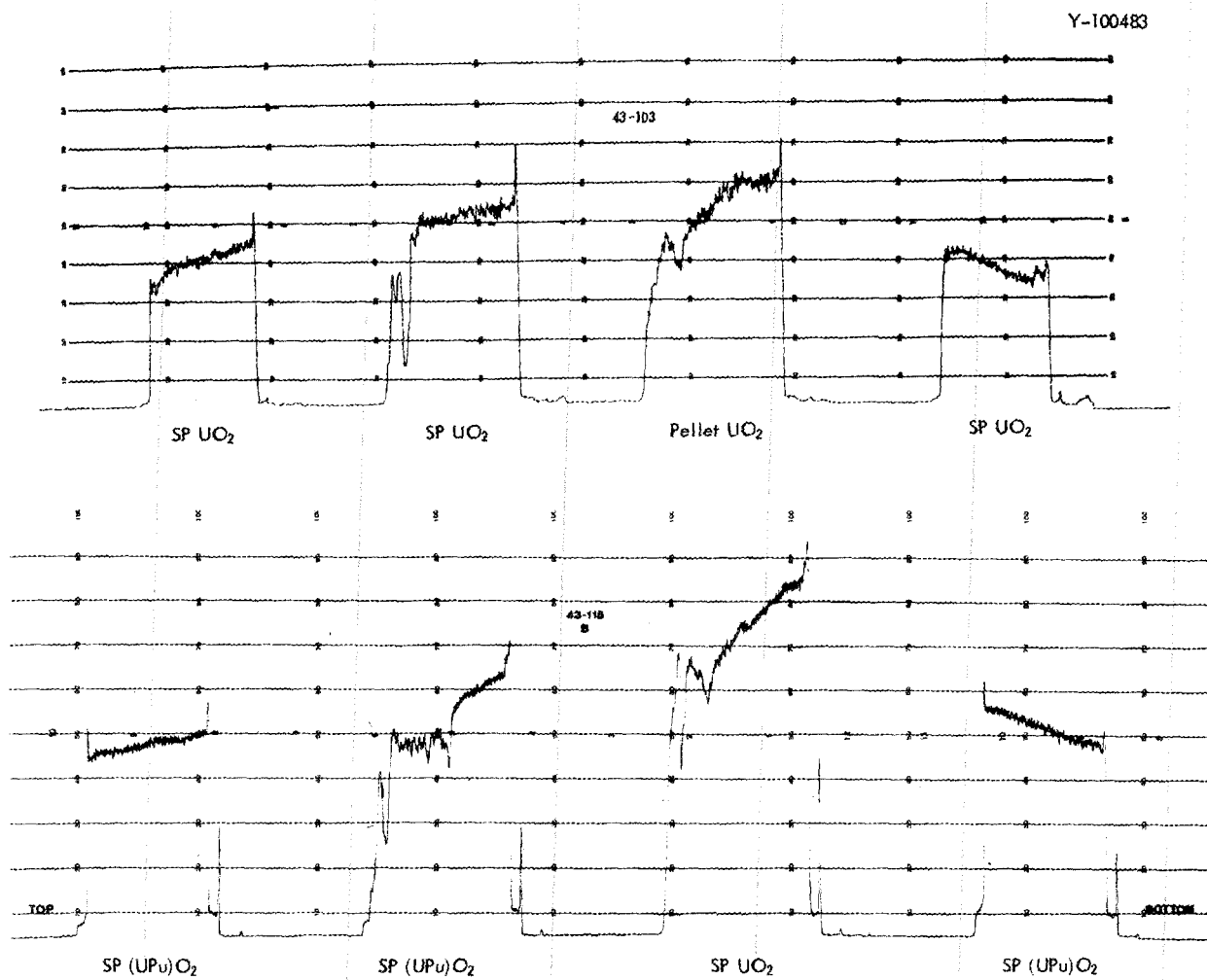


Fig. 5.6. Postirradiation gamma scans of capsules 43-103 and 43-115.

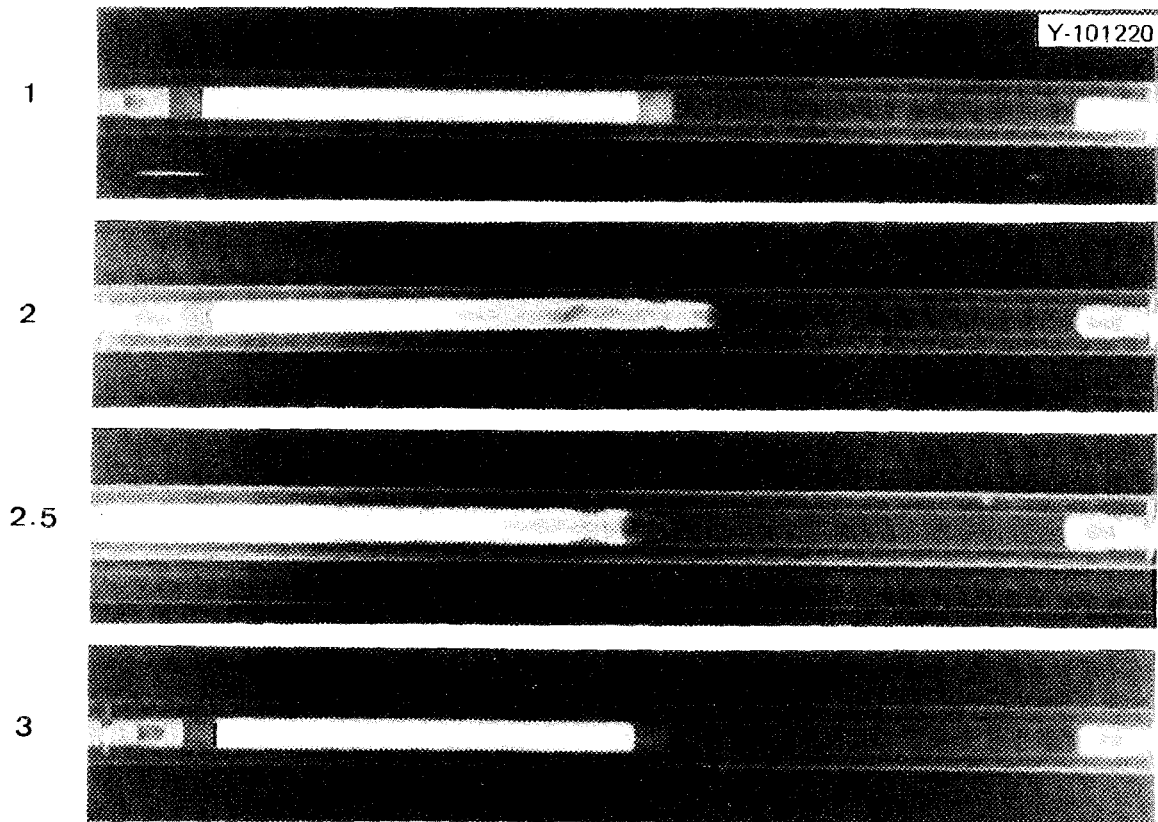


Fig. 5.7. Neutron radiographs of test pins from capsule 43-115.

R-51302

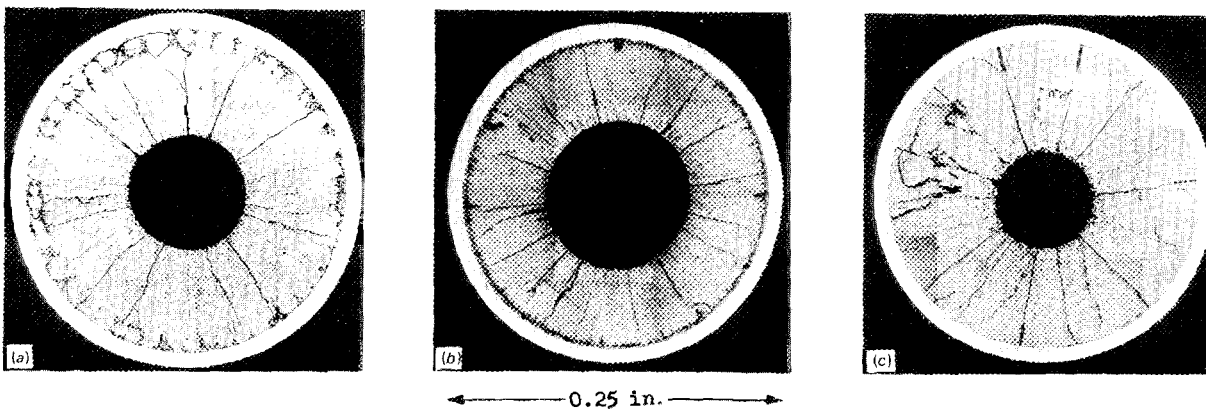


Fig. 5.8. Transverse cross sections of fuel pins after irradiation to moderate burnup. (a) $U_{0.85}Pu_{0.15}O_{1.97}$; 20 kW/ft to 6% FIMA; 82% smear density. (b) Sphere-Pac $UO_{2.02}$; 22 kW/ft to 5.5% FIMA; 73% smear density. (c) Pelletized $UO_{2.00}$; 26 kW/ft to 5.7% FIMA; 84% smear density.

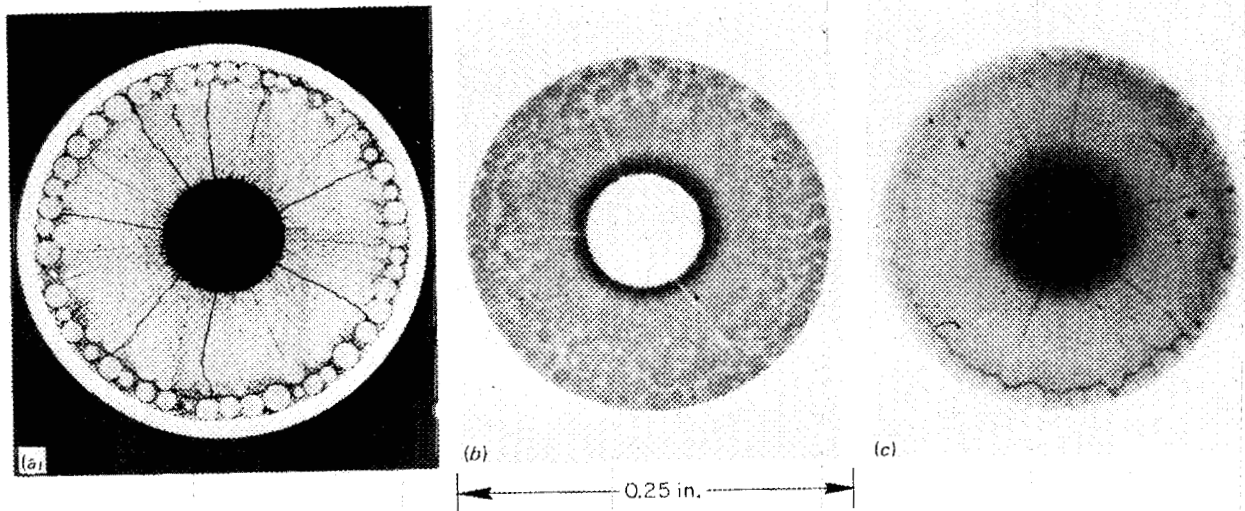


Fig. 5.9. Sphere-Pac $(U-15\%Pu)O_{1.97}$ irradiated at 14 kW/ft to 4.2% FIMA. Smear density 81% of theoretical. (a) Photograph; (b) autoradiograph; (c) beta-gamma autoradiograph.

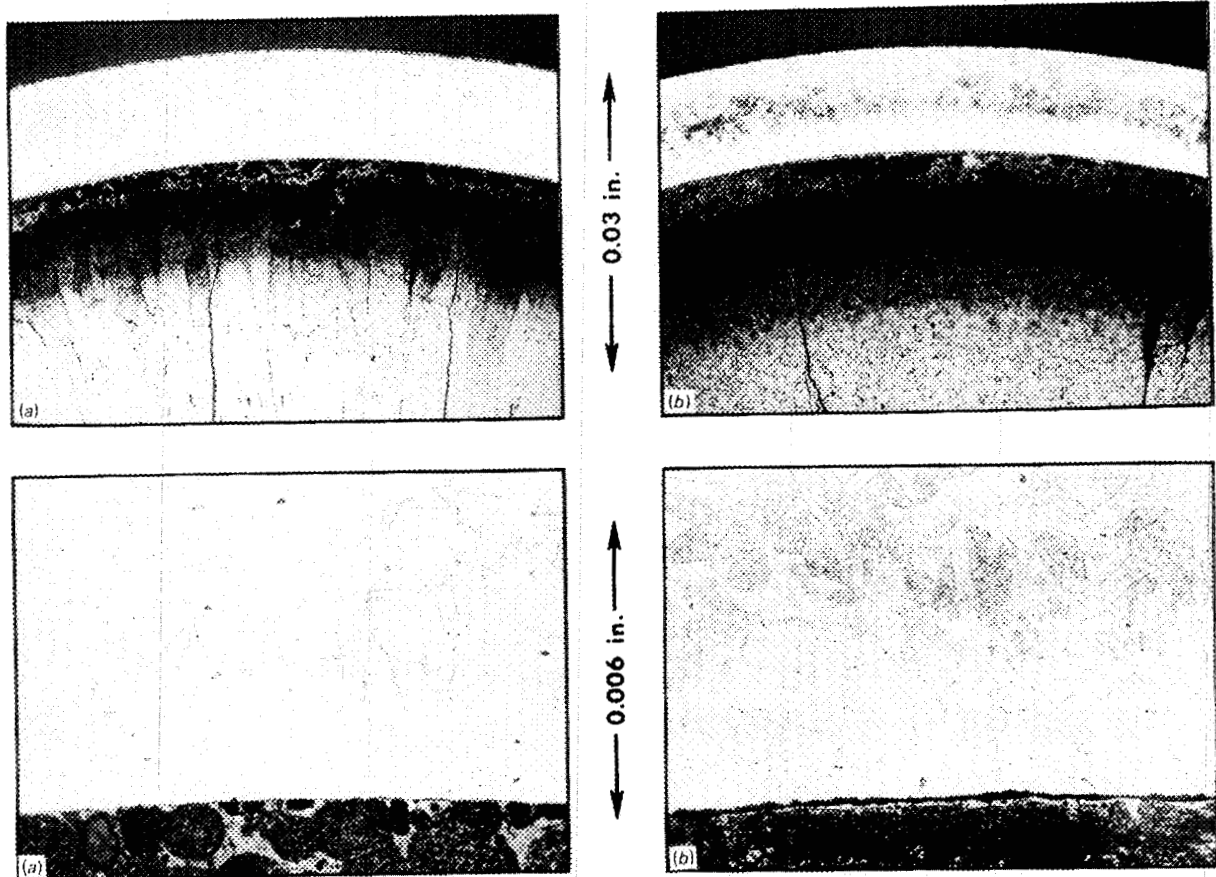


Fig. 5.10. Appearance of type 304 stainless steel cladding after 3000 hr irradiation at inner surface temperatures of (a) 470°C and (b) 540°C.

kW/ft, even though they started at 14.7 and 12.5 kW/ft respectively. The effects of initial fissile content and depletion are seen in the burnup values, which for the (U,Pu)O₂ pins are tending toward a common value despite variations in initial linear heat rates, and the UO₂ with the higher fissile content has achieved the highest burnup. The rate of change of the fission rates as a result of depletion appears to have affected the integrated fission gas release rates. Although with these limited data we can only hypothesize, we know that the more rapid drops in fission rates for pins 3 and 4 from depletion resulted in extended operation at lower

overall fuel temperatures. Therefore, much of the fission gas created in the later stages of irradiation was trapped in the cooler fuel, thus giving lower integrated percentages of gas release.

The neutron radiographs shown in Fig. 5.11, together with the gamma scans on these pins, clearly show no overpower operation. The ThO₂ insulators are intact. Central voids are still present in all pins, roughly proportional to the start-of-life heat rating and increasing with decreasing initial smear density, so fuel swelling has not consumed the available fabrication voidage. In fact, the fuel columns showed a decrease in length of 1

R-59488

PIN 4 (U,Pu)O₂PIN 3 (U,Pu)O₂PIN 2 UO₂PIN 1 (U,Pu)O₂

Fig. 5.11. Neutron radiographs of pins from capsule 43-113.



43-113-1, 8.8 kW/ft, 8.6% FIMA



43-113-4, 9.6 kW/ft, 9.7% FIMA

Fig. 5.12. Comparative microstructures of $U_{0.85}Pu_{0.15}O_{1.98}$ fuel pins. As polished.

to 4%, and this decrease was also greater, the smaller the initial smear density.

An effect of the peak linear heat rate on restructuring can be seen in Fig. 5.12, where the extent of columnar grain growth is proportional to the highest linear heat rates at start of life even though the extent of the more or less solid core region, as defined by the circumferen-

tially oriented crack, has been extended to essentially the same radial position on both pins by more time-dependent sintering processes.

Some of the grain structures in pin 113-1 are shown in Fig. 5.13. At the magnifications available with the metallograph, distinct grains can be seen out to the circumferential crack. Note also the short length-to-

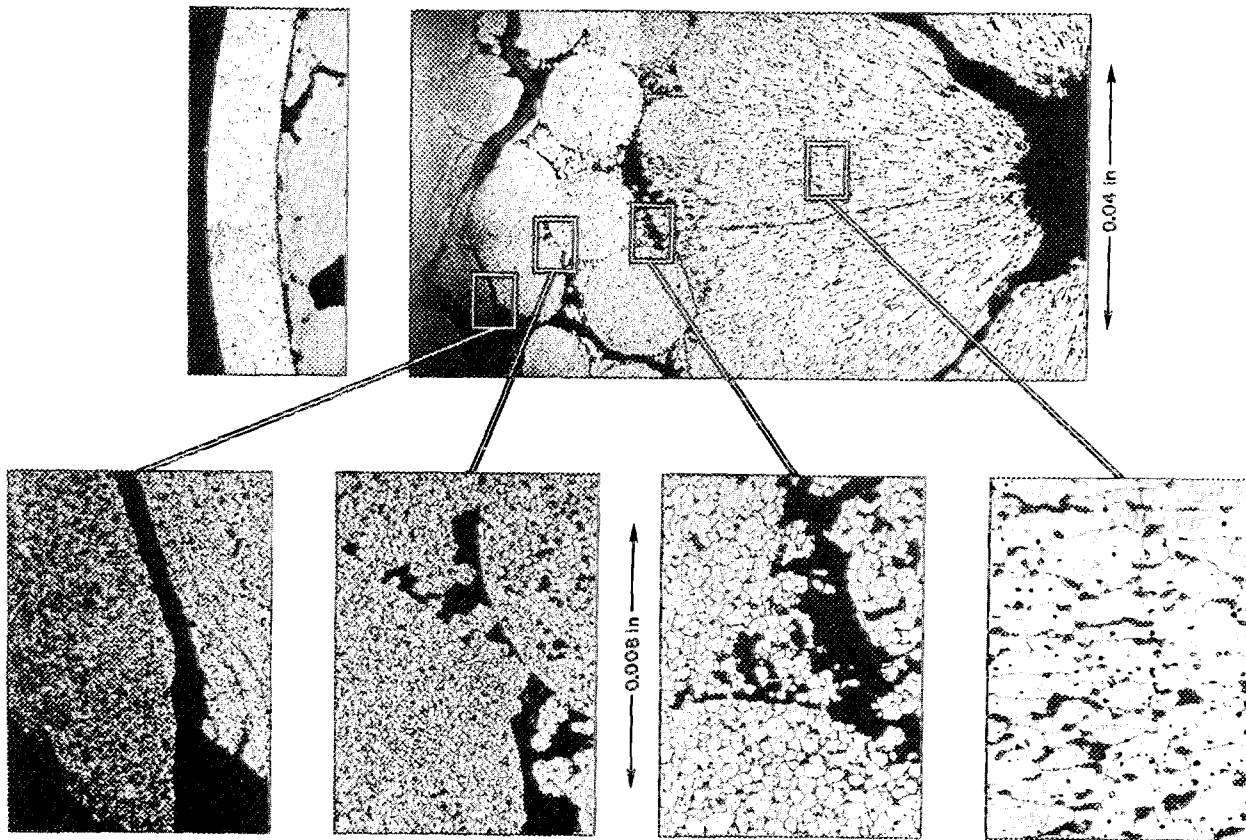


Fig. 5.13. Etched fuel structures in pin 43-113-1.

diameter ratio of the columnar grains, indicating grain refinement during the extended burnup. The columnar grains also contain subgrain boundaries with voids or bubbles on them. With the termination of the program we have not investigated the details of these structures with electron microscopy as we did with earlier structures.⁹⁻¹¹ The general darkening of the structure near the cladding is the result of increased sensitivity to the fuel etchant, making the structure difficult to photograph. The section to the left of the composite

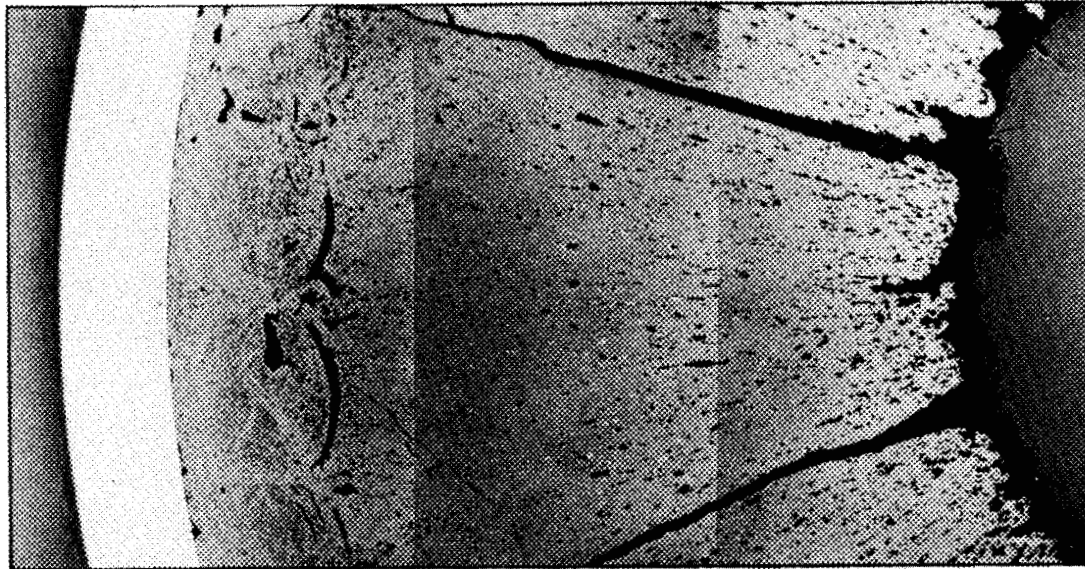
9. A. R. Olsen, R. B. Fitts, and W. J. Lackey, "In-Reactor Restructuring Temperatures and Kinetics for (U,Pu)O₂," pp. 579-602 in *Proc. Conf. Fast Reactor Fuel Element Technology*, ed. by Ruth Farmakes, American Nuclear Society, Hinsdale, Illinois, 1971.

10. W. J. Lackey, R. A. Bradley, and C. M. Cox, "In-Reactor and Out-of-Reactor (U,Pu)O₂ Grain Growth Kinetics" (abstract), *Amer. Ceram. Soc. Bull.* 50(9), 788 (September 1971).

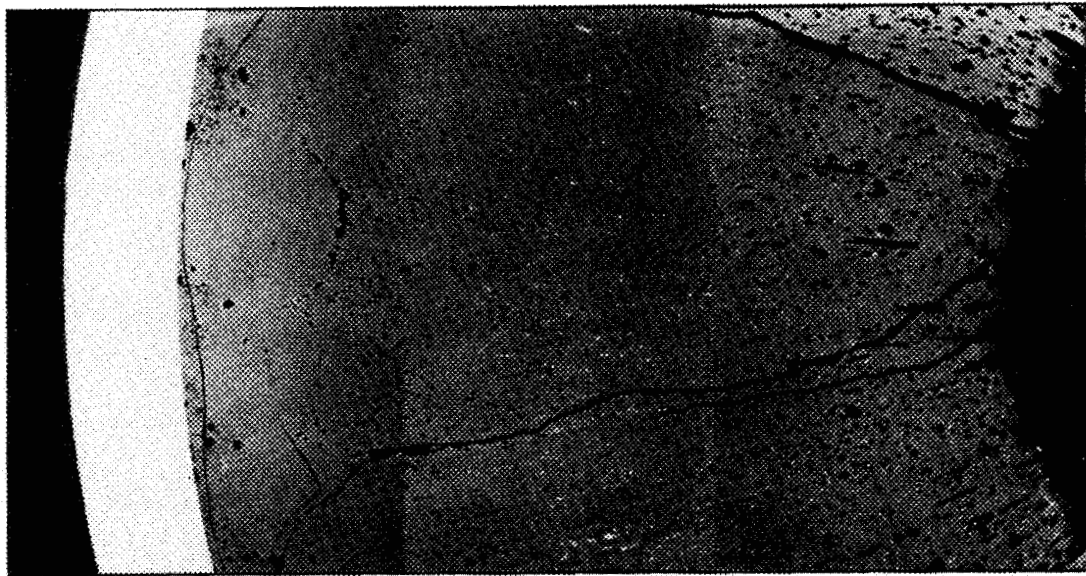
11. W. J. Lackey and F. J. Homan, "Porosity and Actinide Redistribution, Grain Growth, and Desintering in (U,Pu)O₂" (abstract), *Amer. Ceram. Soc. Bull.* 51(4), 387 (April 1972).

shows the unetched fuel and etched cladding. Here it is apparent that material has accumulated to fill the space between spheres. This was true for both UO₂ and (U,Pu)O₂ fuels, as can be seen in Fig. 5.14. When these structures are etched, one can clearly see the original coarse and fine microspheres in a more heavily etched matrix in the regions adjacent to the cladding.

We attempted to identify this matrix material by microprobe analysis. Such analyses were hampered by the significant background caused by the activity, even in sections as thin as $\frac{1}{8}$ in. We found most of the high-yield fission products, including Ba, La, and Zr, but no definite evidence of any particular accumulations other than Cs and Mo. Figure 5.15 shows some of the microprobe data for the peak-burnup (U,Pu)O₂ pin 113-3. On the bottom is plotted the Pu/(U + Pu) ratio as a function of radial location from the central void to the cladding. There is a distinct increase in the ratio near the central void. The distinct peaking in plutonium content just inside the normal dip in plutonium content



43-113-2 $\text{UO}_{2.00}$ 10.8 kW/ft 12% FIMA



43-113-3 $(\text{U}_{0.85}\text{Pu}_{0.15})\text{O}_{1.98}$ 11.3 kW/ft 11.3% FIMA

↑
0.06 in
↓

Fig. 5.14. Comparative microstructures of two fuels, as polished.

at the edge of the columnar grain region is minor but real and was confirmed by several traverses along different radii. With the exception of this minor peak, the distribution is what one would normally obtain from UO_2 -enriched vapor migration down the tempera-

ture gradient during start-of-life restructuring. There is no evidence of a change in actinide distribution as a result of the change in the fuel oxygen-to-metal ratio at these high burnup levels. Certainly the oxygen-to-metal ratio in the fuel should be greater than 2.00 at this

burnup.^{12,13} Some of the effects of this change in oxidation potential can be seen in the two fission product analyses shown in the center of the figure.

We measured the molybdenum-to-ruthenium ratios for at least ten metallic inclusions at selected radial locations and attempted to measure the relative molybdenum and ruthenium content of the oxide adjacent to each of these ingots. The ruthenium analyses in the oxide were masked by the activity and therefore are not reported. Both the ratio numbers and the relative molybdenum intensity readings clearly show a migration of molybdenum down the temperature gradient. The lack of metallic inclusions in the colder regions may indicate a movement of ruthenium up the temperature gradient or a lack of segregation at the lower fuel temperatures. The increasing molybdenum content in the oxide clearly indicates a change in the oxidation potential, with the molybdenum oxidizing in the cooler regions.

In summary then, the high-burnup thermal flux tests of Sphere-Pac fuel have:

1. confirmed that columnar grains are limited to the regions of active vapor transport and that extended exposure simply refines the columnar structure while extending the area of the time-dependent sintering;
2. provided indirect evidence that fission gas release depends more on fuel temperature than on burnup (this has also been indicated in data reported by others¹⁴);
3. provided clear evidence of molybdenum migration down the temperature gradient and its incorporation into the oxide phase in the cooler regions;
4. clearly shown that Sphere-Pac fuels can achieve very high burnup with essentially no mechanical interaction between fuel and cladding.

Additional work needs to be done to define the composition of the matrix material found in the cooler

12. J. M. Leitnaker, J. P. DeLuca, and R. B. Fitts, "Influence of Burnup on Reactivity of Oxide Fuel with Cladding" (summary), *Trans. Amer. Nucl. Soc.* 14(1), 177 (June 1971).

13. A. R. Olsen, R. B. Fitts, and C. M. Cox, "Analysis of the Validity of Fast Reactor Fuel Tests in Existing Test Reactors," pp. 127-50 in *National Symposium on Developments in Irradiation Testing Technology Held at Sandusky, Ohio, September 9-11, 1969*, CONF-690910.

14. J. B. Lambert et al., "Performance of Mixed-Oxide Fuel Elements - ANL Experience," pp. 517-33 in *Proc. Conf. Fast Reactor Fuel Element Technology*, ed. by Ruth Farmakes, American Nuclear Society, Hinsdale, Ill., 1971.

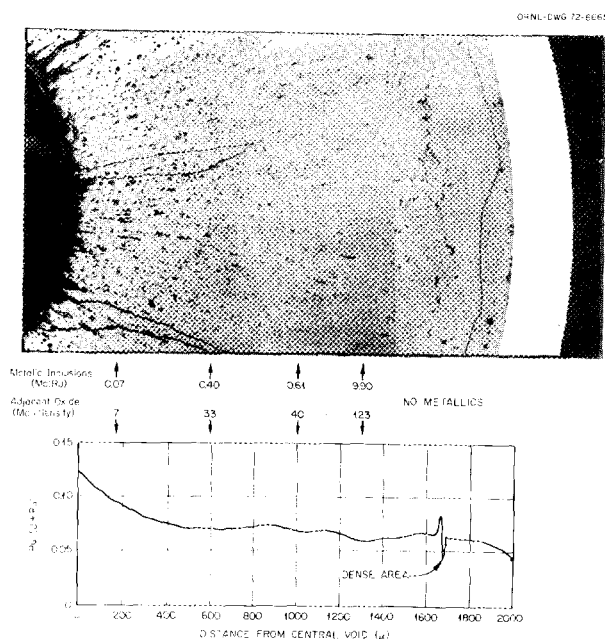


Fig. 5.15. Radial variations in composition for pin 43-113-3. Between the photomicrograph and the plutonium ratio tracing are molybdenum-to-ruthenium ratios measured in metallic inclusions at various locations and relative molybdenum concentrations in adjacent oxide.

fuel regions after high burnup, and electron microscope examinations should be made to establish the mode of gas retention in the cooler fuels.

5.2 ORR THERMAL PERFORMANCE TESTS

R. B. Fitts F. L. Miller¹⁵

5.2.1 Experimental Plan

The ORR instrumented thermal performance tests (SG series) were conducted to determine and compare the effective thermal conductance of low-burnup pellet¹⁶ and Sphere-Pac¹⁷ (U,Pu)O₂ fuels with similar smear densities and operating conditions. In addition,

15. Mathematics Division.

16. R. A. Bradley, *Fuels and Materials Development Program Quart. Progr. Rep. Sept. 30, 1969*, ORNL-4480, pp. 6-8; see also Sect. 5.2 of this report.

17. F. G. Kitts, R. B. Fitts, and A. R. Olsen, "Sol-Gel Urania-Plutonia Microsphere Preparation and Fabrication into Fuel Rods," pp. 195-210 in *Intern. Symp. Plutonium Fuels Technol., Scottsdale, Ariz., 1967*, *Nucl. Met.* 13, American Institute of Mining, Metallurgical, and Petroleum Engineers, New York, 1968; see also Sect. 3.1 of this report.

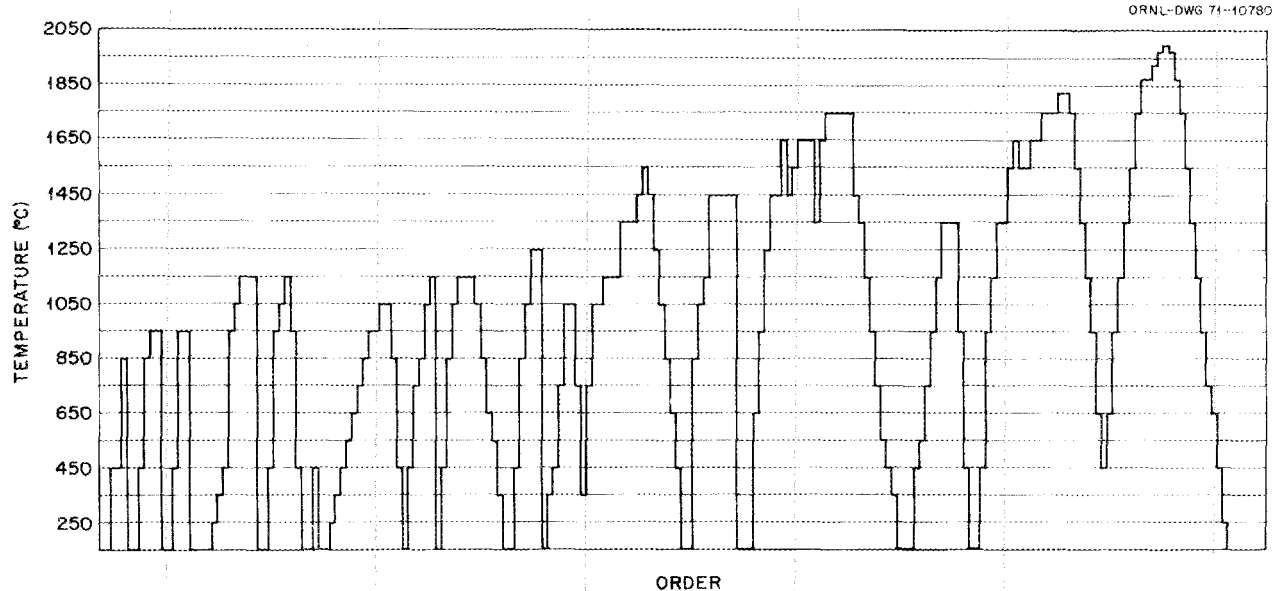


Fig. 5.16. Capsule SG-3 operating sequence.

these tests were used to examine the temperature-structure relationship in the fuels and the chemical interactions between the fuels and claddings.

Three capsules were irradiated in this series. Each contained two fuel pins for direct comparison of their performance. The first capsule (SG-1)¹⁸ was used to evaluate the capsule design, the second capsule (SG-2)^{19,20} was operated at low power (≈ 12 kW/ft) to examine Sphere-Pac fuel structures at central temperatures below 1500°C , and the third capsule²⁰⁻²² (SG-3) compared Sphere-Pac and pellet fuel pins at fuel central temperatures up to 2000°C .

5.2.2 Design and Operation

The SG irradiation capsules were operated in the Poolside Facility²³ of the Oak Ridge Research Reactor, where the highly instrumented capsule can be moved so as to operate at any desired heat generation rate up to 20 kW/ft at any time during the test. A typical operating sequence is plotted in Fig. 5.16, where the fuel central temperature was held constant for periods ranging from 15 min to 3 days, with the long holds occurring at each new maximum temperature.

The capsule design is shown in Fig. 5.17 for SG-1 and -2, in which the lower fuel pin contained a dummy thermocouple well. Capsule SG-3 contained an active thermocouple in both fuel pins. Each capsule contained two $(\text{U,Pu})\text{O}_2$ fuel pins clad in titanium-modified type 304 stainless steel. The fuel pins operated one above the

other, immersed in NaK contained in a double-wall capsule. Each pin was monitored at fuel midlength by 12 thermocouples, as shown schematically in Fig. 5.18. These measured the fuel central temperature, the cladding temperature at three points, and the radial heat flow. The heat flow was determined from four pairs of thermocouples embedded in the outer capsule wall.

The fabrication and operating conditions for the fuel pins are summarized in Table 5.4. Fuel pin 6 was shielded by a cadmium sleeve during the final stages of operation to keep the pellet central temperature from exceeding 2000°C while the Sphere-Pac fuel was operating at 2000°C .

18. R. B. Fitts and V. A. DeCarlo, "Instrumented Tests," *Metals and Ceramics Div. Annu. Progr. Rep. June 30, 1968*, ORNL-4370, pp. 145-49.

19. R. B. Fitts and V. A. DeCarlo, "ORR Instrumented Tests," *Metals and Ceramics Div. Annu. Progr. Rep. June 30, 1969*, ORNL-4470, pp. 135-37.

20. R. B. Fitts et al., "ORR Instrumented Tests," *Metals and Ceramics Div. Annu. Progr. Rep. June 30, 1970*, ORNL-4570, pp. 56-57.

21. R. B. Fitts, "ORR Instrumented Thermal Performance Tests," *Metals and Ceramics Div. Annu. Progr. Rep. June 30, 1971*, ORNL-4770, pp. 50-51.

22. R. B. Fitts and F. L. Miller, "Analysis of ORR Instrumented Thermal Performance Tests," *Metals and Ceramics Div. Annu. Progr. Rep. June 30, 1972*, ORNL-4820, pp. 66-67.

23. D. B. Trauger, *Some Major Fuel Irradiation Test Facilities of the Oak Ridge National Laboratory*, ORNL-3674 (April 1964).

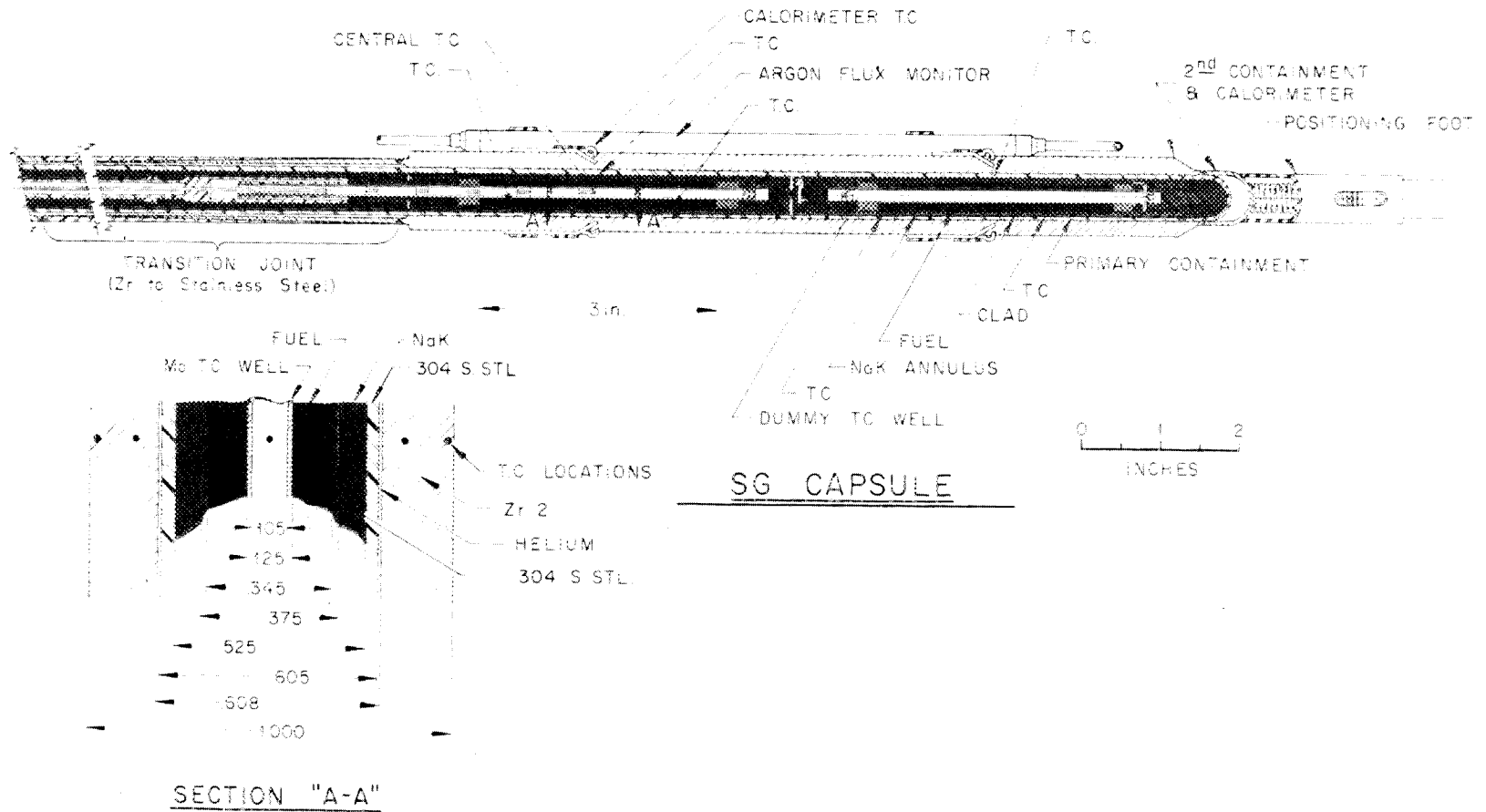


Fig. 5.17. SG capsule design.

Table 5.4. ORR instrumented capsules

| Capsule | Fuel pin ^a | Fuel | | | | Operation | | | |
|---------|-----------------------|---------------------|-----------------|------|--------------------------------------|-----------------|---------------------------------------|----------------------------------|---------------------------------|
| | | Form | Pu/(U + Pu) (%) | O/M | Smear ^b density (% theo.) | Total time (hr) | Maximum ^c temperature (°C) | Time at maximum temperature (hr) | Maximum heat generation (kW/ft) |
| SG-1 | 1 | Sphere-Pac | 15 | 1.99 | 81 | 1200 | >1800 | <i>d</i> | 15 |
| | 2 | Sphere-Pac | 15 | 1.99 | 81 | 1200 | <i>e</i> | <i>d</i> | 15 |
| SG-2 | 3 | Sphere-Pac | 20 | 1.99 | 81 | 1763 | 1500 | 72 | 12 |
| | 4 | Sphere-Pac | 20 | 1.99 | 82 | 1763 | <i>e</i> | 72 | 12 |
| SG-3 | 5 | Sphere-Pac | 20 | 1.98 | 82 | 2180 | 2000 | 35 | 16 |
| | 6 | Pellet ^f | 20 | 1.98 | 82 | 2180 | 2000 | 120 | 14.5 |

^aClad with titanium-modified type 304 stainless steel, 0.375 in. OD × 0.015 in. wall.

^bFuel density between central thermocouple and cladding inner surface.

^cMaximum fuel central temperature.

^dNot determined.

^eNot recorded, no central thermocouple.

^fPellet was 83.5% dense, pellet-cladding radial gap was 0.0014 in., pellet OD = 0.3423 in.

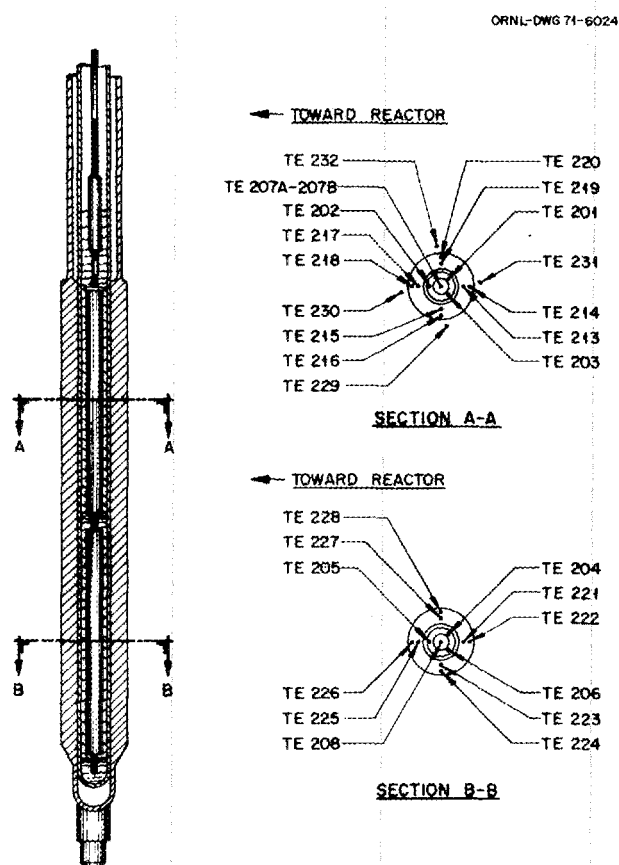


Fig. 5.18. SG capsule instrumentation.

5.2.3 Results

The SG capsules performed very well in obtaining the desired experimental data. The only difficulty was the failure in the first capsule (SG-1) of the molybdenum sheath used on the BeO-insulated W-3% Re vs W-25% Re fuel center-line thermocouple.²⁴ This was remedied in subsequent capsules by using a W-26% Re sheath in place of molybdenum. The three tungsten-rhenium-sheathed tungsten-rhenium thermocouples used in the fuel in capsules SG-2 and -3 performed satisfactorily, but detailed postirradiation examination of the assemblies revealed degradation of the tungsten-rhenium components. Even though the thermocouples did not fail, the presence of this degradation, probably material transport by an oxidation mechanism,²⁴ indicates a need for improvement of the thermocouple system for long-term application.

5.2.3.1 Fuel Restructuring

The postirradiation examination of the fuel structures from the SG capsules revealed the temperature-structure relationship developed during irradiation. The appearance of the Sphere-Pac fuel up to 1500°C (from

24. R. B. Fitts, J. L. Miller, Jr., and E. L. Long, Jr., *Observations on Tungsten-Rhenium Thermocouples Used In-Reactor in (U,Pu)O₂ Fuel Pins*, ORNL-TM-3617 (February 1972). (See also Proceedings of 5th Symposium on Temperature, Its Measurement and Control in Science and Industry, Washington, D.C., June 1971.)

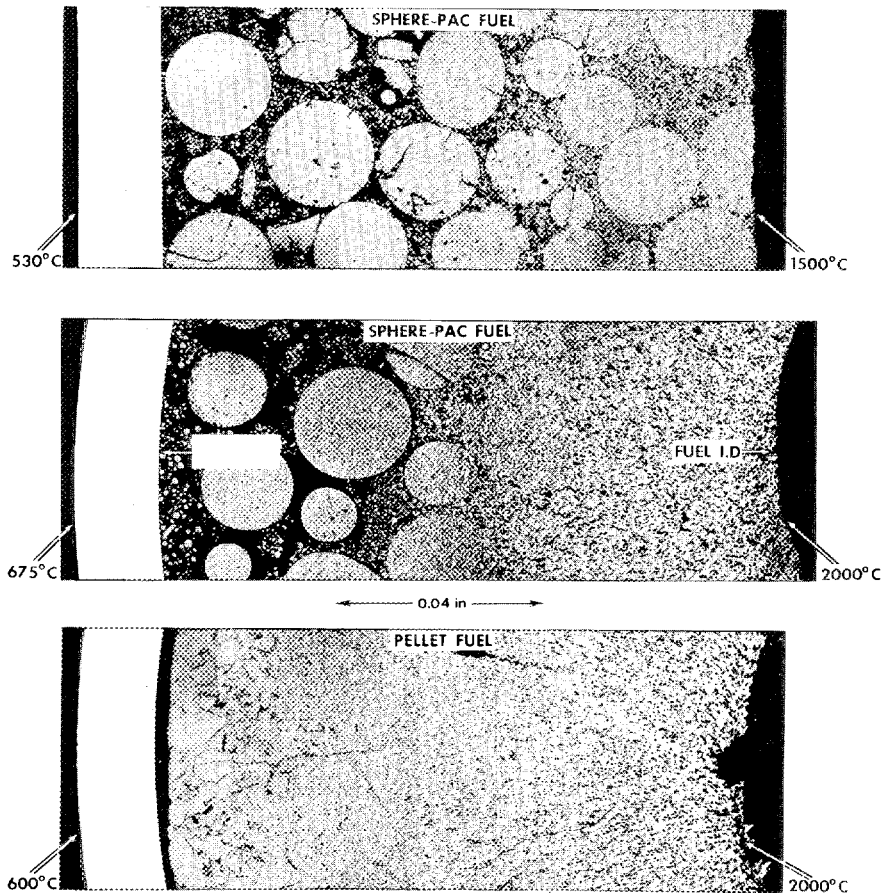


Fig. 5.19. Appearance of $U_{0.8}Pu_{0.2}O_{1.99}$ fuel after irradiation to low burnups.

capsule SG-2) and of both fuels up to 2000°C (from capsule SG-3) is shown in Fig. 5.19. The 2000°C fuel central temperature was developed in the pellet fuel at a lower heat rating than in the Sphere-Pac fuel, and this fact accounts for the lower cladding surface temperature on the pellet fuel pin. Both fuels restructured completely above about 1650°C (columnar grain growth region), and equiaxed grain growth is observable above about 1300°C. We also observed an increase in the fuel-to-cladding gap in the pellet fuel pin from 1.4 mils before irradiation to about 3 mils after the test. This increase may be evidence of in-reactor densification of the pellet fuel.

5.2.3.2 Temperature Analysis

From the thermometry data from the SG-3 capsule, we conclude that the fuel surface was hotter in the pellet fuel pin than in the Sphere-Pac fuel pin, despite the cooler cladding surface on the pellet pin. This

condition is illustrated in Fig. 5.20, where the average temperature profile at maximum operating condition is superimposed on the postirradiation fuel structures. The temperature scales were computed²⁵ from the measured fuel center-line and cladding surface temperatures and heat generation rates using reported data²⁶ on thermal conductivity of 82%-dense $(U,Pu)O_2$ fuel. The calculation, therefore, assumes only that the conductivity is the same for pellet and Sphere-Pac fuel of this density. Using the indicated fuel surface temperatures and the measured cladding surface tempera-

25. C. M. Cox and F. J. Homan, *PROFIL - A One-Dimensional FORTRAN IV Program for Computing Steady-State Temperature Distribution in Cylindrical Ceramic Fuels*, ORNL-TM-2443 (March 1969) and Addendum (August 1969).

26. W. E. Baily et al., "Thermal Conductivity of Uranium-Plutonium Oxide Fuels," pp. 293-308 in *Intern. Symp. Plutonium Fuels Technol., Scottsdale, Ariz., 1967, Nucl. Met. 13*, American Institute of Mining, Metallurgical, and Petroleum Engineers, New York, 1968.

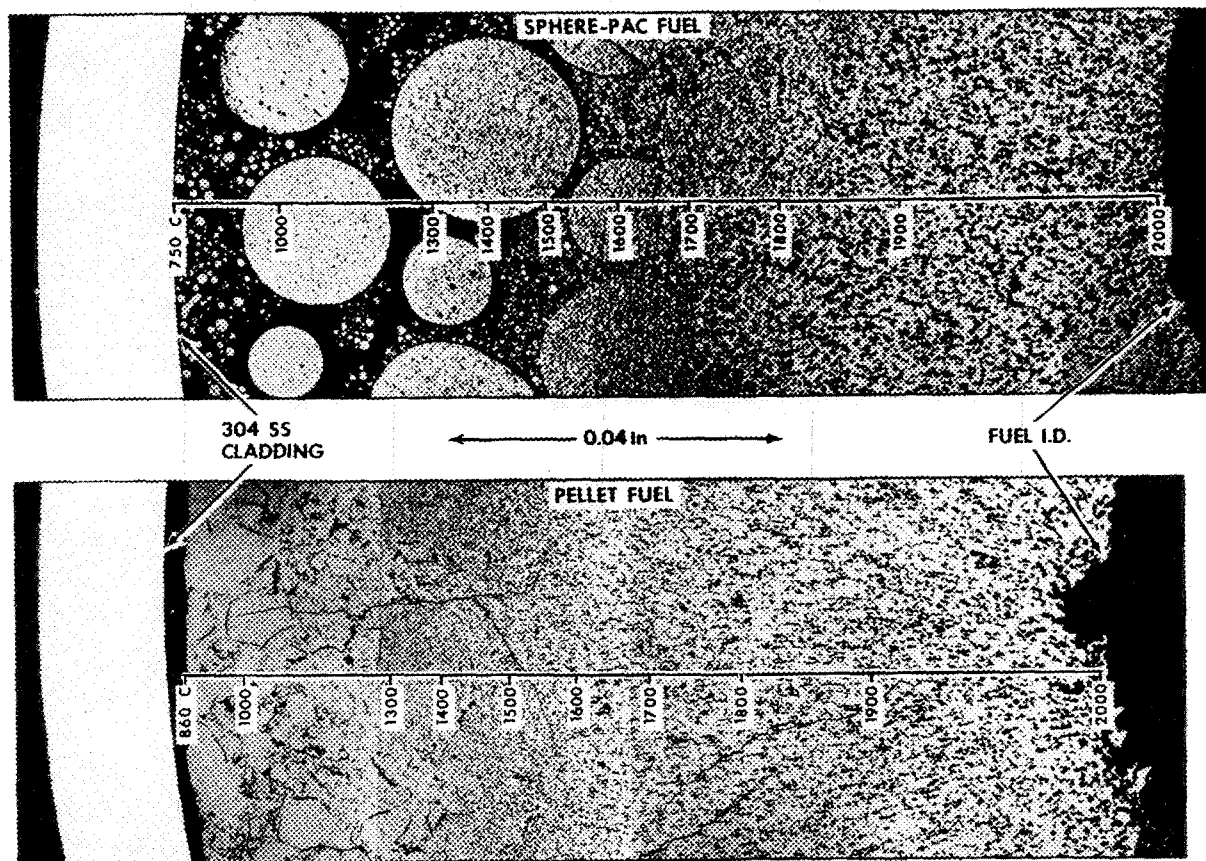


Fig. 5.20. Fuel restructuring in ORR instrumented tests of $U_{0.8}Pu_{0.2}O_{1.99}$. The structure of Sphere-Pac and pellet fuel is compared with calculated temperature profiles from the type 304 stainless steel cladding to the inner surface of the annular fuel.

tures we evaluated the surface heat transfer coefficient (gap conductance) between fuel and cladding for the two fuel forms. The gap conductance is $0.73 \text{ W cm}^{-2} (\text{°C})^{-1}$ for the pellet fuel, which is consistent with the results of similar analyses,²⁷ and $1.93 \text{ W cm}^{-2} (\text{°C})^{-1}$ for the Spere-Pac fuel, which is consistent with analyses²⁸ of transient irradiations of Sphere-Pac fuel. The only alternate explanation for the production of the same central temperature in both fuels at different heat ratings (14.5 kW/ft in the pellets and 16 kW/ft in the Sphere-Pac) requires the coincident assumption of (1) lower fuel thermal conductivity for the pellet fuel and

(2) lower restructuring temperatures for the pellets. Since the thermal conductivity used in the temperature calculations was that published for pellet fuels, and other work²⁹ has also indicated similar restructuring temperatures for both fuel forms, we believe that the correct explanation is the lower gap conductance and the resulting higher fuel surface temperature with the pellet fuel.

5.2.3.3 Fuel-Cladding Chemical Interaction

One further result obtained from the postirradiation examination of the SG-3 capsule was the observation of fuel-cladding chemical interaction in the pellet fuel pin,

27. C. N. Craig et al., *Heat Transfer Coefficients Between Fuel and Cladding in Oxide Fuel Rods*, GEAP-5748 (1969).

28. C. M. Cox, D. R. Cuneo, and E. J. Manthos, "Performance of Sphere-Pac and Pelletized (U,Pu)O₂ During Severe Overpower Transients," pp. 701-24 in *Proc. Conf. Fast Reactor Fuel Element Technology*, American Nuclear Society, Hinsdale, Illinois, 1971.

29. A. R. Olsen, R. B. Fitts, and W. J. Lackey, *In-Reactor Restructuring Temperatures and Kinetics for (U,Pu)O₂*, ORNL-TM-3387 (July 1971). (See also pp. 579-602 in *Proc. Conf. Fast Reactor Fuel Element Technology*, American Nuclear Society, Hinsdale, Illinois, 1971.)

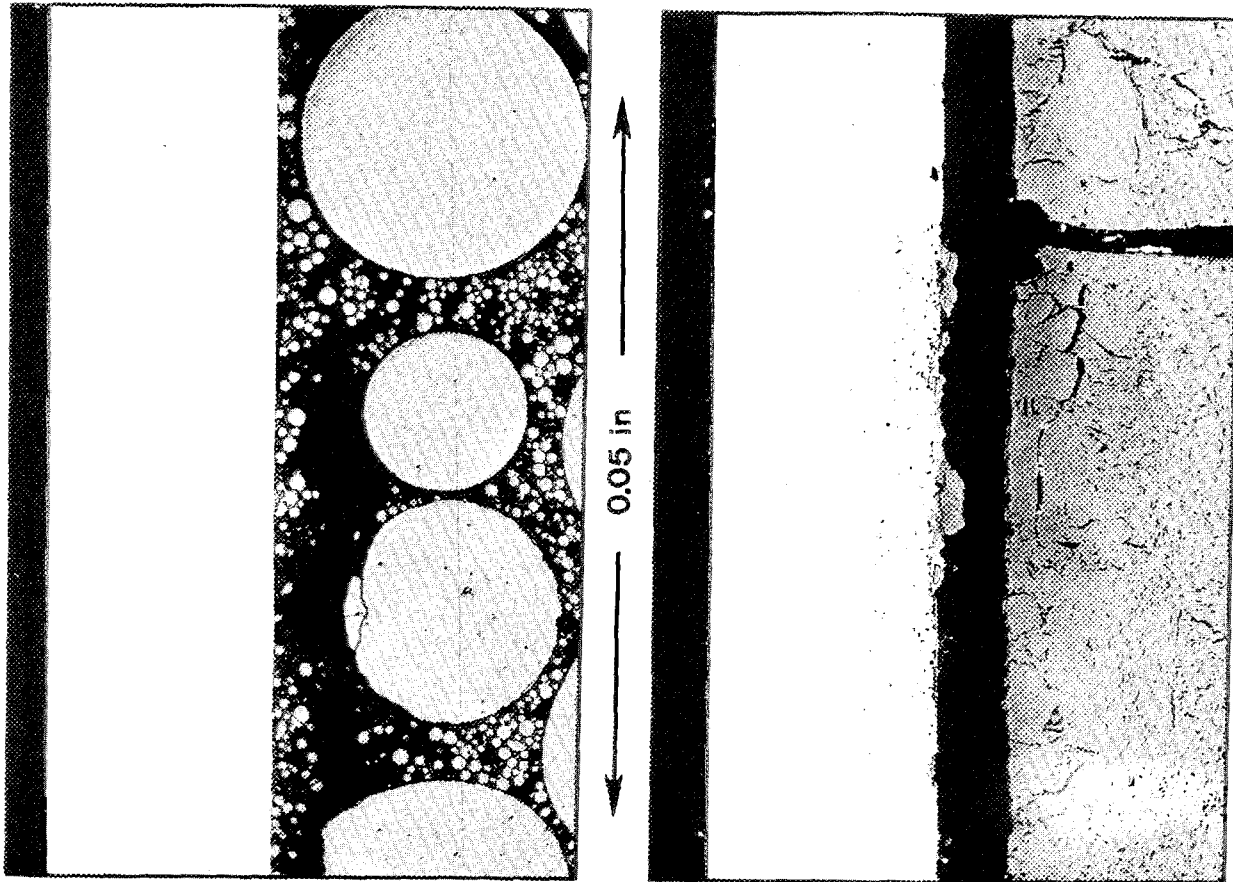


Fig. 5.21. Comparison of interactions of $(U-20\% Pu)O_2$ fuel with type 304 stainless steel cladding at about 5% FIMA. At left is sol-gel Sphere-Pac fuel with cladding inner surface that had been above $650^\circ C$ for 430 hr. At right is sol-gel pellets with cladding that had been above $650^\circ C$ for 265 hr.

but no evidence of any such interaction in the Sphere-Pac fuel pin. The fuel-cladding interface from both pins is illustrated at higher magnification in Fig. 5.21. Three localized regions of attack were found in the pellet pin. Two were very minor, consisting of less than 1 mil penetration of the cladding over a length less than 5 mils along the interface. The third and most severe area is shown in Fig. 5.21. Here the maximum penetration was about 5 mils over an area 50 mils long located below a pellet-to-pellet interface in the fuel column. Reaction product layers visible on the cladding and on the fuel are similar to those observed by others.³⁰ No attack occurred near any of the other

eight pellet-to-pellet interfaces examined in this pin. Grain boundary porosity shows clearly in the cladding. Surface layers of reaction product metal or oxide phases are visible along the reaction zone, and two particles of fuel are adhering to the cladding. The smaller one is surrounded by reaction product, and the larger is mixed with reaction product on the cladding side and overlaid with a small amount of reaction product on the side toward the bulk of the fuel.

A shielded electron microprobe was used to examine the reaction zone and adjacent fuel. Neither the porosity in the cladding grain boundaries nor the areas of grain boundary delineation or reaction contained any detectable amount of fission products. This may be due to the low burnup in these fuel pins. The delineated grain boundaries were depleted in chromium and iron but not in nickel. The mottled or large reaction product layer on the cladding consists of alternating iron-rich

30. R. B. Fitts, E. L. Long, Jr., and J. M. Leitnaker, *Observations of Fuel-Cladding Chemical Interactions as Applied to GCBR Fuel Rods*, ORNL-TM-3385 (May 1971). (See also pp. 431-58 in *Proc. Conf. Fast Reactor Fuel Element Technology*, American Nuclear Society, Hinsdale, Illinois, 1971.)

and chromium-rich layers containing traces of nickel. The layer of reaction product around the fuel particles adhering to the cladding is predominantly iron, and the layer adhering to the surface of the bulk fuel is principally chromium, either metal or oxide. A trace of nickel is also found in these layers along with a trace of chromium in the iron-rich layer. The metallic-appearing material found in the pellet-to-pellet interface and in the porosity within the fuel is primarily iron. A smaller amount of chromium-rich material, perhaps an oxide, is also present at these locations.

The structure of these fuels shows that the heat generation was approximately 8% off-center. This condition exists in all tests irradiated in facilities outside a reactor core. The phenomenon leads to a hot side on each fuel pin, and the thermocouple measurements of cladding temperatures supported this observation. However, as was discussed above, the fuel surface temperature was also higher in the pellet fuel pin than in the Sphere-Pac pin. These data are given in Table 5.5, and the operating times at selected thermal conditions are given in Table 5.6. The average and hot-side thermal conditions were determined from the measured variation of the cladding temperature and heat flow and the gap conductance found for the average condition as described above.

Table 5.5. Operating temperatures in SG-3 fuel pins at 2000°C fuel central temperature

| Fuel pin | Maximum inner cladding temperature (°C) | | Maximum fuel surface temperature (°C) | |
|------------|---|----------|---------------------------------------|----------|
| | Average | Hot side | Average | Hot side |
| Pellet | 625 | 665 | 860 | 900 |
| Sphere-Pac | 700 | 745 | 750 | 800 |

Table 5.6. Approximate operating time at various conditions for SG-3 fuel pins

| Fuel pin | Operating time (hr) | | | |
|------------|-----------------------------------|----------|-----------------------|------------------|
| | Cladding inner surface over 650°C | | Hot-side fuel surface | |
| | Average | Hot side | Over 800°C | At or over 900°C |
| Pellet | 0 | 265 | 550 | 60 |
| Sphere-Pac | 120 | 430 | 20 | 0 |

5.2.4 Discussion

5.2.4.1 Thermometry Data Analysis

The final detailed analysis^{31,32} of the thermometry data from the SG-3 capsule produced a statistically valid quantified comparison of the relationship between fuel central temperature and heat generation rate within the two fuel pins. The techniques developed for this analysis and the results are both significant and are described below.

The operating sequence (see Fig. 5.16) of the SG-3 capsule was designed to yield data over most of the operating power-temperature range at intervals throughout the operating period. This approach permits an analysis of the effects of time and history on the response of the experiment. We sampled the 12 thermocouples with an automatic recording system for 3 min every 2 hr and whenever we made a change in operating conditions. This procedure yielded 44,500 data sets or over one million recorded thermocouple readings. Analysis of this amount of data, of course, required reduction to a smaller representative sample. We therefore obtained average values for the data from each thermocouple during each 3-min period of sampling, which yielded 1550 sets of averaged data. We then selected at least one sample from every temperature hold and more samples from the longer holds. This selection provided 261 of these averaged sets to examine in detail.

This set of data for the Sphere-Pac fuel pin is shown in Fig. 5.22. The fuel central temperature and the cladding temperature (proportional to heat generation rate in the fuel) are related, but considerable scatter shows. We refined the data by analysis of residuals. This is an effective technique for isolating and identifying the various populations in a large data set, thereby permitting the formation and analysis of meaningful groupings of the data. A quadratic function of average cladding temperature (or in other cases a quadratic in average heat generation rate) was fit by least squares to the fuel central temperature, and then the patterns in the residuals were analyzed. The results for the data in Fig. 5.22 are shown in Fig. 5.23. The residuals, plotted in this case against the order in which the data were collected, showed periods of excessive deviation during

31. R. B. Fitts and F. L. Miller, "Analysis and Performance of Instrumented Fuel Pins," *Trans. Amer. Nucl. Soc.* 15(1), 180 (June 1972).

32. F. L. Miller and R. B. Fitts, *Statistical Analysis of SG-3 Data*, ORNL-TM-4034 (in preparation).

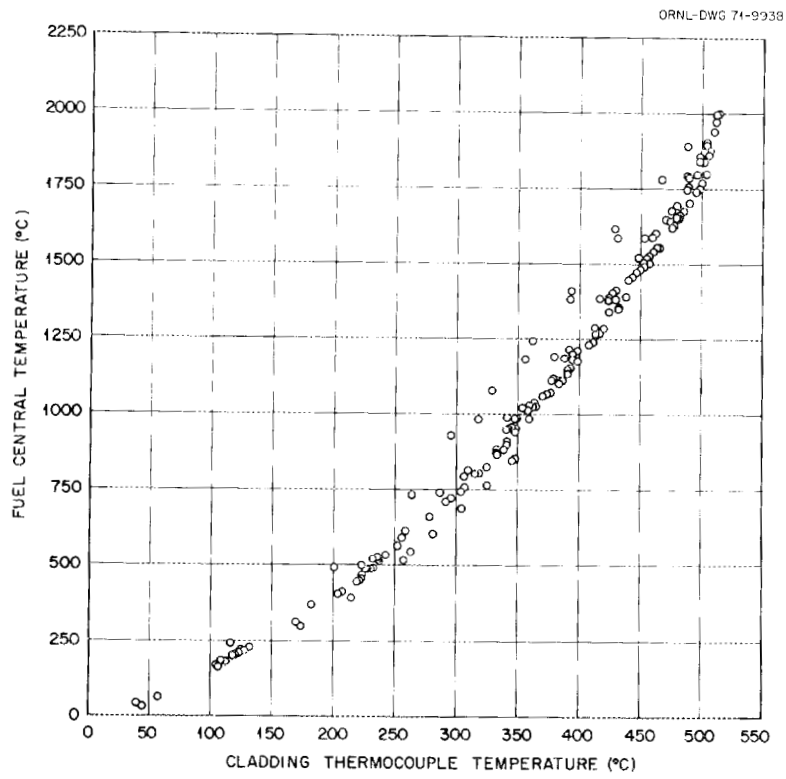


Fig. 5.22. Measured temperatures in SG-3 Sphere-Pac fuel tests.

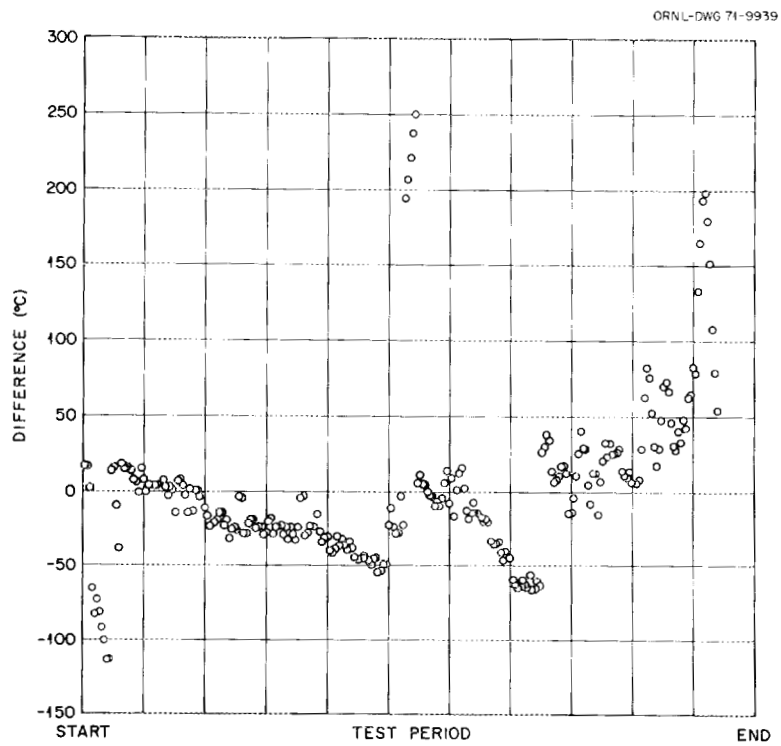


Fig. 5.23. Difference between measured fuel central temperature and those calculated from quadratic fit of all data.

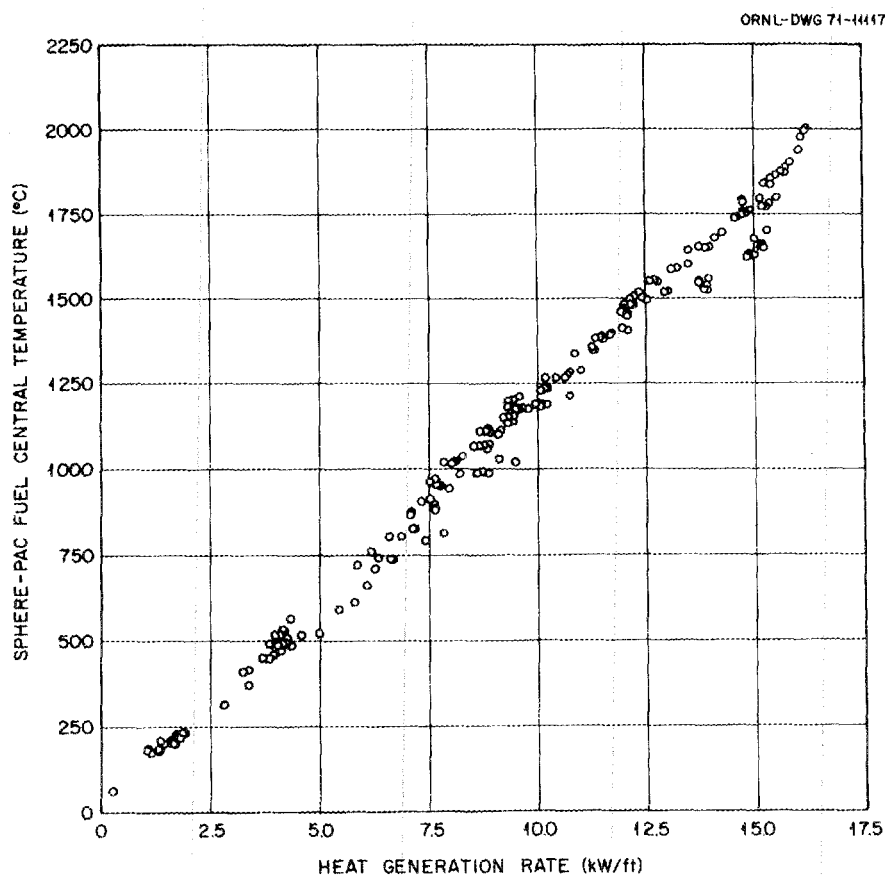


Fig. 5.24. Sphere-Pac fuel central temperature in SG-3 as a function of heat generation rate. Only steady-state data included.

initial start-up and twice during rapid shutdown after operation at high fuel temperatures.

The steady-state data, with these shutdown or transient data removed, are shown in Fig. 5.24. In this case we show the fuel central temperature correlated with average heat generation rate in the fuel pin. The scatter in the data is greatly reduced by elimination of the data from transient periods, and a reasonable relationship describing all of these data can be obtained. However, if we look again at Fig. 5.23 we see a sharply dropping set of data near the middle of the time period. These data, although not greatly different, were associated with a period in which an experiment was installed in an adjacent test position; and upon close inspection of these data, we found a shift in the pattern of heat flow from the experiment. These data points were therefore discarded as not typical of the bulk of the steady-state temperature data and were set aside to be analyzed separately. This produced the final data set displayed in Fig. 5.25, where the relationship between Sphere-Pac fuel

central temperature and heat generation rate at steady-state condition is shown.

The same procedure was followed to refine the pellet fuel pin data. The full data set is displayed in Fig. 5.26. The scatter is worse in the pellet pin data, but analysis of residuals showed much of the scatter to be associated with the same time periods as in the Sphere-Pac pin data. The refined steady-state data set for the pellet pin is shown on Fig. 5.27. There is still more scatter among these data than in the Sphere-Pac pin data. The greater scatter probably reflects a greater sensitivity to the formation and healing of thermal-stress-induced cracks within this type of fuel.

The results for both pins are compared in Fig. 5.28. This analysis showed that at the 99% confidence level, the central temperature of the Sphere-Pac fuel was always $11.7 \pm 1.2\%$ cooler than that of the pellet fuel at any given steady-state heat generation rate. This result is important, not so much because of the lower temperatures in the Sphere-Pac fuel, but because there

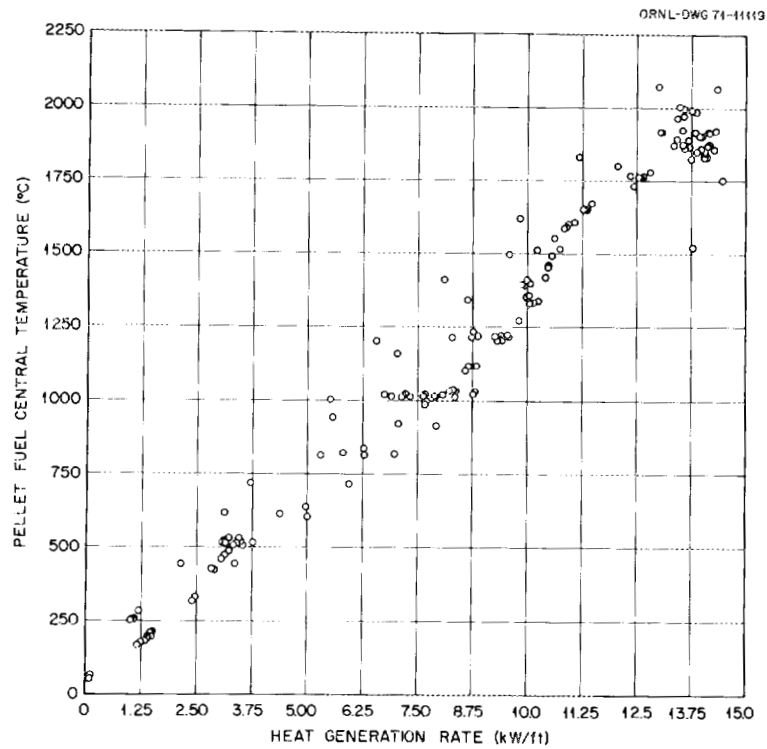


Fig. 5.25. Sphere-Pac fuel central temperature in SG-3 as a function of measured heat generation rate — refined data.

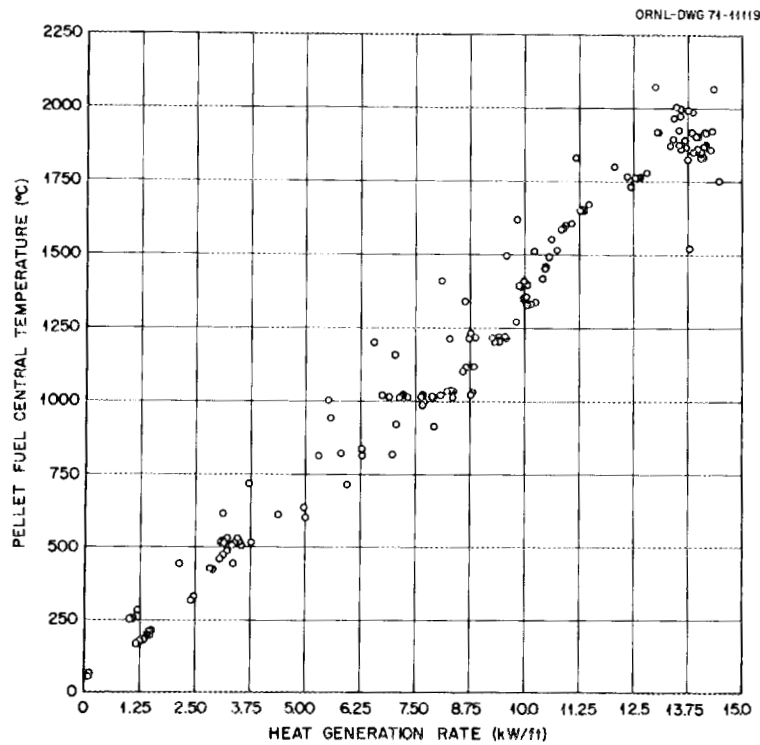


Fig. 5.26. Measured pellet fuel central temperature and heat generation rates from capsule SG-3 — all data included.

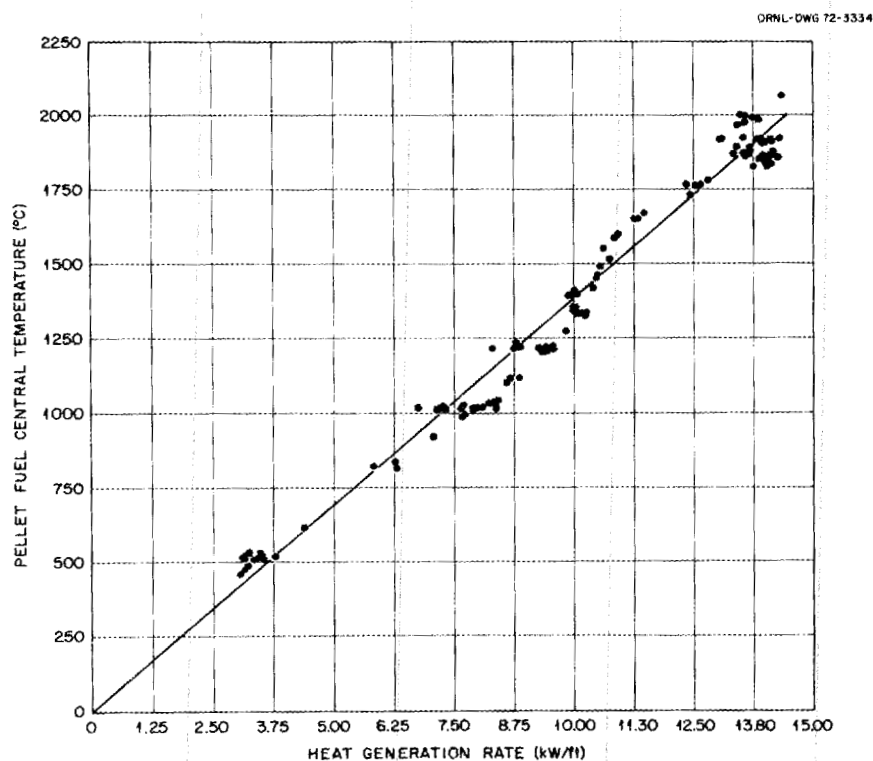


Fig. 5.27. Measured pellet fuel central temperature and heat generation rates from capsule SG-3 -- refined data.

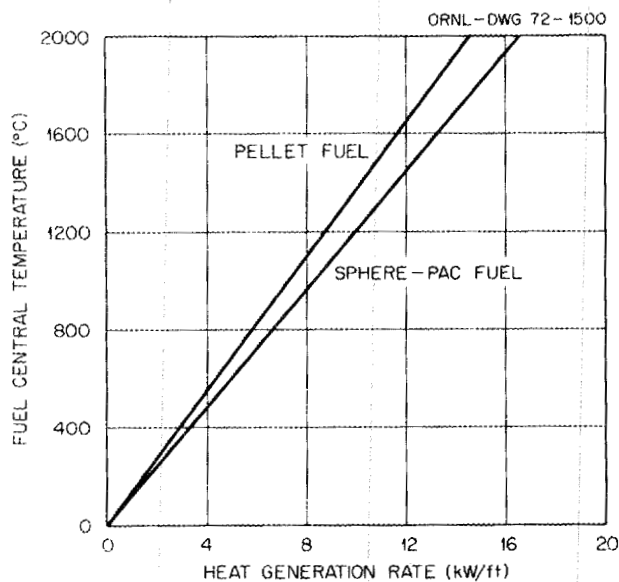


Fig. 5.28. Final relationship between fuel central temperature and power for capsule SG-3.

have been indications from both experiment and calculation that angular particulate (Vi-Pac) fuels might have lower thermal conductance than solid fuels, and this result had been extrapolated to predict poor thermal conductance for Sphere-Pac fuel.

In addition, the SG-3 thermometry data have yielded qualitative information on the effects of power cycling on the two fuels. Power cycling significantly affected the fuel pin central temperature. In both fuel pins the central temperature at 8 to 13 kW/ft was about 250°C higher upon initial return to power after a reactor shutdown than it was at the same heat rate during steady-state operation. The duration of this fluctuation was a function of the operating conditions and fuel form, with the pellet fuel requiring about 3 hr and the Sphere-Pac about 1 hr to recover.

Finally, the abnormalities detected in these data, related to reactor shutdown and reactor configuration or loading changes, indicate that the design of in-reactor experiments should provide for such effects. This may be accomplished through frequent replication of test conditions or, as in this experiment, by very careful analysis of the data collected in highly instrumented tests.

5.2.4.2 Cladding Attack

The form of attack on the cladding observed in the pellet fuel pin is consistent with the oxidation mechanism reported^{33,34} earlier for this phenomenon. The following differences in fuel form and operating conditions could be invoked to explain the lack of reaction in Sphere-Pac pins and existence of the localized reaction observed in pellet pins:

1. localized composition variations,
2. cladding temperature differences,
3. fuel surface temperature differences,
4. cladding hot-spot temperatures, stresses, or both,
5. differences in gas phase access to the internal fuel structure.

The chemical interactions between fuel and cladding can be affected by local variations in fuel composition. Fuel inhomogeneity and pellet surface contamination during fabrication and fuel pin loading are likely sources of such variations. However, both pellet and Sphere-Pac sol-gel fuels have consistently shown excellent homogeneity, and both fuels were made from the same starting sol. Since no significant chemical composition differences and no metallographic evidence of surface contamination was found on the pellets for this test, we believe that local composition variations played no part in our observed results.

The cladding temperatures, both average and hot-side, were highest on the Sphere-Pac fuel pin; this should have caused the reverse of the observed different compatibility behavior. Therefore, this factor will not explain the results. Some chemical interactions might have been expected in both fuel pins, on the basis of cladding temperature, if longer operating times had been employed in this test.

The fuel surface temperature has not been previously considered as a controlling factor in fuel-cladding chemical interaction. This is partly due to the difficulty of measurement and uncertainty in calculation of the fuel surface temperature for an operating fuel pin.

However, an interesting possibility has come to light as a result of the analysis of this experiment. The pellet surface temperature is higher than the Sphere-Pac fuel surface temperature and, at its maximum, is approaching what one would normally expect³⁵ in LMFBR-type fuel pins,³⁶ where reactions have been observed at cladding temperatures above 650°C. On this basis the present results are consistent with earlier work.

Another explanation of our observations may be based on the effect of higher surface temperatures for pellets than for Sphere-Pac fuels coupled with short-circuit heat transfer at the contact points in the pellet-cladding interface. Such contact points (see Fig. 5.21 for an example involving chips of fuel at the interface) should cause both localized stress and hot spots in the cladding. Both factors would increase the probability of fuel-cladding chemical interaction. It is worthy of note that such hot spots were observed³⁷ in-reactor in TREAT tests of stainless-steel-clad fuel pins. Such severe localized contact is minimized in Sphere-Pac fuel operating under normal conditions, however, because many points of contact between fuel and cladding exist in a Sphere-Pac fuel pin.

A final contributing factor that may be important in the difference in fuel-cladding compatibility in Sphere-Pac and pellet fuel is the difference in porosity configuration in the two and a consequent difference in oxygen and/or fission product activity at localized surface areas. In the low-burnup Sphere-Pac fuel the gas phase communicates directly, and by a short path, between the fuel surface and the hotter fuel away from the surface. In pellet fuels some regions of the fuel surfaces adjacent to the cladding have poor gas phase communication with the fuel away from the surface. Several mechanisms of oxygen redistribution are apparently operative in the mixed-oxide fuels.³⁸ For nearly stoichiometric fuels, where the gas phase is continuous and well distributed within the fuel pin, the oxygen

35. One predicts a fuel surface temperature of around 920°C at a cladding outer surface temperature of 650°C on an LMFBR fuel pin operating at 13 kW/ft with a surface heat transfer coefficient of $1 \text{ W cm}^{-2} (\text{°C})^{-1}$.

36. K. J. Perry and C. N. Craig, "Austenitic Stainless-Steel Compatibility with Mixed-Oxide Fuel," *Trans. Amer. Nucl. Soc.* 12(2), 564-65 (1969).

37. L. Harrison, R. C. Liimatainen, and F. J. Testa, "Photographic Studies of Metal Clad, UO₂-Core Fuel Rods in TREAT," *Chem. Eng. Div. Semiannu. Rep. July-December 1966*, ANL-7325, p. 160.

38. E. A. Aitken, "Thermal Diffusion in Closed Oxide Fuel Systems," *J. Nucl. Mater.* 30, 62-73 (1969).

33. R. B. Fitts, E. L. Long, Jr., and J. M. Leitnaker, *Observations of Fuel-Cladding Chemical Interactions as Applied to GCBR Fuel Rods*, ORNL-TM-3385 (May 1971). (See also pp. 431-58 in *Proc. Conf. Fast Reactor Fuel Element Technology*, American Nuclear Society, Hinsdale, Illinois, 1971.)

34. J. W. Weber and E. D. Jensen, "Effect of O/M on Irradiated Mixed-Oxide Stainless-Steel Cladding Compatibility," *Trans. Amer. Nucl. Soc.* 14(1), 175-76 (June 1971).

potential is controlled by gas phase equilibration.³⁸⁻⁴⁰ Conversely, by solid-state chemical diffusion theory, excess oxygen not accessible to the gas phase but trapped in solid fissioned fuel would tend to diffuse toward the cold surface.^{38,41} Thus, a local buildup of oxygen might be expected in any region where a pellet surface is not readily accessible to the gas phase. This cannot occur in low-burnup Sphere-Pac fuels under normal operating conditions.

5.2.5 Conclusions

The following principal conclusions may be drawn from the ORR instrumented thermal performance tests.

1. The effective thermal conductance of the Sphere-Pac fuel pin was $11.7 \pm 1.2\%$ better (at the 99% confidence level) than that of the pellet fuel pin during irradiation to 0.5% FIMA with fuel smear densities of 82% of theoretical.

2. The better conductance (lower fuel temperatures) in the Sphere-Pac fuel pin is probably due to higher thermal conductance between the fuel and cladding with the Sphere-Pac fuel. We estimated a gap conductance of $0.73 \text{ W cm}^{-2} (\text{°C})^{-1}$ for the pellet fuel and $1.93 \text{ W cm}^{-2} (\text{°C})^{-1}$ for the Sphere-Pac fuel in these tests.

3. The temperature-structure relationship was the same in both fuels. Complete restructuring of the fuels (columnar grain growth region) occurred above 1650°C , and equiaxed grain growth was evident at all temperatures between 1300 and 1650°C .

4. Power cycling significantly affected fuel pin central temperature. In both pins at 8 to 13 kW/ft, the central temperature was about 250°C higher immediately after a rapid shutdown and return to power than before. The temperature decreased to normal during the first few hours of steady-state operation after the shutdown.

5. The chemical interaction of fuel and cladding was more severe in the pellet than in the Sphere-Pac pin despite somewhat higher cladding temperatures on the Sphere-Pac pin. This difference may be related to (1) lower fuel surface temperature with Sphere-Pac fuel, (2)

less severe cladding hot spots or stresses with Sphere-Pac fuel, or (3) better access of gases to the fuel-cladding interface in the Sphere-Pac fuel at low burnup.

6. The performance of the W-26% Re-clad W-3% Re vs W-25% Re fuel center-line thermocouples used in these tests was satisfactory for the time-temperature regime of these tests; however, we identified chemical changes that could pose problems for long-term high-temperature use.

5.3 ETR TESTS -- INSTRUMENTED SERIES

A. R. Olsen

5.3.1 Experimental Plans

The plans for instrumented irradiation tests in the ETR called for two series of tests utilizing a similar capsule design. The series I tests were to provide a direct comparison of the performance of pellet and Sphere-Pac fuel forms in the same capsule. The series II tests were designed for a similar comparison but with extended fuel column lengths to investigate the effects of length on fuel pin performance and also to measure fission gas pressures during irradiation.

Series I consists of two capsules, 43-120 and 43-121. Each capsule contained four fuel pins with two thermocouples on the cladding at the fuel midlength of each pin. The fuel column length in each pin was 3 in. These tests were designed to investigate fuel swelling and fuel-cladding chemical interactions of Sphere-Pac and pelletized $(\text{U,Pu})\text{O}_2$ fuels over a range of cladding temperatures up to a maximum of 650°C . Both capsules have completed their irradiation exposures. Capsule 43-121 was discharged on January 10, 1972, and capsule 43-120 on May 9, 1972. Only capsule 43-121 was returned to ORNL for postirradiation examination. With the termination of the program, capsule 43-120 was transferred to ANL for examination.

The series II group was originally planned to include three capsules. Each capsule was to contain a single fuel pin with a 20-in.-long fuel column. Each pin was to be instrumented with a pressure transducer to measure gas pressure in the plenum region during irradiation and nine thermocouples to measure cladding temperatures at selected locations along the fuel column and in the gas plenum region. One capsule was to contain FTR-type pellets of the highest permissible density (94% of theoretical), the second was to contain FTR pellets of the lowest permissible density (88% of theoretical), and the third was to contain a packed bed of Sphere-Pac

39. K. E. Spear, A. R. Olsen, and J. M. Leitnaker, *Thermodynamic Applications to $(\text{U,Pu})\text{O}_{2+x}$ Fuel Systems*, ORNL-TM-2494 (April 1969).

40. W. J. Lackey, F. J. Homan, and A. R. Olsen, *Porosity and Actinide Redistribution During Irradiation of $(\text{U,Pu})\text{O}_2$* , ORNL-TM-3762 (August 1972).

41. M. G. Adamson, "Thermal Diffusion of Oxygen in Hyperstoichiometric Urania with Low Carbon Content," *J. Nucl. Mater.* 38, 213-16 (1971).

U-Fines fuel.⁴² In the U-Fines fuel, all the plutonium is contained in the coarse fraction (about 400- μm -diam) microspheres, and a fine fraction (<44- μm -diam) of depleted UO_2 microspheres is infiltrated into the coarse bed. The primary objective of these tests was to determine the rate of release of fission gases during irradiation as a function of operating conditions and of the method of void deployment in the as-fabricated fuel. Secondary objectives included investigations of both chemical and mechanical interaction of fuel and cladding, restructuring of the different fuel types, comparison of fission gas data obtained during tests with those obtained during postirradiation examination, and evaluation of the performance characteristics of the Sphere-Pac U-Fines fuel.

The two capsules containing the low-density FTR pellets and the Sphere-Pac fuel are partially fabricated. We have been instructed by the AEC to store these for possible use by others.

5.3.2 Design and Construction

The design of the series I capsule is shown in Fig. 5.29. The outer shell of the capsule is a 1-in.-OD, type 304 stainless steel tube with a wall thickness of 0.065 in. Within this shell there is a 0.5-in.-OD, type 304 stainless steel sleeve tube with holes drilled near the bottom, tack welded to the bottom end plug of the capsule, and with a flared top protruding above the NaK heat transfer medium level. This sleeve centers the fuel pin assembly in the capsule and subdivides the NaK into two narrow annuli, thus reducing the possibility of thermal convection loops developing. The fuel pin array is shown schematically in Fig. 5.30. Only the top and bottom pins are shown, but the two central pins are similar. Each fuel pin is $8\frac{1}{16}$ in. long, including the two end caps. The 3-in. fuel columns have two 0.25-in.-long ThO_2 insulators at each end. The fuel columns are held in place by Inconel X springs in the plenum region. The cladding on these pins is annealed type 316 stainless steel 0.250 in. OD with a 0.016-in. wall thickness. The bottom two pins in each capsule (Nos. 1 and 2) contain sol-gel-derived pellets and are arranged with the plenum on the bottom. The two Sphere-Pac pins (Nos. 3 and 4) are loaded with the fuel on the bottom. The eight thermocouples are strapped to the pins before assembly

and are brazed through the thermocouple seal bulkhead at the top of the capsule.

The design of the series II capsules is similar. The sleeve assembly is fastened to the top of the capsule and ventilated with holes above the top of the NaK fill. The pins, one in each capsule, are approximately 32 in. long and contain a 20-in.-long fuel column. The insulator material was depleted UO_2 , and both the upper and lower insulator sections are 2 in. long. The gas plenum contains a stainless steel sleeve $\frac{3}{16}$ in. in diameter \times $6\frac{1}{4}$ in. long and an Inconel X spring. The cladding material is 20%-cold-worked type 316 stainless steel, 0.230 in. OD with a 0.015-in. wall thickness. The instrumentation includes a pressure transducer connected to the pin gas plenum by a capillary tube. A report containing the design details, safety analysis, and status of fabrication of the series II capsules has been prepared.⁴³

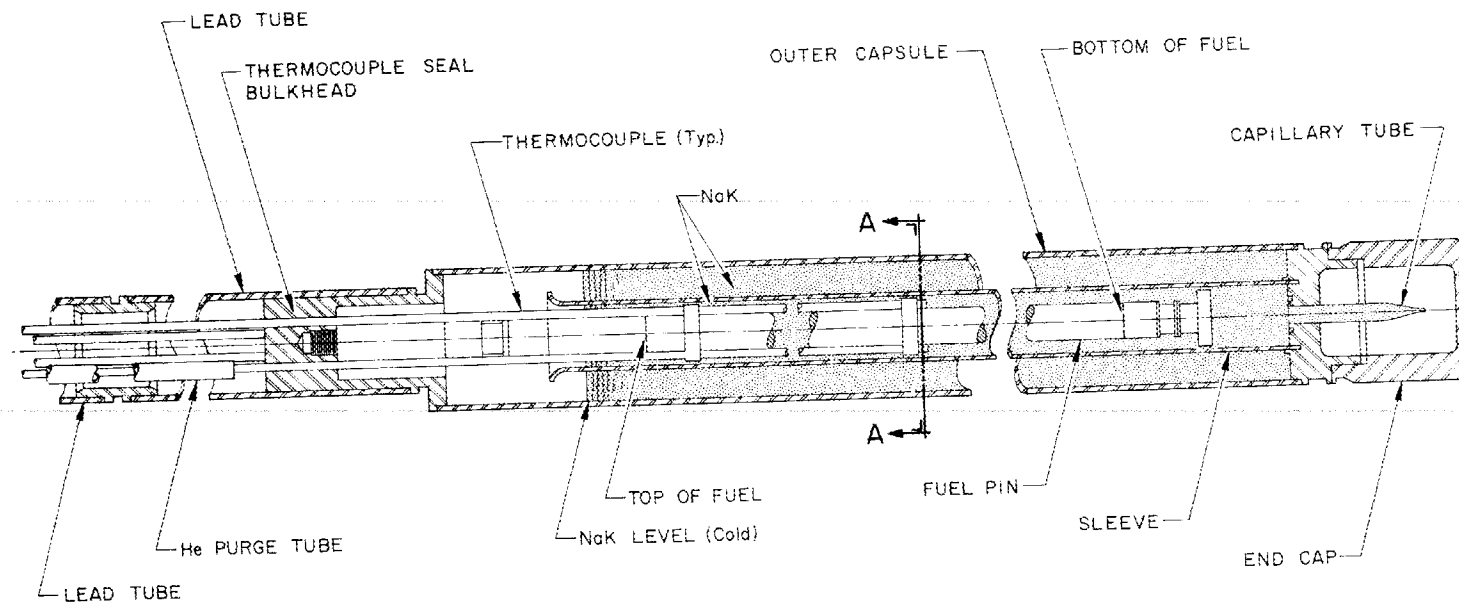
The capsules both have similar thermal analyses, so only the analysis for the series I group is shown in Fig. 5.31. This analysis was made with our GENGTC⁴⁴ code, assuming pure radial heat transfer, which is quite accurate for the thermocouple locations at the centers of the fuel columns.

Since only the series I group has been completely fabricated and irradiated, only the preirradiation data on these eight pins are complete. These data are presented in Table 5.7. Before irradiation, a series of calculations was made to determine the desired irradiation conditions at different levels of burnup. These conditions were a peak unperturbed (2200-m/sec) flux of 0.9×10^{14} neutrons $\text{cm}^{-2} \text{sec}^{-1}$ for the first 3% burnup, 1.1×10^{14} neutrons $\text{cm}^{-2} \text{sec}^{-1}$ for the next 3% FIMA, and 1.23×10^{14} neutrons $\text{cm}^{-2} \text{sec}^{-1}$ for the final 4% of the total burnup. Because of the need for bending the instrumentation lead tube and other restrictions, we chose two positions in the ETR core, which could provide two levels of flux rather than three. Capsule 120 was placed in position C10SW with a flux of 0.9×10^{14} neutrons $\text{cm}^{-2} \text{sec}^{-1}$. The adjacent position, C10SE, had a measured peak flux of 1.45×10^{14} neutrons $\text{cm}^{-2} \text{sec}^{-1}$, which was too high, but we did not plan to step this capsule. Capsule 43-121 was placed in position C11SW at a flux of 0.9×10^{14} neutrons $\text{cm}^{-2} \text{sec}^{-1}$. The adjacent C11SE position had

42. J. D. Sease, R. A. Bradley, C. R. Reese, W. H. Pechin, and A. L. Lotts, "Sphere-Pac and Pelletization of (U,Pu) O_2 ," pp. 323-41 in *Symposium on Sol-Gel Processes and Reactor Fuel Cycles*, Gatlinburg, Tennessee, May 4-7, 1970, CONF-700502.

43. A. R. Olsen, R. A. Bradley, and E. J. Mantos, *Fabrication and Safety Analysis of (U,Pu) O_2 Instrumented Capsules - Series II* (in preparation).

44. H. C. Roland, GENGTC, a One-Dimensioned CEIR Computer Program for Capsule Temperature Calculations in Cylindrical Geometry, ORNL-TM-1947 (December 1967).



87

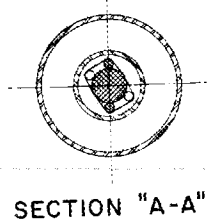


Fig. 5.29. ETR series I instrumented capsule.

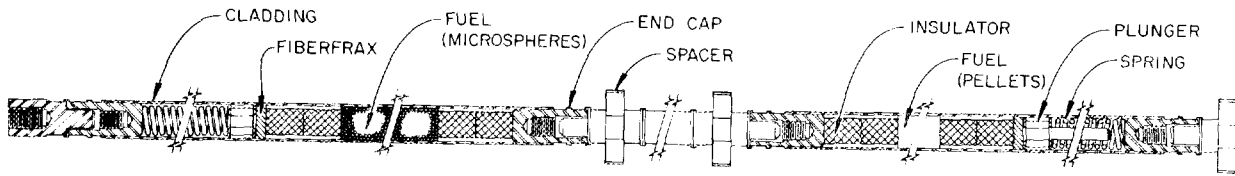


Fig. 5.30. Fuel pin array in ETR series I instrumented capsule.

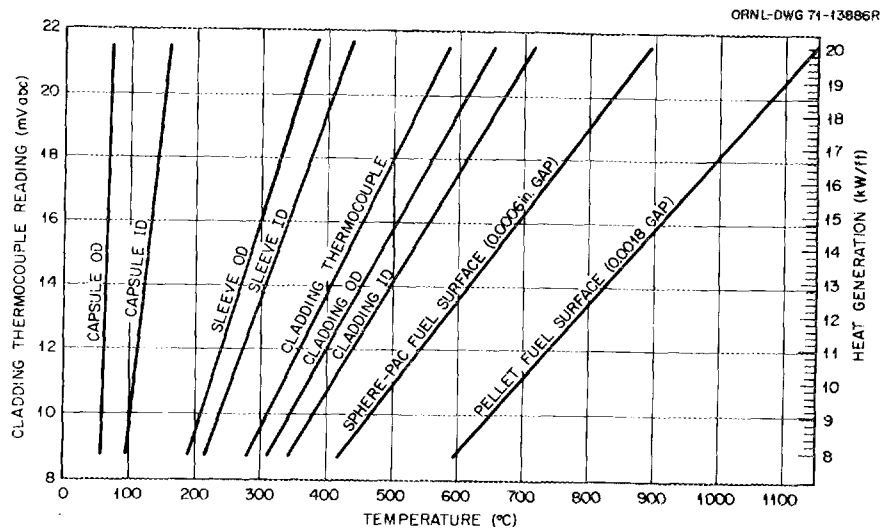


Fig. 5.31. Temperature distribution in ORNL-43-120 and ORNL-43-121.

Table 5.7. Preirradiation data for ETR instrumented tests 120 and 121

| Fuel pin | Tube | Type of fuel | Weight of fuel (g) | Height of fuel (in.) | Smear density (% of TD) | O/M | Material batch | Pu (%) | U (%) | OD | ID | Wall thickness (mils) |
|----------|---------|--------------|--------------------|----------------------|-------------------------|-------|----------------|--------|-------|--------|--------|-----------------------|
| 120-1 | 19-9-A | P | 16.34 | 2.985 | 81.1 | 1.985 | ET-3N | 16.67 | 70.24 | 0.2491 | | |
| 120-2 | 19-10-A | P | 16.22 | 2.973 | 81.5 | 1.985 | ET-3N | 16.67 | 70.24 | 0.2496 | | |
| 120-3 | 19-4-C | S-P | 17.144 | 3.02 | 84.8 | 1.980 | PUM-11-C | 16.89 | 69.91 | 0.2495 | | |
| 120-4 | 19-4-F | S-P | 17.057 | 3.01 | 84.6 | 1.980 | PUM-11-F | 16.70 | 68.26 | 0.2495 | 0.2174 | 16.1-15.5 |
| | | | | | | 1.975 | PUM-11-C | 16.89 | 69.91 | 0.2472 | 0.2171 | |
| 121-1 | 19-11-D | P | 16.32 | 2.995 | 81.0 | 1.975 | PUM-11-F | 16.70 | 68.26 | 0.2496 | 0.2171 | 16.1-15.6 |
| | | | | | | 1.985 | ET-3N | 16.67 | 70.24 | 0.2485 | | |
| 121-2 | 19-9-C | P | 16.27 | 2.976 | 81.2 | 1.985 | ET-3N | 16.67 | 70.24 | 0.2494 | | |
| | | | | | | | | | | 0.2493 | | |
| 121-3 | 19-4-B | S-P | 16.866 | 3.00 | 83.9 | 1.980 | PUM-11-C | 16.89 | 69.91 | 0.2495 | | |
| | | | | | | 1.975 | PUM-11-F | 16.70 | 68.26 | 0.2491 | 0.2175 | |
| 121-4 | 19-4-E | S-P | 17.055 | 2.98 | 85.5 | 1.980 | PUM-11-C | 16.89 | 69.91 | 0.2495 | 0.2175 | 16.1-15.5 |
| | | | | | | 1.975 | PUM-11-F | 16.70 | 68.26 | 0.2490 | 0.2171 | |
| | | | | | | | | | | 0.2495 | 0.2171 | 16.2-15.6 |

a measured peak flux of 1.3×10^{14} neutrons $\text{cm}^{-2} \text{sec}^{-1}$, and we planned to move the capsule to this position when the burnup would permit, thus making a single large step instead of two smaller steps.

5.3.3 Irradiation History

Both series 1 capsules started their irradiation in May 1970. The operating conditions near the start of the irradiation period are shown in Table 5.8. Both the strip-chart recordings and the thrice-daily manual readings of the thermocouples showed some variations, with the primary variation resulting from control rod movements during any one reactor cycle. As expected, the linear heat rates gradually changed due to fissile depletion. After seven reactor cycles, a total exposure of 295 effective full-power days (EFPD), the peak cladding inner surface temperatures had fallen to approximately 520°C for capsule 43-120 and 550°C for capsule 43-121. At that time capsule 43-121 was moved to the higher flux position. This transfer did not produce the anticipated increase in fission rate, so the peak cladding temperature rose only to 585°C . Consequently, we decided to discharge capsule 43-121 at the next reactor shutdown and move capsule 43-120 to its higher flux position for continued irradiation. Capsule 43-121 was discharged from the reactor on January 10, 1972, after 335 EFPD of irradiation at a calculated

burnup of 7.6% FIMA. The change in linear heat rate for capsule 43-120 was again not as large as expected. In fact, the peak linear heat rate changed only 14%, going from 12.8 to 13.8 kW/ft. From the flux measurements before irradiation, an increase of approximately 70% was anticipated. This change in the flux distribution is not abnormal for the varying loading sequence in the ETR. There is no evidence of a drift in the thermocouples in either capsule. Since the program was terminating and the desired high cladding inner surface temperatures could not be maintained, this capsule was discharged on May 9, 1972. The total irradiation time was 391 EFPD, and the calculated burnup was 8.2% FIMA. A computer program was written to correlate the daily thermocouple readings and the reactor power history to provide a graphical history of irradiation for each pin in each capsule. Examples of this for the highest heat-rate pins in each of the capsules are given in Figs. 5.32 and 5.33.

Capsule 43-121 was returned to ORNL for postirradiation examination, and capsule 43-120 was shipped to Los Alamos for postirradiation examination under the auspices of Argonne National Laboratory.

Although a complete comparison of the pellet and Sphere-Pac fuel performance in these capsules cannot be made until 43-120 is examined, the data from 43-121 have been very informative. A topical report concerning the irradiation of both capsules and the postirradiation examination of 43-121 is in preparation.⁴⁵ The highlights are included here.

5.3.4 Results

Before capsule 43-121 was dismantled, it was scanned for gamma activity distributions. The fuel columns were intact, and there was no evidence of any pin failures. Two unusual peaks in the gamma scan were located near the bottom of the fuel columns for the pins with the two highest heat rates (121-2, a pellet fuel pin, and 121-3, a Sphere-Pac fuel pin). These peaks were associated with what appeared to be metallic ingots in the neutron radiographs. The neutron radiographs also showed some fuel bridging in the central voids, particularly for the pins with the two highest heat rates. Figure 5.34 is a composite of the gamma scan, neutron radiograph, and sectioning diagram for fuel pin 43-121-2, showing these features. The sections for metallographic examination were selected to investigate

Table 5.8. Operating conditions for capsules 43-120 and 43-121 at start of irradiation

| Pin | Thermocouple | Temperature of inner surface of cladding ($^\circ\text{C}$) | Heat rate (kW/ft) |
|----------|--------------|---|-------------------|
| 43-120-1 | 1 | 595 | 16.0 |
| | 2 | 575 | 15.4 |
| 43-120-2 | 3 | 625 | 17.0 |
| | 4 | 630 | 17.2 |
| 43-120-3 | 5 | 595 | 16.0 |
| | 6 | 545 | 14.5 |
| 43-120-4 | 7 | 440 | 11.0 |
| | 8 | 380 | 9.5 |
| 43-121-1 | 1 | 545 | 14.5 |
| | 2 | 545 | 14.5 |
| 43-121-2 | 3 | 565 | 15.0 |
| | 4 | 610 | 16.4 |
| 43-121-3 | 5 | 475 | 12.1 |
| | 6 | ^a | ^a |
| 43-121-4 | 7 | 407 | 10.0 |
| | 8 | 407 | 10.0 |

^aInoperative thermocouple; lost during shipment.

45. A. R. Olsen and R. A. Buhl, *Comparative Tests of Sol-Gel Pellet and Sphere-Pac (U,Pu)O₂ Fuels in Instrumented Thermal Flux Tests* (in preparation).

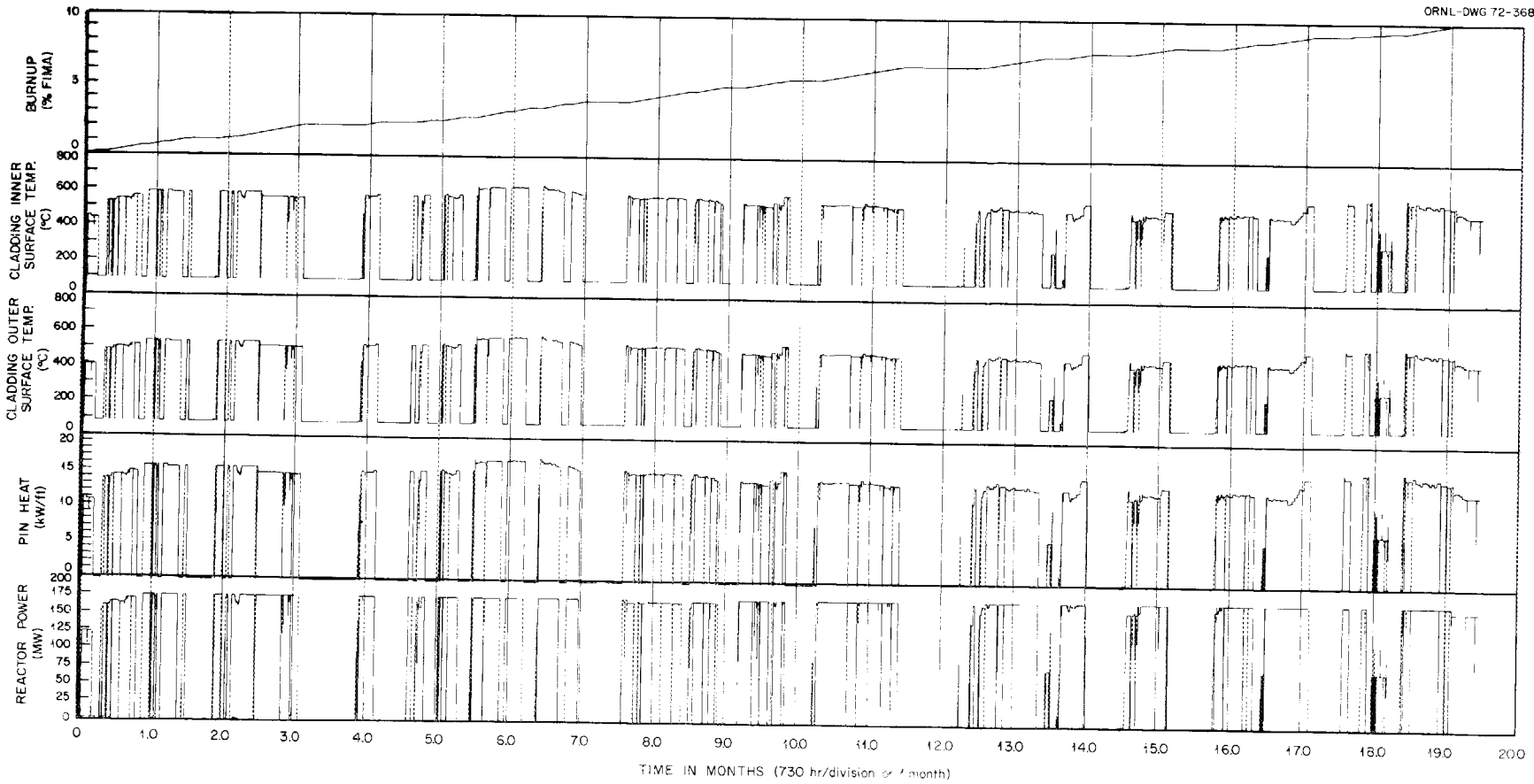
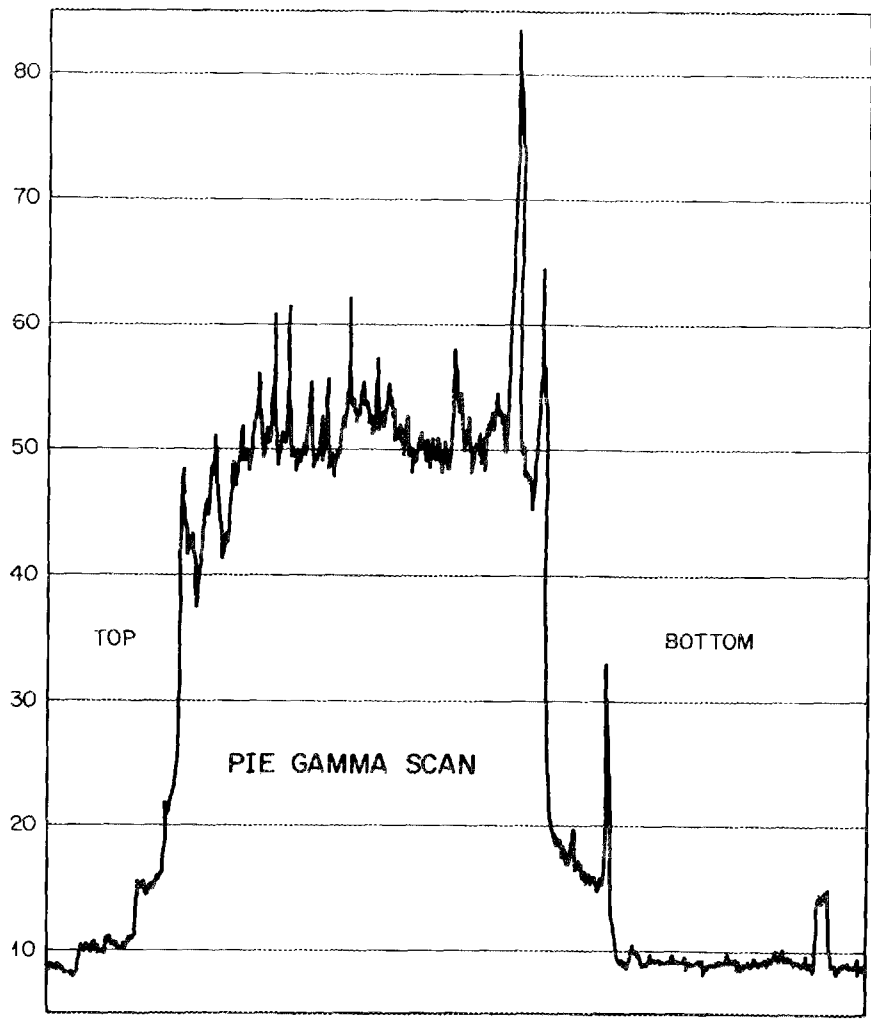


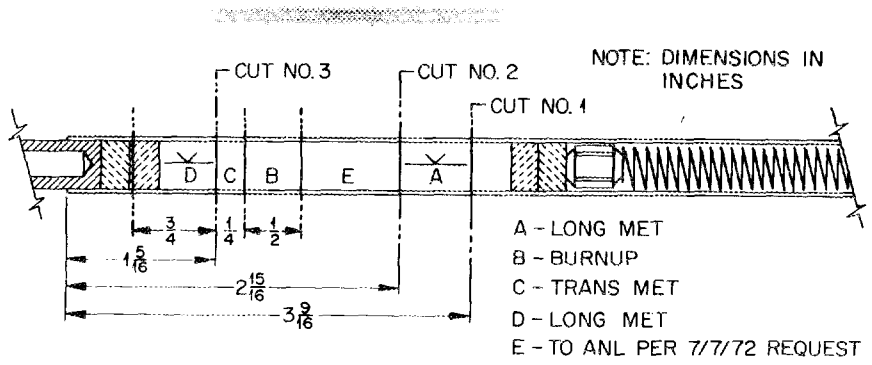
Fig. 5.32. History of capsule ORNL-43-121, fuel pin 2.



Fig. 5.33. History of capsule ORNL-43-120, fuel pin 3.



NEUTRON RADIOGRAPH



SECTIONING DIAGRAM

Fig. 5.34. Postirradiation gamma scan, neutron radiograph, and sectioning diagram for series I ETR instrumented capsule pellet pin 121-2.

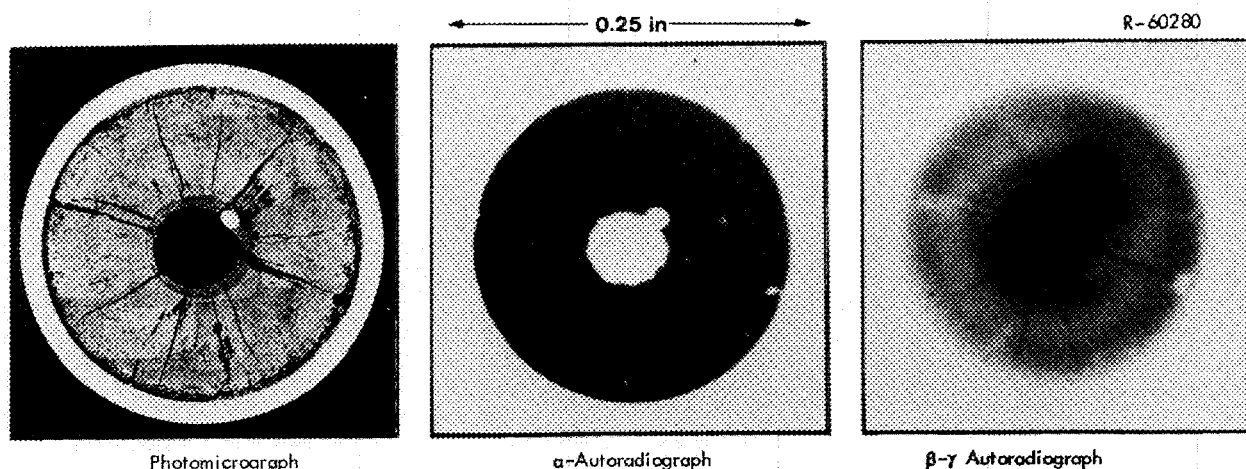


Fig. 5.35. Cross section of pellet fuel pin 121-1 irradiated to 9.3% FIMA with a peak linear heat rate of 15.7 kW/ft.

these phenomena. An example of the metallic ingot can be seen in Fig. 5.35, and metallic ingots and fuel bridging can be seen in Fig. 5.36. The metallographic examinations confirm the presence of metallic ingots within the central void regions of both pellet pins (positions 1 and 2) and one Sphere-Pac pin (position 3). Adjacent to these ingots we have found a two-phase cast structure consisting of a matrix of $(U,Pu)O_2$ with barium in the second phase. A similar structure was seen previously in a Fast Gas-Cooled Breeder Reactor test fuel pin.⁴⁶ Part of the columnar grain region surrounding this structure was relatively free of metallic particles.

The general structures of all four pins can be seen in Figs. 5.37 and 5.38. Since these structures indicate the possibility of peak power excursions near melting, we examined the daily log sheet data on the thermocouple readings to see if there had been a short period of very high-power operation that had been overlooked. None was found. However, the peak power levels during the last cycle of irradiation, in which the capsule had been moved to the higher flux position, were very close to the maximum recorded at anytime during the irradiation history. A change in calibration of the thermocouples during irradiation could mean they saw their peak power operation at the end of life. The low power readings do not substantiate this postulate.

The most likely explanation of the center melting, which had to occur during the later stages of irradiation,

can be ascribed to a variety of causes, each contributing to the final result. These are:

1. The thermal conductivity of the fuel is changed. Recently Moore⁴⁷ has calculated the effects of fission products in solid solution in UO_2 . He predicts an increase in thermal resistivity of $0.37 W^{-1} cm (^{\circ}C)$ at all temperatures for each 1% FIMA. Thus, the mean thermal conductivity in these fuels at 10% FIMA would be reduced approximately 10%.

2. The fuel melting point near the central void has been reduced by the higher concentration of plutonium in this region and the migration of barium up the temperature gradient.⁴⁸

3. The fission rate radial distribution in these fuels has been changed by both a reduction in self-shielding and the radial change in plutonium concentrations.

Thus, at a linear heat rate near the start-of-life peak heat rate, which resulted from the movement of the capsule to a higher flux position, some central fuel melting is likely. The effects of self-shielding will not be significant in a fast flux, so the examination of the EBR-II series I test pins discussed in Sect. 5.5, which also received a step in flux after achieving a burnup of approximately 5% FIMA, should provide additional information on this phenomenon.

46. R. B. Fitts, E. L. Long, Jr., and D. R. Cuneo, *Gas-Cooled Reactor Program Semiannual Progr. Rep. Mar. 31, 1970*, ORNL-4589, pp. 80-91.

47. J. P. Moore, ORNL, private communication on Nov. 13, 1972.

48. M. Conti, M. Mochiuto, and F. K. Lohmütz "Postirradiation Observations of Mixed Oxides with Initial Addition of Fission Product Elements," *Nucl. Technol.* 16(1), 143-55 (October 1972).

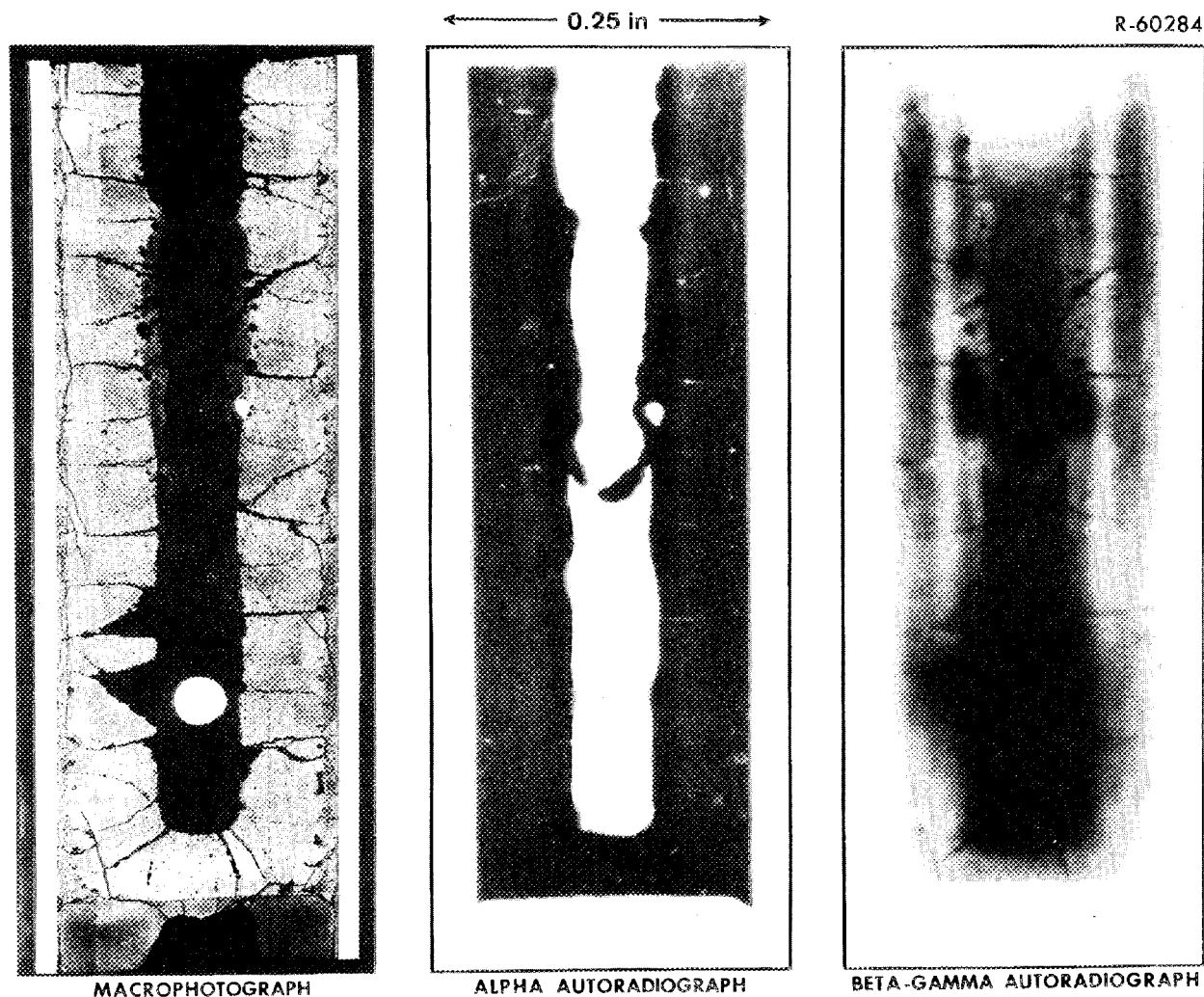


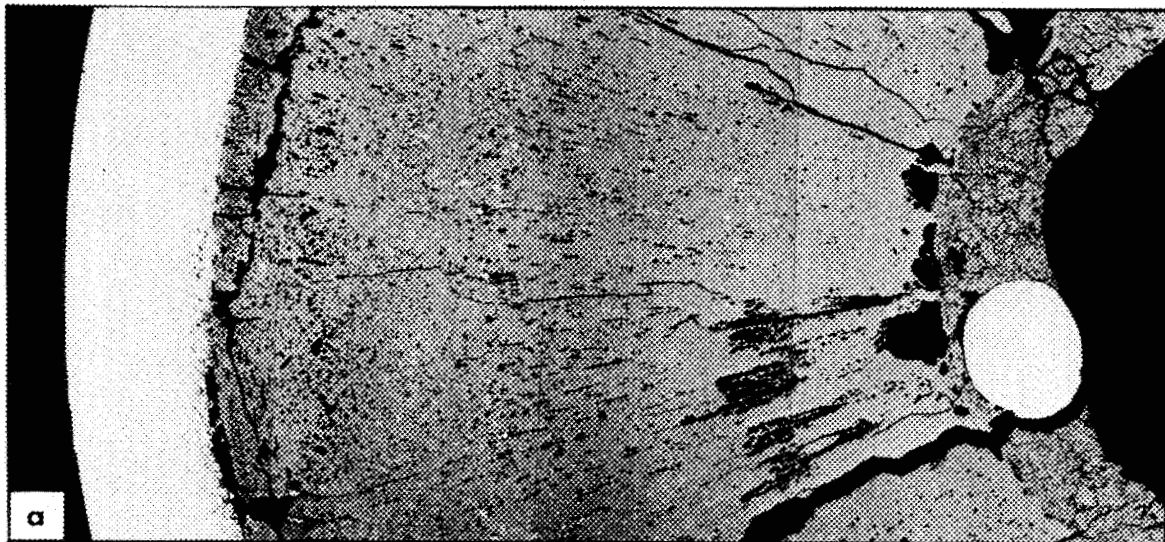
Fig. 5.36. Longitudinal section at bottom of fuel column in Sphere-Pac fuel pin 121-3.

Table 5.9 is a summary of the available operating and postirradiation data on both capsules. The data on all pins except 43-121-3 were consistent with preirradiation calculations. One of the thermocouples on this pin failed during insertion of the capsule into the reactor. Since there is a flux gradient across the capsules, the average of two thermocouples is needed to define the linear heat rate. It was apparent from the difference in the calculated and measured burnups on 43-121-3 that the thermocouple on the low-flux side of the capsule was operative, so the apparent linear heat rates and cladding temperatures for this test pin were all low. Assuming a consistent flux gradient and adjusting all heat rates by the ratio of measured to calculated burnups (1.15), the peak heat rates and cladding

temperatures were calculated, and these are the values reported in the table. These corrections seem to be thoroughly justified by the fact that the other three pins have calculated and measured burnup levels within 5% of each other. The power distribution in the nearby 43-120 capsule also indicates that 121-3 operated at a higher power than the thermocouple was indicating.

The metallography clearly shows fuel-cladding chemical interaction for three of the four pins. Typical micrographs of the fuel-cladding interfaces are shown in Fig. 5.39. With the exception of the pellet pin in the SG-3 ORR instrumented test (see Sect. 5.2), we have not seen this type of attack in our irradiation tests. A comparison of the depth and type of attack on the two pellet pins shows the total attack depth to be equal at

R-60287



0.05 in

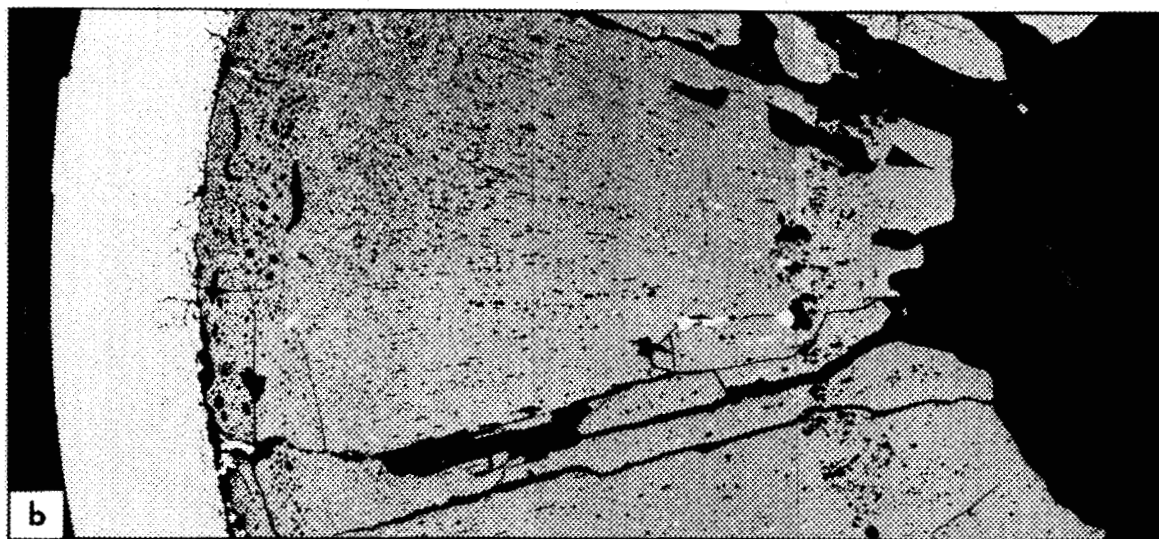


Fig. 5.37. As-polished microstructures from pellet pins (a) 121-1 and (b) 121-2.

R-60288

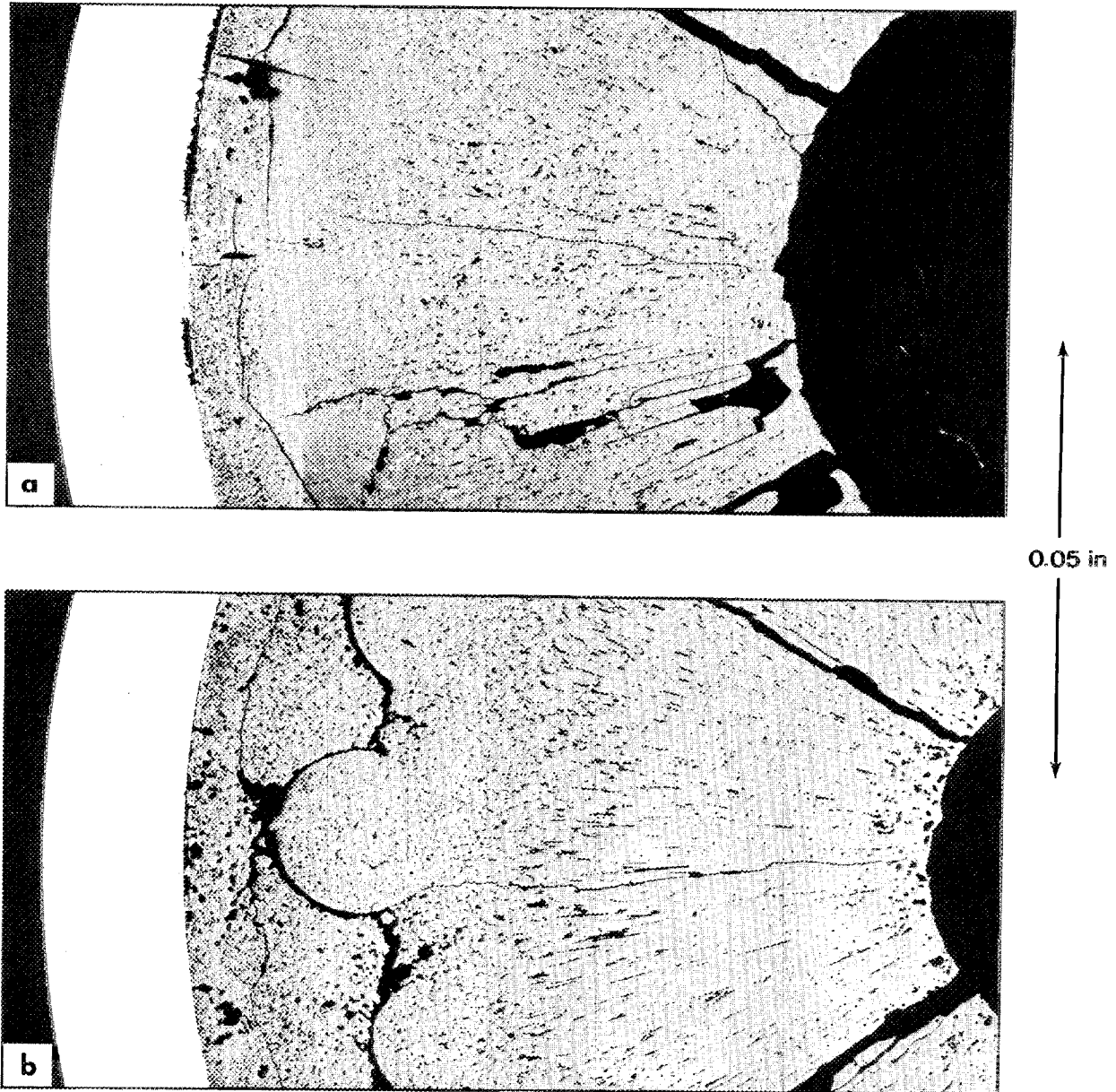


Fig. 5.38. As-polished microstructures from Sphere-Pac pins (a) 121-3 and (b) 121-4.

Table 5.9. Fabrication and operating conditions for capsules 43-120 and 43-121 derived from in-reactor thermocouple data

| Pin | Fuel | | | Peak linear heat rate (kW/ft) | | | Peak inner cladding surface temperatures (°C) | | | Peak burnup (% FIMA) | | Fission gas release (% ⁸⁵ Kr) | Equiv. full-power days | Number of power cycles ^e |
|--------------------|------------|-------------------------|-------|-------------------------------|------|---------------------|---|------|--------|-------------------------|-----------------------|--|------------------------|-------------------------------------|
| | Form | Smear density (% of TD) | O/M | S.O.L. ^a | Max. | E.O.L. ^b | Peak inner cladding surface temperatures (°C) | | | Peak burnup (% FIMA) | | | | |
| | | | | | | | S.O.L. | Max. | E.O.L. | Calculated ^c | Measured ^d | | | |
| 120-1 | Pellet | 81.1 | 1.986 | 15.7 | 16.9 | 13.6 | 575 | 610 | 510 | 11.1 | | | 351 | 106 |
| 120-2 | Pellet | 81.5 | 1.986 | 16.6 | 16.8 | 13.4 | 595 | 605 | 505 | 11.0 | | | 351 | 106 |
| 120-3 | Sphere-Pac | 84.8 | 1.977 | 17.0 | 17.0 | 13.4 | 615 | 615 | 505 | 9.7 | | | 351 | 106 |
| 120-4 | Sphere-Pac | 84.6 | 1.977 | 11.1 | 12.5 | 12.5 | 395 | 480 | 480 | 7.4 | | | 351 | 106 |
| 121-1 | Pellet | 81.0 | 1.986 | 14.4 | 15.7 | 15.7 | 535 | 575 | 570 | 9.2 | 9.3 | 81.2 | 335 | 79 |
| 121-2 | Pellet | 81.2 | 1.986 | 16.1 | 17.3 | 16.8 | 585 | 625 | 610 | 10.3 | 9.8 | 99.3 | 335 | 79 |
| 121-3 ^f | Sphere-Pac | 83.9 | 1.977 | 15.2 | 16.5 | 16.2 | 565 | 605 | 600 | 8.2 | 9.5 | 86.3 | 335 | 79 |
| 121-4 | Sphere-Pac | 85.5 | 1.977 | 10.2 | 12.0 | 12.0 | 405 | 460 | 460 | 6.7 | 6.7 | 74.9 | 335 | 79 |

^aS.O.L. -- start of life or the first time the reactor reached the 175-MW power level.

^bE.O.L. -- end of life or the last time the reactor was at 175 MW before the capsule was removed. Note: This was obtained for the pins after the capsule had been moved to a higher flux position for the last cycle of irradiation.

^cPeak burnup was calculated on integrated heat rates derived from the thermocouple readings using an energy of 180 MeV per fission and using the reactor power history for interpolation.

^dPeak burnup was measured by the analysis of the ¹⁴⁸Nd fission product.

^eThe number of power cycles is the number of times the reactor power went from greater than 50% of full power to less than 50% of full power during the irradiation.

^fOnly one thermocouple was functioning on this pin, so all data are less reliable than for the other seven pins in the two capsules. Peak linear heat rates were derived by multiplying the thermocouple data by the ratio of measured to calculated burnup. Cladding temperatures are reported for the adjusted heat rates.

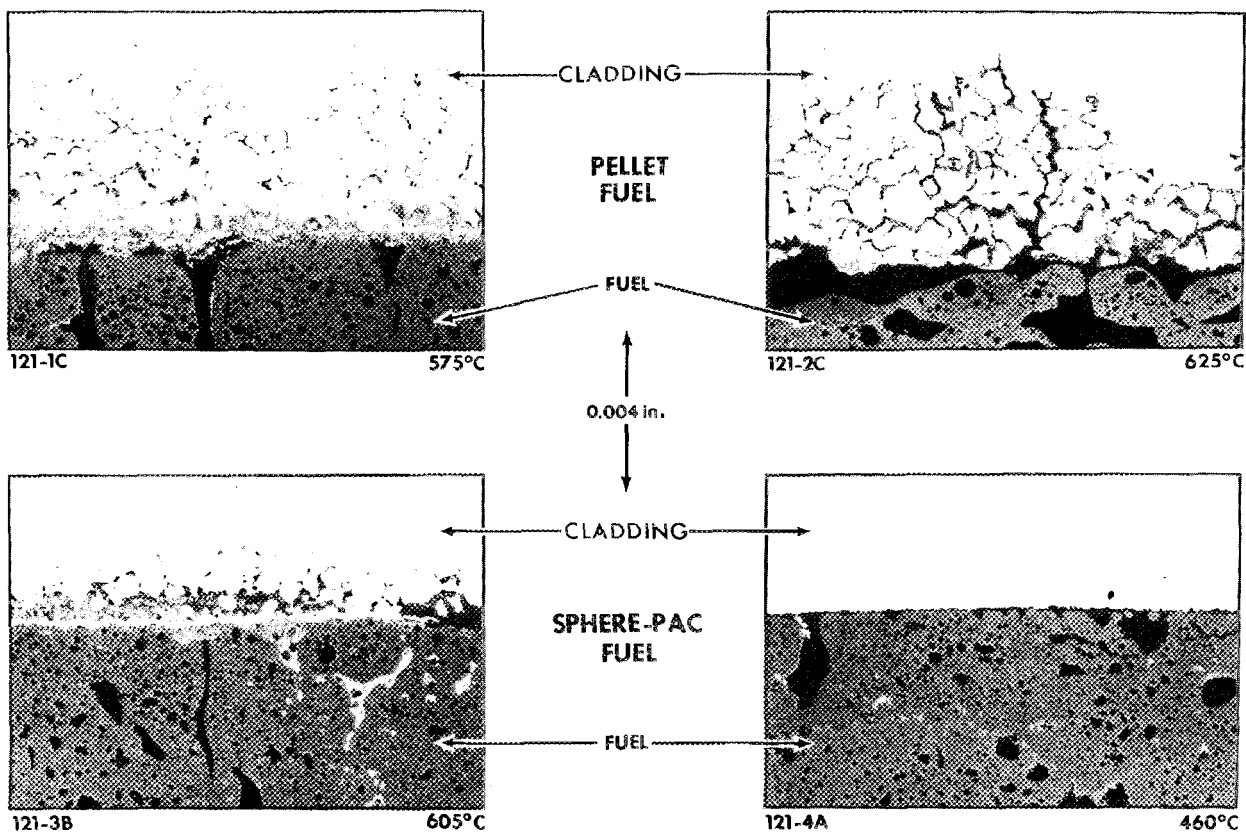


Fig. 5.39. Fuel-cladding interface micrographs, showing intergranular attack at various peak cladding inner-surface temperatures.

0.0054 in.; however, the distribution of the two types of attack is different, with matrix attack being greater at the higher temperature. The extent of attack on the Sphere-Pac pins is significantly less. However, because of the uncertainty in the true cladding temperature on pin 121-3 this conclusion will need to be verified by the examination of the pins from capsule 43-120. That examination should provide the best comparison of pellet and Sphere-Pac fuel-cladding chemical interaction, as can be seen from the comparable operating conditions summarized in Table 5.9. Additional discussion of the fuel-cladding chemical interaction phenomena is presented in Sect. 5.8.6.

A limited amount of microprobe data was obtained on transverse sections from pins 121-1 and 121-3 at ORNL. Similar sections from pins 121-2 and 121-3 were sent to Argonne for additional metallography and detailed microprobe analysis. The actinide redistribution found on pins 43-121-1 and 43-121-3 was typical,⁴⁵⁻⁵⁰ with more uranium movement in the pin with the higher heat rating, as can be seen by comparing

Figs. 5.40 and 5.41. Ruthenium was the only fission product found in the large metallic inclusions at the central void. This centrally located two-phase oxide structure contained large amounts of barium and detectable amounts of cerium in the second phase. These features can be seen in the electron-beam scanning images in Fig. 5.42. Similar scanning images of the fuel-cladding interface can be seen in Fig. 5.43. Tellurium and cesium, in small concentrations, were found at the oxide-metal interfaces. The metallic stringers in the oxide were iron and chromium from the cladding. We tried to detect fission products in the intergranular attack areas of the cladding. None were

49. A. R. Olsen, R. B. Fitts, and W. J. Lackey, *In-Reactor Restructuring Temperatures and Kinetics for (U,Pu)O₂*, ORNL-TM-3387 (July 1971). Also pp. 579-602 in *Proc. Conf. Fast Reactor Fuel Element Technology*, ed. by Ruth Farmakes, American Nuclear Society, Hinsdale, Ill., 1971.

50. W. J. Lackey, F. J. Homan, and A. R. Olsen, "Porosity and Actinide Redistribution During Irradiation of (U,Pu)O₂," *Nucl. Technol.* 16(1), 120-42 (October 1972).

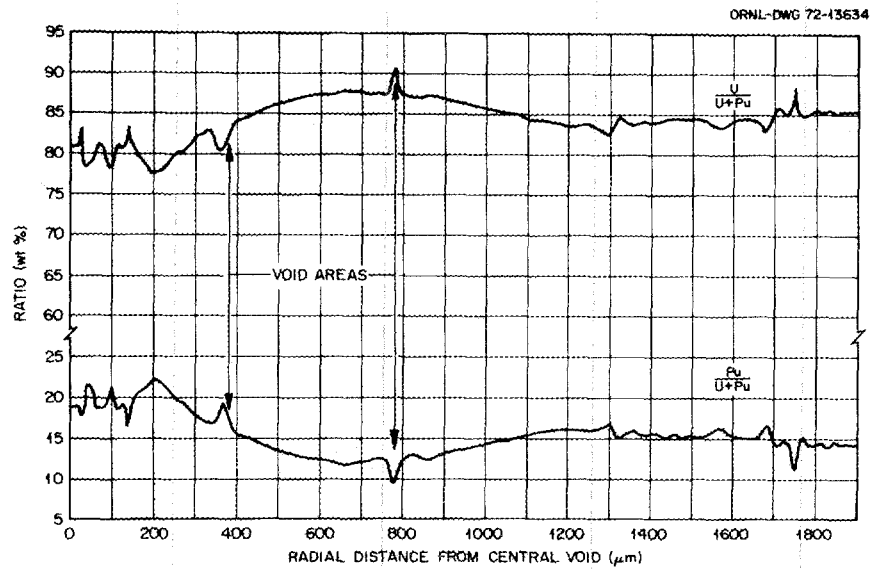


Fig. 5.40. Heavy-metal distribution in sample 43-121-1A.

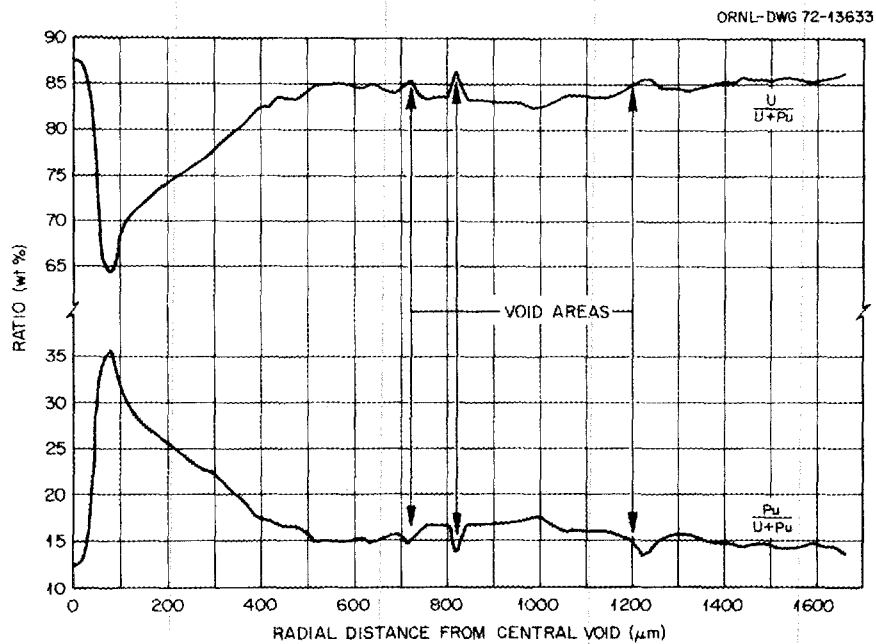


Fig. 5.41. Heavy-metal distribution in sample 43-121-3B.

found. Because of the high activity of these metallographic-size samples, minor amounts may have escaped detection. The noticeable decreases in the cladding primary constituents -- iron, nickel, and chromium -- in the intergranular areas suggest they are filled with

compounds such as carbides or oxides. More information on the fission product distributions should be derived from the thin sections specifically prepared for microprobe analysis at Argonne.

Y-114325

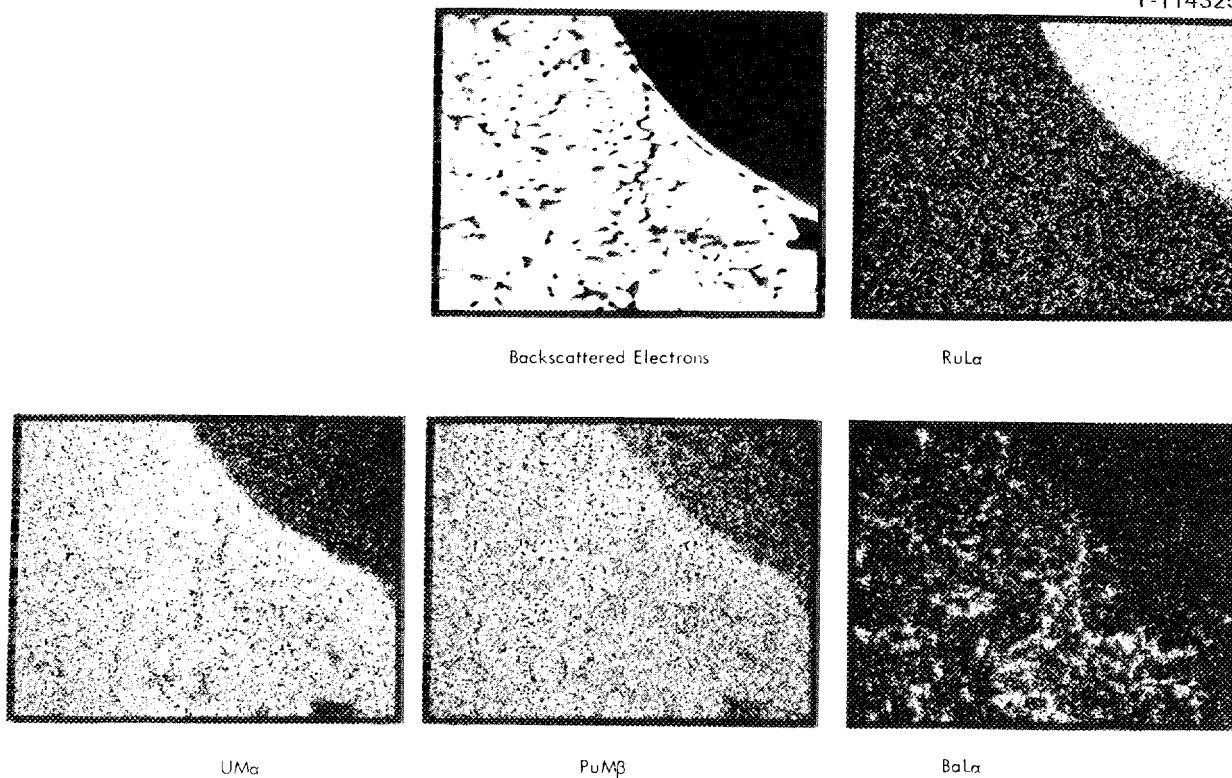


Fig. 5.42. Electron-beam scanning images of metallic structure (43-121-1A, MX-4668).

Y-114324

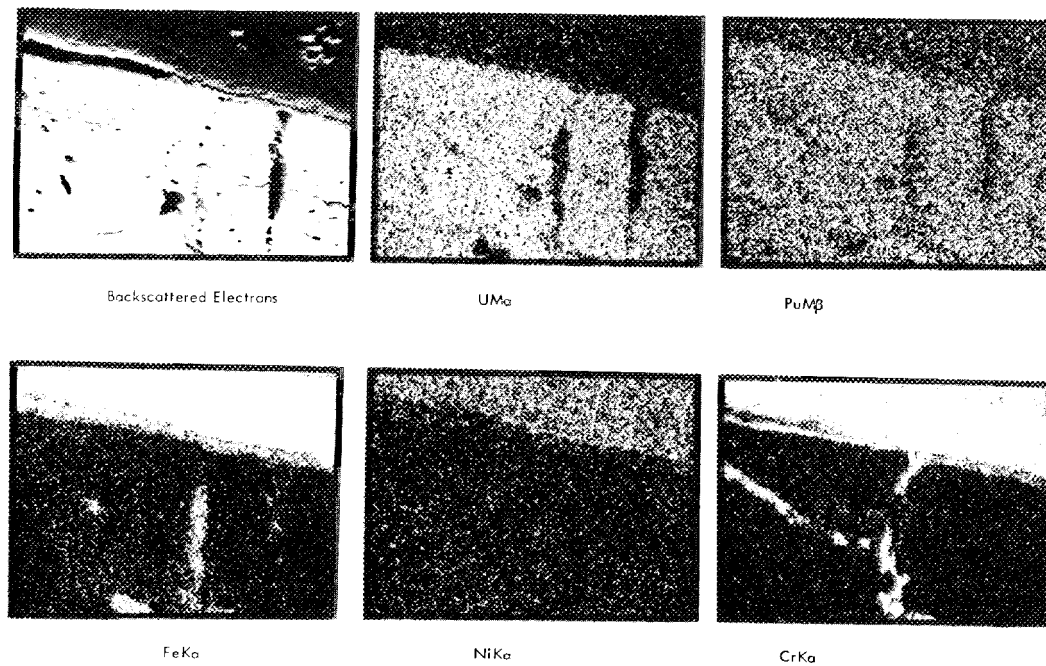


Fig. 5.43. Electron-beam scanning images of fuel-cladding interface (43-121-1A, MX-4668).

5.4 MECHANICAL INTERACTION TEST

B. Fleischer R. L. Senn⁵¹
R. B. Fitts J. A. Conlin⁵¹

5.4.1 Experimental Plan

The possibility of failure of fuel pins through mechanical interaction between fuel and cladding has become an important question in assessing the life of metal-clad pellet fuel pins.⁵²⁻⁵⁴ The objective of the mechanical interaction series of tests was to investigate this phenomenon with Fast Test Reactor (FTR) and Liquid-Metal Fast Breeder Reactor (LMFBR) type fuel pins.

Our general test plan included an initial experiment, *Mechanical Interaction Test-1 (MINT-1)*, to develop our basic test equipment while also attempting to evaluate a "typical" FTR fuel pin. Typical was defined as a pin whose dimensions and makeup were in the middle of those allowed by FTR specifications. An operation power level of 17 kW/ft in the thermal flux Oak Ridge Reactor (ORR) was selected to match the fuel centerline temperature with that expected in the peak-power FTR pin with hot channel factor added (see Fig. 5.44). The operation plan also included an occasional 20% overpower condition and rapid shutdown to simulate reactor scrams. Heat-up to power for each cycle was done at a rate selected to achieve full power (17 kW/ft) in 2 to 3 hr. The amount of time at power was variable, depending upon the experimental information desired and the manpower availability for shutdown. Shutdown to zero power was done in 2 min by continuously retracting the capsule from the face of the reactor. Because of high gamma heating rates in the capsule instrumentation causing higher than acceptable temperatures in the delicate instruments, we were unable to cycle at the 20% overpower condition.

5.4.2 Design and Construction

The conceptual design of the capsule for the first of this test series is presented in Fig. 5.45. This design provides for in-test measurement of fuel column and cladding length changes, internal fission gas pressure,

51. Reactor Division.

52. G. Kjerheim and E. Rolstad, "In-Core Study of the Mechanical Interaction between Fuel and Cladding," *Nucl. Appl. Technol.* 7, 347-60 (October 1969).

53. J. F. Giovenyo, *In-Pile Dimensional Changes of ThO₂ UO₂ Fuel Rods with Non-Free-Standing Cladding* (LWBR Development Program), WAPD-TM-986 (November 1970).

54. E. Rolstad and K. D. Knudsen, "Studies of Fuel-Clad Mechanical Interaction and the Resulting Interaction Failure Mechanism," *Nucl. Technol.* 13, 168-76 (February 1972).

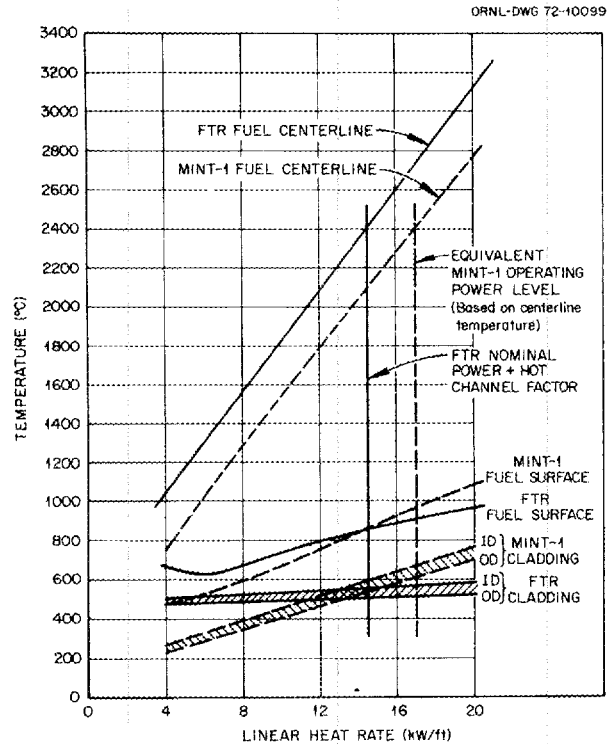


Fig. 5.44. Comparison of FTR and MINT-1 fuel element operating temperatures.

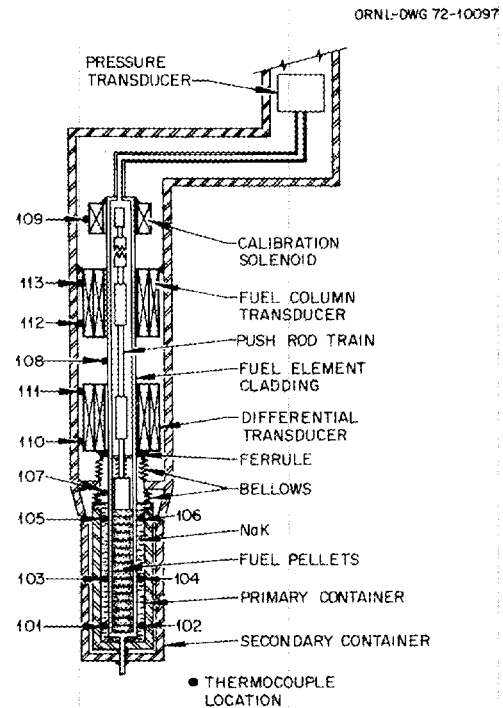


Fig. 5.45. Conceptual drawing of MINT-1 capsule lower portion.

and temperatures as shown. Motion of the fuel and cladding was determined with variable permeance differential transducers (VPDT's). Motion was detected by movement of the transducer cores, which were attached to a pushrod that responded to fuel column movement. The upper transducer coil, which was fixed with respect to the bottom of the fuel column, measured fuel column movement. The lower transducer coil was attached to the cladding above the fuel column and moved with the cladding. It therefore measured the difference between movement of the fuel column and the cladding. The movement of the cladding could then be deduced from these two measurements. The capsule also contained instruments and equipment for in-test calibration of the motion transducers. A flux monitor tube was included for periodic determination of the axial flux distribution.

5.4.3 Results

The MINT-1 capsule was inserted into the ORR in November 1971 and removed in June 1972, having accumulated 1.7% FIMA exposure. A total of 32 cycles to power included 6 cycles at low power (≤ 10 kW/ft) during start-up, 17 cycles to 14 kW/ft, 4 cycles to 16 kW/ft, 2 cycles to 17 kW/ft, and 3 multilevel cycles between 10 and 17 kW/ft.

MINT-1 was instructive in identifying some problems in the design and apparatus. In addition, it provided useful insight into gas release behavior for FTR prototypic fuel and confirmed the expansion behavior expected for dished fuel pellets. Details of the experiment are reported elsewhere.⁵⁵ The specific conclusions and recommendations are itemized below.

1. No evidence of significant mechanical interaction was found.
2. The cladding length was governed by its average temperature and normal thermal expansion.
3. The fuel column expansion during power transients was controlled by temperature changes near the outer surface of the FTR dished pellet. The thermal expansion was in the range predicted on the basis of out-of-reactor thermal expansion data and the fuel temperature at the outer surface and at the inner edge of the dish.
4. The fuel column was shortened each time the fuel pin was operated at any *new high* power level above 10 kW/ft, probably due to irradiation-enhanced creep of

the fuel. This phenomenon appears to be accelerated by operation at higher fuel linear heat ratings.

5. The fuel column expanded slightly during constant power operation, probably due to burnup accumulation.

6. The net fuel column length change after operating 15,783 kWhr to a burnup of 1.7% FIMA at power levels from 10 to 17 kW/ft was a shrinkage of 61 mils for the 9.6-in.-long fuel column.

7. Fission gas release for prototypic FTR fuel was continuous with respect to time at power and did not significantly depend upon power cycling.

8. The fission gas release rate increased with increasing operating power level. At 13.5 and 14 kW/ft the estimated steady-state release at low burnup was 30 and 36%, respectively. The total gas release after 1.7% FIMA with an end-of-life heat rating of 16.6 kW/ft was 56%.

9. Most of the adsorbed gases were released from the fuel at low power (≈ 4 kW/ft) and quickly reacted and/or diffused out, thus having an inconsequential effect upon internal gas pressure.

10. Future capsule designs incorporating VPDT's should provide for their use in cold regions to avoid effects of thermal gradients and minimize chances of damage by thermal cycling.

11. Future capsule designs should provide better centering of the fuel elements and sufficient supports to prevent bowing of the element.

5.5 FAST REACTOR TESTS – EBR-II ENCAPSULATED PINS

A. R. Olsen A. Jostsons⁵⁶ J. O. Stiegler

The fast flux irradiation tests were all planned for irradiation in the Experimental Breeder Reactor-II (EBR-II). These tests were designed to obtain data in an environment where the fission rate distributions in the fuel would be comparable with those in commercial LMFBR fuels and where the fast flux effects on the cladding material would be occurring concurrently. The tests were subdivided into three series. The series I group involved enriched uranium and fuel pin encapsulation; the series II group, enriched uranium and no encapsulation; the series III group, normal uranium and no encapsulation. Both the series I and series II tests were carried to the point of irradiation, and these are discussed respectively in this and the following sections.

55. R. B. Fitts, B. Fleischer, and R. L. Senn, *Fuel-Cladding Interaction and Gas Pressure Buildup in a Shortened FTR Type Fuel Pin*, ORNL-4875 (June 1973).

56. On attachment from the Australian Atomic Energy Commission Research Establishment.

The series III tests were proposed in March 1971 and preliminary design work was completed. These tests would have provided the most realistic tests of LMFBR conditions in that they would have operated at typical design temperatures and heat rates, and the fission product yields would have been only from plutonium. This way their effect on oxygen potential would have been similar to that in commercial LMFBR fuels, and the fast-flux-to-fission ratio would have been essentially the same as in commercial fuel pins, rather than 40% as much, which is typical of enriched uranium fuel tests in the EBR-II. Approval-in-principle was withheld because of the termination of the ORNL program, so the test design was not completed and no fabrication was initiated.

5.5.1 Experimental Plan

The series I oxide fuels tests in the EBR-II, as originally proposed, would have included both pellet and Sphere-Pac fuels. However, since other sites were also proposing tests of Sphere-Pac (notably the Babcock & Wilcox Company and Argonne National Laboratory), and there was no experience with such fuels in a fast flux environment, the AEC suggested the test series be reduced to a limited number of pins containing only Sphere-Pac with secondary encapsulation. These pins would then serve as lead experiments to unencapsulated pin tests, which could be run in larger numbers in the EBR-II with companion pins containing fuel from the other processes for comparison. Five encapsulated pins were fabricated in 1968 and inserted into a row 4 position in the reactor.

The primary purposes of the series I tests were:

1. to establish the effects of fast flux irradiation on the performance of fuel pins fabricated by the Sphere-Pac process from fuels derived from the ORNL sol-gel process,
2. to provide assurance that pins containing Sphere-Pac fuels would not fail prematurely, so that a larger number of unencapsulated pins containing Sphere-Pac fuel could be irradiated in the EBR-II with other pins containing different fuel forms for comparative evaluation, and
3. to preirradiate two of these pins for subsequent transient testing in the TREAT reactor.

The first purpose includes the collection of data on the effects of fast flux irradiation on fission gas release, fuel swelling, in-reactor restructuring, fuel and fission product distribution, and fuel-cladding chemical and

mechanical interaction. The second purpose was fully satisfied with the initiation of the unencapsulated series II irradiations in June 1971. The third purpose was incorporated because of some evidence that particulate fuels (Vi-Pac) might be more susceptible to power transient failures than pelletized fuels.⁵⁷ Subsequent tests of unirradiated Sphere-Pac fuels⁵⁸ summarized in Sect. 5.7 showed this was not the case, so transient testing of preirradiated fuel was deferred in favor of normal postirradiation examination of both the pins removed at the 5% FIMA burnup level.

5.5.2 Test Capsule Design and Fabrication

Details of the experiment design and fabrication have been reported.^{59,60} A schematic drawing of the capsule and fuel pin is shown in Fig. 5.46. Each pin was fabricated with a 13.5-in.-long fuel column of $U_{0.8}Pu_{0.2}O_{1.98}$ microspheres. The uranium was 93% enriched. Two ThO_2 insulator pellets were located on each end of the fuel column. A nickel reflector rod was located above the upper insulators. All pins contained a spring-loaded extensometer to prevent segregation in the packed fuel bed by providing axial restraint during preirradiation handling and to indicate the maximum fuel column length reached during testing. The gas plenum was designed to be approximately equal to the volume of the fuel at 100% density and to accommodate 100% release of the fission gases at a peak burnup of 11% FIMA. The cladding was 0.250-in. stainless steel tubing with a 0.016-in. wall thickness. Two pins, identified as S-I-A and S-I-B, had type 304 stainless steel cladding and three, S-I-C, S-I-D, and S-I-E, had type 316 stainless steel cladding. Both claddings were in the annealed condition. The bottom end plug in each pin had a threaded length, which was designed for use in the remote assembly of the transient test capsules.

57. G. R. Thomas and J. H. Field, "Transient Performance of Mixed Oxide Powder Fuel with Up to 60% Melting" (summary), *Trans. Amer. Nucl. Soc.* **12**(1), 343-44 (1969).

58. C. M. Cox, D. R. Cuneo, and E. J. Manthos, "Performance of Sphere-Pac and Pelletized (U,Pu)O₂ During Severe Overpower Transients," pp. 701-24 in *Proc. Conf. Fast Reactor Fuel Element Technology*, ed. by Ruth Farmakes, American Nuclear Society, Hinsdale, Ill., 1971.

59. A. R. Olsen, *Experiment Description and Hazards Evaluation for the Series I ORNL Oxide Fuels Irradiation in EBR-II*, ORNL-TM-2635 (April 1970); A. R. Olsen and F. J. Homan, ORNL-TM-2635 (supplement) (June 1970).

60. W. L. Moore, M. K. Preston, and J. D. Sease, *Fabrication of ORNL Series I Irradiation Test Capsules for Experimental Breeder Reactor II*, ORNL-TM-2922 (July 1970).

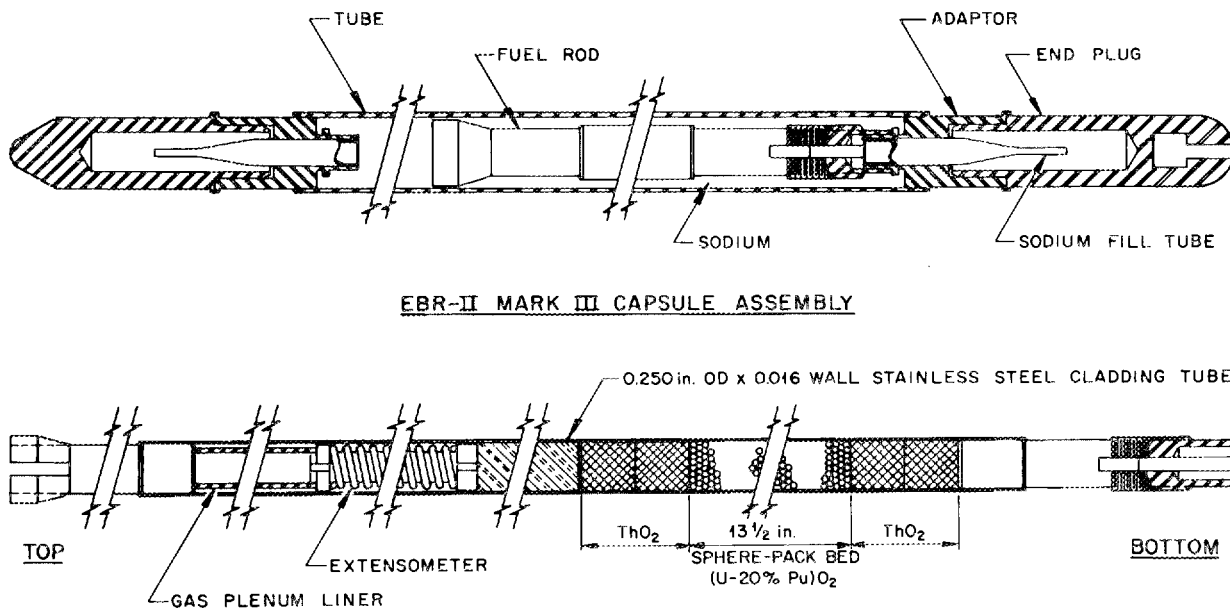


Fig. 5.46. Capsule and fuel rod for series I ORNL oxide fuels tests in EBR-II.

The pins were encapsulated with static sodium in a modified EBR-II Mark III capsule of annealed type 304 stainless steel. The capsule and end plugs were supplied by the EBR-II project and inspected by ORNL before use. The adapters on each end of the capsule were incorporated to permit sodium loading after the pin had been installed in the capsule tube.

The Sphere-Pac fuel beds were made up of two sizes of microspheres. The coarse spheres (420 to 595 μm in diameter) were loaded first. The resulting beds were then constrained and infiltrated with the fine spheres (<25 μm in diameter) to attain the final packed beds. It should be noted that these fuels were produced in laboratory-scale equipment early in this process development with enriched uranium sols, and the tests were initiated before all the current fuel characterization procedures were developed. The product microspheres were not perfectly spherical and did contain numerous pits and some fragments. The lack of sphericity was not considered serious in its effect on the performance characteristics, so, in view of the scheduling delays that would have been encountered otherwise, this fuel was used. The shape factors and the fragmentation undoubtedly contributed to the variations in final packed bed densities achieved. The variations can be seen in the summary loading data presented in Table 5.10.

5.5.3 Test Results

All five capsules were designed for irradiation in a standard EBR-II A-19 subassembly. The predicted heat rates, based on advertised EBR-II fission rates for a subassembly in one of the highest flux positions in a row 4 position, were to be between 12 and 16 kW/ft, depending on the location of the capsules in the subassembly. With the given subassembly loading, the predicted start-of-life operating conditions for the capsules were calculated as shown in Table 5.11.

Subassembly X 050 was inserted into position 4C2 of the EBR-II grid on February 23, 1969. The subassembly was irradiated continuously during runs 33 through 42 and discharged on May 18, 1970. During this period the reactor generated a total of 11,706 MWD of energy. This irradiation included 64 reactor power cycles from greater than 50% of maximum to less than 10% of maximum. The operating histories for the two pins (S-I-A and S-I-E) removed for destructive examination are summarized graphically in Fig. 5.47. The calculated burnups for all five capsules at the time subassembly X 050 was discharged are also listed in Table 5.11. Capsules S-I-B, S-I-C, and S-I-D were incorporated in subassembly X 119 for continued irradiation up to a target peak burnup level of 11.8% FIMA.

Table 5.10. Summary of preirradiation data

| Capsule | S-I-A | S-I-B | S-I-C | S-I-D | S-I-E |
|---|-------------------|-------------------|------------------|-------------------|-------------------|
| Fuel pin | 14-27-E | 14-23-A | 17-1 | 17-4-A | 17-4 |
| Type stainless steel cladding for fuel pin | 304 | 304 | 316 | 316 | 316 |
| Fuel | | | | | |
| Lot | 100 | 100 | 100 | 101 | 100 |
| Ratio of oxygen to metal | 1.99 | 1.99 | 1.99 | 1.98 | 1.99 |
| Weight, g | 76.84 | 77.18 | 73.97 | 70.76 | 73.09 |
| Bed height, in. | 13 $\frac{7}{16}$ | 13 $\frac{3}{64}$ | 13 $\frac{1}{2}$ | 13 $\frac{7}{64}$ | 13 $\frac{2}{64}$ |
| Density | | | | | |
| Smear, % of theoretical | 83.28 | 86.10 | 82.66 | 79.71 | 82.02 |
| Variation (by gamma scan), % (av) | ±8.6 | ±6.1 | ±2.3 | ±5.8 | ±8.1 |
| Oxygen in sodium, ppm (av) | 16 | 18 | 21 | 12 | 16 |

Table 5.11. Series I Sphere-Pac $U_{0.8}Pu_{0.2}O_{1.98}$ capsules irradiated in EBR-II

| Capsule | Peak linear ^a heat rate (kW/ft) | Peak temperature at inside surface of cladding (°C) | Peak burnup (% FIMA) | |
|---------|--|--|-------------------------|--------|
| | | | Current ^b | Target |
| S-I-A | 14 | 570 | 5.9 | 5.9 |
| S-I-B | 14 | 600 | 6.0 | 11.8 |
| S-I-C | 14 | 590 | 6.2 | 11.8 |
| S-I-D | 13 | 580 | 6.1 | 11.8 |
| S-I-E | 14 | 590 | 6.0 | 6.0 |

^aCalculated with EBR-II fission rates.^bCalculated through EBR-II run 42.

The results of the postirradiation examination of the two encapsulated pins S-I-A and S-I-E have been presented previously⁶¹ and a complete report is in preparation.⁶² The data from the two pins examined are summarized in Table 5.12 together with the cladding type and fuel smear density.

Pin S-I-A was slightly larger in diameter (0.254 instead of 0.250 in.) and had a higher smear density (83% instead of 82% of theoretical). These differences explain the higher linear heat rate for S-I-A with equivalent peak inner cladding temperatures and a lower burnup in the same irradiation time. We lost the

fission gas sample from pin S-I-A in postirradiation examination, but the 80% release value for S-I-E is similar to release rates reported by others.⁶³ The measured fluence seen by the cladding shows very good agreement with the predicted fluence, according to data supplied by the EBR-II operations group. Although S-I-E was located slightly closer to the core center, it was in an interior position in the subassembly and therefore may have seen a somewhat softer neutron spectrum. There was undoubtedly some flux suppression within this subassembly. We measured the burnup by radiochemical analysis of fission products and changes in the actinide isotopic analysis as well as the ¹⁴⁸Nd analysis reported in the table. The various

61. A. R. Olsen, "Sol-Gel Sphere-Pac (U,Pu)O₂ Fuel Performance in EBR-II Irradiation Tests" (summary), *Trans. Amer. Nucl. Soc.* 14(2), 596-98 (1971).

62. A. R. Olsen, *Series I Sol-Gel Sphere-Pac (U,Pu)O₂ Fuel Performance in EBR-II Irradiation Tests at Intermediate Burn-up*, ORNL report in preparation.

63. J. D. B. Lambert et al., "Performance of Mixed-Oxide Fuel Elements - ANL Experience," pp. 517-54 in *Proc. Conf. Fast Reactor Fuel Element Technology*, ed. by Ruth Farmakes, American Nuclear Society, Hinsdale, Ill., 1971.

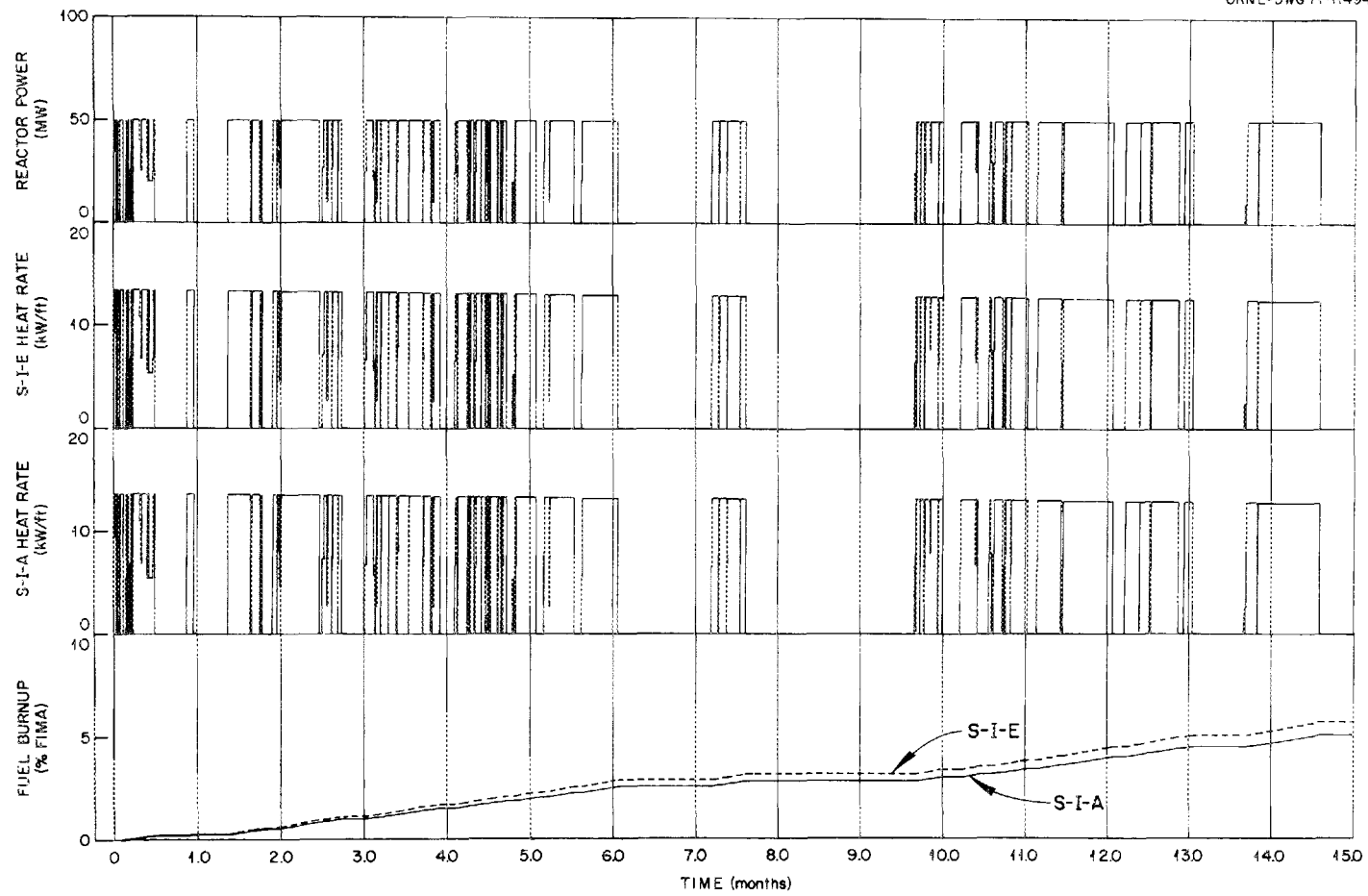


Fig. 5.47. Operating history for ORNL-EBR-II series I pins S-I-E and S-I-A.

Table 5.12. Fabrication and operating data for EBR-II series I
Sphere-Pac $U_{0.8}Pu_{0.2}O_{1.98}$ tests^a

| | S-I-A | S-I-E |
|---|----------------------|----------------------|
| Cladding, stainless steel | 304 | 316 |
| Outer diameter, in. | 0.254 | 0.250 |
| Fuel smear density, % of theoretical | 83 | 82 |
| Linear heat rate, kW/ft | | |
| Peak | 13.7 | 13.5 |
| Average | 12.2 | 12.0 |
| End-of-life peak | 12.7 | 12.5 |
| Peak cladding inner surface temperature, °C | 570 | 570 |
| Peak cladding fluence, neutrons/cm ² | | |
| Total | 4.2×10^{22} | 4.0×10^{22} |
| >0.1 MeV | 3.6×10^{22} | 3.4×10^{22} |
| Fuel burnup, % FIMA by ¹⁴⁸ Nd analysis | | |
| Peak | 5.11 | 5.74 |
| Average | 4.56 | 5.12 |
| Fission gas release, % | | 80 |
| Peak cladding diametral change, % | 0.71 ± 0.16 | 0.40 ± 0.08 |
| Peak capsule diametral change, % | 0.29 | 0.32 |

^aPins removed after 234.1 effective full-power days. Three similar capsules are continuing irradiation in subassembly X 119.

analyses agreed reasonably, but the averages were 8 to 14% below the values predicted from the EBR-II published fission rates for this core position.

More information on diametral changes for the fuel pins is presented in Fig. 5.48. Here we have plotted the mean diametral change as a function of axial location. The fueled region is located in the 1- to 14.5-in. section of this plot. A statistical analysis of the data indicates that any change greater than roughly 0.0005 in. is significant. Thus, all dimensional changes plotted in the 3- to 15-in. range are significant. The dimensional changes for the type 304 stainless steel cladding (S-I-A) are approximately twice the changes for comparable positions with the type 316 stainless steel (S-I-E) cladding. This difference agrees qualitatively with GE data reported by Craig et al.⁶⁴

In an effort to define the source of these dimensional changes and to investigate the effects of the temperature gradient across the cladding on void swelling, sections were examined from near the bottom, peak burnup region, and top of the fuel column. The fuel was removed and the cladding cut into small samples. A jet polishing technique was used to obtain specimens for transmission electron microscopy from areas within

0.001 in. of the inner and outer surfaces of each section.

In all locations except one, the microstructural features reflected the variations in temperatures across the cladding. At the hotter inner surfaces, voids were larger but fewer, and carbide precipitation in the grain boundaries was more massive and continuous. The exception was the section taken from near the peak flux position on the type 316 stainless steel cladding of pin S-I-E, where no significant variation was found.

Void swelling was calculated from the measured void diameters and concentrations and compared with quantities calculated from current empirical correlations^{65,66} for both types 304 and 316 stainless steel. In both cases measured values of the swelling are only about half the calculated values. Otherwise most of the trends found in other studies are followed. Type 304 stainless steel swells appreciably more than does type 316 stainless steel, mainly on account of higher void concentrations. In general, voids are larger in type 316 than in type 304 stainless steel. In the type 316 stainless steel cladding, measured void concentrations and sizes are both slightly less than calculated values, but in the type 304 stainless steel cladding, measured

64. C. N. Craig et al., "Steady State Performance of PuO_2-UO_2 Fast Reactor Fuels," pp. 555-78 in *Proc. Conf. Fast Reactor Fuel Element Technology*, ed. by Ruth Farmakes, American Nuclear Society, Hinsdale, Ill., 1971.

65. H. R. Brager et al., "Irradiation Produced Defects in Austenitic Stainless Steel," *Met. Trans.* 2, 1893 (1971).

66. H. R. Brager, Westinghouse Hanford Company, to J. O. Stiegler, ORNL, private communication, August 1972.

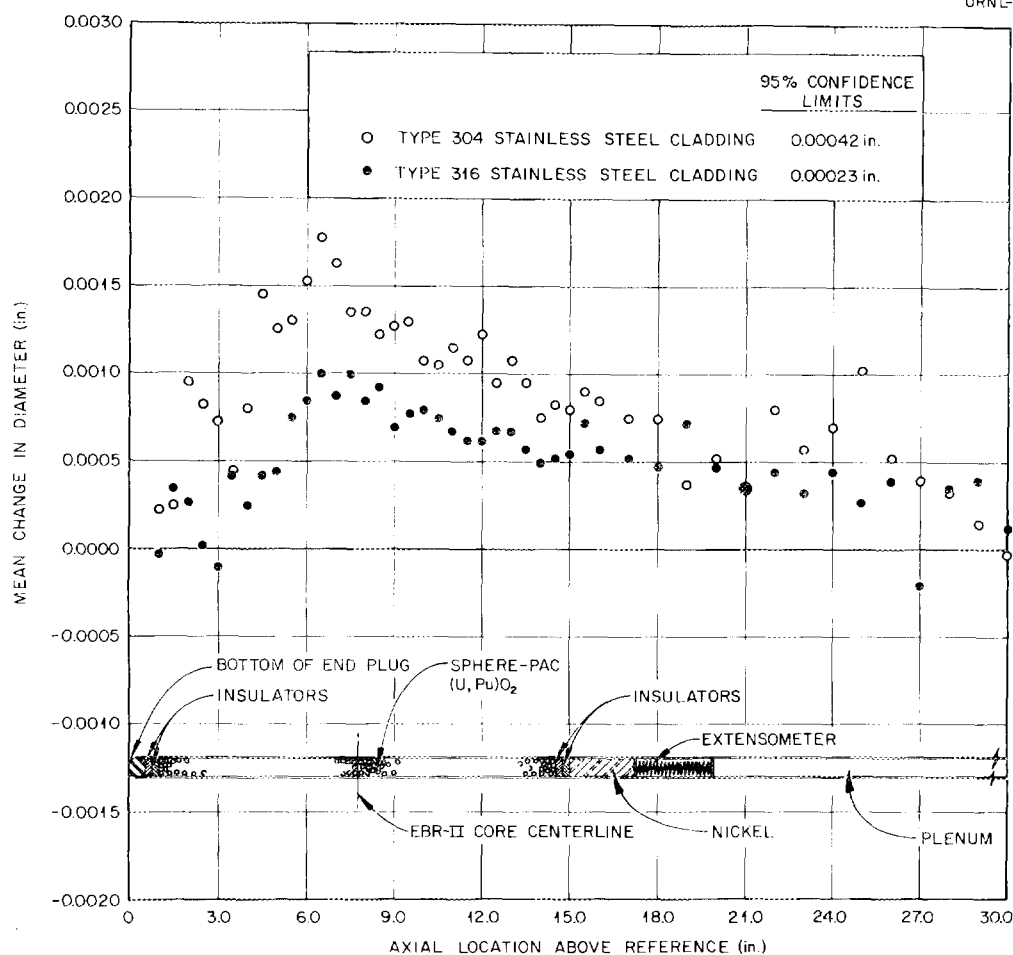


Fig. 5.48. Comparison of diametral changes for pins clad in type 304 or 316 stainless steel.

concentrations are much lower and measured sizes slightly larger than calculated.

These differences between measured and calculated values could reflect variations in composition of the steels or in the initial microstructures. Significant heat-to-heat variations in void concentrations and sizes but not in swelling have been noted.⁶⁷ We do not now attach any significance to the differences in void concentrations and sizes. The differences between measured and calculated values of swelling are outside our experimental error and must be considered real. The fluences may not be as high as we have estimated.

67. E. E. Bloom, "Nucleation and Growth of Voids in Stainless Steels During Fast-Neutron Irradiation," pp. 1-30 in *Radiation-Induced Voids in Metals*, ed. by J. W. Corbett and L. C. Ianniello, AEC Symp. Ser. 26, CONF-710601, U.S. Atomic Energy Commission Office of Information Services, April 1972.

Since in this temperature range the swelling appears to increase with fluence at a rate faster than linear, the correction would be appreciably less than the ratio of measured to calculated values of swelling would indicate. Alternatively, the temperatures may be in error.

The measured volumetric changes due to void formation will not account for the measured changes in diameter of the cladding. Using the approximation that diameter changes are one-third the volumetric changes, we find the cladding diameter measurements also show a change twice that calculated from the volumetric changes. This difference could be explained by small amounts of plastic deformation in the cladding during irradiation. This deformation might also account for the differences in void concentrations and sizes between these specimens and those used to develop the empirical formulas. A detailed study of the dislocations in these specimens may help resolve this question and will be conducted under another program.

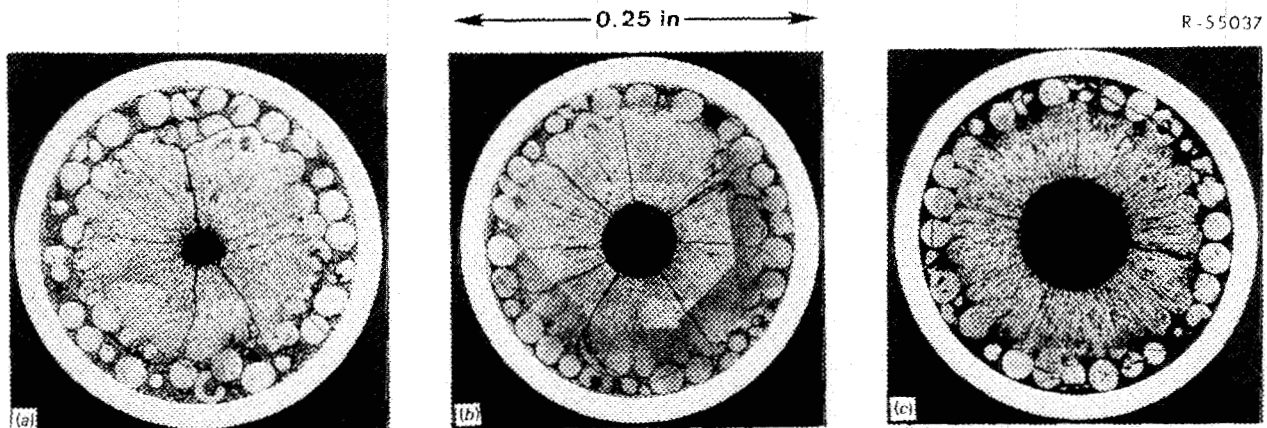


Fig. 5.49. Transverse metallographic sections from pin S-1-E. (a) Section A, bottom; (b) section B, center; (c) section D, top.

Fuel restructuring was similar to that in the thermal flux irradiation tests of Sphere-Pac fuel. Figure 5.49 shows transverse metallographic sections from pin S-1-E taken from the bottom, center, and top of the fuel column. These are also typical of similarly located sections from pin S-1-A. All the sections show the unstructured Sphere-Pac bed surrounding a columnar grain growth region and a central void. Section D from the top of the fuel column is unusual in that no fine spheres are in the unstructured region. Because we failed to add sufficient fine material in loading these pins, a distinctly low-density bed was formed in the top 2 in. This low-density region was shown in preirradiation gamma-densitometry measurements and very clearly in the postirradiation gamma scans and neutron radiography in Fig. 5.50. Here we have oriented the gamma scan trace and the neutron radiograph with the destructive examination sectioning diagram. It can be clearly seen that section D was taken from the top of the pin, where a dip occurred in the gamma activity, and the neutron radiograph shows a sudden increase in the central void diameter.

The open structure of the fuel bed in this area would provide an easy path for volatile fission products to migrate to the fuel-cladding interface. Nevertheless, as we can see in Fig. 5.51, there is no evidence of either gross uniform attack of the cladding or of intergranular penetration at the peak-heat-rate section with the cladding inner surface at 550°C or at the low-density fuel region where the cladding temperature was up to 570°C. A similar lack of attack was seen on the S-1-A pin with type 304 stainless steel cladding.

Microprobe analysis confirmed the absence of fission products from the cladding but did show concentra-

tions of Cs, Te, some Mo, and a little Nd in the deposit on the cladding surface. We looked for (but did not find) a concentration of uranium in the interface area.

The postirradiation fuel structure analysis also provided some confirmatory evidence for a high fuel-cladding gap conductance. The microstructural features in the fuel are shown in Fig. 5.52 together with a temperature scale calculated by the PROFIL⁶⁸ code. The columnar grain region has a density of 96% and is achieved at all temperatures above 1700°C. By use of the fuel thermal conductivity values reported by Baily et al.,⁶⁹ the calculated radii of the central voids and columnar grain growth regions were matched to the measured radii. This could not be done until the fuel outer surface temperature was established by assuming a gap conductance of $1.9 \text{ W cm}^{-2} (\text{°C})^{-1}$. This high gap conductance value is the one derived from the ORR instrumented tests. Although this is not concrete evidence for high gap conductance with Sphere-Pac fuels, it does strongly support the other data.

The results of the examination of the first two Sphere-Pac fuel pins examined after irradiation in a fast flux environment have confirmed the evidence of good performance seen in thermal flux irradiations. They

68. C. M. Cox and F. J. Homan, *PROFIL - A One-Dimensional FORTRAN IV Program for Computing Steady-State Temperature Distributions in Cylindrical Ceramic Fuels*, ORNL-TM-2443 (March 1969); Addendum, ORNL-TM-2443 (August 1969).

69. W. E. Baily et al., "Thermal Conductivity of Uranium-Plutonium Oxide Fuels," pp. 293-308 in *Intern. Symp. Plutonium Fuels Technol.*, Scottsdale, Arizona, 1967, *Nucl. Met.* 13, American Institute of Mining, Metallurgical, and Petroleum Engineers, New York, 1968.

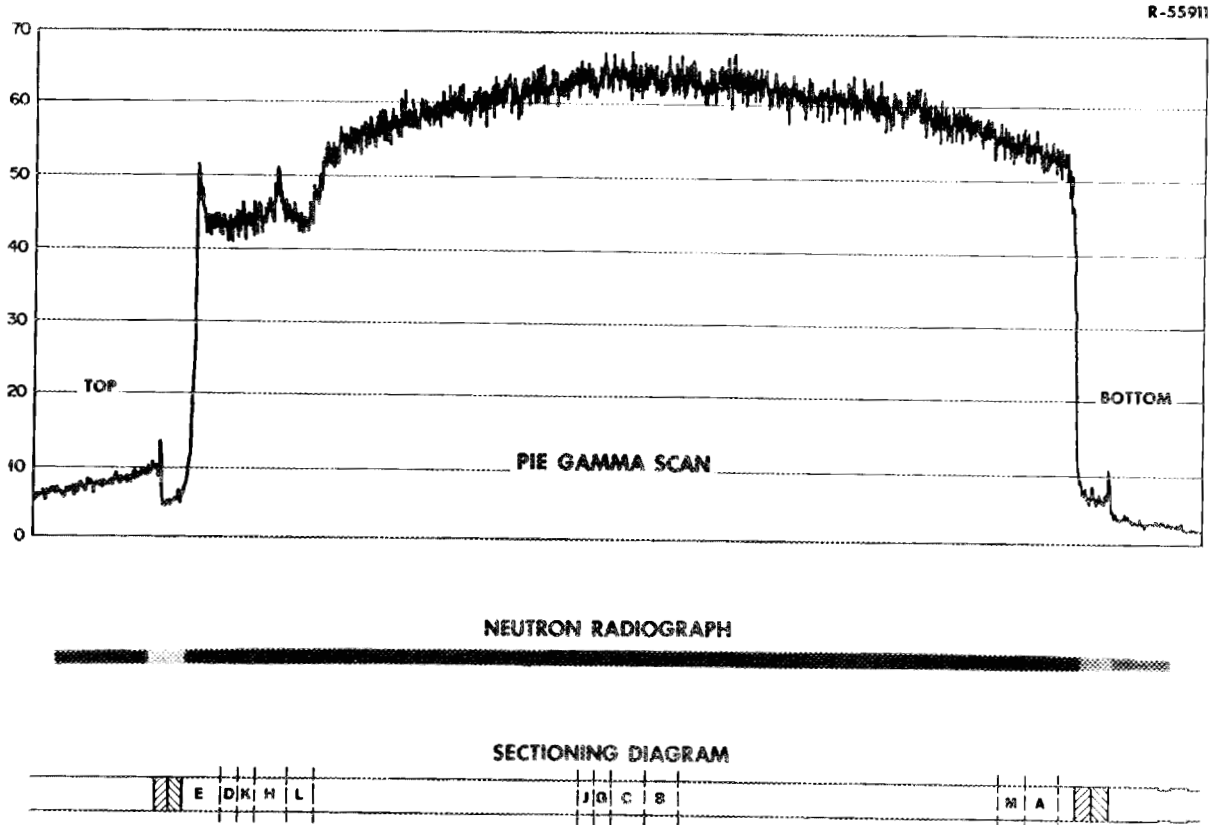


Fig. 5.50. Postirradiation gamma scan, neutron radiograph, and sectioning diagram for pin S-I-E.

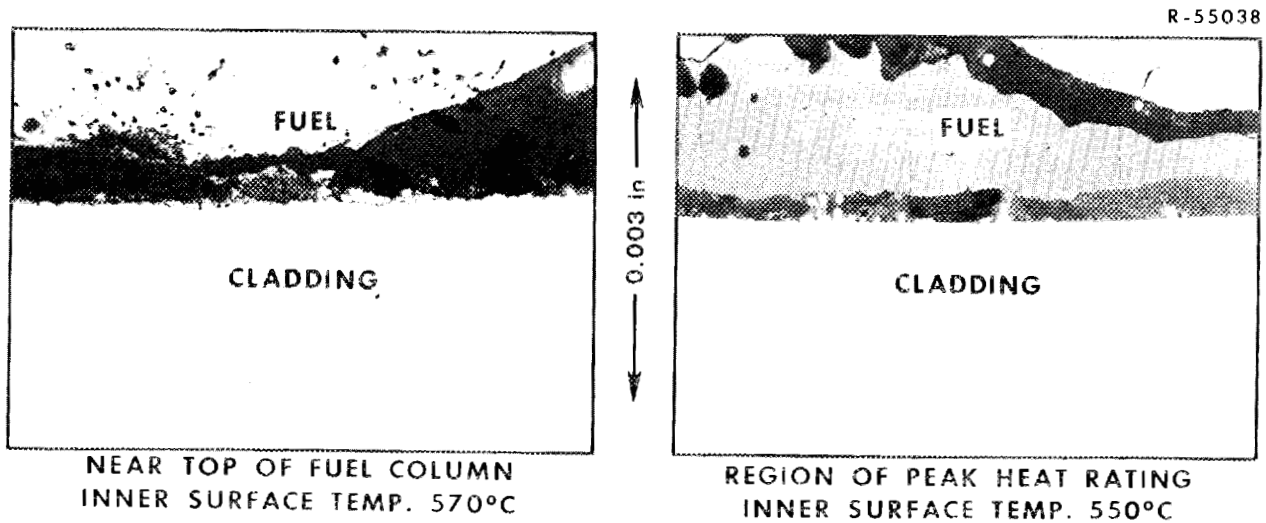


Fig. 5.51. Maximum degree of chemical interaction observed between fuel and cladding in fuel pin S-I-E.

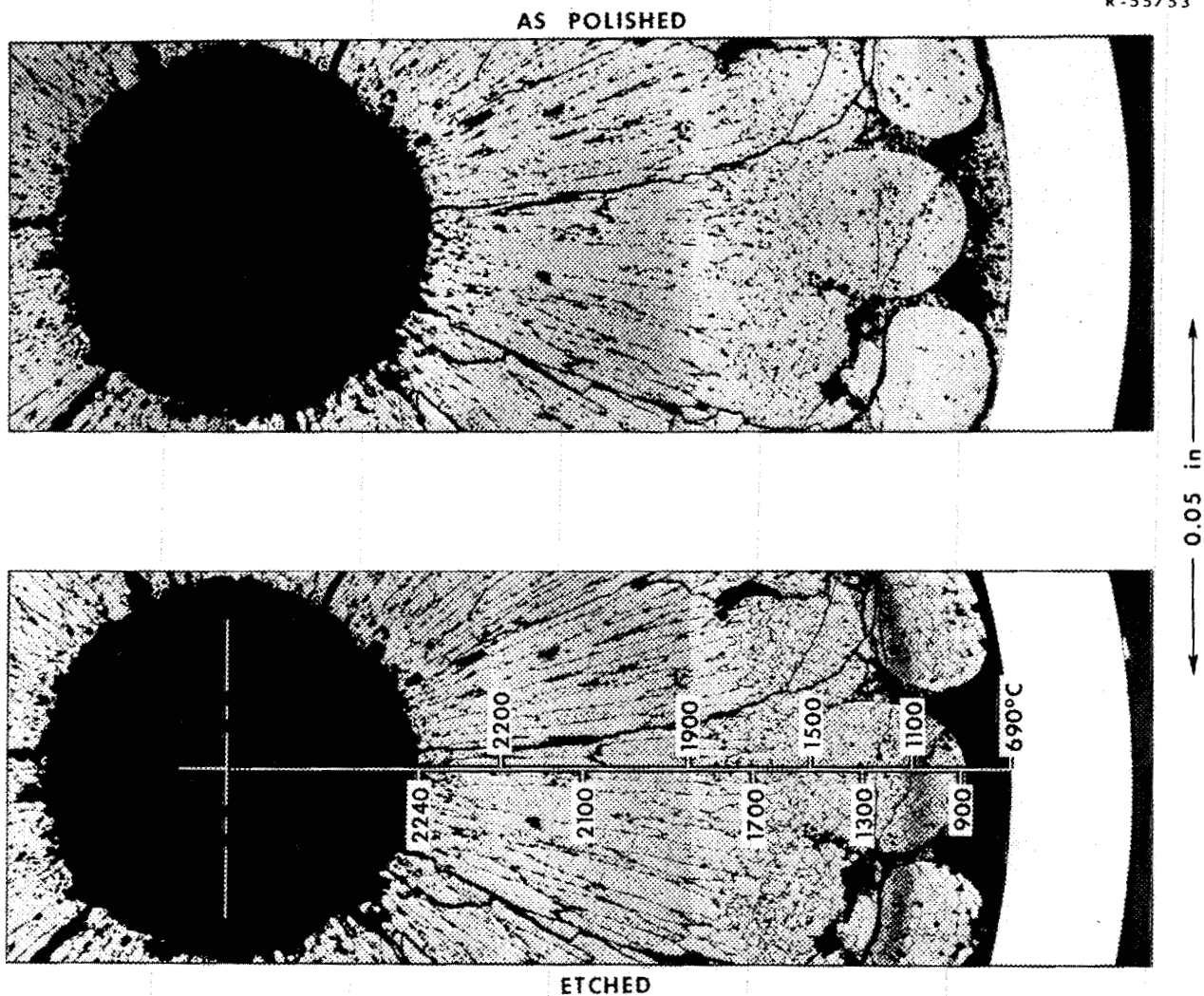


Fig. 5.52. Microstructure and calculated temperatures in peak-heat-rate section G, pin S-I-E.

have shown little if any fuel-cladding mechanical interaction at burnup levels in excess of 5% FIMA, a distinct lack of fuel-cladding chemical interaction at temperatures up to 570°C, and additional evidence indicating a high fuel-cladding gap conductance for the Sphere-Pac fuels.

5.6 FAST REACTOR TESTS -- EBR-II UNENCAPSULATED PINS

A. R. Olsen

5.6.1 Experimental Plan

The EBR-II series II test pins are designed for irradiation in a 37-pin subassembly. The test program

was a coordinated effort between the Babcock & Wilcox Company and ORNL. The overall test plan is designed to provide comparative performance data on a variety of fuel forms, densities, and oxygen-to-metal ratios.

All fuels are $(^{235}\text{U}-20\% \text{Pu})\text{O}_2$. The ORNL pins contain sol-gel-derived fuel, while the Babcock & Wilcox pins contained pellets and Vi-Pac shards processed from coprecipitated powder. The tests have been coordinated to provide data for:

1. the evaluation of particulate fuels (Sphere-Pac and Vi-Pac) for LMFBR use,
2. the comparison of performance characteristics of pellets fabricated from coprecipitated or sol-gel-derived powders.

Table 5.13. Number of test pins of various fuel forms in test subassembly X 112

| Fabrication form and type designation | Fuel production process | Oxygen-to-metal ratio | Number of test pins at each design smear density (% of theoretical) | | | | Total pins of each fuel form |
|---------------------------------------|-------------------------|-----------------------|---|---------|------|----|------------------------------|
| | | | 80 | 83 | 85 | 90 | |
| | | | Sphere-Pac (SP) | Sol-gel | 1.98 | 4 | |
| Sphere-Pac (SPL) | Sol-gel | 1.94 | 2 | 1 | 1 | 4 | |
| Pellet (PEL) | Sol-gel | 1.98 | | | 2 | 2 | 4 |
| Pellet (PEL) | Coprecipitation | 1.98 | | 5 | | | 5 |
| Pellet (PELL) | Sol-gel | 1.94 | 2 | | 1 | | 3 |
| Vi-Pac (VP) | Coprecipitation | 1.98 | 6 | 1 | | | 7 |
| Totals | | | 14 | 11 | 10 | 2 | 37 |

The emphasis in these tests is on the effects of fuel form and void distribution on the release of fission gas, fission product redistribution, and mechanical and chemical interactions of fuel and cladding. A linear heat rate of 14 kW/ft, cladding temperatures of 550 to 650°C, and burnup levels to 100,000 MWd/metric ton are planned.

The initial plan⁷⁰ was to discharge the subassembly twice during its irradiation period for interim non-destructive examination and replacement of selected pins. Thus, all fuel variables were included in the initial subassembly loading, as shown in Table 5.13.

Initially, Babcock & Wilcox was to supply 18 pins for the subassembly plus 10 replacements, while ORNL was to fabricate 19 pins for the initial subassembly plus 11 replacement pins. With the termination of the ORNL program we fabricated 19 pins plus 1 replacement, while Babcock & Wilcox produced 18 pins plus 16 replacements before their program was terminated. Thus, the original plan for 58 pins was reduced to 54 pins, and some fuel forms will not see all of the proposed irradiation conditions.

The initial irradiation schedule⁷⁰ also had to be modified to comply with EBR-II regulations on gas plenum pressures, which required a move of the N-37-type subassembly from a row 6 position to a row 7 position after the installation of the stainless steel reflector in the EBR-II. Since not all of the Babcock & Wilcox replacement pins passed the preirradiation quality control inspection, only a tentative replacement program could be proposed before the program responsibility was transferred to ANL in July 1972. This

70. A. R. Olsen et al., *Preirradiation Data for ORNL Series II and B & W Oxide Fuel Tests in EBR-II*, ORNL-TM-3446 (November 1971).

Table 5.14. Pins to be replaced after first incremental exposure

| Subassembly position | Pin removed | | Pin installed | |
|----------------------|-------------|-------------------|---------------|-------------------|
| | Number | Fuel ^a | Number | Fuel ^a |
| 6 | OS-8 | SP-82 | D-39 | SP-78 |
| 8 | D-9 | PEL-83 | D-42 | PEL-83 |
| 9 | OP-5 | PEL-86 | OP-4 | PEL-84 |
| 26 | D-18 | VP-78 | D-53 | VP-78 |

^aFuel designation defines fabrication form - smear density (as fabricated).

proposal is shown in Tables 5.14 and 5.15. The inspection defects of the pins that will require repair work before they can be irradiated are also given in Table 5.15.

Only two replacement sequences are proposed on the assumption that the second incremental exposure will be approved to a lead pin peak burnup of $8.7 \pm 0.2\%$ FIMA. This limit on the second incremental exposure is required because the calculated peak plenum pressure will be approaching the 1000-psi limit for unencapsulated pins in an N-37 subassembly. Unless this pressure limit is changed by the end of the second incremental exposure, continued irradiation of the remaining pins and the second group of replacements will require a change in type of subassembly. We have not included this situation specifically in our proposal. However, with the inclusion of a spare pin in the test series, two groups of 19 pins each will be available for irradiation in two Mark E 19E subassemblies.

It should be noted that the four pins to be destructively examined after the initial increment of exposure include both sol-gel-derived and coprecipitated fuels and all three fuel forms. They have been selected from

Table 5.15. Pins to be replaced after second incremental exposure

| Subassembly position | Pin removed | | Pin installed | | Pin defects ^a requiring repair |
|----------------------|-------------|---------|---------------|--------|---|
| | Number | Fuel | Number | Fuel | |
| 1 | D-2 | SP-78 | D-44 | SP-79 | A |
| 10 | OP-3 | PELL-80 | D-50 | PEL-83 | |
| 12 | D-10 | SP-78 | D-35 | SP-78 | A |
| 14 | OS-6 | SP-83 | D-43 | SP-79 | A |
| 15 | D-22 | VP-78 | D-40 | VP-78 | B |
| 17 | D-21 | VP-78 | D-37 | VP-78 | |
| 20 | D-17 | PELL-83 | D-38 | PEL-85 | |
| 25 | D-19 | SP-78 | D-52 | SP-79 | B |
| 27 | OS-3 | SP-83 | D-54 | VP-79 | |
| 29 | D-27 | SP-79 | D-36 | SP-78 | B |
| 30 | D-4 | PELL-83 | D-41 | PEL-82 | |
| Spare | | | D-34 | VP-78 | A, B |
| Spare | | | D-51 | PEL-85 | |

^aDefect types: A -- insufficient weld penetration (>20% porosity); B -- weld is oversize.

central positions in the subassembly where the peak cladding temperatures are highest. Thus, they will give information on the fuel-cladding chemical interaction at the higher temperature.

5.6.2 Design and Construction

Although the pins fabricated by each of the sites varied slightly in details to accommodate different methods of introducing the xenon tag gas, they are quite similar. Each pin is 0.250 in. in diameter and has an overall length of 40 in. Detailed drawings and as-fabricated data are included in the original data package.⁷⁰ A nominal test pin description is given in Table 5.16. The pin design will allow irradiation in three types of standard EBR-II subassemblies, N-37, J-37, and E 19E.

5.6.3 Irradiation Results

The initial group of 37 pins was irradiated in an N-37 subassembly (X 112) in two row 6 positions. This subassembly was inserted into position 6-B-2 during run 49 and moved to the desired higher flux 6-E-3 position for irradiation during runs 50 through 55. Thus, the initial incremental exposure was for 10,600 MWd of EBR-II operation. The lead pin calculated peak burnup was 3.8% FIMA. At this burnup the calculated peak plenum gas pressure was 470 psi, just below the 500-psi limit imposed by the EBR-II operations on unencapsulated pins in this type of subassembly for positions adjacent to control rod or safety rod thimbles. All row 6 positions are adjacent to such thimbles, so the

Table 5.16. Nominal test pin description

| | | |
|---|--|--------------------------------|
| Fuel: | | |
| Material | (U,Pu)O ₂ | |
| Pu/(U + Pu) | 0.20 ± 0.01 | |
| ²³⁵ U/U | 0.93 | |
| (²³⁹ Pu + ²⁴¹ Pu)/Pu | 0.90 | |
| Fuel bed length, in. | 13.5 | |
| Theoretical density, g/cm ³ | 10.90 at 1.98 oxygen-to-metal ratio | |
| Bed smear density | Variable (80 to 90% of theoretical) | |
| Cladding: | | |
| Material | Type 316 stainless steel (solution treated) | |
| Outer diameter, in. | 0.250 ± 0.001 | |
| Inner diameter, in. | 0.218 ± 0.001 | |
| Wall thickness, in. | 0.015 + 0.0015 - 0.0010 | |
| Insulator pellets: | | |
| Material | ORNL | B & W |
| Length, in. | ThO ₂ | ²³⁸ UO ₂ |
| | 1 | 1 |
| Blanket pellets: | | |
| Material | ²³⁸ UO ₂ | |
| Length (of stack), in. | ~6 | |
| Shield rod: | | |
| Material | Nickel | |
| Length, in. | 2 ⁷ / ₃₂ | |
| Diameter, in. | 0.212 | |
| Bed retainers: | | |
| Material | ORNL | B & W |
| Plug | Type 316 stainless steel | None |
| Spring | Inconel X | Type 302 stainless steel |
| Plenum liner: | | |
| Material | ORNL | B & W |
| | Type 304 stainless steel | Type 316 stainless steel |
| Outer diameter, in. | 0.188 | 0.187 |
| Wall thickness, in. | 0.020 | 0.014 |
| Pads: | | |
| Material | "Fiberfrax" Al ₂ O ₃ -SiO ₂ | |
| | Al ₂ O ₃ 50 ± 5% | |
| | SiO ₂ 50 ± 5% | |
| | Other oxides <3% | |

subassembly was discharged. No detailed data on the interim examination are available, but no failures or unusual behavior characteristics were noted.

The variations in coolant channels in the subassembly lead to two peak cladding temperature groups. Pins located in the central regions operate at peak calculated cladding temperatures approximately 100°C higher

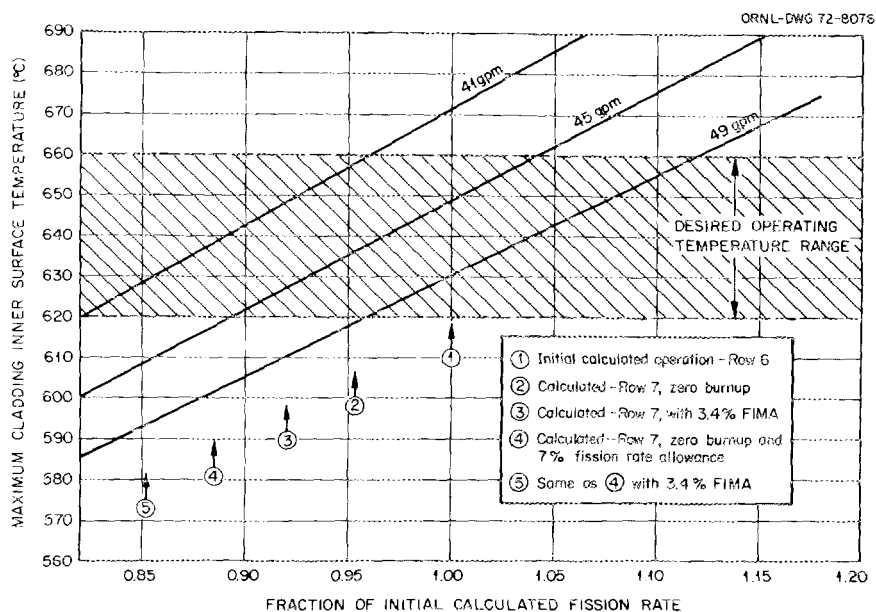


Fig. 5.53. Parametric analysis of the effects of changing fission rates and subassembly coolant flow rates on the maximum cladding inner surface temperature of pin OS-12.

than the pins in peripheral locations. The control of this temperature for central pins thus establishes the total subassembly coolant flow rate. With the initial row 6 fission rates we requested a flow of 45 gpm to limit the start-of-life peak cladding temperature to 650°C. The measured flow rate for subassembly X 112 was 49 gpm, so the start-of-life peak cladding temperature was lowered to 630°C and had fallen to the bottom of the desired range (650 to 620°C) at the end of run 55.

The reconstituted subassembly X 112A is scheduled for irradiation in a row 7 position, where the plenum gas pressure limit is 1000 psi. This move will also result in lower fission rates, so a parametric study was made to define the effects of coolant flow on peak cladding temperature. The results of this study are shown in Fig. 5.53. The fission rate allowance included in points 4 and 5 in the figure are from EBR-II data and represent the uncertainty extreme. Because of subassembly coolant outlet temperature limitations, the minimum allowable flow rate in the X 112A subassembly is 41.4 gpm. The subassembly is to be orificed to provide a flow rate between 42 and 44 gpm. This will keep the peak cladding temperature for the central pins in the desired range during the second incremental irradiation period.

All postirradiation examination data and further test results will be provided by Argonne National Laboratory.

5.7 TRANSIENT TESTS IN TREAT

C. M. Cox⁷¹ E. J. Manthos

5.7.1 Experimental Plan

Understanding the behavior of fuel pins under transient operating conditions is important in determining the overpower allowance of fuel element designs, in predicting the influence of temporary abnormal conditions on future pin lifetimes and safety margins, and in predicting the initial consequences of pin failures. There is no facility in which the temperature or power transients hypothesized for LMFBR accidents can be imposed on a (U,Pu)O₂ fuel pin operating at typical steady-state conditions. However, transients from zero power typical of a major control rod ejection accident can be reasonably well simulated in the Transient Reactor Test Facility (TREAT). The objective of the ORNL TREAT experiment was to compare the behavior of unirradiated sol-gel-derived (U,Pu)O₂ Sphere-Pac and pellet fuel pins during severe power transients causing various amounts of fuel melting. The principal test variables were fuel smear density (81 and 88% of theoretical) and fuel fabrication form (pellets and

71. Now at Hanford Engineering Development Laboratory, Richland, Wash.

vibratorily compacted microspheres from the Sphere-Pac process). Details of the analyses performed in conjunction with this experiment have been previously published.^{72,73}

5.7.2 Design and Construction

The transient tests were conducted with two capsules, each containing three fuel pins in tandem. The fuel pins were encapsulated in stagnant sodium-filled capsules as shown in Fig. 5.54. The capsules contained electrical heaters to heat the fuel pins to about 430°C before the

transients, and thermocouples were adjacent to the fuel pins at various circumferential positions in the capsules at the fuel column midlengths. Each fuel pin had an 8-in.-long fuel column and was clad with 0.254-in.-OD × 0.016-in.-wall type 304 stainless steel tubing. The fuel columns were partially restrained axially with a spring-loaded extensometer, which allowed up to $\frac{3}{16}$ in. fuel length increase. Reactor data are given in Table 5.17 and fuel fabrication data in Table 5.18. Two columns appear in Table 5.17 for TR-1, because this capsule was initially subjected to a calibration transient to verify the design techniques. This verification was based on excellent agreement between calculated and measured temperatures in the sodium annulus around the fuel pins. The calculated maximum fuel center-line temperature was about 1800°C for this calibration transient. The test transients were designed to melt approximately one-fourth of the fuel in the peak power region of the first capsule and half for the second capsule (TR-2).

72. C. M. Cox and R. E. Adams, *Safety Analysis and Test Specifications for Transient Test of Sol-Gel (U,Pu)O₂ Fuel Pins (ORNL Series I)*, ORNL-TM-3574 (December 1971).

73. C. M. Cox, D. R. Cuneo, and E. J. Mantlos, "Performance of Sphere-Pac and Pellerized (U,Pu)O₂ During Severe Overpower Transients," pp. 701-24 in *Proc. Conf. Fast Reactor Fuel Element Technology*, ed. by Ruth Farmakes, American Nuclear Society, Hinsdale, Illinois, 1971.

Table 5.17. Reactor data for ORNL TREAT capsules TR-1 and TR-2

| Capsule | TR-1 | TR-1 | TR-2 |
|------------------------------------|----------|----------|----------|
| TREAT transient | 1293 | 1294 | 1295 |
| Date | 10-29-69 | 10-30-69 | 10-31-69 |
| Initial reactor period, msec | 630 | 204 | 200 |
| Peak reactor power, MW | 29.8 | 202 | 202 |
| Integrated reactor power, MWsec | 88 | 140 | 172 |
| Pulse width at half max power, sec | 3.6 | 0.78 | 0.85 |

Table 5.18. Fabrication data for ORNL TREAT capsules TR-1 and TR-2

| Fuel pin | TR-1A | TR-1B | TR-1C | TR-2A | TR-2B | TR-2C |
|---|-------|-------|-------|-------|-------|-------|
| Fuel fabrication form ^a | P | S | P | S | S | P |
| U/(U + Pu) ^b | 0.801 | 0.801 | 0.801 | 0.801 | 0.801 | 0.801 |
| O/M | 1.983 | 1.980 | 1.991 | 1.980 | 1.980 | 1.990 |
| Gas release, cm ³ /g (STP) at 1600°C | 0.07 | 0.14 | 0.23 | 0.14 | 0.14 | 0.19 |
| Fuel smear density, % of theoretical | 88.9 | 80.9 | 79.7 | 82.0 | 80.9 | 80.2 |
| Fuel length, in. | 8.03 | 8.00 | 7.98 | 8.01 | 8.00 | 8.10 |
| Fuel-cladding diametral gap, mils | 5 | | 5 | | | 5 |
| Gas plenum volume, cm ³ (STP) ^c | 1.1 | 1.3 | 1.5 | 1.3 | 1.3 | 1.4 |

^aP = solid pellets; S = Sphere-Pac.

^bNatural U.

^cIncluding all porosity.

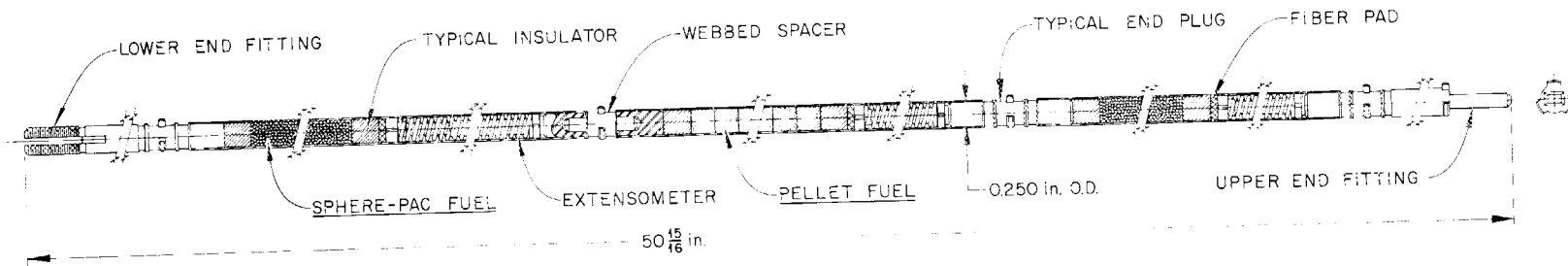


Fig. 5.54. Typical TREAT experiment fuel rod.

5.7.3 Results

The fuel pin operating and examination data for the two TREAT capsules are summarized in Table 5.19. The time variation of heat rate at the fuel column midplanes during the transient for each pin is shown in Fig. 5.55. Figures 5.56 and 5.57 show neutron radiographs taken after the transient experiments. These indicate no definite central voids in any of the pellet pins; however, two of these pins had fuel column separations, apparently at pellet interfaces. Subtracting the measured separations from the total change in fuel column length indicates that some fuel restructuring and densification occurred in rod TR-1A and perhaps in rod TR-2C. Figure 5.58 shows the as-polished microstructure of each of the fuel pins at the fuel column midplane after the transient tests. The large circular voids evident in these photographs are believed to be bubbles formed during the high-temperature transients by coalescence of adsorbed gases present in the fuel from fabrication. The greater amount and larger bubbles in pin 1B as compared with 1A follow from the lower density of the fuel and the higher as-fabricated

adsorbed gas content. Although appreciable restructuring in these two pins was apparent, there was no indication that the fuel had melted except near the ends of the pins, where flux peaking was evident, as shown in Fig. 5.59. After being etched, the fuel pins were examined for the extent of melting and grain growth, as shown in Fig. 5.60 for pin 2B. Only the two pins with the highest energy release, 2A and 2B, were identified as having melted at the fuel midplane. It also appears in Fig. 5.60 that Sphere-Pac fuel, after appreciable densification during the transient, shrank away from the cladding (leaving a gap). The chevron-shaped low-density regions observed on the neutron radiographs are shown in Fig. 5.61 to have been due to the formation of voids as the fuel melted and due to axial relocation of the oxide fuel.

Figures 5.62 and 5.63 show the postirradiation visual appearance of the pins from the two TREAT capsules. As can be seen, the pins are in excellent condition, indicating that unirradiated sol-gel Sphere-Pac (U,Pu)O₂ fuel pins can accommodate severe TREAT-type transients, which cause fuel volume melts up to at least 50% without failing.

Table 5.19. Summary of operating and examination data for ORNL TREAT capsules^a

| Fuel pin | TR-1A | TR-1B | TR-1C | TR-2A | TR-2B | TR-2C |
|---|---------------------|-----------------|-------------------|---------------------|-------------------|---------------------|
| Operating data ^b | | | | | | |
| Fuel pin temperature before transient, °C | 410 | 449 | 414 | 400 | 436 | 410 |
| Peak instantaneous linear power, kW/ft | 175 | 155 | 118 | 178 | 164 | 103 |
| Energy release, cal/g | 390 | 380 | 292 | 525 | 491 | 313 |
| Postirradiation examination | | | | | | |
| Cladding maximum ovality, ^c max diam - min diam, mils | <0.5 | <0.5 | 1.5 | <0.5 | <0.5 | 1.8 |
| Overall fuel column length change, ^d mils | 90 | -20 | -30 | -60 | -30 | 40 |
| Radius of fuel central void, ^b mils | 0 | 0 | 0 | 17 | 28 | 0 |
| Volume of fuel melting, ^b % | 0 | 0 | 0 | 50 ^{±2} | 51 ^{±2} | 0 |
| Radius of equiaxed grain growth, ^b mils | 94 | 111 | 0 | 111 | 111 | 78 |
| Fuel-cladding radial gap, ^b mils | 2.4 ^{±1.2} | 3 ^{±3} | 1.5 ^{±1} | 4.4 ^{±2.6} | 3.7 ^{±3} | 1.2 ^{±1.2} |

^aFabrication data are given in Table 5.18.

^bAt fuel column midplane.

^cMaximum diametral increase <0.5 mil.

^dBased on neutron radiographs; estimated accuracy, ±20 mils.

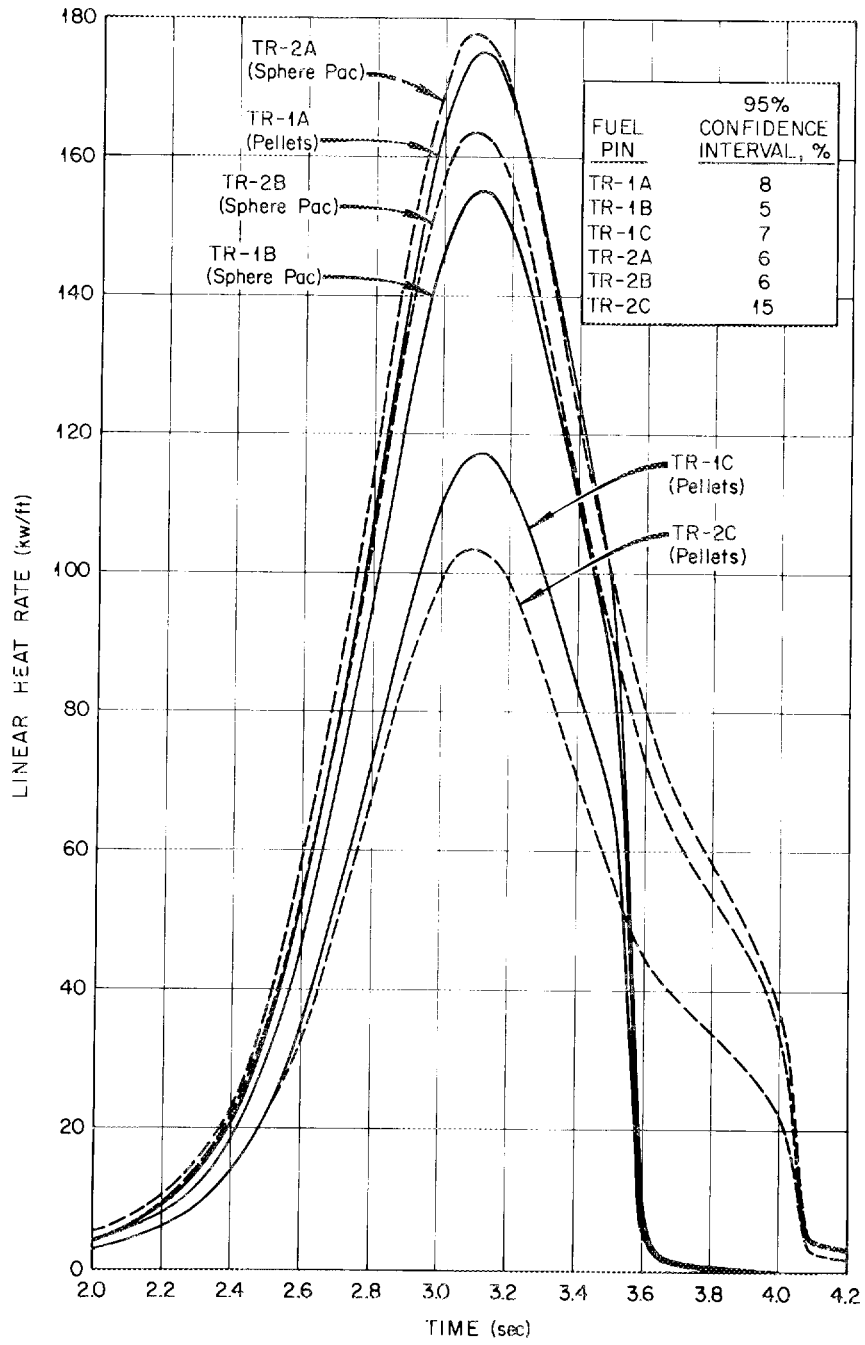


Fig. 5.55. Time variation of heat rate at fuel column midplanes.

R-50108

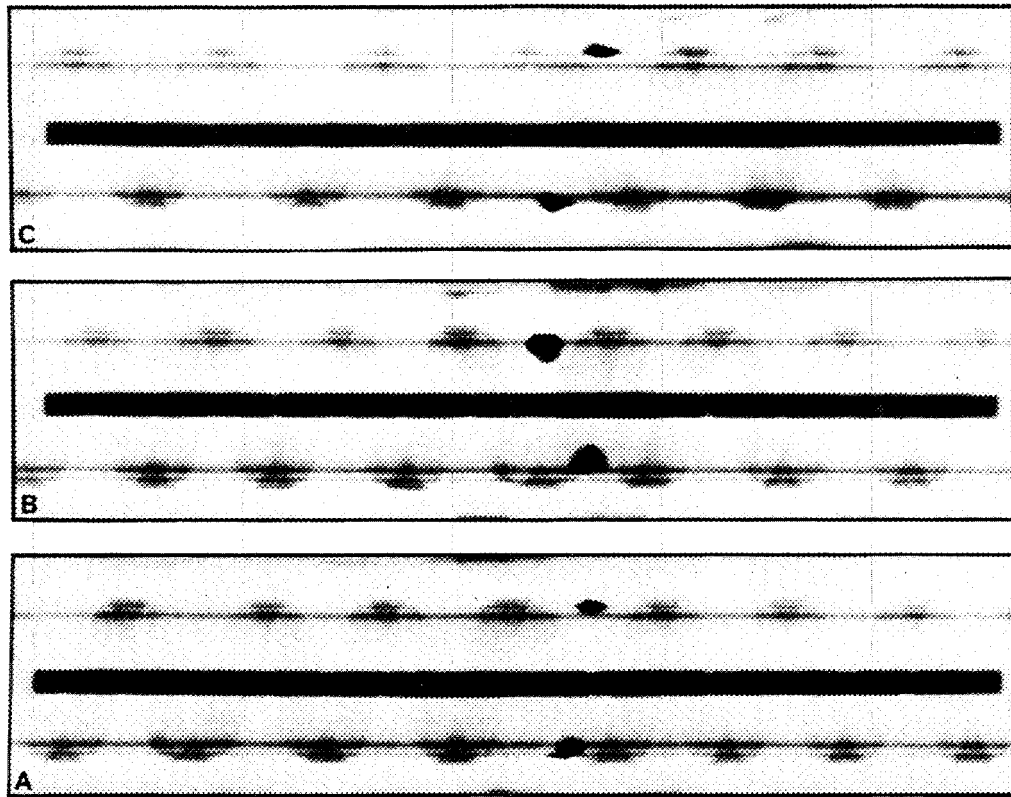


Fig. 5.56. Postirradiation neutron radiographs of capsule TR-1.

R-50108

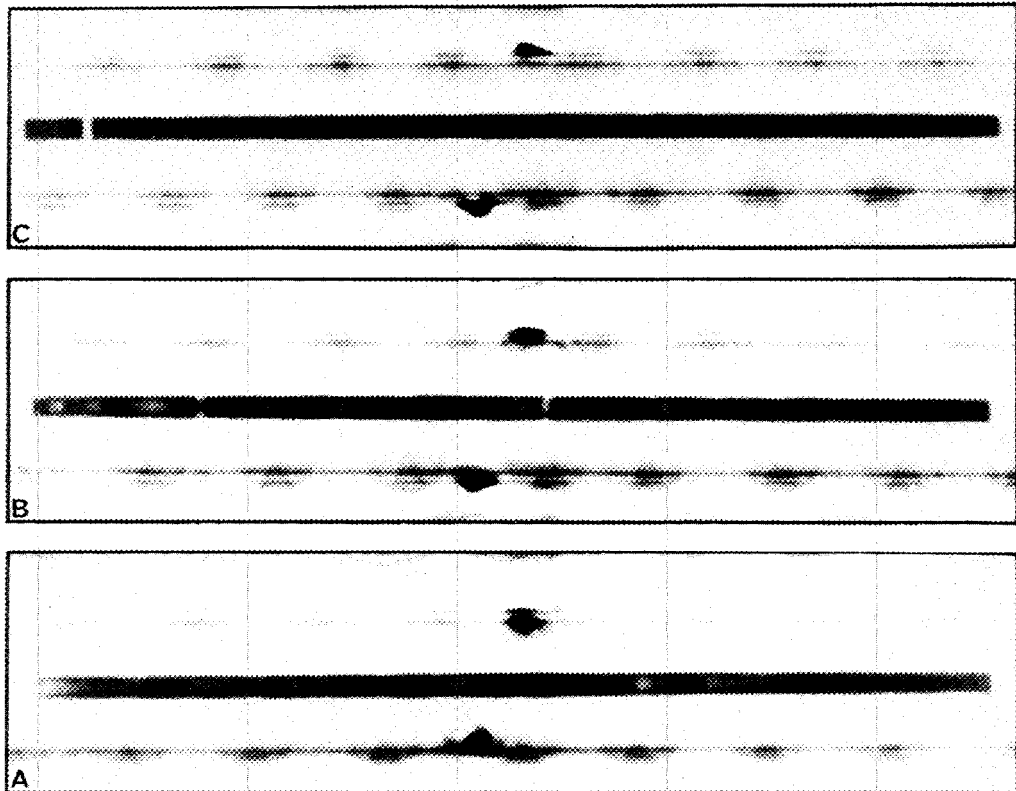


Fig. 5.57. Postirradiation neutron radiographs of capsule TR-2.

R-54832

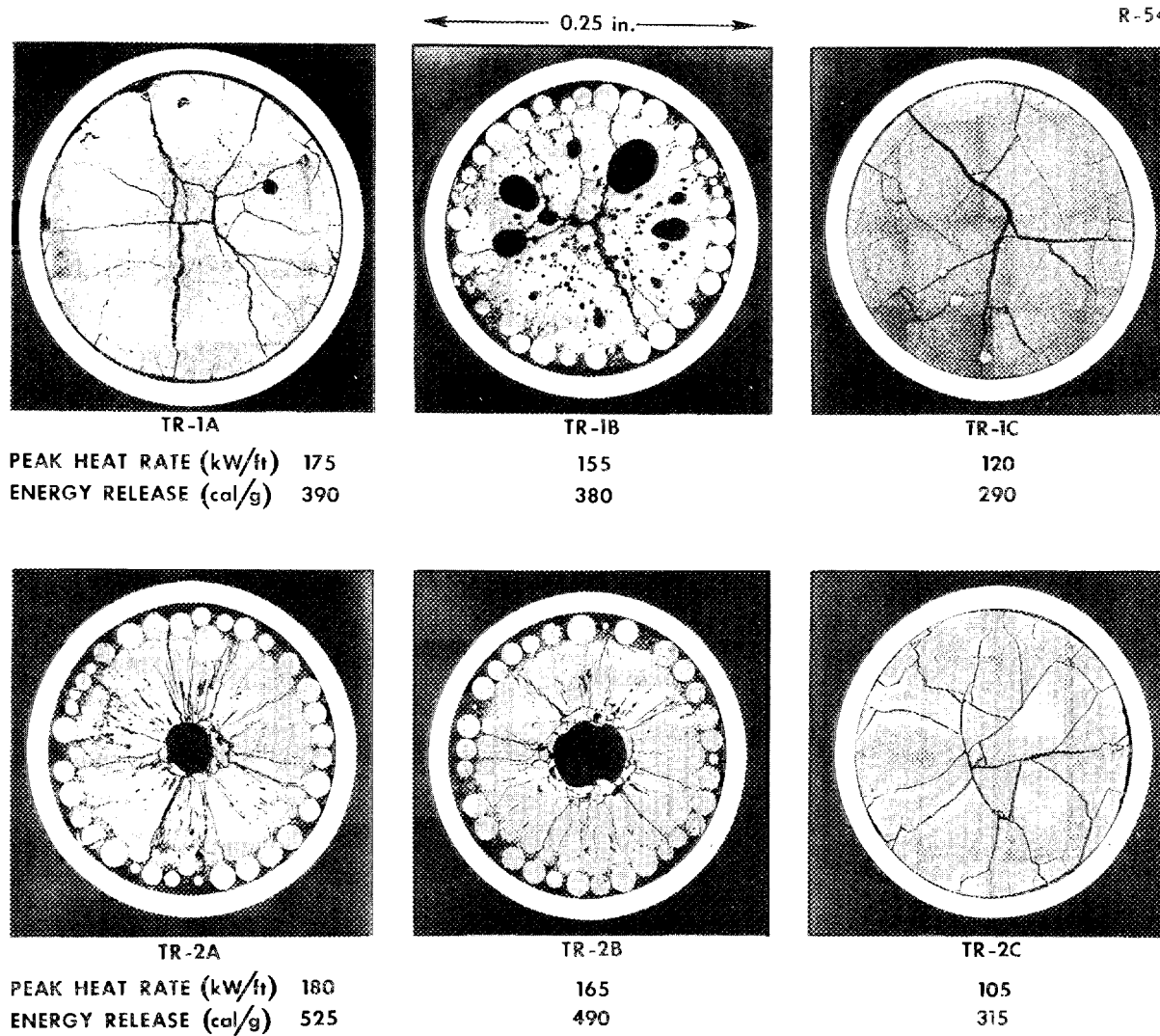


Fig. 5.58. Transverse sections taken from the midlengths of fuel pins irradiated in TREAT experiments and fueled with $U_{0.8}Pu_{0.2}O_{1.98}$.

R-54900

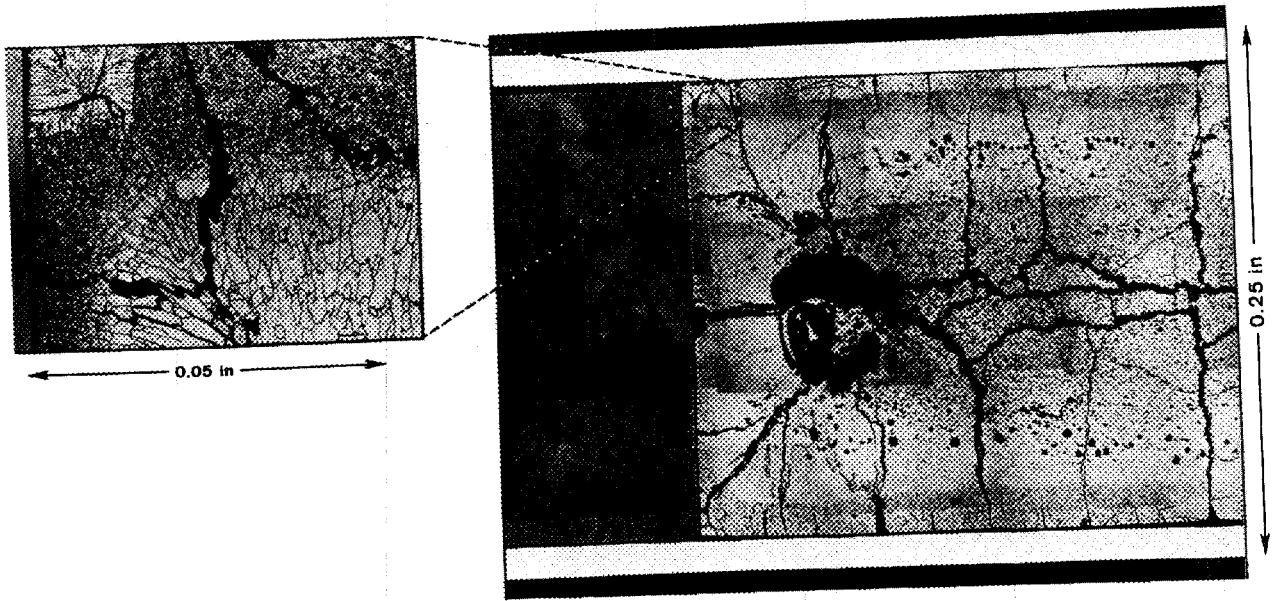


Fig. 5.59. Effect of flux peaking on fuel microstructure.

R-53348

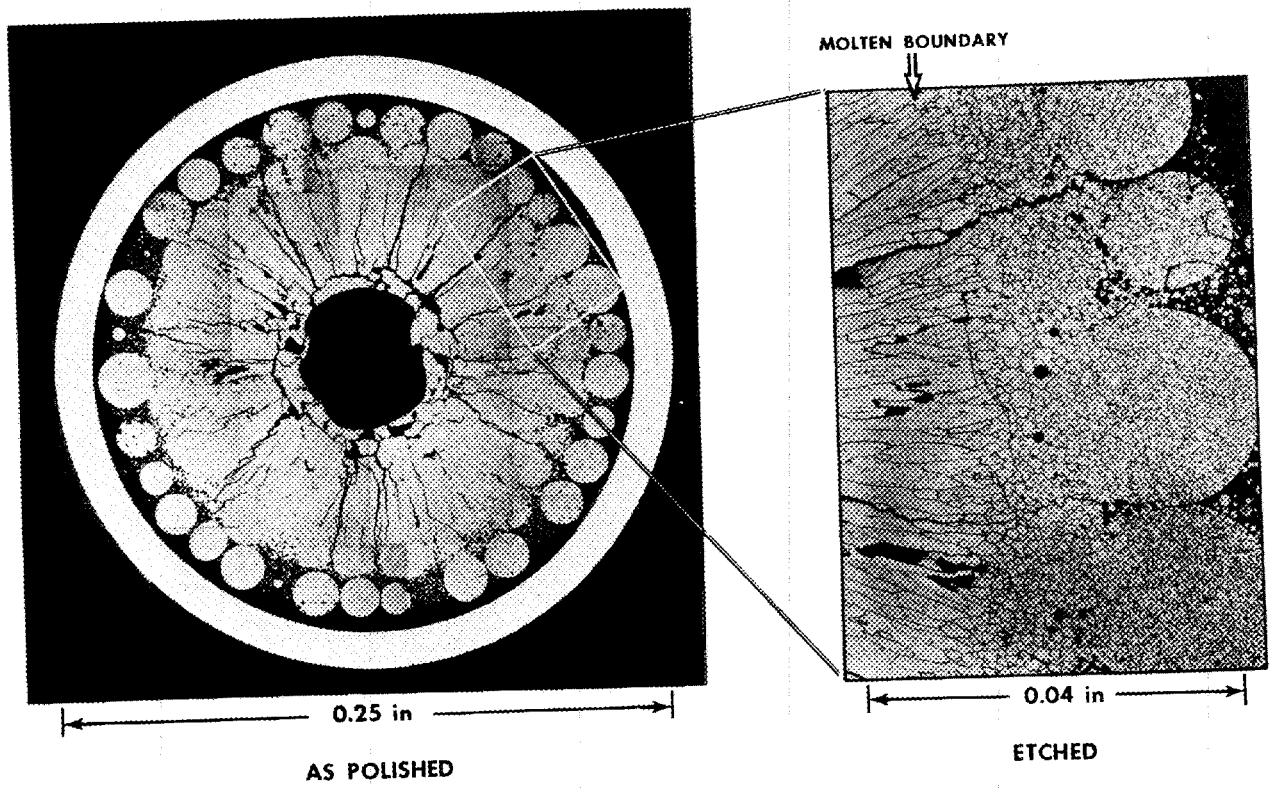


Fig. 5.60. Location of melt radius in fuel pin TR-2B.

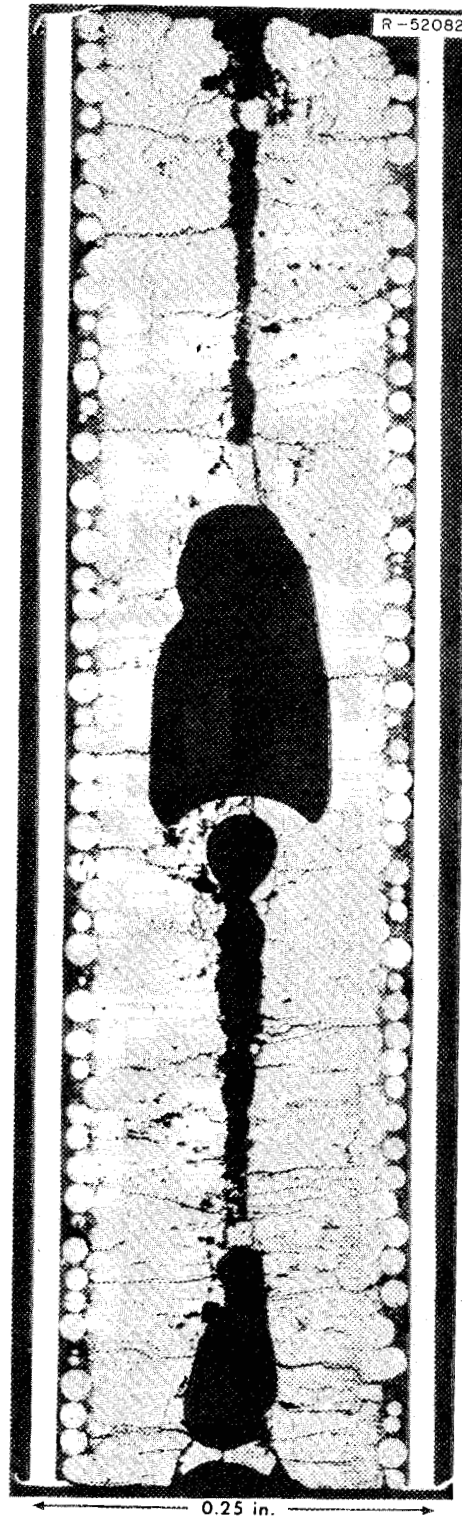


Fig. 5.61. Gross restructuring of $U_{0.8}Pu_{0.2}O_{1.98}$ microsphere fuel irradiated at a peak heat rate of 165 kW/ft (TR-2B-1-3).

R 53170

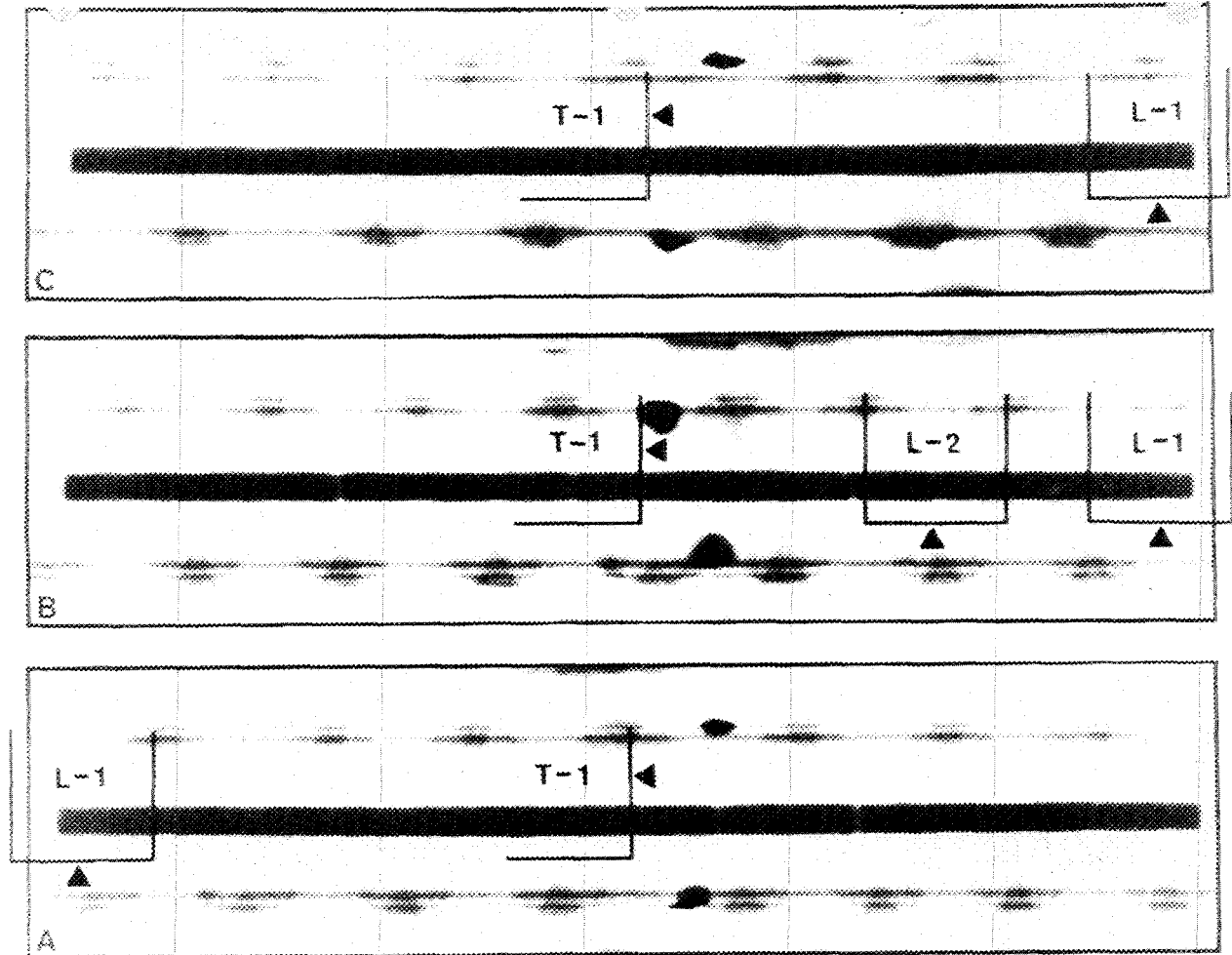


Fig. 5.62. Postirradiation visual appearance of T-1 fuel pins. Sectioning sites are indicated.

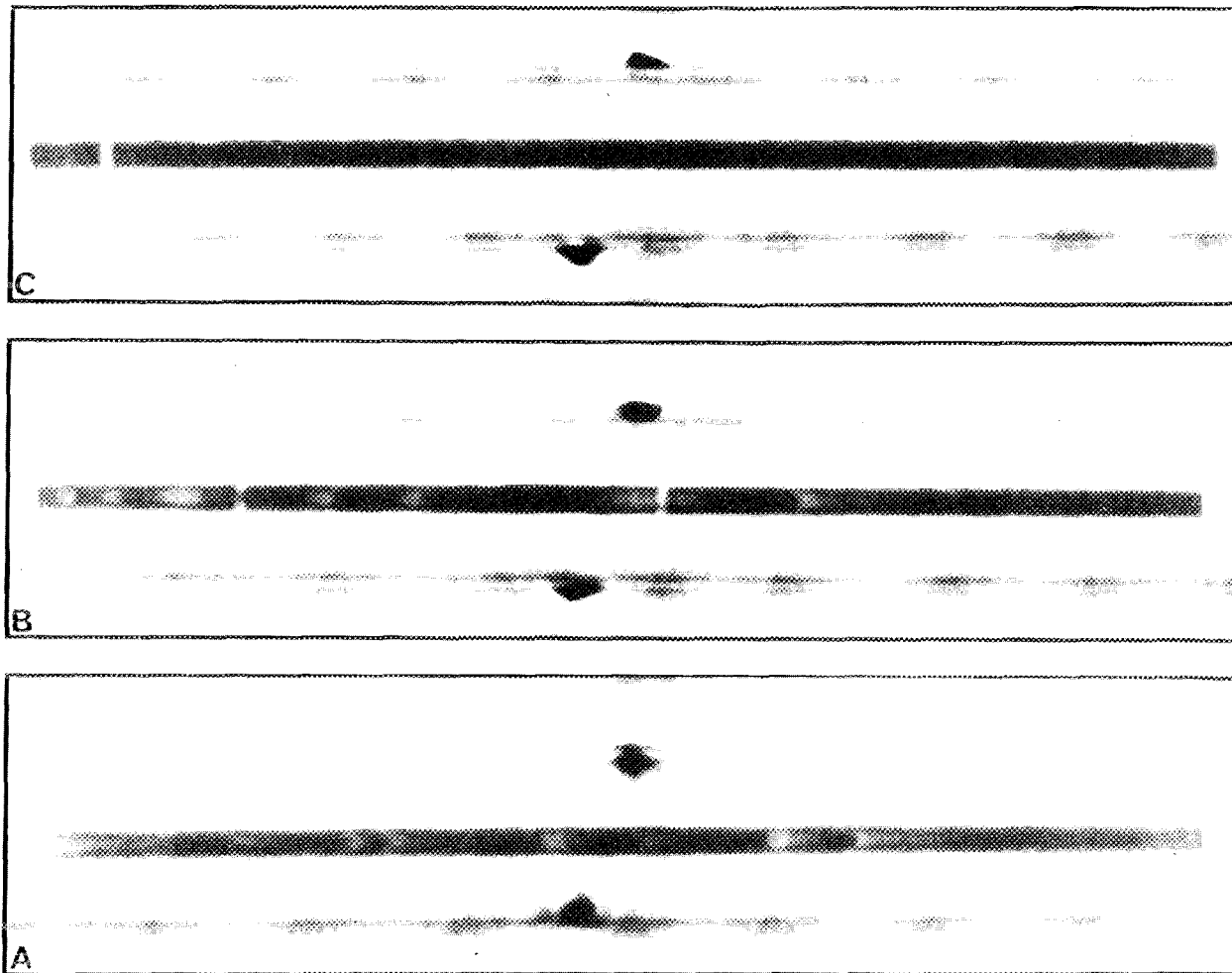


Fig. 5.63. Postirradiation visual appearance of TR-2 fuel pins.

5.8 DISCUSSION OF RESULTS OF IRRADIATION PROGRAM

A. R. Olsen F. J. Homan R. B. Fitts
W. J. Lackey E. L. Long, Jr.

The following discussion of the results of irradiation testing has been organized to discuss individual performance areas and the data derived from all of the tests as applied to each area.

5.8.1 Thermal Performance

The integrated thermal conductance of a fuel pin is important if the maximum operating power of a fuel

pin is based on a fuel temperature limit below melting. This thermal conductance is made up of two major parts: the fuel thermal conductivity and the fuel-cladding gap conductance. The oxide fuel thermal conductivity is sensitive to temperature, porosity, and composition, all of which change during irradiation. The thermal resistance of the gap between fuel and cladding is a function of gap dimensions, gas composition, and the surface characteristics and mechanical properties of both the fuel and cladding.

Although none of these tests provided a direct measurement of fuel thermal conductivity, they have provided indirect evidence that the fuel fabrication form has no significant effect on this conductivity. The

high-burnup tests discussed in Sect. 5.1.2.3 provided some qualitative data on the degradation of fuel thermal conductivity with burnup. Additional qualitative data on this phenomenon without the additional variable of self-shielding should be available from the series I EBR-II tests (Sect. 5.5) still in the reactor.

On the other hand, the instrumented tests in the ORR poolside facility (Sect. 5.2) have provided data on the integrated fuel thermal performance that have permitted an analysis of fuel conductivity and gap conductance. These tests measured simultaneously fuel center temperatures, cladding outer surface temperatures, and heat rate. The results of these tests are summarized in Fig. 5.64, where the fuel center temperature is plotted against heat rate for a pellet and a Sphere-Pac fuel pin, both with a fuel smear density 82% of theoretical. The dashed line, identified as calculated, is based on the GE thermal conductivity equations for the fuel⁷⁴ combined with a gap conductance of $1 \text{ W cm}^{-2} (\text{°C})^{-1}$. Statistical analysis of the many thousands of data points obtained from these tests clearly indicates a lower central temperature for the Sphere-Pac fuel at any given linear heat rate. Assuming equivalent fuel restructuring temperatures for both pins and no significant difference in fuel conductivity, the differences in center temperatures can be accounted for by differences in gap conductance. Analysis of the data indicates the pellet fuel with a small initial radial gap (0.0015 in.) had a gap conductance of $0.73 \text{ W cm}^{-2} (\text{°C})^{-1}$, while the Sphere-Pac gap conductance was $1.93 \text{ W cm}^{-2} (\text{°C})^{-1}$. These conductances would yield the measured fuel temperatures shown in Figs. 5.64 and 5.33. Indirect substantiation of the high gap conductance for the Sphere-Pac fuel was obtained from the series I EBR-II tests (Sect. 5.5). Since these were uninstrumented tests, we had to use fuel structure as a temperature indicator. The temperature distributions given in Fig. 5.52, which are normalized to a 1700°C limit for columnar grain growth, could only be obtained by using a high gap conductance of $1.9 \text{ W cm}^{-2} (\text{°C})^{-1}$.

Thus, the data obtained indicate that the gap conductance for Sphere-Pac fuel at linear heat rates up to 16 kW/ft and at burnup levels up to 6% FIMA is approximately twice that of pellet pins under similar conditions. This would permit operation of Sphere-Pac fuels at 110% of the linear heat rate of pellet fuels while

74. W. E. Baily et al., "Thermal Conductivity of Uranium-Plutonium Oxide Fuels," pp. 293-30 in *Intern. Symp. Plutonium Fuels Technol., Scottsdale, Ariz., 1967, Nucl. Met. 13*, American Institute of Mining, Metallurgical, and Petroleum Engineers, New York, 1968.

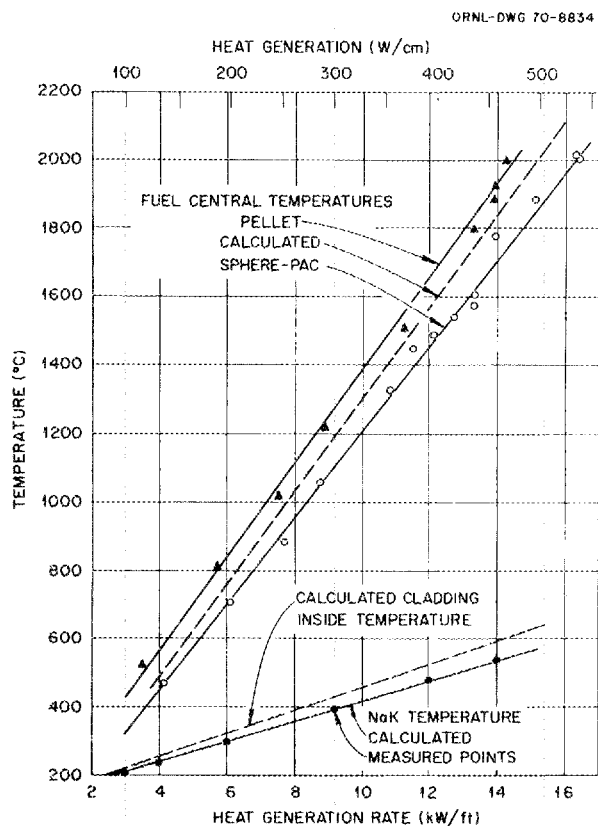


Fig. 5.64. Variation of calculated and measured fuel and capsule temperatures with heat generation rate in capsule SG-3.

maintaining the same fuel center temperatures. The lower fuel surface temperatures may also affect fuel-cladding chemical interaction, which will be discussed later. The data at higher burnup levels are not yet available. The macroscopic appearance of the fuels operating at moderate linear heat rates of less than 12 kW/ft (Figs. 5.38 and 5.28) indicates that this high gap conductance may prevail to at least 10% FIMA. However, at higher linear heat rates the fuel near the cladding interface appears to be similar for both pellet (Fig. 5.37) and Sphere-Pac [Fig. 5.38(a)]. For steady-state operations the linear heat rate in a pin generally decreases with burnup, so decreases in the gap conductivity should not be significant. Under accident or overpower conditions at high burnup, the gap conductance should not be worse in Sphere-Pac fuel than in pellet fuels under similar conditions and may still be better. A transient test of at least one of the series I EBR-II tests still in the reactor was planned and should still be conducted to investigate this possibility.

5.8.2 Fuel Restructuring

As indicated in the previous section, fuel restructuring has appreciable effects on fuel operating temperatures. The Sphere-Pac fuel tests have provided a unique structure for the visual observations of the mechanisms of fuel structural changes. A general discussion of these mechanisms and a qualitative evaluation of these has been presented.⁷⁵ A mathematical model for predicting the changes in structure and actinide distribution was developed.⁷⁶

The primary mode of restructuring at high temperatures was clearly defined as a vaporization-condensation mechanism, as shown by the photograph of fuel at the outer periphery of the columnar grain structure (Fig. 5.4). With the instrumented tests (Sect. 5.2), we were able to define the temperature limit for columnar grain growth at 1650°C. No definite temperature limit could be established for grain growth in the cooler regions. Grain growth was measured, and the results, as discussed in Chap. 6, were fit to the classical phenomenological model involving time and temperature.

The kinetics of restructuring have not been fully defined, although the tests have shown a distinct time dependence, as can be seen in the structural evolution with time shown in Fig. 5.65. The structures shown are from instrumented and uninstrumented thermal flux tests and show that under these conditions (2000°C at the surface of the central void) restructuring is not complete in 28 days of irradiation. The rate of restructuring for the columnar grain growth regions is controlled primarily by the linear heat rate as it affects fuel temperatures and temperature gradients and by the initial oxygen-to-metal ratio in the fuel and secondarily by the plutonium content of the fuel. The rate of restructuring increases rapidly with increasing temperature and oxygen potential and decreases slowly with increasing plutonium content. These same phenomena affect the actinide redistribution in the fuel, as will be discussed later.

Although the principal structural changes are associated with early life, some structural changes occur at higher burnup levels. At moderate end-of-life heat

rating (less than 10 kW/ft), the densified fuel in the original columnar grain growth region shows grain refinement, with short columnar grains and radially elongated porosity in the grain boundaries. Additional sintering of sphere to sphere in Sphere-Pac fuel is seen in the cooler regions, and the fuel in this region is heavily decorated with spherical pores or bubbles, as can be seen in Fig. 5.13. A distinct subgrain structure is developed. The distribution of metallic inclusions in the microstructures also varies with burnup. More will be said on this in discussing the observations on fission product distribution. At higher end-of-life linear heat rates and burnup levels near 10% FIMA, the general structural features are similar, with the one difference being the possibility of additional structural changes near the central void due to limited-volume melting, as discussed in Sect. 5.3.

One macroscopic effect of restructuring is the observation of in-reactor fuel dimensional changes, which may be attributed to sintering in the cooler regions of the fuel. Since most of our work involved Sphere-Pac fuel, there is very little information on diametral changes. The one diametral change recorded is for the low-burnup pellet pin in the ORR instrumented tests (Sect. 5.2), where the pellet-to-cladding gap apparently increased from 0.0014 to 0.003 in. This was a diametral shrinkage of approximately 0.5% at approximately 0.5% FIMA in a pellet that had a starting density approximately 84% of theoretical. Better information is available on fuel column length changes. The best data are from the instrumented MINT pin (Sect. 5.4), where the fuel column length decreased approximately 0.5% during the initial period of irradiation (57.0 hr at 10 to 13 kW/ft). This capsule was irradiated at several power levels, and the length change was first definitely seen on going to 10 kW/ft, with subsequent definite decreases in length on later going to 15.5 and 16.3 kW/ft. Fuel column length changes for the series I EBR-II Sphere-Pac fuel pins, which operated at 15 kW/ft to a burnup of approximately 6% FIMA, were derived from neutron radiographs. These data are less reliable, and the apparent changes were both positive and negative, with the maximum for the 13.5-in.-long columns being 1.5%. At high burnup (10% FIMA) the fuel columns in capsule 113 (Sect. 5.1) all showed a measurable decrease in length, ranging from 1.2 to 4.2%, with the amount of shrinkage being roughly proportional to peak linear heat rate (temperature) and decreasing with initial fuel smear density, as would be expected for a sintering process. Insufficient data were obtained to define the extent or kinetics of this process.

75. A. R. Olsen, R. B. Fitts, and W. J. Lackey, *In-Reactor Restructuring Temperatures and Kinetics for (U,Pu)O₂*, ORNL-TM-3387 (July 1971). (See also pp. 579–602 in *Proc. Conf. Fast Reactor Fuel Element Technology*, ed. by Ruth Farmakes, American Nuclear Society, Hinsdale, Ill., 1971.)

76. W. J. Lackey, F. J. Homan, and A. R. Olsen, *Porosity and Actinide Redistribution During Irradiation of (U,Pu)O₂*, ORNL-TM-3762 (August 1972).

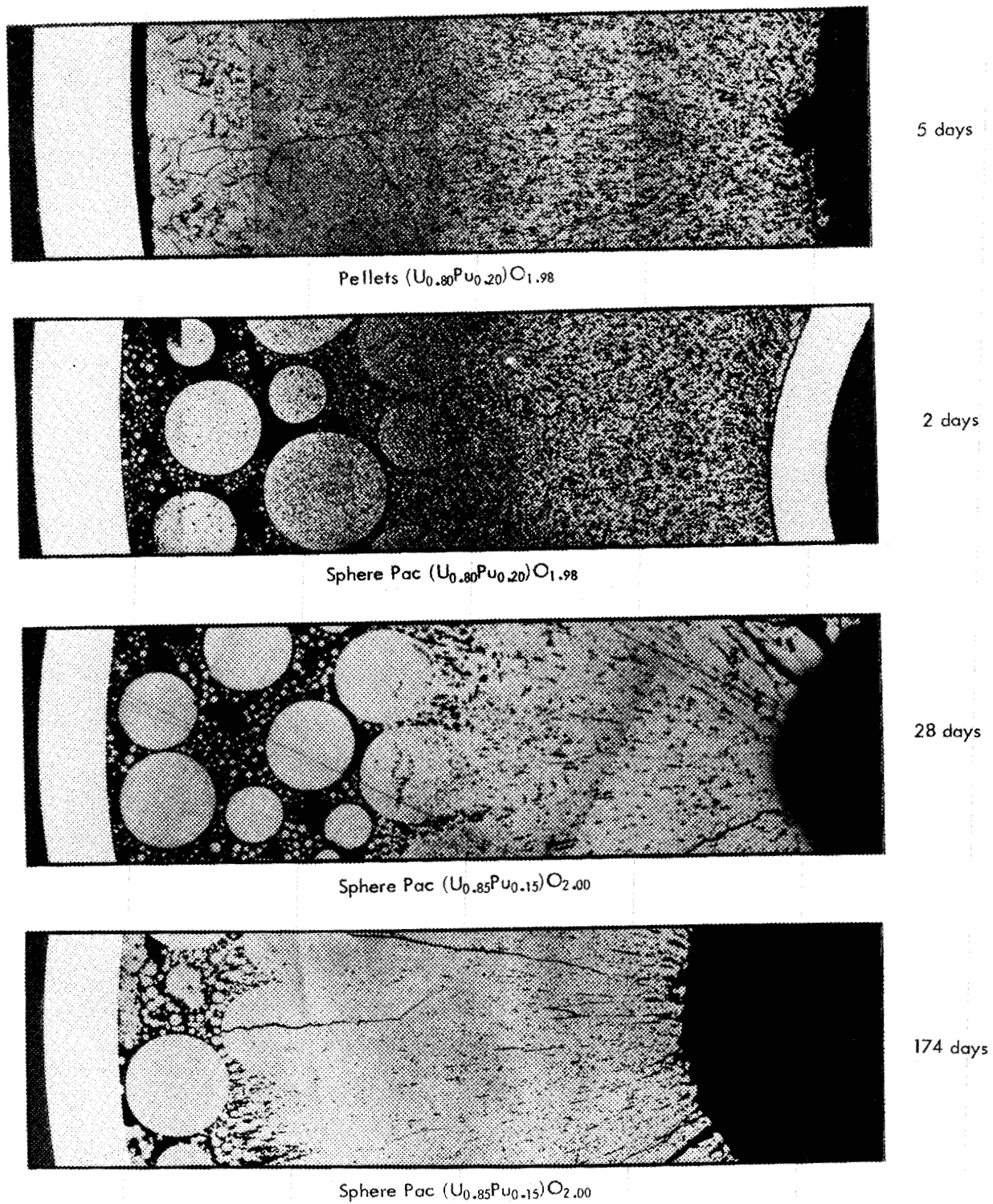


Fig. 5.65. Effect of irradiation time on restructuring of $(U,Pu)O_2$ fuels with a center temperature of approximately $2000^\circ C$.

5.8.3 Actinide and Fission Product Redistribution

The movement of the actinides and the fission products in the fuel can have significant effects on the performance characteristics of the fuel. As we have stated previously, there was clear evidence of the preferential movement of uranium down the temperature gradients in the columnar grain growth regions (temperatures greater than 1650°C). This led to the formation of regions depleted in uranium and thus concentrated plutonium in the regions near the central void. That increased the fission heat generation rate there and simultaneously lowered the local melting point. This could lower the permissible linear heat rating⁷⁷ by as much as 2.5 kW/ft. A secondary effect of this change in actinide distribution has been seen in fuel reprocessing studies.⁷⁸ The fuels with higher plutonium content are less soluble in nitric acid and may require a secondary dissolution step with a fluoride addition to the solvent. The kinetics of this redistribution as well as the limits of plutonium enrichment are primarily controlled by the oxygen-to-metal ratio in the initial fuel. This has been discussed in detail,⁷⁵ and a model to predict the actinide redistribution is discussed in Chap. 6.

Concurrent with the actinide redistribution, oxygen redistributes. This can affect the form of fission product inclusion in the fuel structure and the fuel-cladding chemical interaction. The effect of the oxygen potential on the form of the fission product molybdenum was clearly seen in the uninstrumented high-burnup tests and the EBR-II series I tests, where the molybdenum concentration in the metallic inclusions decreased with distance from the center of the fuel to the cladding. There was evidence of molybdenum migration down the temperature gradient, but it was incorporated in the oxide at the lower temperatures.

Distinct accumulations of barium and ruthenium in the higher-temperature fuel regions were found, particularly in the ETR instrumented tests, where the barium in the oxide fuel may have lowered the melting point. Distinct accumulations of molybdenum, cesium, and tellurium in the fuel adjacent to the cladding were found. The buffering effect of the molybdenum on the

oxygen potential⁷⁹ has been recognized but not fully explained. The cesium and tellurium concentrations may have a significant effect on the fuel-cladding chemical interaction rate.^{80,81} Additional investigation of the extent of concentration of the cesium and tellurium as well as identification of the distribution and oxidation states of the molybdenum⁸² and rare-earth fission products⁸³ was planned. Data on this should come from the EBR-II series II tests currently in the reactor. Since the type of atom fissioned will significantly affect the fission product inventory, we began early⁸⁴ to take this into account. In fact, the thermal flux test provides the best simulation of LMFBR composition changes, because the only fissile material is the plutonium, while in the tests in the EBR-II, ²³⁵U is usually incorporated to obtain the desired fission rates.

5.8.4 Electron Microscopy of Irradiated (U,Pu)O₂

Replica electron microscopy of irradiated (U,Pu)O₂ was conducted to improve our understanding of restructuring, fuel swelling, and fission gas release. We examined fuel irradiated in the ETR to burnups of 0.7 and 4.2% FIMA with cladding inner surface temperatures of 325 to 370°C at time-averaged linear heat rates of 13 to 14 kW/ft. The higher-burnup fuel is shown in Fig. 5.66. The microstructure of both fuels immediately adjacent to the cladding was unchanged from that of the

79. K. E. Spear, J. M. Leitnaker, and N. Engel, "Thermodynamic Calculations: Chemical Effects of Nuclear Burnup on UPuO₂ Fuels," *Fuels and Materials Development Program Quart. Progr. Rep. June 30, 1969*, ORNL-4440, pp. 18-22.

80. E. A. Aitken et al., "Transport and Reaction of Fission Products with Stainless-Steel Cladding Out-of-Pile Thermal Gradient Testing," *Trans. Amer. Nucl. Soc.* **14**(1) 176-77 (1971).

81. H. E. McCoy, Jr., J. H. Shaffer, and B. McNabb, Jr., "Intergranular Cracking of Materials Exposed to Several Fission Products and Sulphur," *Metals and Ceramics Div. Annu. Progr. Rep. June 30, 1972*, ORNL-4820, pp. 118-19.

82. J. M. Leitnaker and F. J. Homan, "Molybdenum Concentration Distribution in Fuel Pins," *Fuels and Materials Development Program Quart. Progr. Rep. Dec. 31, 1971*, ORNL-TM-3703, pp. 23-33.

83. J. M. Leitnaker, J. P. DeLuca, and R. B. Fitts, "Influence of Burnup on Reactivity of Oxide Fuel with Cladding," *Trans. Amer. Nucl. Soc.* **14**(1), 177 (1971).

84. A. R. Olsen, R. B. Fitts, and C. M. Cox, "Analysis of the Validity of Fast Reactor Fuel Tests in Existing Test Reactors," pp. 127-50 in *National Symposium on Developments in Irradiation Testing Technology Held at Sandusky, Ohio, September 9-11, 1969*, CONF-690910.

77. W. T. Sha, P. R. Huebotter, and R. K. Lo, "The Effect of Plutonium Migration on Allowable Power Rating and Doppler Broadening," *Trans. Amer. Nucl. Soc.* **14**(1), 183-84 (1971).

78. Personal communication from J. H. Goode of ORNL Chemical Technology Division on Nov. 30, 1972.

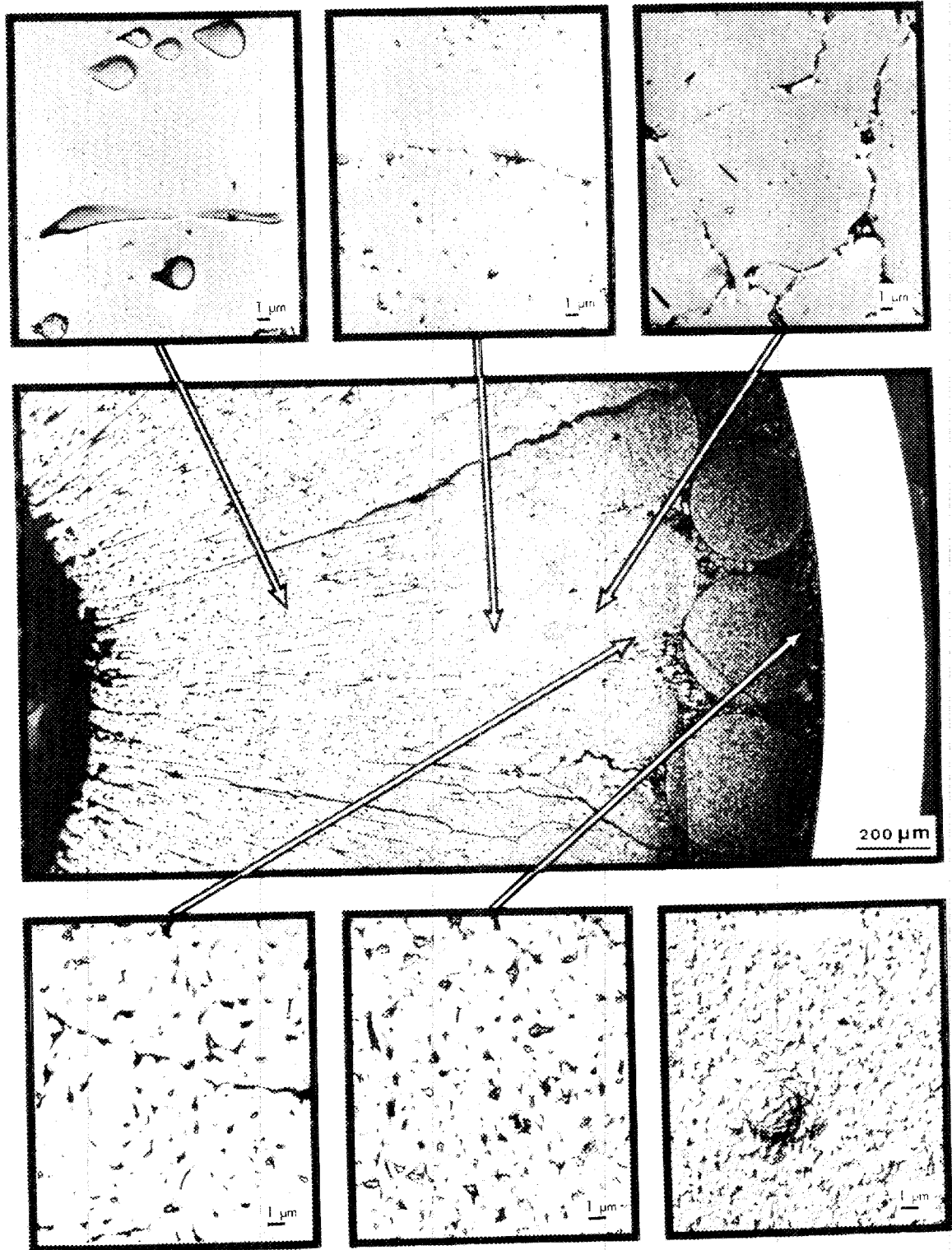


Fig. 5.66. Selected-area replica electron micrographs of $U_{0.85}Pu_{0.15}O_{2.00}$ fuel pin 43-115-4 irradiated to a burnup of 4.2% FIMA.

unirradiated material. This is strong evidence that intergranular pores as large as $0.2\ \mu\text{m}$ in diameter do not disappear during irradiation. This is not to say that a large number of considerably smaller fission gas bubbles do not disappear by redissolving. There were indications that fission gas bubble migration and coalescence were influenced by movement of columnar grain boundaries perpendicular to the thermal gradient as well as by the presence of subgrains 1 to $3\ \mu\text{m}$ across within the equiaxed grain region. The bubbles or pores located within the four grains shown in the lower left micrograph of Fig. 5.66 are located on subgrain boundaries.

5.8.5 Fuel-Cladding Mechanical Interactions

Two types of fuel-cladding interactions can have a significant effect on fuel pin failure. These are mechanical and chemical interactions. Mechanical interaction may occur:

1. as a result of differential thermal expansion between the fuel and the cladding, particularly under start-of-life conditions, or when there is a sudden increase in pin linear heat rate because of a change in reactor loading,
2. as a result of fuel volume changes resulting from fission product accumulation at high burnup.

Our experiments to date have not provided any evidence for significant mechanical deformation that can be attributed to fuel-cladding mechanical interaction. This is not surprising, since most of the fuel pins have had smear densities less than 85%, and the majority of the burnup levels have been less than 50,000 MWd/ton – a combination of conditions under which General Electric investigators⁸⁵ have also reported no significant mechanical interaction.

We noted two cases in which the cladding has plastically deformed. In the transient tests on unirradiated Sphere-Pac fuel⁸⁶ there was metallographic evidence of spheres having been forced against the cladding, as seen in Fig. 5.67, by the differential thermal expansion during the rapid power excursion.

85. C. N. Craig, et al., "Steady-State Performance of PuO_2 - UO_2 Fast Reactor Fuels," pp. 555–75 in *Proc. Conf. Fast Reactor Fuel Element Technology*, ed. by Ruth Farmakes, American Nuclear Society, Hinsdale, Ill., 1971.

86. C. M. Cox, D. R. Cuneo, and E. J. Manthos, "Performance of Sphere-Pac and Pelletized (U,Pu) O_2 During Severe Overpower Transients," pp. 701–24 in *Proc. Conf. Fast Reactor Fuel Element Technology*, ed. by Ruth Farmakes, American Nuclear Society, Hinsdale, Ill., 1971.

The second observation is not clearly defined, since it derives from a comparison of predicted diametral changes and measured changes for the EBR-II series I pins as discussed in Sect. 5.5.

Tests currently under irradiation in the EBR-II include higher-density fuel and will go to higher burnups so that additional data on mechanical interaction will be available from them.

5.8.6 Fuel-Cladding Chemical Interactions

Chemical interactions between the fuel and stainless steel cladding have been repeatedly observed by a number of experimenters⁸⁷ at cladding temperatures as low as 500°C (certainly at temperatures above 550°C) and burnup levels in excess of 3 to 5% FIMA. These reactions have been recognized as a potential limiting factor on operating conditions and attainable burnup. The fact that oxidation of the cladding is the primary reaction has also been established.^{83,88} Two types of oxidation have been seen: (1) a general or matrix oxidation, with the buildup of a significant surface oxide layer and a more or less uniform reduction in wall thickness, and (2) an intergranular attack, which is often only in localized areas but which proceeds to significant depths, sometimes greater than 50% of the 0.016-in. tube wall thickness. The intergranular attack, which usually shows some fission products such as cesium in the grain boundaries, is the source of greatest concern, since it has been seen most often in the irradiation tests conducted to date.⁸⁹

The intergranular type of attack has occurred at the lower temperatures with penetrations up to 0.009 in. at temperatures near 600°C . Significant general matrix oxidation is usually not seen until the cladding surface temperatures are well above 600°C . Figure 5.68 shows the compilation of the data as of November 1971, with the ORNL data from the tests reported in Sect. 5.3 added. The bulk of the postirradiation data at that time lay in the cross-hatched area in the lower left of this plot and at temperatures below 500°C .

87. R. B. Fitts, A. R. Olsen, C. M. Cox, and E. L. Long, Jr., *Metals and Ceramics Div. Annu. Progr. Rep. June 30, 1971*, ORNL-4770, pp. 57–59.

88. R. B. Fitts, E. L. Long, Jr., and J. M. Leitnaker, "Observations of Fuel-Cladding Chemical Interactions as Applied to GCBR Fuel Rods," pp. 431–58 in *Proc. Conf. Fast Reactor Fuel Element Technology*, ed. by Ruth Farmakes, American Nuclear Society, Hinsdale, Ill., 1971.

89. R. E. Adams and R. B. Fitts, "Compilation of Data on Oxide-Fuel-Stainless Steel Cladding Interaction," *LMFBR Fuel Cycle Studies Progr. Rep. November 1971, No. 33*, ORNL-TM-3663, pp. 47–56.

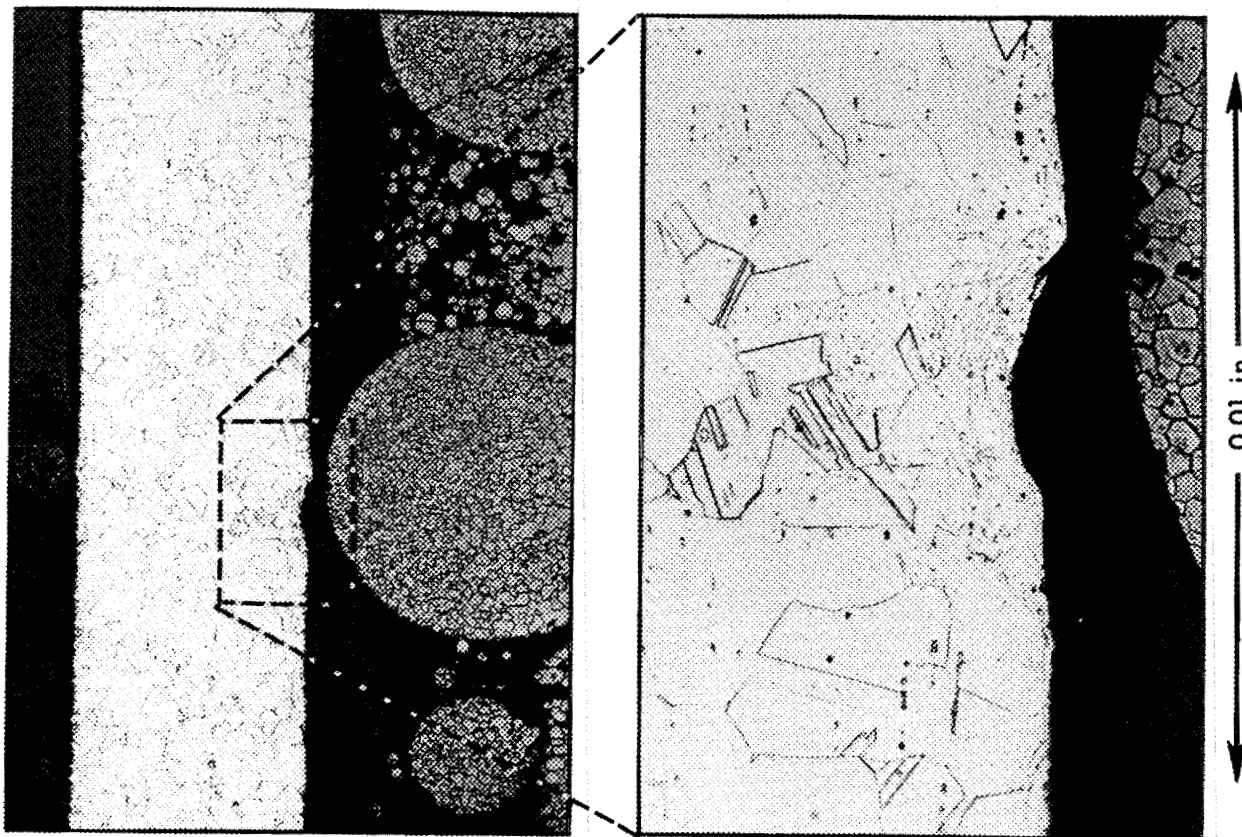


Fig. 5.67. Point of contact of large microsphere with cladding during irradiation.

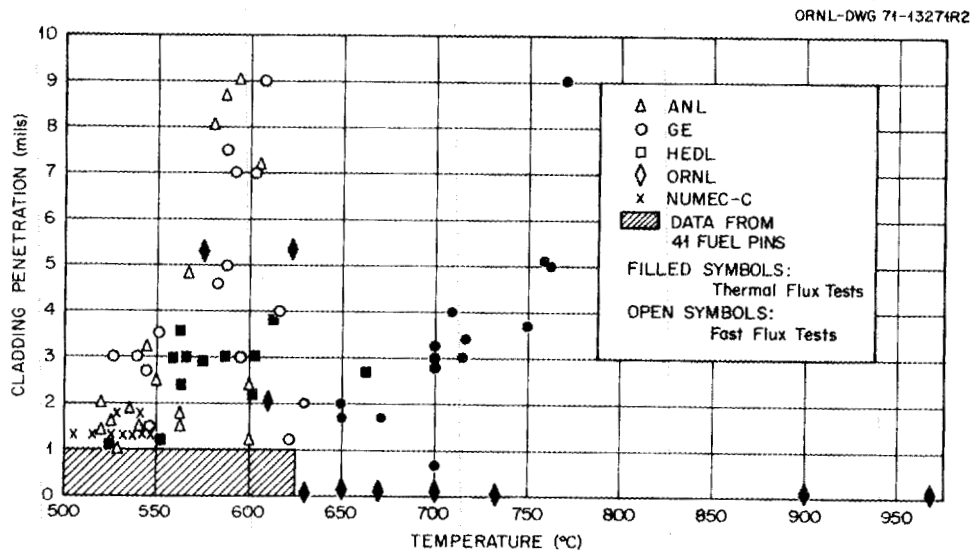


Fig. 5.68. Summary of stainless steel attack in mixed oxide fuel pins.

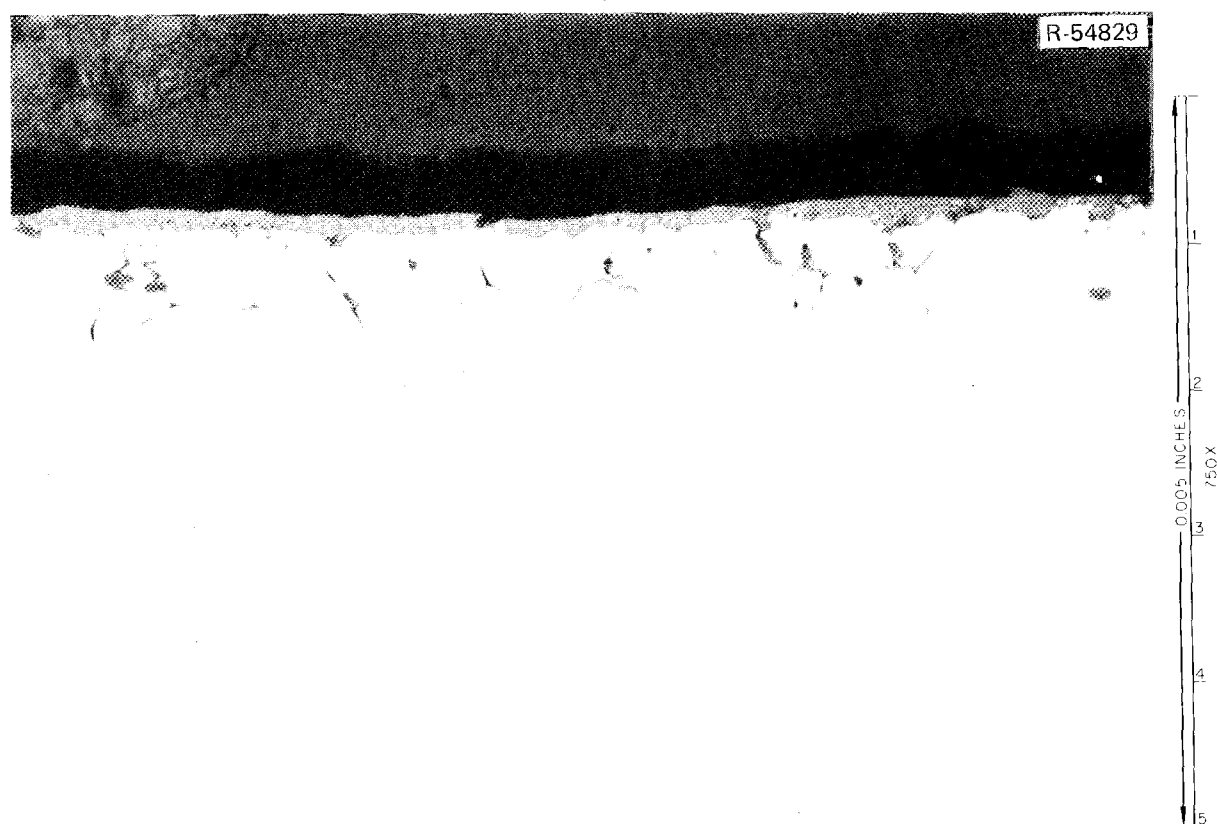


Fig. 5.69. Type 316 stainless steel oxidized at 925°C for 500 hr in Ar-4% H₂-4000 ppm H₂O.

The mechanisms of the attack have not been defined, although a number of hypotheses have been proposed.^{83,88,90,91} Most of the hypotheses have been associated with the effects of fission products, particularly cesium, on the attack with a recognition of the strong effect of oxygen potential in the fuel and a distinct temperature dependence. Early work suggested that fission products were responsible, in that mixed oxides out-of-reactor did not show extensive corrosion⁹² and that the extent of attack was proportional to the temperature.⁹³ Still others⁹⁴ felt that low-density fuel would lead to more concentration of the fission products at the cladding interface and increased reactions.

The out-of-reactor oxidation studies⁸⁸ conducted as an adjunct to the ORNL irradiation program showed that both types of attack could be developed in the absence of both fission products and fuel, as seen in Fig. 5.69. There was evidence of a threshold temperature for some cladding microstructural changes (see Fig. 5.10) in the uninstrumented thermal flux tests we ran, but even at temperatures above this threshold we did

not see intergranular attack with the Sphere-Pac fuels in the uninstrumented tests (Sect. 5.1), the thermal performance tests (Sect. 5.2), or the series I EBR-II tests (Sect. 5.5). The EBR-II tests also failed to show any density effect, even at fuel smear densities as low as

90. C. E. Johnson, I. Johnson, and C. E. Crouthamel, "Fuel-Cladding Chemical Interactions in UO₂-20 wt % PuO₂ Fast Reactor Fuel Clad with Stainless Steel," pp. 393-410 in *Proc. Conf. Fast Reactor Fuel Element Technology* ed. by Ruth Farmakes, American Nuclear Society, Hinsdale, Ill., 1971.

91. P. S. Maign, "Interaction of Volatile Fission Products with Austenitic Stainless-Steel Cladding Alloys," *Trans. Amer. Nucl. Soc.* 14(2), 599 (1971).

92. K. J. Perry et al., "Fuel-Cladding Reactions Observed in Stainless-Steel-Clad Mixed-Oxide Fuel Pin Irradiations," pp. 411-29 in *Proc. Conf. Fast Reactor Fuel Element Technology*, ed. by Ruth Farmakes, American Nuclear Society, Hinsdale, Ill., 1971.

93. C. E. Johnson and C. E. Crouthamel, "Fuel-Clad Interactions in Mixed-Oxide UO₂-PuO₂ Fuel," *Trans. Amer. Nucl. Soc.* 14(1), 173 (1971).

94. J. W. Webber and E. D. Jensen, "Effect of O/M on Irradiated Mixed Oxide Stainless-Steel Cladding Compatibility," *Ibid.*, p. 175.

76% and very high temperatures up to 1000°C in tests to low to intermediate burnup.⁹⁵

The only significant fuel-cladding chemical interaction with Sphere-Pac fuels seen to date was in the high-burnup instrumented thermal flux series I tests, and here the Sphere-Pac fuel showed approximately one-half the extent of attack seen in a companion pin with pellet fuel. A similar result with no attack for Sphere-Pac fuel and some attack for pellet fuel was seen in the ORR thermal performance test, Sect. 5.2. Additional data on low rates of chemical interaction between Sphere-Pac fuel and cladding have been reported by Neimark,⁹⁶ who also reported both matrix and intergranular attack in companion fuels in the same EBR-II subassembly.

Although the improved performance of Sphere-Pac fuel with respect to fuel-cladding chemical interactions has not been proven incontrovertibly, the evidence overwhelmingly supports this conclusion. In every test examined to date the Sphere-Pac fuel has shown less reaction. Examination of the pins from the second ETR instrumented capsules (Sect. 5.3) and from EBR-II series II tests (Sect. 5.6) should provide conclusive evidence.

The EBR-II pins should also help in defining the reasons for this improved behavior, because the Vi-Pac fuel pins, which have a different porosity distribution, will retain open paths for gas phase communication between the fuel surface and the hotter fuel. Thus, a comparison of the chemical interactions for the Vi-Pac and Sphere-Pac pins should help to define the role of this mechanism in the rates of interaction. It should be pointed out here that of all the possible explanations presented in the discussion in Sect. 5.2.4.2, the gas-phase oxygen transport argument is the least likely, because of the high rates of chemical interaction seen by others⁹⁰ in Vi-Pac fuels, and because in our series I ETR instrumented tests (Sect. 5.3) the Sphere-Pac porosity gas paths at high burnup were plugged with fission product oxides, but still the extent of interaction was less than in the adjacent pellet pins. The most likely sources of improved performance are the better gap conductivity and possibly the reduced cladding stresses with Sphere-Pac fuels.

One additional finding in the area of chemical interaction that has come to light during our investiga-

tions is the fact that the intergranular form of attack does not increase monotonically with temperature but in fact has a peak at intermediate temperatures. The data presented in Fig. 5.68 show an apparent peak in the extent of reaction in the 540 to 610°C range. This peak we believe is associated with the kinetics of carbide precipitation in the grain boundaries of the stainless steel.

Evidence to support this hypothesis was developed in another out-of-reactor adjunct test⁹⁷ of oxidation in the absence of both fuel and fission products. In a series of experiments, solution-treated type 316 stainless steel tubing was exposed to flowing Ar-4% H₂ with controlled moisture contents of 4000 or 40 ppm to control the oxidation potential. A temperature gradient was maintained along each 10-in.-long tube. Two gradients were used: 450 to 650°C and 500 to 710°C. In all, nine tubes were tested in three groups of three tubes each. The entire length of each tube was nondestructively inspected for wall thickness with an eddy-current technique.⁹⁸ Two tests were conducted for 500 hr each and one for 1000 hr. All nine tubes showed an apparent wall thickness reduction, which was localized in the 560 to 650°C range, with the maximum change at 585 to 605°C. In the 1000-hr test with the higher oxygen potential, a second and greater change in wall thickness was indicated above 660°C. The effect of oxidation potential is shown in Fig. 5.70, while the effect of time is shown in Fig. 5.71.

Standard metallographic examinations of the tests show no significant change in the geometric wall thickness. Although there are other metallographic differences, the most pronounced observation is the distinct increased sensitivity to etching (glyceria regia at room temperature) of all sections cut from the 600°C region. The grain boundaries are most rapidly attacked; this effect is less on sections from higher or lower temperature regions.

Thinned sections from one tube in the 500-hr test with 4000 ppm H₂O were examined by transmission electron microscopy. These samples, one from the 650°C region and one from the 615°C region, showed only M₂₃C₆ precipitate in the structure. However, the morphology of these precipitates was distinctly different, as shown in Fig. 5.72, with thin sheetlike precipitate covering most of the grain boundary in the lower

95. C. M. Cox, A. R. Olsen, R. B. Fitts, and E. L. Long, Jr., "Fuel-Cladding Chemical Interactions in Low-Density (U,Pu)O₂ Fuel Pins," *ibid.*, pp. 173-75.

96. L. A. Neimark, "Fuel Element Performance," *Argonne National Laboratory Reactor Development Program Progr. Rep. June 1971*, ANL-7833, pp. 5-13-15.

97. A. R. Olsen, J. M. Leitnaker, and R. A. Buhl, "Cladding Chemical Reactions," *Metals and Ceramics Div. Annu. Progr. Rep. June 30, 1972*, ORNL-4820, pp. 59-61.

98. C. V. Dodd and W. A. Simpson, Jr., *Thickness Measurements Using Eddy-Current Techniques*, ORNL-TM-3712 (March 1972).

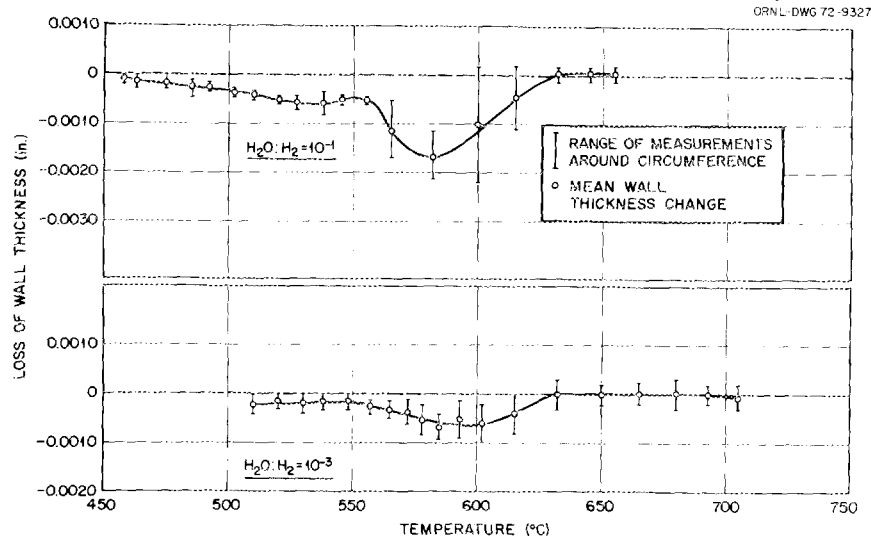


Fig. 5.70. Effect of oxidation potential reaction of stainless steel with Ar-H₂-H₂O in 500-hr tests.

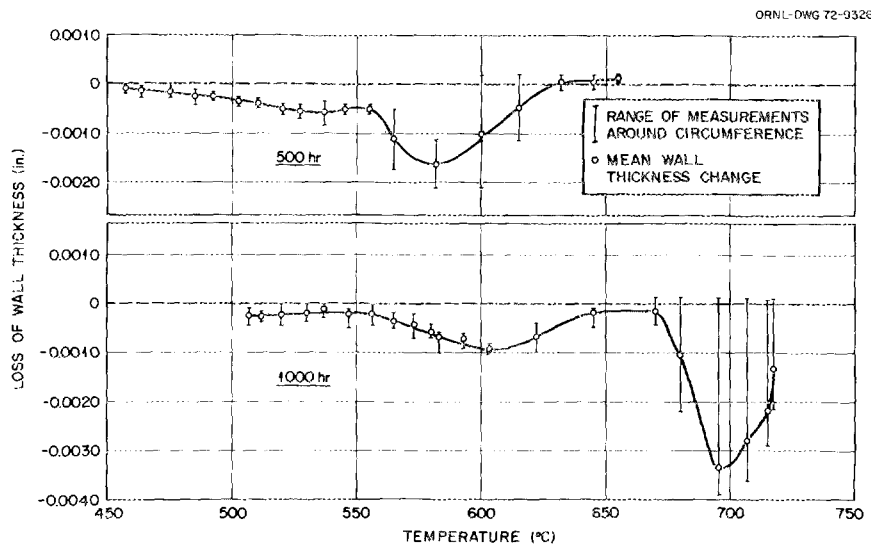


Fig. 5.71. Effect of time at constant H₂O:H₂ = 10⁻¹ on reaction of stainless steel with Ar-H₂-H₂O.

temperature section and thicker, separated, agglomerated precipitate in the higher temperature section. This observation is in excellent agreement with the findings of Stickler and Vinckier.⁹⁹ These same authors report a maximum in intergranular embrittlement after exposure to Strauss solution for samples heat treated in

the range 565 to 650°C. In another experiment in a dry environment, Pickering, Beck, and Fontana¹⁰⁰ report on corrosion tests in the range 93 to 760°C with NaCl with and without the presence of oxygen. Oxygen was required for both matrix and intergranular attack. Also, the reaction occurred most rapidly with M₂₃C₆ com-

99. R. Stickler and A. Vinckier, "Morphology of Grain-Boundary Carbides and Its Influence on Intergranular Corrosion of 304 Stainless Steel," *Trans. Amer. Soc. Metals* 54, 362-80 (1961).

100. H. W. Pickering, F. H. Beck, and M. G. Fontana, "Rapid Intergranular Oxidation of 18-8 Stainless Steels by Oxygen and Dry Sodium Chloride at Elevated Temperatures," *Trans. Amer. Soc. Metals* 53, 793-803 (1961).

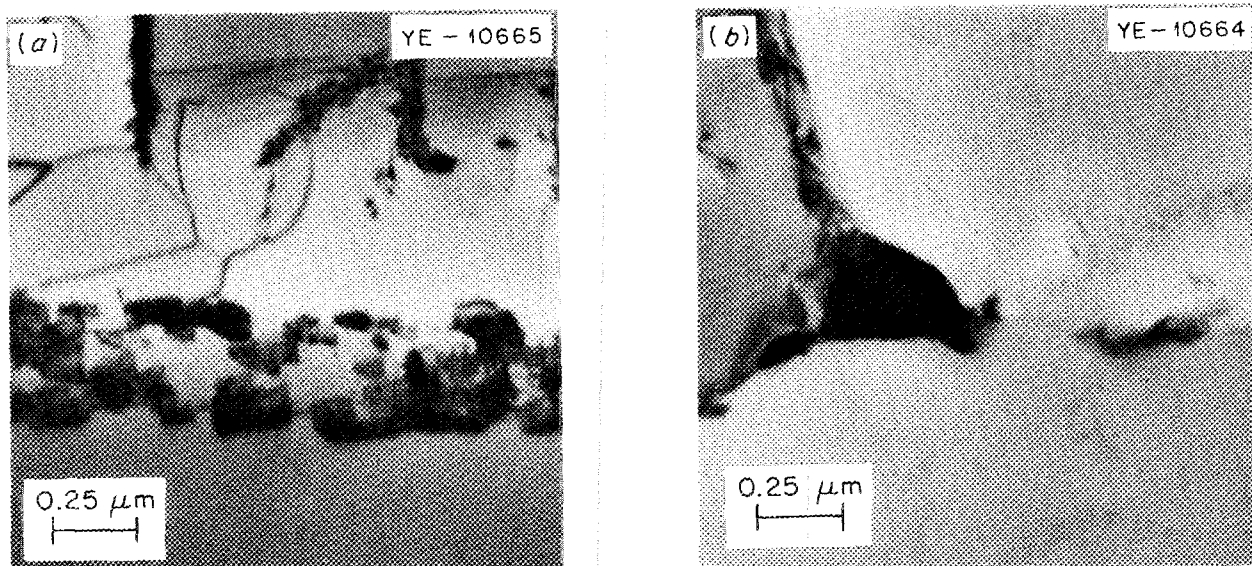


Fig. 5.72. Morphology of precipitates in stainless steel tubing heated in Ar-4% H₂-4000 ppm H₂O for 500 hr. (a) 615°C region; (b) 650°C region.

pounds. The salt led to the production of Na₂CrO₄ instead of a protective chromic oxide. Matrix attack producing large amounts of surface scale occurred only at 704 to 760°C, whereas intergranular attack was very pronounced at 593°C.

Thus, the work of others on intergranular corrosion may help explain our nondestructive test results in stainless steel heat treated in a pure oxidizing atmosphere. The postulated reaction for the apparent wall thickness reduction measured by the eddy-current technique is the formation of thin intergranular oxide layers where the thin interconnected sheets of M₂₃C₆ are formed near 600°C. Agglomerated carbide at higher temperatures does not provide a continuous path, so less penetration occurs until the matrix oxidation rate increases and a thicker continuous carbide precipitate is formed at the highest temperatures of our tests. The intergranular oxide would electrically insulate the grains and increase the resistivity, thus causing an apparent reduction in wall thickness.

The presence of fission product cesium in the grain boundaries of intergranularly attacked cladding on irradiated oxide fuel pins may also be the result of the formation of compounds of cesium, chromium, and oxygen by removal of carbon from the M₂₃C₆ precipitate as CO. This would yield a surface area relatively free of carbide, as we have noted in some of our high-temperature tensile tests of previously heat-treated

type 316 stainless steel.¹⁰¹ The postulated reactions require additional experimental proof. The known effects of neutron irradiation on carbide precipitation kinetics^{102,103} may lower the temperature range to the 540°C seen in Fig. 5.68.

Thus, the irradiation tests in this program together with the simple out-of-reactor oxidation study tests have shown that the oxygen activity is the primary variable in fuel-cladding reactions, that temperature is important particularly for the intergranular form of attack, and finally that the cladding is a very important part of the reaction, with intergranular attack varying from one lot to another depending on as yet undefined variations in composition and fabrication history. They have also shown that for any given lot of tubing the Sphere-Pac fuels appear to be much less reactive than pellet fuels.

101. J. M. Leitnaker and H. Mateer, *Fuels and Materials Development Program Quart. Progr. Rep. March 31, 1972*, ORNL-TM-3797, pp. 92-96.

102. T. T. Claudson, R. W. Barker, and R. L. Fish, "The Effects of Fast Flux Irradiation on the Mechanical Properties and Dimensional Stability of Stainless Steel," *Nucl. Appl. Technol.* 9, 10-23 (1970).

103. P. J. Barton, *Some Observations on the Structure and Tensile Properties of AISI Type 316 Steel as a Function of Fast Reactor Irradiation Temperature*, AERE-R-6435 (June 1970).

5.8.7 Recommendations for Further Work on Irradiation Effects

Following are the salient recommendations of this program for work in the near future:

1. An experiment similar to the SG-3 experiment should be conducted. The pellet and Sphere-Pac fuel pins would be brought to power over about 10 hr (in an attempt to duplicate a typical power ramp for a commercial power reactor) and held at constant power throughout the test. We would of course be constrained by the cycle durations of the test reactor, but cyclic data would also be useful. The center-line and cladding thermocouples would then monitor the kinetics of sintering, restructuring, and gap conductance changes. In this manner data applicable to LMFBR safety analyses would be obtained. It would be desirable to compare pellet and Sphere-Pac fuels and to investigate a range of initial densities and fabrication techniques.

2. Transient testing should be conducted on selected EBR-II series II pellet and Sphere-Pac pins. These tests were planned to supplement our transient testing on unirradiated pins but were not conducted because of the program termination.

3. EBR-II tests should be conducted with plutonium and natural or depleted uranium. As is pointed out in the section on thermodynamics in Chap. 6, the amount

of oxygen used by oxide-forming fission products is significantly greater for ^{235}U fuel than for plutonium fuel because of the important shift in fission product distribution. Since all EBR-II fuel pins have contained enriched uranium, the chemical interactions between fuel and cladding could be substantially reduced. A request for Approval in Principle for such EBR-II tests was submitted to the USAEC shortly before announcement of program termination.

4. The out-of-reactor chemical interaction studies initiated in this program should be followed up to investigate the influence of cold work and cladding composition on the results. This type of experimentation is inexpensive and can shed valuable light on the mechanisms, temperature ranges, and magnitudes of both uniform attack and intergranular penetration. Sufficient information could be developed to specify cladding composition and metallurgical processing variables to minimize cladding-fuel chemical interaction.

5. The results of the program have shown some potential performance advantages for Sphere-Pac fuels, both in regard to mechanical interaction between fuel and cladding, and chemical compatibility. These potential advantages should be pursued both experimentally, to establish the limits of superiority, and analytically, to define the mechanisms that lead to better performance.

6. Fuel Performance, Process, and Economic Evaluations

F. J. Homan A. L. Lotts

The performance and economic evaluation studies were conducted primarily in an effort to optimize the design of oxide fuel pins for fast breeder reactors. While there were several other objectives of the modeling work, which will be discussed below, we hoped that the behavior models would be capable of accurately predicting the useful lifetime of a fast reactor fuel pin. Coupling this information with cost analyses, such as provided by the FABCOST 9 computer code,¹ would then permit trade-off studies to be made to select a fuel pin design that would result in minimum fuel cycle costs consistent with achievement of desired burnup levels.

6.1 FUEL PERFORMANCE MODELING

F. J. Homan R. A. Bradley
W. J. Lackey A. R. Olsen
J. M. Leitnaker

As indicated earlier, the fast breeder reactor oxide fuels program was structured so that information developed through irradiation testing was incorporated into computerized behavior models. The modeling work had several objectives. The first, of course, was to develop the means to analytically predict how a fast reactor fuel pin will behave in service, particularly when it will fail. Secondary objectives included providing guidance for the planning of irradiation tests for the program and interpretation of the results from these tests. In addition, the models were used to establish the sensitivity of fuel performance to different material properties and operating parameters. We hoped that this would enable us to use our research money more effectively, in reducing the uncertainty in the most critical areas.

The fuel model (FMODEL) computer code² was written to predict the in-reactor performance of a single LMFBR fuel pin consisting of pelletized oxide fuel clad with stainless steel. The code is sufficiently flexible to

predict performance of other types of fuel pins. For example, the irradiation behavior of a fuel pin in a thermal flux can be modeled, and pins clad with materials other than stainless steel can be analyzed with a few minor modifications to the code. FMODEL could be used for carbide and nitride fuels, but changes in the built-in fuel properties will be necessary for such use. The code can also be used for particulate fuel forms, including powders, shards, and microspheres such as those loaded by the Sphere-Pac process developed at ORNL.

6.1.1 Integrated Code Description

FMODEL represents an integration of three fairly complex models: a heat transfer model, a fuel and cladding mechanical model, and a chemical performance model. The heat transfer model is similar to that described in the write-up of the PROFIL code,³ except that the empirical restructuring model has been replaced with a time-dependent pore migration model based on a vaporization-condensation mechanism. The details of the restructuring model are given in Appendix C of ref. 2. A sophisticated model has been recently developed⁴ to calculate the conductance of heat across the fuel-cladding gap. Total gap conductance is viewed

1. A. L. Lotts, T. N. Washburn, and F. J. Homan, *FABCOST 9, a Computer Code for Estimating Fabrication Costs for Rod-Bundle Fuel Elements*, ORNL-4287 (August 1968).

2. F. J. Homan, W. J. Lackey, and C. M. Cox, *FMODEL - a FORTRAN IV Computer Code to Predict In-Reactor Behavior of LMFBR Fuel Pins*, ORNL-4825 (January 1973).

3. C. M. Cox and F. J. Homan, *PROFIL - a One-Dimensional FORTRAN IV Program for Computing Steady-State Temperature Distributions in Cylindrical Ceramic Fuels*, ORNL-TM-2443 (March 1969) and Addendum (August 1969).

4. C. M. Cox, F. J. Homan, and R. L. Diamond, "Description of Fuel-to-Cladding Gap Conductance," *Fuels and Materials Development Program Quart. Progr. Rep. Mar. 31, 1972*, ORNL-TM-3793, pp. 25-38.

in the model as the sum of a conductance term from solid-solid contact (when the gap has closed from differential thermal expansion or fuel swelling) and from heat transport across a gas phase separating the fuel and cladding. Accommodation effects are considered, as well as the changing conductivity of the gas in the gap from the introduction of fission gases into the plenum during irradiation.

The mechanical model uses a generalized plane strain, finite difference approach. The code user can supply his own plasticity equations and creep equations to describe both thermal and irradiation creep of the cladding. The mechanical model is applied to the fuel in a somewhat different manner than to the cladding, because of the extreme plasticity of the central portion of the fuel and because of the cracks that form in the cooler fuel regions. The mechanical model has been incorporated into a fuel cracking model, which is described in Appendix F of ref. 2. The details of the mechanical model are given in Appendix E of ref. 2.

The chemical model describes the transport of oxygen, uranium, and plutonium during irradiation. Thermodynamic considerations are employed in these calculations, and the results are extremely sensitive to the initial oxygen-to-metal ratio of the fuel. The details of this model have recently been published.⁵ Component redistribution is very important in a performance model because of the influence of plutonium content and stoichiometry on thermal conductivity, thermal expansion, the melting temperature, and the creep characteristics of mixed oxide fuels. Failure to account for these changes will result in a model that does not properly compute temperature changes with irradiation and can lead to serious errors in other performance characteristics.

The general approach used in FMODEL is to divide the fuel pin into a user-specified number of axial regions, with each axial region further divided into concentric rings. Then the performance of each region at an axial node located in the axial center of the region is calculated. The irradiation history of interest is broken down into components or cycles, and the performance of each axial node is calculated in turn for each cycle. This process is repeated until all cycles have been completed. Thus two noding systems are required – axial and radial. Storage locations are required to store the performance calculations from one axial node

while calculations are being performed on other nodes. At the end of each cycle the performance information can be output for examination. The code user has complete control of the amount of information output.

Performance calculations at a given axial node begin with the temperature distribution in the fuel and cladding, based on fuel and cladding geometry and reactor operating conditions. Mechanical and physical properties are then determined for each fuel and cladding node, based on the temperature, porosity, grain size, and other parameters for the fuel or cladding at that node. The temperatures and properties calculated are assumed to remain constant for a time period Δt . The length of Δt is under the control of the code user. The continuously changing real-life situation can be approximated more closely by making Δt small, but a penalty is paid in greater computer time requirements. During any Δt both the fuel and cladding will be subjected to various types of stresses. Both will have a temperature gradient, fission gas pressure, and perhaps pressure due to fuel-cladding mechanical interaction. In addition, both will swell, the cladding because of void formation and the fuel because solid fission products and retained fission gas accumulate in its lattice. The geometry changes brought about by response to the fuel and cladding stresses are calculated at the end of each time period, and the temperature distribution is recalculated. Then the physical and mechanical properties are redetermined and the process repeated until the entire time period of interest has been covered.

Changes in power are modeled as occurring stepwise. A linear power ramp is replaced by a series of vertical steps, followed by horizontal periods of constant power. The number of such steps in a given power change is under the control of the user. The code has been designed to follow the broad changes in reactor power history with the characteristics of each cycle input. However, if the detailed power history is to be followed, it is more convenient to merely read in the reactor power as a function of time and write a small routine to generate the other necessary cycle characteristics. See Appendix B of ref. 2 for a description of the cycle characteristics required.

Several assumptions and simplifications are inherent in the FMODEL code. A listing and brief discussion of each is given below.

1. The heat transfer analysis considers heat flow in the radial direction only. The axial length is divided into a user-specified number of regions, for which the calculations representing the entire region are performed for the axial midpoint of the region. Axial heat

5. W. J. Lackey, F. J. Homan, and A. R. Olsen, "Porosity and Actinide Redistribution During Irradiation of (U,Pu)O₂," accepted for publication in *Nuclear Technology*. Also available as ORNL-TM-3762 (August 1972).

flow near the ends of the rod probably causes a temperature distribution in those regions somewhat different than that calculated with the one-dimensional analysis at the region midpoint. This effect is ignored in the present version of the code.

2. The cladding mechanical analysis assumes circumferential symmetry as well as plane strain. Thus the effects of cladding bowing due to asymmetrical distributions of neutron flux and coolant temperature are ignored. Similarly, the stress effects due to the presence of wire wrap or grid spacers are ignored. Friction forces between fuel and cladding are also ignored.

3. One simplification used in the code is to neglect time-dependent cladding wastage. This is somewhat difficult to treat analytically, because the nature of intergranular penetration of fission products at the cladding inner surface is such that the cladding strength may be lost, but its volume is still present to influence fuel-cladding mechanical interaction. In addition, swelling and plastic strain are being accumulated as functions of time and radial position across the cladding. If cladding nodes are "disappearing" because of wastage, it is difficult to keep track of these quantities. Therefore, our present position is that because of the lack of data and understanding concerning this effect, it is better to make allowances for wastage in the initial cladding thickness than to attempt to describe the wastage phenomenon as a time-dependent event.

4. Cladding creep and tensile properties are presently treated in the code as independent of plastic strain and irradiation. It is well-known qualitatively that annealed claddings harden and cold-worked claddings soften from irradiation, and it would be a simple matter to substitute quantitative relationships to describe the changes when such relationships are available.

5. Fuel creep is expressed in the code as a function of temperature, porosity, stress, and grain size. Equations for UO_2 developed by Bohaboy⁶ are used for fuel with density greater than 92% of theoretical, and by Clauer⁷ for fuel with densities below this value. Again, it is well-known qualitatively that the fissioning event, substitution of plutonium for uranium, stoichiometry, porosity form, and plutonium concentration will influence creep strength in the fuel, and it is a simple matter to use suitable equations for the fuel under consideration when such quantitative relationships are available.

6. P. E. Bohaboy et al., *Compressive Creep Characteristics of Stoichiometric Uranium Dioxide*, GEAP-10054 (1969).

7. A. H. Clauer et al., *Progress Report on Development of Materials and Technology for Advanced Reactors*, January-March 1969, BMI-1862, p. c-22.

The FMODEL fuel pin performance code has proven to be a valuable tool for planning and design of irradiation experiments and interpretation of data from the experiments. The code contains models to describe most of the phenomena known to occur in an operating fuel pin. Some of the models are derived from first principles, whereas others are empirical or semiempirical. The overall calculational framework is logically and efficiently laid out so that individual models can be replaced when more sophisticated models are available. The code has been able to reasonably reproduce experimental measurements without the use of adjustable parameters to force fit code predictions to experimental observations. The code is flexible, containing many user options to attain the degree of analytical detail desired. The code requires about 300 K of core storage on the IBM 360/91 computer, and running times are under 10 min for most cases of interest. Most of the cases run to date have included 9 axial nodes, 20 fuel nodes, 5 cladding nodes, and 2 to 5 time cycles. Running times could be substantially reduced (to less than 1 min) for cases with fewer nodes and cases where fuel and cladding do not mechanically interact.

6.1.2 Comparison of Code Results with Experimental Results

The veracity of any model is of course determined by comparing its predictions with measured behavior of the real-life system being modeled. Each of the individual models (mechanical, thermal, and chemical) contained in the FMODEL code has been thoroughly confirmed by comparing prediction with experimental measurement. It should be emphasized at this point that FMODEL contains no adjustable parameters for artificially "fitting" predicted performance to measured performance. Predicted performance depends only on the fabrication data and irradiation conditions input, the thermophysical and mechanical properties of the fuel and cladding, and the validity of the models. If agreement with experimental results is not satisfactory, the reason is sought in erroneous data, faulty assumptions, or omission of an important factor from the model.

Measured performance of fuel pins irradiated under fast flux conditions is presently limited to what can be observed during postirradiation examination. This is because instrumentation is very limited in the EBR-II, the only fast reactor in this country in which a substantial number of mixed-oxide pins have been irradiated. In-test data can be obtained from irradiation tests in several thermal flux facilities. Although it is

recognized that thermal flux tests are generally unsuitable for proof tests of fast reactor fuel elements, such tests can be valuable for understanding certain aspects of fuel performance. Pending the availability of instrumented test data from fast reactors, we have utilized thermal flux test data to test the accuracy of our thermal performance models. Fast-flux test data were used for the comparison between predicted and measured diametral expansion.

Comparisons between predicted and measured performance are divided into the five areas (1) diametral expansion of the pins, (2) fuel radial porosity distributions, (3) diameters of central void, columnar, and

equiaxed-grain regions, (4) fuel center-line temperatures, and (5) uranium and plutonium redistribution.

6.1.2.1 Diametral Expansion

Permanent diametral expansion of an irradiated fuel pin is due to cladding density decrease from void formation, plastic strain accumulated throughout irradiation, and elastic strain present at room temperature due to fission gas pressure and cladding swelling gradients. Predicted diametral expansions are sensitive to the assumed cladding strength and pin fabrication and operating conditions.

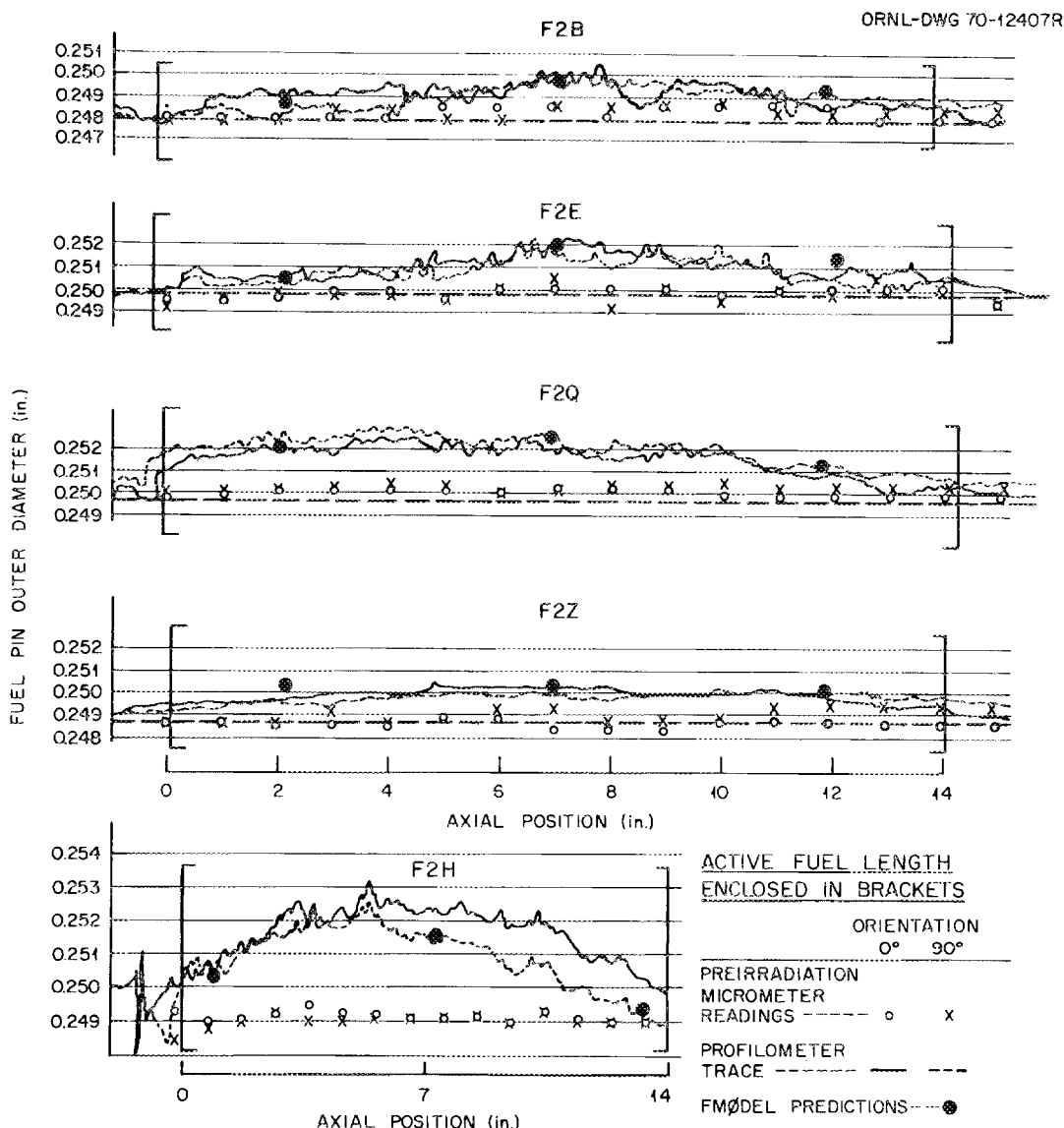


Fig. 6.1. Postirradiation profilometer traces for five fuel pins from General Electric F-2 series.

Figure 6.1 summarizes some early FMODEL analyses on diametral expansions of several pins from the General Electric F-2 series irradiation experiments⁸ in the EBR-II. Irradiation-enhanced creep of the cladding was not considered in the calculations reflected in this figure, and the August 1969 version of the WARD-PNL cladding swelling correlation⁹ was used. Mechanical interaction on start-up due to differential thermal expansion between fuel and cladding was predicted for F2Q and F2H. Notice that the greatest measured diametral expansion for both these pins occurred at the cold end (bottom), where the fuel and cladding differed most in thermal expansion.

Two of the pins shown in Fig. 6.1, F2Z and F2H, were included in the modeling round-robin exercise.¹⁰ The measured and predicted diametral expansions for these pins are compared in more detail in Figs. 6.2 and 6.3. Calculations performed with the data provided for this exercise agreed far better with measurement for F2Z than for F2H. However, we have noted¹⁰ that both the heat rate and neutron fluence provided in the round-robin data package were below those reported in the literature for F2H. These effects account for part of the bias between observed and predicted diametral expansion for this pin.

Figure 6.4 compares predicted and measured diametral expansions for fuel pin F2S. This pin is particularly interesting, because the fabricated smear density and heat rate were high, the fuel was axially restrained, and the cladding was 30 mils thick. The postirradiation profilometer trace for F2S indicates a greater diametral expansion at the hot end of the pin than at the cold end. Recall that this is opposite to the observations made for F2H and F2Q. It has been suggested¹¹ that the axial restraint at the top of F2S prevented any axial movement of fuel in that portion of the pin, whereas the fuel at the bottom of the pin, being more remote from the restraint, may have been freer to move axially.

8. R. C. Nelson et al., *Performance of Plutonium-Uranium Mixed-Oxide Fuel Pins Irradiated in a Fast Reactor (EBR-II) to 50,000 MWd/Te*, GEAP-13549 (1969).

9. A. Biancheria et al., *Oxide Fuel Element Development Quart. Progr. Rep. Sept. 30, 1969*, WARD-4135-1, p. 12-4.

10. F. J. Homan, *Oak Ridge National Laboratory Solutions to a Modeling Round-Robin Exercise*, ORNL-TM-3360 (August 1971).

11. W. E. Baily and E. L. Zebroski, *Sodium-Cooled Reactors, Fast Ceramic Reactor Development Program, Thirty-Second Quarterly Report, August-October 1969*, GEAP-10028-32, p. 12-4.

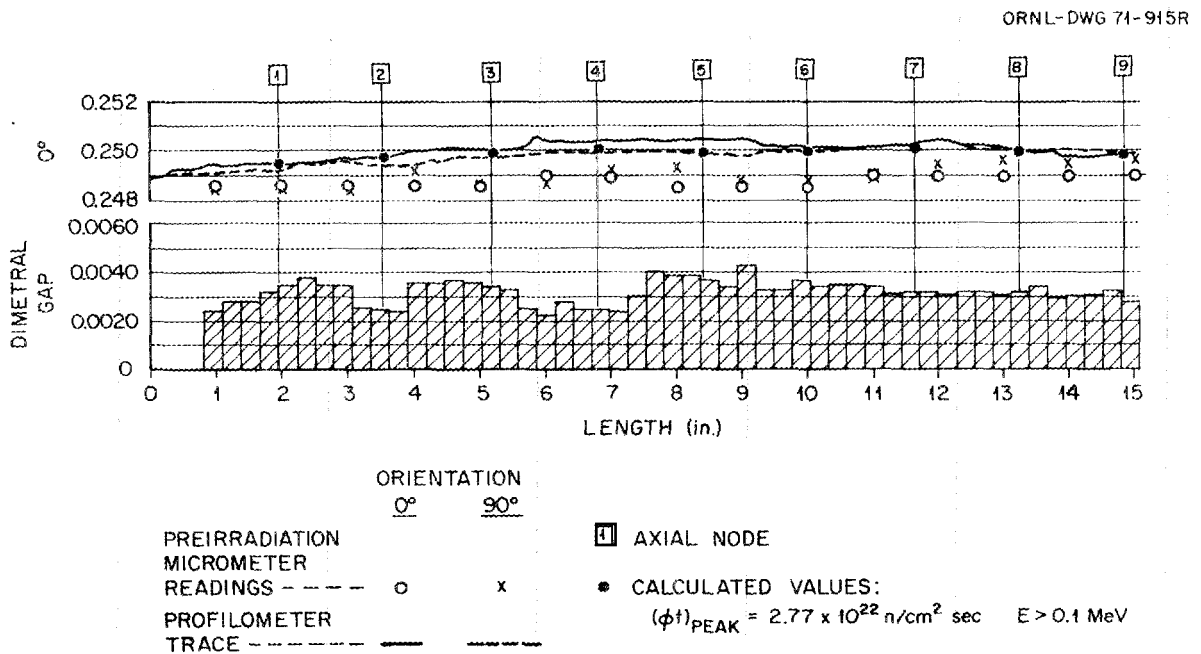


Fig. 6.2. Comparison of predicted and measured diametral expansions for pin F2Z.

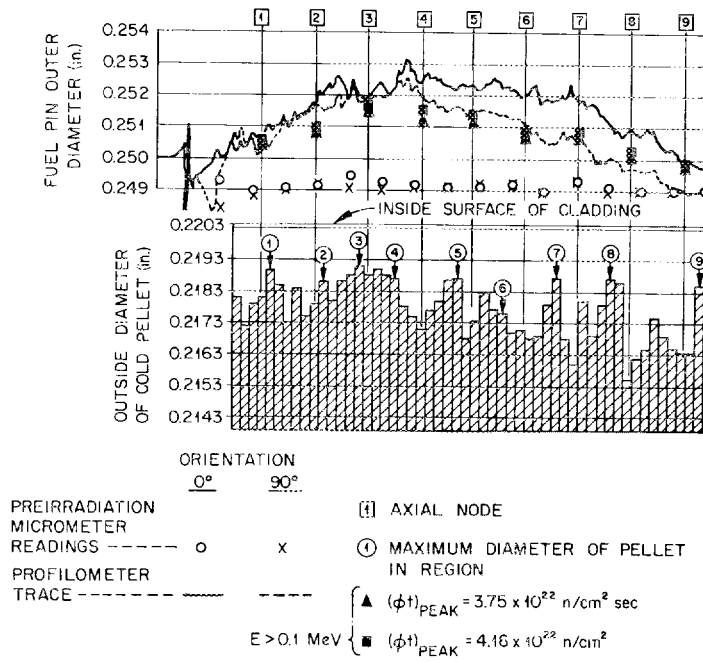


Fig. 6.3. Comparison of predicted and measured diametral expansions for pin F2H.

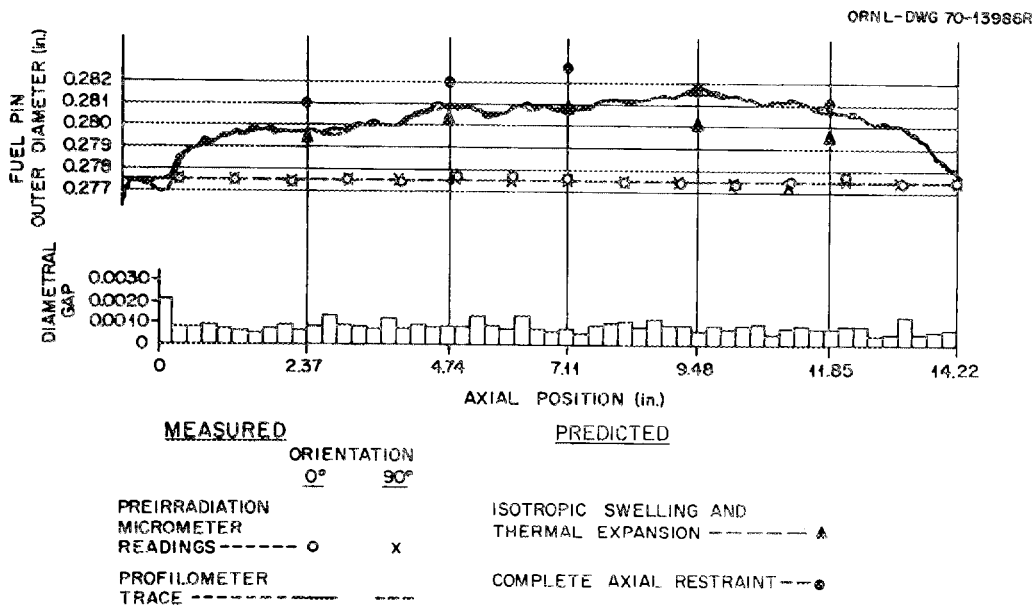


Fig. 6.4. Comparison of predicted and measured diametral expansions for pin F2S as a function of axial position.

Our analysis supports this hypothesis. Two sets of assumptions were made in calculating the predictions plotted in Fig. 6.4. First, we assumed that thermal expansion and swelling of the fuel occurred isotropically; then we assumed complete axial restraint in all regions of the pin. Good agreement between prediction and measurement was achieved at the bottom of the pin, using the isotropic assumption, and at the top of the pin, using the axial restraint assumption.

All comparisons between predicted and measured fuel pin diametral expansion are summarized graphically in Fig. 6.5. Each point of the plot represents one axial position for the pin indicated. The measured values are the average of the 0 and 90° profilometer traces. The predicted values are those plotted on the previous figures, with the exception of F2S. The predicted values for this pin were based on the isotropic assumption at the bottom of the pin and the axial restraint assumption at the top of the pin. With the exception of pin F2H, where the actual operating conditions were uncertain, agreement is excellent. Even in this case the agreement was within 30%. Exact agreement for any pin must be considered fortuitous, since the cladding density changes generally accounted for at least half the predicted diametral expansions, and the data from

which the swelling correlations were derived have a wide scatter band.

6.1.2.2 Fuel Radial Porosity Distribution

FMODEL utilizes a continuous, time-dependent fuel restructuring model adapted¹² from Nichols' equation¹³ for pore motion by a vaporization-condensation mechanism. One measure of the validity of such a model is the comparison of predicted and measured void diameters and diameters of the columnar and equiaxed-grain regions. However, a difficulty with such comparisons is that axial movement of fuel will influence the measured diameters and thus distort the comparison. In addition, columnar and equiaxed grains are not exact indicators of the porosity present in a given fuel region. Therefore, actual comparison of predicted and measured radial porosity distributions in the fuel provides a much sounder basis for judging the usefulness of this model. Unfortunately, few systematic measurements of radial porosity distributions of pins irradiated under fast flux conditions are reported in the literature. Lackey and Kegley¹⁴ measured the radial porosity distribution for a Sphere-Pac fuel pin operated at 13.6 kW/ft to about 0.7% FIMA in the Engineering Test Reactor. A postirradiation metallographic cross section of this pin is shown in the center portion of Fig. 6.6, and their porosity distribution data are shown in the upper portion of the figure. The solid curve shown on the upper portion of the figure is the porosity distribution predicted by FMODEL. The agreement between prediction and experiment here is excellent, except that FMODEL overpredicts the size of the central void at this axial location by about 10%.

6.1.2.3 Actinide Redistribution

The model to describe actinide redistribution is interrelated with the porosity redistribution model. We consider an axial segment of the fuel pin of unit length. After calculation of the radial temperature profile, it and the overall oxygen-to-metal ratio of the fuel are used to calculate the oxygen-to-metal distribution

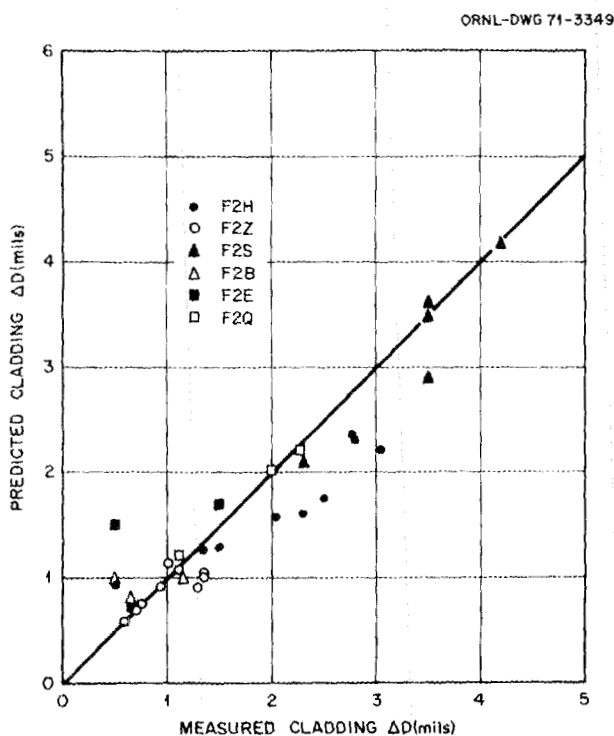


Fig. 6.5. Summary of comparison between predicted and measured cladding diametral expansions.

12. F. J. Homan, "Development of a Fuel-Restructuring Model," *LMFBR Fuel Cycle Studies Progress Report for December 1970, No. 22*, ORNL-TM-3281, pp. 56-62.

13. F. A. Nichols, "Theory of Columnar Grain Growth and Central Void Formation in Oxide Fuel Rods," *J. Nucl. Mater.* **22**, 214 (1967).

14. W. J. Lackey and T. M. Kegley, Jr., "Microscopy of (U,Pu)O₂ Fuels," *LMFBR Fuel Cycle Studies Progress Report for October 1970, No. 20*, ORNL-TM-3217, pp. 79-82.

according to a previously proposed irreversible thermodynamic approach.¹⁵ Next, the porosity of each radial increment at the end of a short time period is determined from knowledge of the initial porosity and calculation of the movement of pores, or equivalently the movement of material, into and out of each radial

increment. Similarly, since the initial $Pu/(U + Pu)$ ratio for each radial increment and the amount of fuel transported into and out of each increment are known, the $Pu/(U + Pu)$ ratio of each increment at the end of the time period can be calculated if the composition of the transported vaporous material is known. This composition was calculated¹⁶ by equilibrium thermodynamics as a function of the temperature, oxygen-to-metal ratio, and $Pu/(U + Pu)$ ratio of the solid fuel. Repeating the calculations for a series of time periods spanning the irradiation time can give the porosity, actinide, and oxygen radial profiles at any desired time.

Predicted and measured actinide redistributions for the fuel pin discussed previously are compared in the bottom portion of Fig. 6.6. The agreement is very good, supporting the validity of the models used to make this calculation.

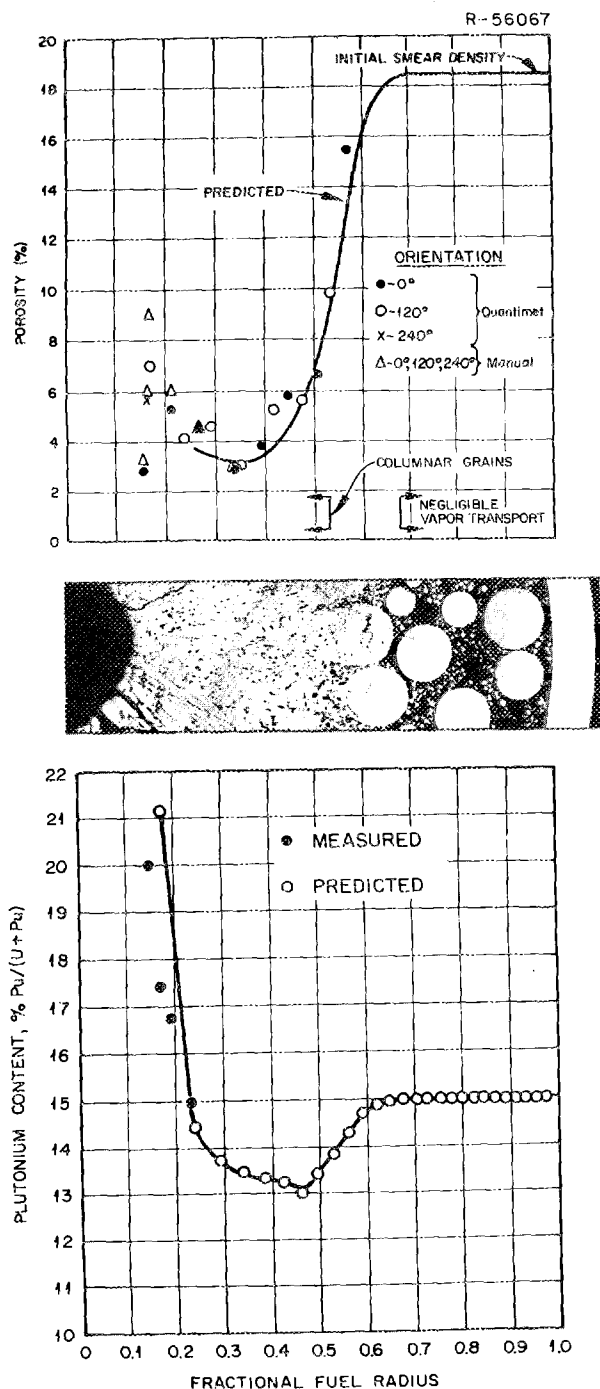


Fig. 6.6. Comparison of measured and predicted porosity and $Pu/(U + Pu)$ profiles.

6.1.2.4 Diameters of Central Void, Columnar, and Equiaxed-Grain Regions

As mentioned earlier, another measure of the validity of any fuel restructuring model is the comparison between predicted and measured void diameters and diameters of the columnar and equiaxed-grain regions. Although this comparison is not as useful as one between predicted and measured radial porosity distributions, considerably more data are available. Predictions with measurements reported⁸ for General Electric F2 series irradiations are summarized in Fig. 6.7. The beginning-of-life heat rates for the pins considered ranged from 9.7 to 17.4 kW/ft, and the fabricated fuel densities ranged from 83.8 to 98.2% of theoretical. It should be emphasized that FMODEL does not predict columnar and equiaxed regions as such. Rather, it predicts porosity distributions. The columnar region has been arbitrarily assigned as any portion of the fuel with less than 2% porosity. Similarly, the equiaxed region has been arbitrarily assigned as the region between the columnar region and the region of as-fabricated density.

The results presented in Fig. 6.7 indicate that FMODEL somewhat overpredicts fuel restructuring. This conclusion is reached through the observation that most of the plotted points lie above the diagonal line, and it is in agreement with the discussion and results

15. W. E. Baily and E. L. Zebroski, *Sodium-Cooled Reactors, Fast Ceramic Reactor Development Program, Thirty-Seventh Quarterly Report, November 1970–January 1971*, GEAP-10028-37, pp. 38–40.

16. W. J. Lackey, F. J. Homan, and A. R. Olsen, "Porosity and Actinide Redistribution During Irradiation of $(U,Pu)O_2$," accepted for publication in *Nuclear Technology*. Also available as ORNL-TM-3762 (August 1972).

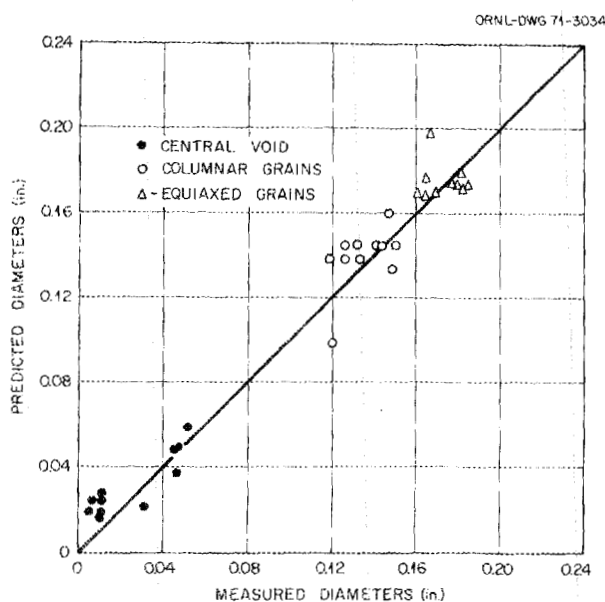


Fig. 6.7. Summary of comparisons between predicted diameters for central void, columnar, and equiaxed-grain regions.

presented in the section on radial porosity distributions. Recall that in the upper portion of Fig. 6.6 the predicted central void was some 10% larger than the experimentally measured void.

We feel that the present model is a significantly better approximation of fuel restructuring than the three-zone empirical model we have used in the past.¹⁷ The ability to predict fuel restructuring on a time-dependent basis is particularly necessary when related to the need to determine fuel-cladding mechanical interactions due to differential thermal expansion during start-up. Using the earlier three-zone model we would assume that restructuring occurred "instantaneously" and would thereby underestimate the thermal expansion of the fuel and plastic deformation of the cladding.

6.1.2.5 Fuel Center-Line Temperatures

Irradiation experiments in which fuel center-line temperatures are measured have not yet been conducted with (U,Pu)O₂ fuel pins in the limited instrumented facilities available in the EBR-II. Therefore, we have used thermal reactor data to test the heat generation and transfer portion of the FMODEL code. Fitts¹⁸ recently completed irradiation in the ORR of an instrumented capsule that contained 82%-smear-density (U,Pu)O₂ Sphere-Pac and pellet fuel pins in tandem. Variable heat rates were achieved by moving the capsule to different flux positions within the ORR poolside facility. Fuel center-line temperatures, clad-

ding surface temperatures, and fuel pin heat generation rates were continuously measured and recorded during the 109 days in-reactor.

Data points representing the entire range of heat rates from 0 to 16 kW/ft were selected randomly for each pin. Using the measured cladding surface temperatures and a radial power distribution predicted by the ANISN neutron transport code,¹⁹ we calculated fuel center-line temperatures with FMODEL for both the Sphere-Pac and pellet pins. Calculated and measured fuel center-line temperatures are compared in Fig. 6.8.

Examination of Fig. 6.8 reveals that, in general, good agreement between predicted and measured fuel center-line temperatures was achieved for the Sphere-Pac fuel. However, several measured data points between 14 and 16 kW/ft appear to be low on the temperature scale. The agreement between predicted and measured pellet center-line temperatures above 9 kW/ft is poor. Because of this poor agreement, and because Fitts²⁰ suspected that one or more of the four calorimeter thermocouple pairs used to measure the heat generation rate may have been giving erroneous readings and thereby affecting the average heat generation rates plotted, a rigorous statistical analysis was performed on the SG-3 data to see if any of the data points can be justifiably discarded. The techniques and results of the statistical analysis have been reported in several sources.²¹⁻²⁵

17. C. M. Cox and F. J. Homan, "Performance Analysis of a Mixed-Oxide LMFBR Fuel Pin," *Nucl. Appl. Technol.* **9**, 317-25 (1970).

18. R. B. Fitts, V. A. DeCarlo, E. L. Long, Jr., and A. R. Olsen, "Thermal Performance and Restructuring of Pellet and Sphere-Pac Fuels," *Trans. Amer. Nucl. Soc.* **13**, 549-51 (1970).

19. W. W. Engle, Jr., *A Users Manual for ANISN, a One-Dimensional Discrete Ordinates Transport Code with Anisotropic Scattering*, K-1693 (March 30, 1967).

20. R. B. Fitts, "ORR Instrumented Tests," *LMFBR Fuel Cycle Studies Progress Report for February 1971, No. 24*, ORNL-TM-3345, p. 52.

21. R. B. Fitts and F. L. Miller, "ORR Instrumented Tests," *LMFBR Fuel Cycle Studies Progress Report for August 1971, No. 30*, ORNL-TM-3571, pp. 31-34.

22. R. B. Fitts and F. L. Miller, "ORR Instrumented Tests," *LMFBR Fuel Cycle Studies Progress Report for July 1971, No. 29*, ORNL-TM-3534, pp. 50-51.

23. R. B. Fitts and F. L. Miller, "ORR Instrumented Tests," *LMFBR Fuel Cycle Studies Progress Report for September 1971, No. 31*, ORNL-TM-3614, pp. 32-38.

24. R. B. Fitts and F. L. Miller, "Analysis and Performance of Instrumented Fuel Pins," *Trans. Amer. Nucl. Soc.* **15**(1), 180 (1972).

25. R. B. Fitts and F. L. Miller, "A Comparison of Sphere-Pac and Pellet (Pu,U)O₂ Fuel Pins in Low-Burnup Instrumented Irradiation Tests," submitted for publication. See also Sect. 5.2 of this report.

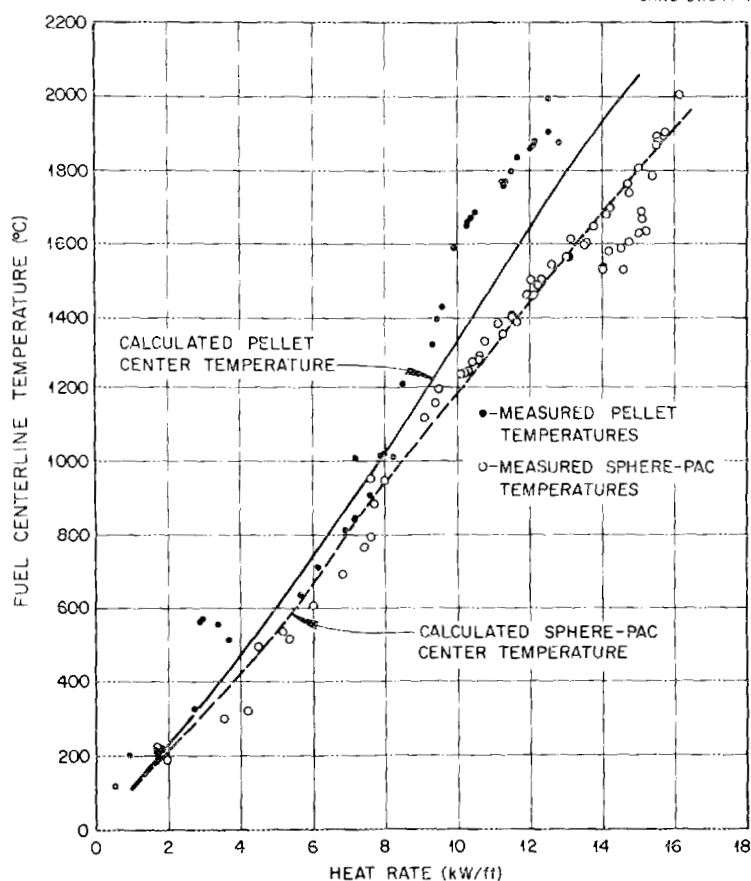


Fig. 6.8 Comparison between predicted and measured fuel center-line temperature variation with heat rate for pellet and Sphere-Pac pins in capsule SG-3.

In the SG-3 experiment, thermocouple readings were automatically recorded for 3 min every 4 hr and whenever a change in power was made. This procedure yielded 44,500 data sets or over one million recorded thermocouple readings. The temperature vs heat rate plots shown in Fig. 6.8 were generated from randomly selected sets of data. The statistical analysis mentioned earlier revealed that much of the data taken during start-ups, shutdowns, power changes, and periods when the SG-3 experiment was being markedly influenced by adjacent experiments did not follow the same trends of center temperature vs heat rate that were observed during extended periods of operation at constant heat rate. When these data are eliminated from consideration, the center temperature vs heat rate relationships for the pellet and Sphere-Pac pins from the SG-3 capsule are as shown in Fig. 5.28. Notice the excellent agreement between the FMODEL predictions (solid lines in Fig. 6.8) and the statistically verified center temperature vs heat rate curves shown in Fig. 5.28. It

should be emphasized that the analysis shown in Fig. 6.8 was done in March 1971, and the statistical analysis culminating in Fig. 5.28 was not completed until February 1972. This demonstrates graphically one of many instances where use of FMODEL rendered great assistance in the interpretation of the data from an irradiation experiment.

6.1.3 Discussion of Individual Models

The individual models contained in the FMODEL code are complex and have been well documented. Therefore only brief descriptions will be provided here, with references to more detailed accounts.

6.1.3.1 Porosity, Actinide, and Oxygen Redistribution

Thermal-gradient-induced redistribution of porosity and fuel components during irradiation of $(U,Pu)O_2$ will sufficiently alter the radial heat-generation pro-

file,²⁶ fuel conductivity,²⁷⁻²⁹ melting point,^{30,31} oxygen activity,^{32,33} and mechanical properties to significantly influence fuel pin performance. Accordingly, we have measured radial porosity and actinide profiles of irradiated fuel pins. Further, analytical models, which should prove useful in design and analysis of LMFBR fuels, were developed for predicting radial profiles of porosity, Pu:(U + Pu), and oxygen. These models have been incorporated into FMODEL, permitting determination of the consequences of fuel component redistribution on the thermal and mechanical performance of (U,Pu)O₂ fuel pins.

The interrelated porosity and actinide redistribution models are kinetic and based on the evaporation-condensation mechanism. An axial segment of the fuel pin of unit length is divided into 30 radial increments. After calculation of the radial temperature profile, it and the overall oxygen-to-metal ratio of the fuel are used to calculate the oxygen-to-metal distribution according to a previously proposed irreversible thermodynamic approach.³⁴ Next, the porosity of each of the radial increments at the end of a short time period is determined from knowledge of the initial porosity and calculation³⁵ of the movement of pores (or equivalently material) into and out of each radial increment. Similarly, since the initial Pu:(U + Pu) ratio for each radial increment and the amount of fuel transported

into and out of each increment are known or calculated, the Pu:(U + Pu) ratio of each increment at the end of the time period can be calculated if the composition of the transported vapor is known. This composition was calculated³⁵ by equilibrium thermodynamics as a function of the temperature, oxygen-to-metal ratio, and Pu:(U + Pu) ratio of the solid fuel. Repeating the calculations for a series of time periods spanning the irradiation time can give the porosity, actinide, and oxygen radial profiles at any desired time.

Experimentally measured porosity and Pu:(U + Pu) radial profiles for a U_{0.85}Pu_{0.15}O_{2.00} fuel pin clad with 1/4-in.-OD stainless steel are shown to compare favorably with predicted profiles in Fig. 6.6. This Sphere-Pac fuel pin (43-112-3) was irradiated in the ETR at a linear heat rate of 13.6 kW/ft to a burnup of 0.7% FIMA. The columnar grain region is considerably more porous than previously generally believed. We have observed the same to be true for pins irradiated in a fast-neutron flux. In the present case, the calculated fuel center temperature was 9.6% (200°C) higher when based on the observed porosity distribution rather than the previously generally assumed three-zone porosity distribution model. A report describing this work in detail has been issued.³⁵

6.1.3.2 (U,Pu)O₂ Grain Growth

Because of the influence that grain size is expected to have on release of fission gas, fuel swelling, and Nabarro-Herring creep of (U,Pu)O₂, we investigated the kinetics of in-reactor and out-of-reactor grain growth. The size of the equiaxed grains was determined as a function of radial position for three Sphere-Pac U_{0.85}Pu_{0.15}O_{2.00} fuel pins after irradiation in the ETR. The initial grain size of the fuel was 1.2 μm. Data for two low-burnup pins were combined and analyzed as shown in Fig. 6.9. The least-squares equations given in the figure relate the observed grain size in micrometers (D) to the initial grain size (D_0), the irradiation time in hours (t), and the irradiation temperature in degrees Kelvin (T). In the higher temperature region, solid fission products or gas bubbles retard the rate of grain growth. The in-reactor activation energies are smaller than expected from out-of-reactor grain growth of UO₂ and ThO₂. To determine if the lower temperature dependence was typical of the mixed oxide or was an irradiation effect, out-of-reactor grain growth kinetics of (U,Pu)O₂ were determined. The out-of-reactor data are also of value for estimating the thermal treatment necessary to fabricate fuel of a specified grain size should it be required.

26. W. T. Sha, P. R. Huebotter, and R. K. Lo, *Trans. Amer. Nucl. Soc.* **14**, 183-84 (1971).

27. R. L. Gibby, *J. Nucl. Mater.* **38**, 163-77 (1971).

28. R. L. Gibby, *The Effect of Oxygen Stoichiometry on the Thermal Diffusivity and Conductivity of U_{0.75}Pu_{0.25}O_{2-x}*, BNWL-727 (January 1969).

29. General Electric Breeder Reactor Development Operation, *Sodium-Cooled Reactors, Fast Ceramic Reactor Development Program*, GEAP-10028-35 (September 1970), pp. 44-49.

30. W. L. Lyon and W. E. Bailly, *J. Nucl. Mater.* **22**, 332-39 (1967).

31. E. A. Aitken and S. K. Evans, *A Thermodynamic Data Program Involving Plutonia and Urania at High Temperatures*, *Quart. Rep. No. 4*, GEAP-5672 (1968).

32. J. A. Christensen, "Transport Processes in Oxide Nuclear Fuels," pp. 109-25 in *Ceramic Nuclear Fuels International Symposium, May 3-8, 1969, Washington, D.C.*, American Nuclear Society, Hinsdale, Ill., 1969; also BNWL-1202.

33. E. A. Aitken and S. K. Evans, "Thermodynamic Behavior of Plutonium Oxide Systems in a Temperature Gradient," pp. 772-80 in *Plutonium 1970 and Other Actinides*, *Nucl. Met.* **17** (Part 2), The Metallurgical Society of AIME, New York, 1970.

34. General Electric Breeder Reactor Development Operation, *Sodium-Cooled Reactors, Fast Ceramic Reactor Development Program*, GEAP-10028-37 (March 1971), pp. 38-40.

35. W. J. Lackey, F. J. Homan, and A. R. Olsen, "Porosity and Actinide Redistribution During Irradiation of (U,Pu)O₂," accepted for publication in *Nuclear Technology*; also ORNL-TM-3762 (June 1971).

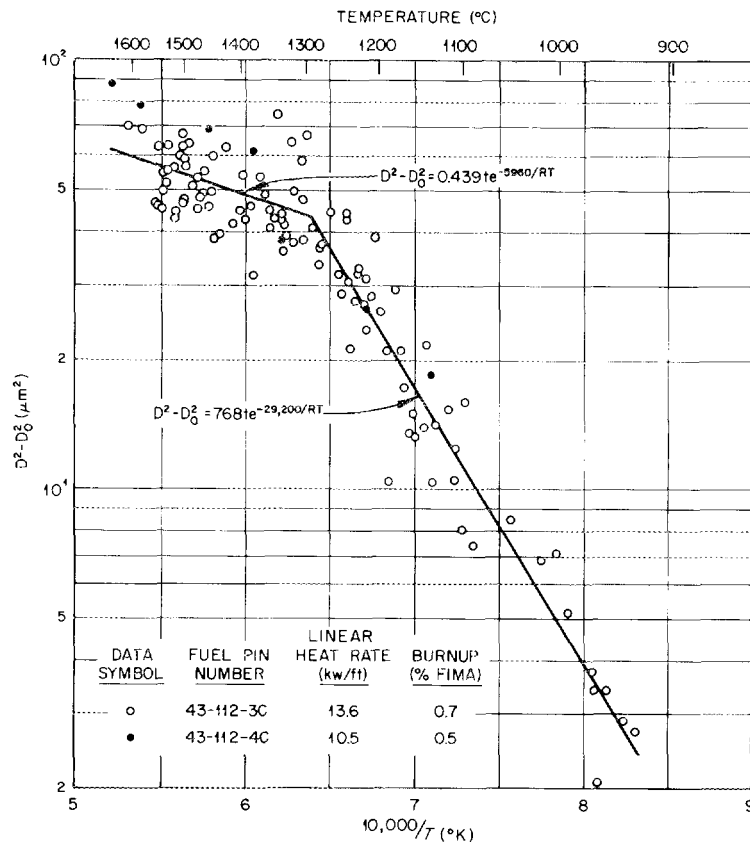


Fig. 6.9. Grain growth of $U_{0.85}Pu_{0.15}O_2$ in-reactor.

The out-of-reactor grain growth study used sol-gel $U_{0.85}Pu_{0.15}O_{2.00}$ microspheres that had been made by the same process used to make the fuel examined in the in-reactor study but from a different batch. The samples were heated isothermally in Ar-4% H_2 at 1200, 1356, and 1550°C for times up to 164 hr. The grain size is plotted as a function of annealing time in Fig. 6.10. Also shown in Fig. 6.10 for comparison are curves for 1356 and 1550°C. They were calculated from the in-reactor grain growth results. At 1356°C the in-reactor and out-of-reactor results are similar; at this temperature irradiation may have increased the rate of grain growth. At 1550°C comparison of the in-reactor and out-of-reactor results shows conclusively that grain growth was retarded by irradiation, perhaps as a result of the presence of fission gas bubbles or solid fission product inclusion.

Least-squares analysis of the out-of-reactor data yielded the following equation:

$$D^2 - D_0^2 = 2.52 \times 10^{21} t \exp(-173,000/RT).$$

The value for the activation energy (173 ± 25 kcal/mole at the 90% confidence level) is comparable to values observed out-of-reactor for UO_2 and ThO_2 but is considerably larger than the values of 29.2 and 5.96 observed in-reactor. This demonstrates that data obtained from isothermal out-of-reactor tests cannot be used to predict in-reactor grain growth of $(U,Pu)O_2$.

6.1.3.3 Cladding Behavior

The models to describe the mechanical behavior of the cladding and its response to the fast neutron environment are included as appendices in the FMODEL report.³⁶ Briefly, the mechanical solution makes use of the finite difference approach and utilizes the assumption of generalized plane strain. Cladding stresses are calculated by assuming values for cladding

36. F. J. Homan, W. J. Lackey, and C. M. Cox, *FMODEL - a FORTRAN IV Computer Code to Predict In-Reactor Behavior of LMFBR Fuel Pins*, ORNL-4825 (January 1973).

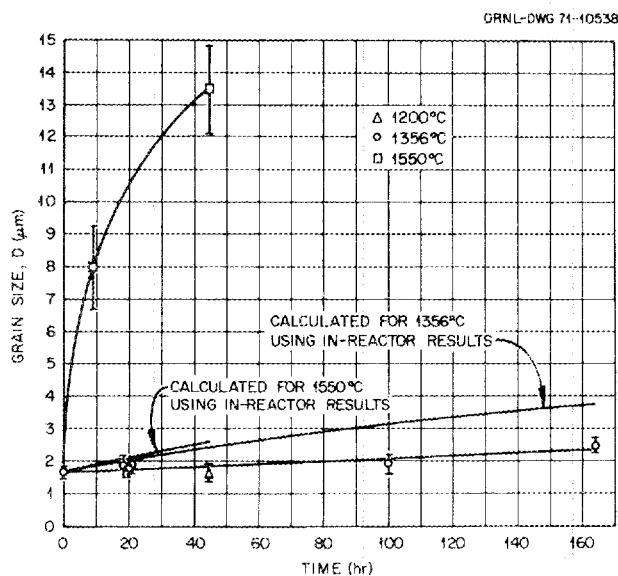


Fig. 6.10. Grain size as a function of time for $U_{0.85}Pu_{0.15}O_2$ isothermally annealed out-of-reactor.

plastic strains and then making new assumptions for the strains based on the stress state. This iterative procedure is continued until convergence on the calculated effective stress is achieved. Plasticity and creep characteristics of the cladding material must be provided by the code user, although equations are built into the code for type 316 stainless steel, both annealed and 20% cold worked. The swelling of the cladding due to fast neutron exposure is treated as an additional component of thermal expansion for stress-strain calculation, and published empirical correlations relating swelling to temperature-fluence combinations are currently used in the code. An iterative method was developed to calculate the mechanical interaction between fuel and cladding due to differential thermal expansion during power changes or due to differential swelling during steady-state operation. This method is outlined in the FMODEL report.³⁶

6.1.3.4 Heat Transfer

The heat transfer model contained in the FMODEL code solves the Fourier heat conduction equation with an internal heat source in cylindrical coordinates. The thermal conductivity in the cladding is temperature dependent and that in the fuel depends upon many variables. Among them are temperature, density, stoichiometry, plutonium content, and the shape and distribution of pores. A description of the method of

solution is given in the PROFIL report.³⁷ Calculating the temperature rise across the fuel-cladding gap presents some special problems, and a recently developed model³⁸ is used to make this calculation. In the gap conductivity model the temperature-dependent thermal conductivity of the gas phase is integrated from cladding inner surface to the fuel outer surface in situations with an open gap. An iterative procedure is used to properly account for thermal expansion, which will change the size of the gap. When the gap is closed, conductance across the points of solid-solid contact is considered as well as conductance across gas pockets that separate the points of contact. Accommodation effects become important here, and also the contact pressure between the fuel and cladding. Thus, the interplay between the different models contained in FMODEL is obvious.

6.1.4 Thermodynamic Considerations in Fuel Behavior

Although we did not have the opportunity to incorporate in FMODEL a large number of the thermodynamic effects, such work was in progress and is reported sequentially as it stood at the terminal date.

The purpose of this work was to provide an understanding of fuel-cladding interaction of $(U,Pu)O_2$ and stainless steel, primarily type 316. This effort was in support of the overall goal of providing safe, reliable, economic fuel elements for LMFBR's, and particularly for sol-gel-derived fuel. In addition, we attempted to indicate those additional data needed to establish confidence in interpolations and extrapolations from experimental data.

Compatibility tests between $(U,Pu)O_{2.0}$ or $(U,Pu)O_{2-x}$ and several stainless steels have shown that no detectable reaction takes place within the times and temperatures of interest in a typical LMFBR. However, when hyperstoichiometric fuel, $(U,Pu)O_{2+x}$, is tested, reactions are seen, and the difference is ascribed to the excess oxygen in the fuel. (See, for example, Lauritzen³⁹ for a review of General Electric work,

37. C. M. Cox and F. J. Homan, *PROFIL - a One-Dimensional FORTRAN IV Program for Computing Steady-State Temperature Distributions in Cylindrical Ceramic Fuels*, ORNL-TM-2443 (March 1969) and Addendum (August 1969).

38. C. M. Cox, F. J. Homan, and R. L. Diamond, "Description of Fuel-to-Cladding Gap Conductance," *Fuels and Materials Development Program Quart. Progr. Rep. Mar. 31, 1972*, ORNL-TM-3793, pp. 25-38.

39. T. Lauritzen, *Compatibility of Urania-Plutonia Fuels with Stainless Steel and Sodium*, GEAP-5633 (June 1968).

which does not differ greatly from that of other workers in this field.) On the other hand, experiments at a number of laboratories have shown that both stoichiometric and hypostoichiometric fuels react with stainless steel cladding when irradiated in the reactor. Three kinds of attack are seen: a uniform attack, an intergranular attack, and transport of cladding elements into the fuel. This lack of ability to extrapolate the out-of-reactor results to the in-reactor results is of concern to the fuel pin designer and indicates that the problem is complicated.

The interaction problem is complicated by the fact that during fissioning, not only does the primary process take place but two other processes directly caused by the fissioning processes also occur. These are the creation of some 26 important additional elements and the release of the oxygen combined with the fissioned element. Much of the oxygen released is taken up by the new elements created. The part that does not combine with the fission products tends to raise the oxidizing potential of the fuel toward the cladding.

A further complicating factor is the temperature gradient within the fuel element. The exact gradient depends on the power at which the pin is being operated as well as the temperature of the coolant. A gradient of $5000^{\circ}\text{C}/\text{cm}$ would not be unusual. The gradient in the temperature leads to a gradient in the oxygen content of the fuel, a condition that is quite different from that tested in out-of-reactor experiments.

We see from the above remarks that the in-reactor experiments are quite different from those out-of-reactor. More detailed investigation reveals a paucity of reliable data on compounds and reactions of interest. Thus, a final complete description of fuel element behavior will be difficult and require a large amount of careful experimentation. Our approach has been to try to understand as completely as possible those data that are available, and to try to point out areas in which additional experimentation is desirable.

6.1.4.1 Description of Intergranular Attack

Toward the end of our program, increasing amounts of experimental data were becoming available from which one could begin to extract rates of intergranular attack. In the time available, we systematized as much of the data as possible. In this section, we show that the logarithm of the attack rate is linear when plotted against $1/T$ ($^{\circ}\text{K}$) within present experimental error. We also note that this relationship did not hold for sol-gel-derived Sphere-Pac fuel – no attack was seen in

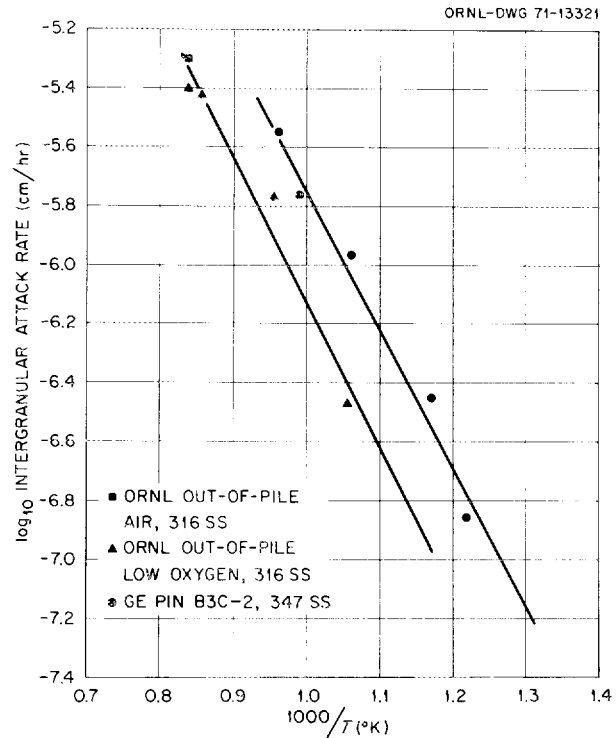


Fig. 6.11. Intergranular attack rates on stainless steels.

the experiments studied, although some attack has been created in later experiments – see Sect. 5.2.

Our initial approach was to seek relationships between rates of attack and the temperature. In the absence of better information, we chose a common rate equation:

$$\text{rate} = A \exp(-E/RT) \quad (1)$$

or

$$\ln(\text{rate}) = \ln A - E/RT, \quad (2)$$

where A is some constant, E is an “activation energy,” R is the gas constant, and T is the Kelvin temperature.

Figure 6.11 shows data plotted in this fashion for two widely differing conditions. One was intergranular attack data from an experiment in which a type 316 stainless steel tube was subjected to a flow of Ar 4% H_2 (4000 ppm H_2) for a period of 500 hr, taken from Fitts et al.⁴⁰ The second condition was taken from the

40. R. B. Fitts, E. L. Long, Jr., and J. M. Leitnaker, “Observations of Fuel-Cladding Chemical Interactions as Applied to GCBR Fuel Rods,” pp. 431–58 in *Proc. Conf. Fast Reactor Fuel Element Technology*, ed. by Ruth Farmakes, American Nuclear Society, Hinsdale, Ill., 1971.

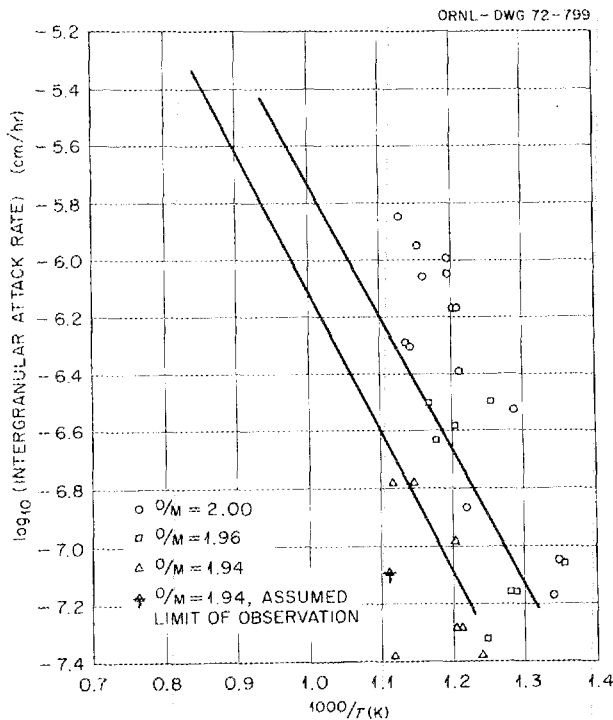


Fig. 6.12. Intergranular attack rates plotted from data contained in ref. 43. Lines shown are from Fig. 6.10.

analysis of Gregorie et al.⁴¹ of a failed fuel element. For both conditions, intergranular attack could be related to both time and temperature with a reasonable degree of confidence. These data were fitted by least squares to Eq. (2), yielding

$$\log_{10}(\text{attack rate}) = \frac{4816}{T} - 1.3129 \quad (3)$$

for the out-of-reactor experiment, and

$$\log_{10}(\text{attack rate}) = \frac{4666}{T} - 1.080 \quad (4)$$

for the failed-pin data. A complete tabulation of the data used is reported elsewhere.⁴² The nearly identical slopes and not dissimilar intercepts of the two equations led us to plot a variety of data in the same fashion.

41. K. E. Gregorie, P. E. Novak, and R. E. Murata, *Failed Fuel Performance in Naturally Convecting Liquid Metal Coolant*, GEAP-13620 (June 1970).

42. J. M. Leijnaker and R. E. Adams, *Fuels and Materials Development Program Quart. Progr. Rep. Dec. 31, 1971*, ORNL-TM-3703, pp. 18-25.

One set of data, plotted in Fig. 6.12, was obtained from depth of penetration measurements on pins irradiated by Battelle Northwest Laboratories.⁴³ Derived calculations from these measurements are shown in Table 6.1. Although Fig. 6.12 shows considerable scatter in the data, two facts stand out. First, there is reasonable agreement between the data plotted and the slopes of the reference lines, superimposed from Fig. 6.11. Second, there is a marked effect of starting oxygen-to-metal ratio on the depth of penetration, the highest O/M corresponding to the highest attack rate.

We also plotted data from sol-gel-derived particulate fuel, Sphere-Pac fuel. Data from these pins were tabulated elsewhere⁴⁰ and are shown in Fig. 6.13. Since no attack was seen in any of the pins, it was necessary to plot a value which represents the lower limit of observation, assuming any attack was present. We have assumed that if the attack were less than 5×10^{-4} cm it would be indistinguishable from fission recoil damage. The lines in the figure are superimposed from Fig. 6.11. Since the starting O/M of the Sphere-Pac fuel was 2.0, the fact that no attack was observed seems remarkable.

It is reasonable to suppose that oxygen, by some unspecified mechanism, is responsible for the attack of the cladding. This is a generally held view, although some alternative explanations have been put forth. (See Sect. 6.1.4.2 for a treatment of one of these.) Oxygen is present in a relatively large amount. Its chemical potential changes during irradiation (see Sect. 6.1.4.3). The similarity of behavior between out-of-reactor tests and in-reactor tests (Fig. 6.11) is too striking to be ignored. And finally, the data in Fig. 6.12, although scattered, seem to establish the postulate beyond more than a very tentative doubt.

The marked lack of reaction of the Sphere-Pac fuel with the cladding seems worthy of further comment. First, it seems clear that both longer irradiation times and higher irradiation temperatures would be desirable to establish exactly what the attack rate is for this fuel. At present, it seems to be true that there is a significant difference between the two kinds of experiments. The reason for the difference is, however, not at all obvious. A number of possible explanations occur to us, but insufficient data are available to evaluate them. However, we list them as follows:

One explanation for the lack of attack might be the lack of high-pressure contact by the Sphere-Pac fuel

43. J. W. Weber and E. D. Jensen, "Effect of O/M on Irradiated Mixed-Oxide Stainless Steel Cladding Compatibility," *Trans. Amer. Nucl. Soc.* 17(1), 175-76 (1971).

Table 6.1. Cladding penetration on BNW thermal irradiations^a

| Temperature ^b (°K) | 1000/T (°K ⁻¹) | Cladding penetration (cm) | Time (hr) | Rate (cm/hr) | log ₁₀ (rate) |
|----------------------------------|-------------------------------|---------------------------------|--------------|-------------------------|--------------------------|
| 827 | 1.209 | 5.08×10^{-4} | 9,800 | 5.18×10^{-8} | -7.286 |
| 830 | 1.204 | 5.08×10^{-4} | 9,800 | 5.19×10^{-8} | -7.286 |
| 827 | 1.209 | 10.16×10^{-4} | 9,800 | 1.036×10^{-7} | -6.985 |
| 900 | 1.112 | $<5 \times 10^{-4}$ | 6,110 | $<8.183 \times 10^{-8}$ | -7.087 |
| 894 | 1.118 | 10.16×10^{-4} | 6,110 | 1.663×10^{-7} | -6.779 |
| 894 | 1.118 | 2.54×10^{-4} | 6,110 | 4.157×10^{-8} | -7.381 |
| 871 | 1.147 | 10.16×10^{-4} | 6,110 | 1.663×10^{-7} | -6.779 |
| 808 | 1.238 | 2.54×10^{-4} | 6,110 | 4.157×10^{-8} | -7.381 |
| 814 | 1.229 | 5.08×10^{-4} | 10,800 | 4.704×10^{-8} | -7.327 |
| 783 | 1.277 | 7.62×10^{-4} | 10,800 | 7.056×10^{-8} | -7.151 |
| 777 | 1.286 | 7.62×10^{-4} | 10,800 | 7.056×10^{-8} | -7.151 |
| 875 | 1.143 | 5.59×10^{-3} | 11,350 | 4.93×10^{-7} | -6.307 |
| 880 | 1.136 | 5.77×10^{-3} | 11,350 | 5.08×10^{-7} | -6.294 |
| 830 | 1.204 | 7.62×10^{-3} | 11,350 | 6.71×10^{-7} | -6.173 |
| 830 | 1.204 | 7.62×10^{-3} | 11,350 | 6.71×10^{-7} | -6.173 |
| 741 | 1.349 | 1.016×10^{-3} | 11,350 | 8.95×10^{-8} | -7.048 |
| 886 | 1.129 | 9.65×10^{-3} | 6,810 | 1.42×10^{-6} | -5.847 |
| 866 | 1.154 | 7.62×10^{-3} | 6,810 | 1.12×10^{-6} | -5.951 |
| 836 | 1.196 | 6.09×10^{-3} | 6,810 | 8.95×10^{-7} | -6.048 |
| 777 | 1.286 | 2.03×10^{-3} | 6,810 | 2.98×10^{-7} | -6.526 |
| 855 | 1.169 | 2.03×10^{-3} | 6,530 | 3.11×10^{-7} | -6.507 |
| 850 | 1.177 | 1.52×10^{-3} | 6,530 | 2.33×10^{-7} | -6.633 |
| 830 | 1.204 | 2.29×10^{-3} | 8,740 | 2.62×10^{-7} | -6.582 |
| 797 | 1.255 | 2.79×10^{-3} | 8,740 | 3.20×10^{-7} | -6.495 |
| 739 | 1.354 | 0.762×10^{-3} | 8,740 | 8.72×10^{-8} | -7.060 |
| 825 | 1.213 | 3.05×10^{-3} | 7,510 | 4.06×10^{-7} | -6.392 |
| 819 | 1.221 | 1.02×10^{-3} | 7,510 | 1.35×10^{-7} | -6.869 |
| 747 | 1.339 | 5.08×10^{-4} | 7,510 | 6.76×10^{-8} | -7.170 |
| 861 | 1.162 | 7.62×10^{-3} | 8,730 | 8.73×10^{-7} | -6.059 |
| 836 | 1.196 | 8.89×10^{-3} | 8,730 | 1.02×10^{-6} | -5.991 |
| 847 | 1.181 | 7.37×10^{-3} | 8,730 | 8.44×10^{-7} | -6.074 |

^aThese data were taken from J. W. Weber and E. D. Jensen, *Trans. Amer. Nucl. Soc.* 17(1), 175-76 (1971).

^bTemperature is a time-averaged value, which may account for scatter in the I.G.A. rate.

compared with the pelletized fuel. Related to this is the stress placed on the cladding by the pelletized fuel, particularly the ratcheting effect postulated on heat-up and cool-down of the reactor. Another possible explanation is that during initial start-up a coating of fuel deposits onto the cladding and effectively acts as a barrier to entrance by the reacting substance. Such a barrier has been seen in some cases but not in others. Its effectiveness, if real, is not known. Still another possibility is formation of a fuel-oxygen-fission product compound on the surface of the Sphere-Pac fuel. Almost nothing is known about the stability of Cs-U,Pu-O compounds, and even less is known about their surface properties.

Further possibilities, as yet essentially unexplored, are fuel impurities and variations in cladding material to

account for the difference in reactivity between Sphere-Pac fuel and more conventional pelletized fuel. Differences in manufacturing methods could account for the former possibility, and chance variation, although unlikely, may account for the latter.

The final possibility that occurs to us is the temperature variation between the two kinds of experiments. After the thermodynamic portion of the work was terminated, Fitts and Miller⁴⁴ analyzed extensively an instrumented comparison between Sphere-Pac and pelletized fuel. This analysis indicated that for the same power output, the fuel close to the cladding was hotter

44. R. B. Fitts and F. L. Miller, "A Comparison of Sphere-Pac and Pellet (U,Pu)O₂ Fuel Pins in Low-Burnup Instrumented Irradiation Tests," submitted for publication in *Nuclear Technology*.

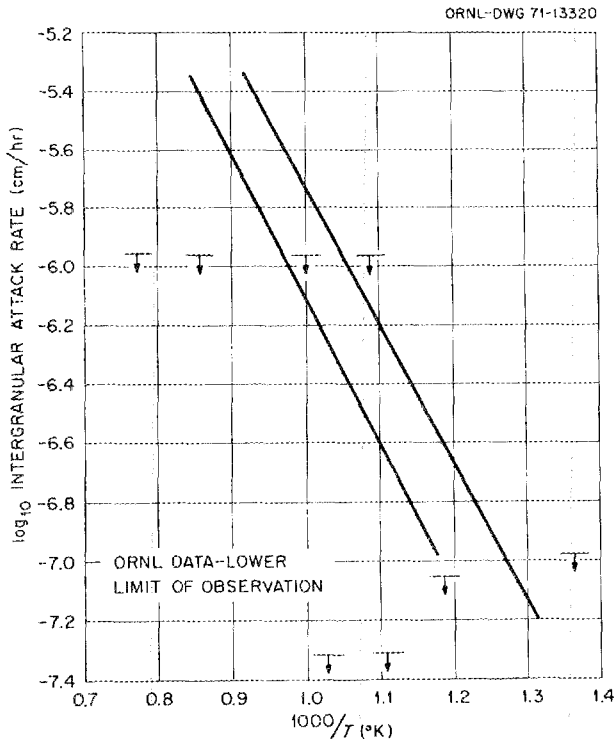


Fig. 6.13. Limit of intergranular attack rate on sol-gel-derived mixed-oxide fuel pins. The lines are taken from Fig. 6.11.

in a Sphere-Pac pin than in a pelletized pin. This temperature difference arises, according to Fitts and Miller, because of the greater gap conductance in the Sphere-Pac pin than in the pelletized pin. As we detail in Sect. 6.1.4.4, the temperature gradient has a strong influence on the oxygen distribution within the pin. Qualitatively, one can see that such behavior would tend to "level" the oxygen content of the fuel, lower the relative difference of the oxygen potential at the fuel surface, and, in view of the marked effect of oxygen potential on fuel-cladding interaction, may reduce the cladding attack by this mechanism.

Insufficient data are available to evaluate the possibilities of reduced fuel-cladding interaction suggested above. Most experiments to date have not been designed to test specific interaction theories, and results are therefore inconclusive. We detail some possibilities in Sect. 6.1.4.4 on further experiments that would relate experimental qualities to reaction rates.

6.1.4.2 Analysis of Reaction Layers and Cladding Transport

Because of our interest in the Gas-Cooled Breeder Reactor (GCBR), numerous irradiation experiments

have been performed investigating the operating behavior of mixed-oxide fuel clad with both types 316 and 304 stainless steel and with Hastelloy X. The higher operating temperatures of a GCBR allow more rapid reactions at the fuel-cladding interface, and the analysis of them is instructive, relative to longer times in the LMFBR at lower temperatures.

An analysis of the interactions observed at ORNL has been performed by Fitts et al.⁴⁰ with the following conclusions: Three types of reaction are seen: (1) a layer of reaction product on the cladding inside surface; (2) grain boundary attack in the cladding (see Sect. 6.1.4.1 for a more extensive analysis); and (3) "rivers" of metallic material along cracks in the fuel. The analysis suggested all forms of the attack, including transport of cladding material, were related to oxide mechanisms. The suggestion that iodine transports stainless steel components⁴⁵ was shown on thermodynamic grounds to be untenable. Both liquid-phase transport and mechanical transport were stated to be tenable mechanisms on the basis of present understanding. Finally, it was stated that although type 316 stainless steel will be satisfactory for early GCBR application, either a more detailed understanding of the reaction involved is needed or alloys that are more oxidation resistant must be proven as cladding materials.

The problem of the GCBR seems not unrelated to the Sphere-Pac fuel success noted in Sect. 6.1.4.1. The reduced oxidizing potential of the Sphere-Pac fuel would logically make it a prime candidate for use in the higher temperature environment proposed for the GCBR. If the early successes already seen were borne out by further experimentation, Sphere-Pac fuel should be considered a major contender for a backup fuel for the LMFBR.

6.1.4.3 Analysis of Oxygen Buildup in Mixed-Oxide Fuel

The ability to predict and understand the equilibrium interactions of a reactor fuel requires, among other things, a knowledge of the effects of nuclear burnup on the fuel. The fissioning of plutonium in (U,Pu)O₂ fuels not only forms fission products, but it also releases the oxygen atoms that had been bound to the plutonium. The final state of such a released atom depends on its relative affinity for the fission products formed and for the remaining fuel. We have used available thermodynamic and phase data to calculate the equilibrium

45. C. E. Johnson and C. E. Crouthamel, *J. Nucl. Mater.* **34**, 101 (1970).

Table 6.2. Uranium-to-plutonium ratio in a (U,Pu)O_{2+x} fast-reactor fuel as a function of time at full power (185 MW/metric ton)^a

| Irradiation time (months) | Burnup (%) | U/Pu ratio |
|---------------------------|------------|------------|
| 0 | 0 | 4.0 |
| 6 | 3.67 | 3.907 |
| 24 | 14.67 | 3.604 |

^aThe plutonium formed from the uranium is assumed to be equal to 0.9 times the plutonium fissioned.

chemical state of the oxide fuel in a fast-reactor environment. As we will show, a major uncertainty in predicting the oxygen potential of the fuel relates to the affinity of rare earths for oxygen in the fuel-fission product environment.

Tables 6.2, 6.3, and 6.4 contain the relative concentrations of atoms in U_{0.8}Pu_{0.2}O₂ and the distribution of bound oxygen atoms after zero time, six months, and two years at full power of 185 MW/metric ton. In calculating the distribution of bound oxygen, we did not consider ternary oxides such as Ba₂ZrO₄ and SrMoO₃, but such oxides probably will not affect the final ratio of oxygen to heavy metal, since most of them are just additions of the binary oxides we considered. For example, Ba₂ZrO₄ can be thought of as 2BaO·ZrO₂.

In using these tables it is important to realize that the fuel contains ²³⁸U rather than ²³⁵U, which has been used for almost all the irradiation experiments. It is also important to recognize that the amount of oxygen used by oxide-forming fission products is significantly greater in the case of ²³⁵U fuel because of the important difference in fission product distribution. Thus the real case would seem to be much worse, with respect to fuel-cladding interaction, than the cases studied experimentally up to the present time.

In Table 6.4 we detail some simple calculations on the amount of "excess" oxygen liberated over and above that used by the fission products. Several things become clear from the table. First, the amount of oxygen used by elements labeled rare earths greatly exceeds that used by all other elements. For that reason, any uncertainties in our understanding of the behavior of these elements is magnified by the very fact of their abundance. Second, we see that two assumptions are listed for the oxygen affinity of the rare earths: a sesquioxide and a dioxide. This diversity requires some explanation.

Table 6.3. Proportions of fission products produced in a (U,Pu)O₂ fast-reactor fuel as a function of time at full power (185 MW/metric ton)^a

| Element | Atoms created per 1000 fissions in | | Chemical form of fission product |
|--------------------|------------------------------------|---------|---|
| | 6 months | 2 years | |
| Kr | 24.5 | 25.2 | Kr |
| Rb | 13.62 | 12.95 | Rb ₂ O |
| Sr | 43.60 | 38.85 | SrO |
| Y | 16.35 | 17.04 | Y ₂ O ₃ or YO ₂ ^b |
| Zr | 201.63 | 187.46 | ZrO ₂ |
| Nb | 10.90 | 4.09 | NbO ₂ |
| Mo | 209.81 | 233.13 | Uncertain |
| Te | 57.22 | 55.21 | Te |
| Ru | 234.33 | 212.00 | Ru |
| Rh | 38.15 | 49.76 | Rh |
| Pd | 103.54 | 120.65 | Pd |
| Ag | 27.25 | 25.90 | Ag |
| Cd | 8.17 | 10.22 | Cd |
| Te | 32.70 | 30.67 | Te |
| I | 27.25 | 25.22 | CsI |
| Xe | 223.43 | 224.95 | Xe |
| Cs | 196.19 | 196.32 | CsI, Cs ₂ O |
| Ba | 68.12 | 68.17 | BaO |
| La | 57.22 | 56.88 | La ₂ O ₃ or LaO ₂ ^b |
| Ce | 141.69 | 117.25 | Ce ₂ O ₃ or CeO ₂ ^b |
| Pr | 46.32 | 52.49 | Pr ₂ O ₃ or PrO ₂ ^b |
| Nd | 138.96 | 153.37 | Nd ₂ O ₃ or NdO ₂ ^b |
| Pm | 19.07 | 15.00 | Pm ₂ O ₃ or PmO ₂ ^b |
| Sm | 29.97 | 36.13 | Sm ₂ O ₃ or SmO ₂ ^b |
| Eu | 8.17 | 6.82 | Eu ₂ O ₃ or EuO ₂ ^b |
| Gd | 8.17 | 8.86 | Gd ₂ O ₃ or GdO ₂ ^b |
| Total ^c | 1986.3 | 1984.3 | |

^aCalculated with the use of a computer program from Hanford converted by E. D. Arnold of the Chemical Technology Division.

^bIn solid solution with the fuel oxide.

^cThe total is not 2000 because several minor elements were not included. These should not affect the analysis.

The highest valence for most of the rare earths, except cerium and praseodymium, is generally taken to be 3+. Substantial evidence exists, however, that the rare-earth oxides dissolve in UO₂ "effectively" as the dioxide, at least at moderately high oxygen potentials. (What actually happens is probably that part of the U(IV) is oxidized to U(V), with the rare-earth ion remaining as R.E.(III). Such behavior has interesting implications concerning the stability of the fluorite lattice.) The simplest direct evidence for this behavior is an experiment in which Eu₂O₃ and UO_{2.00}, both of which had been equilibrated in 10 parts CO and 1 part CO₂, were mixed, pressed into a pellet, and further heated in the same gas mixture at 1000°C. A weight

Table 6.4. Calculations on oxygen use by fission products

| | Quantity (atoms per 1000 fissions) | |
|---|---------------------------------------|---------|
| | 6 months | 2 years |
| Total rare-earth elements created (including Y, La, and Ce-Gd) | 465.92 | 463.54 |
| Atoms of O used if bound as | | |
| R.E.O ₂ | 931.84 | 927.08 |
| R.E.O _{1.5} | 698.88 | 695.31 |
| Atoms of O used by dioxides (excluding rare earths and Mo) | 425.06 | 383.10 |
| Atoms of O used by monoxides | 111.72 | 107.02 |
| Atoms of O left to oxidize Mo and cladding if rare earths are bound as | | |
| R.E.O ₂ | 531.38 | 582.80 |
| R.E.O _{1.5} | 764.34 | 814.57 |
| Atoms of Mo created | 209.81 | 233.13 |
| Excess atoms of O if all Mo were oxidized and rare earths were bound as | | |
| R.E.O ₂ | 111.76 | 116.54 |
| R.E.O _{1.5} | 344.72 | 348.31 |

gain was observed, which corresponded to oxidizing the Eu₂O₃ to EuO_{1.88}. Thus at least some oxidation, outside any reasonable experimental error, took place. Further, more subjective but nonetheless conclusive evidence can be obtained from a consideration of the lattice parameter variation of rare earths in UO₂ as a function of composition.

Lattice parameters of solid solutions of rare-earth sesquioxides in fluorite lattices can be synthesized by means of a general relationship described by Brauer and Gradinger:⁴⁶

$$a_f = 0.3943a_c + 1.2285 (\text{\AA}),$$

where a_c is the lattice constant of a body-centered cubic rare-earth sesquioxide and a_f is the lattice constant of an imaginary rare-earth fluorite phase obtained by extrapolating data for the lattice constants of solutions of rare-earth oxides in fluorite oxides to pure, imaginary rare-earth sesquioxide in the fluorite lattice. By using this equation we are able to calculate the lattice parameters of all solid solutions of rare-earth oxides with UO₂ by simple interpolation, using Vegard's law, between the end members. (The lattice parameter of UO_{2.00} may be taken as 5.4706 ± 0.0002 \AA.) We tabulate the lattice constants of these imaginary, fluorite-structured rare-earth oxides in Table 6.5.

Figure 6.14 graphically illustrates for the case of Y₂O₃-UO₂ a wide range of lattice parameter data as a

Table 6.5. Extrapolated room-temperature lattice parameters for R.E._{1-x}U_xO_{1.5+0.5x} and R.E._{1-x}U_xO_{2.0} as $x \rightarrow 0$... from solid-solution data

| Rare earth | Lattice parameter (\AA) | |
|------------|--|--|
| | R.E. _{1-x} U _x O _{1.5+0.5x} | R.E. _{1-x} U _x O _{2.0} as $x \rightarrow 0$ |
| La | 5.724 | 5.535 |
| Ce | 5.686 | 5.403 |
| Pr | 5.647 | 5.364 |
| Nd | 5.593 | 5.404 |
| Pm | 5.580 | 5.391 |
| Sm | 5.554 | 5.365 |
| Eu | 5.514 | 5.325 |
| Gd | 5.494 | 5.305 |
| Tb | 5.452 | 5.169 |
| Dy | 5.436 | 5.247 |
| Ho | 5.401 | 5.212 |
| Y | 5.399 | 5.210 |
| Er | 5.381 | 5.192 |
| Tm | 5.361 | 5.172 |
| Yb | 5.341 | 5.152 |
| Lu | 5.330 | 5.141 |

function of composition. Only in the case of Aitken and Joseph,⁴⁷ where oxygen potentials were controlled, was a simple Vegard relationship obtained.

We have equilibrated samples of coprecipitated UO₂-Eu₂O₃ in 1 part CO and 1 part CO₂ and plot the room-temperature lattice parameter data in Fig. 6.15.

46. G. Brauer and H. Gradinger, "Binary Solid Solutions of Rare-Earth Oxides," *Z. Anorg. Allgem. Chem.* 276, 14 (1954).

47. E. A. Aitken and R. A. Joseph, "Thermodynamic Study of Solid Solutions of Uranium Oxide-Yttrium Oxide," *J. Phys. Chem.* 70, 1090-97 (1966).

Also shown is the Vegard line between UO_2 and the imaginary fluorite-lattice Eu_2O_3 . The decrease in lattice parameter of the observed solid solution over that

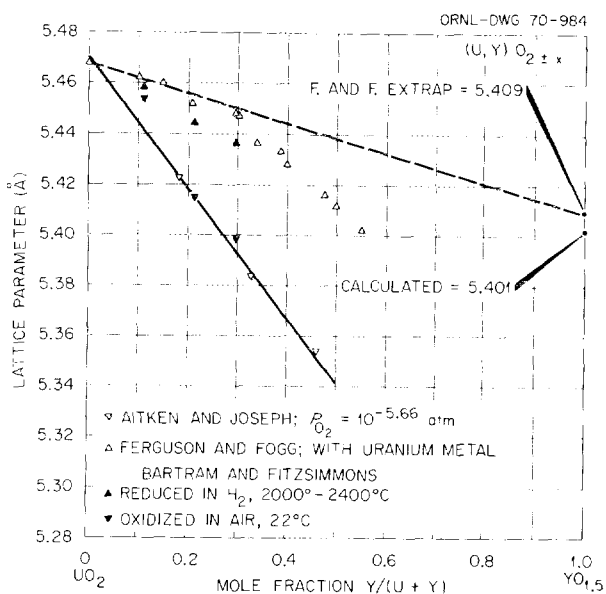


Fig. 6.14. Lattice parameters of U-Y-O solid solutions. [Refs.: E. A. Aitken and R. A. Joseph, *J. Phys. Chem.* **70**, 1090-97 (1966); I. F. Ferguson and P. G. T. Fogg, *J. Chem. Soc.* 3679-81 (1957); S. F. Bartram and E. S. Fitzsimmons, *Studies on the Stabilization of UO_2 and Y_2O_3 Additions*, GEMP-709 (September 1969); also *J. Nucl. Mater.* **35**, 126-30 (1970).]

obtained from the equation of Brauer and Gradinger indicates that the defect fluorite solid solution of $\text{Eu}_2\text{O}_3\text{-UO}_2$ is taking up oxygen to become approximately $(\text{U,Eu})\text{O}_2$. From these data, the data of Aitken and Joseph on $\text{Y}_2\text{O}_3\text{-UO}_2$, and the data of Markin et al.⁴⁸ on the U-Ce-O phase diagram we can compute the rare-earth side of R.E. $\text{O}_2\text{-UO}_2$ solid solutions by means of some reasonable interpolations. We tabulate these values also in Table 6.5.

The data discussed above tend to indicate that the rare earths, of which Y and Eu should be representative examples, dissolve in UO_2 -- and, therefore, probably in $(\text{U,Pu})\text{O}_2$ -- as "effectively" the dioxide. At high temperatures, however, the situation tends to be considerably more complicated. It was to this problem that we were addressing ourselves at the termination of the program. Unfortunately, therefore, the results presented below are fragmentary and incomplete. They strongly suggest that the amount of oxygen taken up by the rare earths does not, at high temperatures, reach "effectively" R.E. O_2 , but something less rich in oxygen. It is this subject to which we now turn our attention.

As one raises the temperature of refractory oxides at a constant oxygen potential, one might expect a loss of oxygen. However, in materials like ZrO_2 , ThO_2 , and Al_2O_3 this loss is too small to detect except with considerable difficulty. This loss may not be small -- and in fact we postulate that it is not -- in rare-earth oxides dissolved in UO_2 . The first indication of a

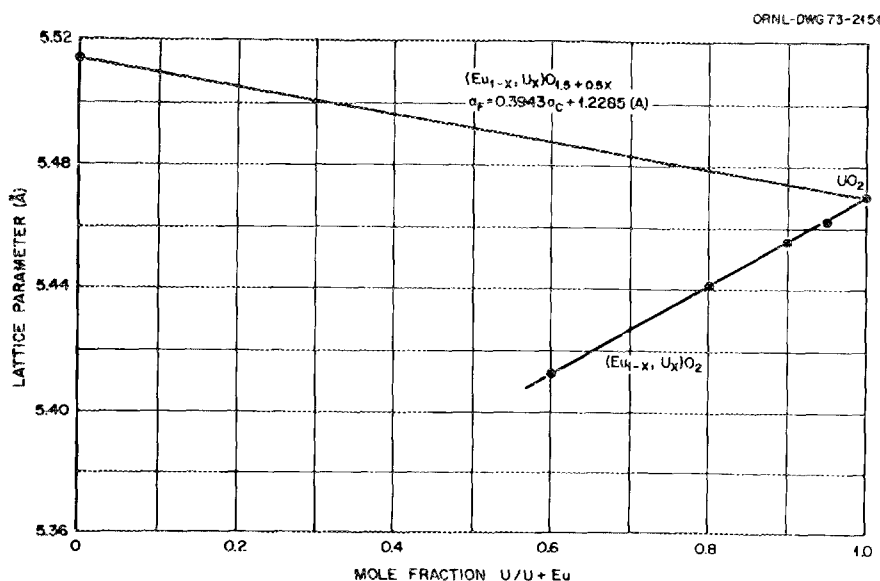


Fig. 6.15. Comparison of measured lattice parameters of the $(\text{U,Eu})\text{O}_2$ solid solution with calculated values.

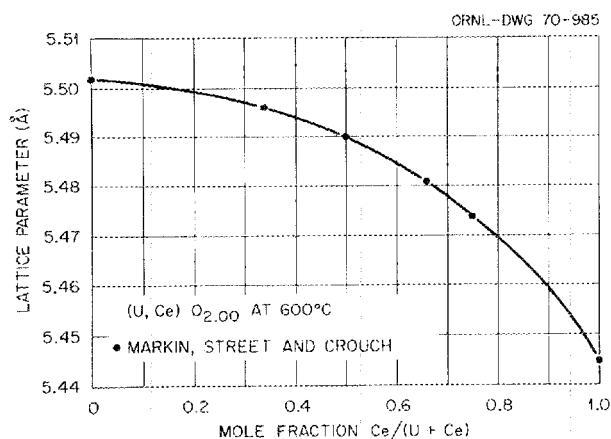


Fig. 6.16. Lattice parameters of $(U,Ce)O_{2.0}$ at $600^{\circ}C$. [Data from Markin et al., *J. Inorg. Nucl. Chem.* 32, 59-75 (1970).]

significant loss came from data of Markin et al.⁴⁸ They state that the UO_2 - CeO_2 pseudobinary obeys Vegard's law. It appears to do so within experimental error at room temperature. However, a plot of their data at $600^{\circ}C$, Fig. 6.16, reveals a system deviating widely from a Vegard relationship. Since the deviation is in the direction of an increased lattice parameter at intermediate compositions, the suggestion that the solid solution may be losing oxygen seems to follow from examination of the data presented above on solid solutions of rare-earth oxides with UO_2 .

We began two programs to attempt to establish on a quantitative basis the extent of any loss. The first was the determination of the lattice parameter of Eu_2O_3 - UO_2 solid solutions as a function of composition, oxygen potential, and temperature. The second program was the direct measurement via weight loss from equilibrated solid solutions of any deviation from stoichiometry as a function of composition, oxygen potential, and temperature. Both programs were terminated before completion, but the lattice parameter measurement was beginning to yield consistent data, and some of those results are presented here. (The weight change measurement was terminated during calibration of the apparatus constructed for the purpose.)

Data for $U_{0.6}Eu_{0.4}O_{2 \pm x}$ are presented in Fig. 6.17. These data represent measurements in the indicated CO- CO_2 mixtures, to fix the oxygen potential, using ThO_2 as an internal standard. We were in the process of

48. T. L. Markin, R. S. Street, and E. C. Crouch, "The Uranium-Cerium-Oxygen Ternary Phase Diagram," *J. Inorg. Nucl. Chem.* 32, 59-75 (1970).

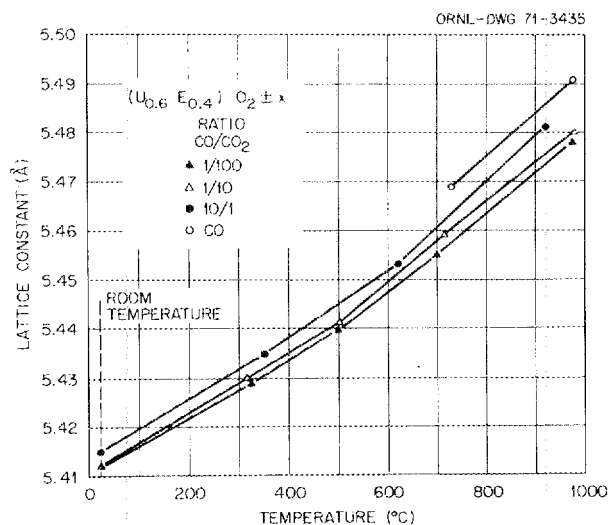


Fig. 6.17. High-temperature lattice parameters of $U_{0.6}Eu_{0.4}O_2$ as a function of oxygen potential.

checking the reversibility of the measurement at program termination, so it is not clear that the results represent the best data obtainable. However, they are internally consistent, and the two points checked at the highest temperatures were reversible. One sees that there is a significant increase in lattice parameter as one decreases the oxygen potential. This is to be expected, since the lattice parameters of these solid solutions increase as the oxygen content decreases. More important, however, is the significant upward curvature to the plots of lattice parameter vs temperature. This upward curvature is similar to the observations of Markin et al. on the UO_2 - CeO_2 lattice parameter as a function of temperature.

The results at $900^{\circ}C$ in Fig. 6.17 can be interpreted as indicating that $U_{0.6}Eu_{0.4}O_2$ not only loses oxygen as the temperature is raised, but it also shows a significant loss of oxygen relative to the room-temperature composition. At $900^{\circ}C$ the total loss from stoichiometry is about 25% of the excess oxygen between $U_{0.6}Eu_{0.4}O_{2.0}$ and $U_{0.6}Eu_{0.4}O_{1.8}$ at an oxygen potential corresponding to 10 parts CO to 1 part CO_2 . Since fuel in a reactor will operate at a much higher temperature, up to $2200^{\circ}C$, the problem would be expected to be magnified. A straight-line extrapolation, which is admittedly dangerous, would indicate as much as 75% of the excess oxygen taken up at room temperature might be lost at $2300^{\circ}C$. Lacking reliable data, we have not even attempted a volume-averaging calculation to guess the average amount of oxygen taken up by the rare earths.

In summary, neither assumption in Table 6.4 for the oxygen content of fuel, relative to the rare earths, can be taken as correct, although both assumptions have been used. The true situation almost certainly lies somewhere in between. A great deal of effort has gone into trying to model the fuel-cladding interaction without considering the oxidation state of the fission product constituents.

The data needed to complete the understanding of the fission product use of oxygen should be the oxygen content of rare-earth-fuel solid solutions as a function of temperature, rare-earth content, and oxygen potential. In principle, the experiments are straightforward and would be highly desirable.

6.1.4.4 Oxygen Gradients in Mixed-Oxide Fuels

In a reactor fueled with mixed oxide, a strong temperature gradient exists, as has been noted previously. Because of the temperature gradient, an oxygen gradient will also exist. This problem is important because in relating oxygen content of the fuel to rates of attack on the cladding, it has been thought important to determine the oxygen potential of the fuel adjacent to the cladding. We have recently pointed out problems with current theories that attempt to solve this problem and have suggested a direct method of measuring oxygen potentials in irradiated mixed-oxide pins as a function of distance across the pin.⁴⁹

6.2 PROCESS AND ECONOMIC EVALUATIONS

A. L. Lotts J. D. Sease

The commercial application of liquid-metal fast breeder reactors will require significant development and extension of technology for the fuel cycle. This requirement arises from the design of the fuel, which will reach burnups of 13 to 15 at. %, which must operate at high heat rates, and which must be shipped and processed quickly and efficiently. The requirement for efficiency and economy arises in part from the fact that capital cost estimates for the construction of LMFBR's indicate that these plants will cost more than light-water reactor systems.⁵⁰

49. J. M. Leitnaker and K. E. Spear, "Elimination of CO₂ and H₂O as Oxygen Transport Species in Mixed-Oxide Fuel Pins," *J. Nucl. Mater.* 45, 195-200 (1972).

50. Systems Analysis Task Force, *Potential Nuclear Power Growth Patterns*, WASH-1098 (December 1970).

As an example of what is required in the economy, McVey et al.⁵¹ stated that, if there is \$20/kW(e) difference between the cost of LMFBR's and light-water reactors and if the LWR fuel cycle costs are in the range 1.2 to 1.4 mills/kWhr, then the LMFBR costs must be between 0.8 and 1.0 mill/kWhr for the LMFBR to be competitive. This is based on an approximation that each \$5/kW(e) installed capacity (capital cost) is equal to 0.1 mill/kWhr in power costs. This is the reason then that considerable resources are being extended by the USAEC and the U.S. nuclear industry to ensure fuel cycle technology and fuel performance technology to achieve low fuel cycle costs by the time LMFBR's reach commercial application.

It is within this context that we have maintained an assessment of the status of the various fuel cycle operations and the need for future development. Information concerning LMFBR fuel fabrication demands and costs, process alternatives, fuel fabrication plant design, and economic optimization is included in this section.

6.2.1 Future Industrial Basis for LMFBR Fuel Fabrication

The fuel industry for LMFBR's in the future will operate within certain constraints imposed by the reactor design, the consumer demand for electricity, and the specific attributes of the fuels to be processed. Also, the industry must take into account the evolutionary process involved in the LMFBR reaching a mature industrial basis. In other words there will be a significant transition period in which these various factors will be changing. This must be taken into account in the processes and plants that are designed to accommodate the fuel cycle operations. Specifically, we are concerned here with the potential demand for fuel to be processed, the composition of these fuels, and the particular fuel element designs that must be fabricated and reprocessed.

6.2.1.1 Demand for LMFBR Power Plants

The study completed by the Systems Analysis Task Force⁵⁰ in December 1970 considered five LMFBR's, as indicated in Table 6.6. Systems analyses for power economies including fossil fuel plants, LWR's, LMFBR's, HTGR's, gas-cooled fast reactors, molten-salt

51. W. H. McVey, N. Haberman, and C. A. Sege, "Fast Reactor Fuel Cycle Economics," pp. 12-29 in *Symposium on Sol-Gel Processes and Reactor Fuel Cycles*, Gatlinburg, Tenn., May 4-7, 1970, CONF-700502.

Table 6.6. Summary of design and performance parameters for carbide- and oxide-fueled liquid-metal-cooled reactors

| | Reference carbide | Advanced carbide | Reference oxide | Advanced oxide (negative) ^a | Advanced oxide (positive) ^a |
|--|-------------------|------------------|-----------------|--|--|
| Core region | | | | | |
| Active height, ft | 4 | 4.83 | 4.0 | 3.5 | 4.0 |
| Diameter, ft | 3.3 | 5.71 | 4.5 | 4.0 | 6.5 |
| Number of control rods | 1.3 | 21 | 21 | 21 | 19 |
| Number of fuel elements | 48 | 148 | 252 | 162 | 189 |
| Fuel pin diameter, in. | 0.286 | 0.400 | 0.25 | 0.23 | 0.23 |
| Number of fuel pins per element | 168 | 91 | 217 | 271 | 217 |
| Average coolant velocity, fps | 27.1 | 32.9 | 25 | 34 | 38 |
| Power, MW(t) | 2300 | 2295 | 2197 | 1975 | 2103 |
| Average specific power, MW(t)/metric ton | 113 | 167.9 | 175 | 230 | 230 |
| Peak linear rod power, kW/ft | 33.2 | 66.9 | 16 | 20 | 20 |
| Fuel average discharge exposure, MWd/metric ton | 79,360 | 110,300 | 80,000 | 101,000 | 97,000 |
| Hot-spot cladding temperature, °C | 700 | 730 | 665 | 730 | 735 |
| Maximum fuel temperature, °C | 1285 | 1975 | 2620 | 2750 | 2750 |
| Coolant outlet temperature, °C | 540 | 580 | 570 | 650 | 650 |
| Nominal coolant temperature rise, °C | 110 | 190 | 150 | 150 | 150 |
| Axial blanket | | | | | |
| Length, ft (each end) | 1.25 | 1.0 | 1 | 1.5 | 1.5 |
| Power, MW(t) | 54 | 51 | 40 | 54 | 45 |
| Average specific power, MW(t)/metric ton | 4.26 | 9.02 | 5.5 | 6.7 | 6.0 |
| Fuel average discharge exposure, MWd/metric ton | 3000 | 5930 | 2500 | 2900 | 2500 |
| Radial blanket | | | | | |
| Number of fuel elements | 102 | 162 | 234 | 198 | 114 |
| Power, MW(t) | 346 | 204 | 263 | 271 | 152 |
| Average specific power, MW(t)/metric ton | 5.43 | 8.46 | 10 | 10 | 10.9 |
| Fuel average discharge exposure, MWd/metric ton | 3870 | 8340 | 8100 | 5900 | 6000 |
| System | | | | | |
| Breeding ratio | 1.45 | 1.50 | 1.27 | 1.34 | 1.31 |
| Specific inventory, kg fissile/MW(e) | 2.84 | 1.44 | 3.9 | 2.8 | 2.3 |
| Simple system doubling time, years | 8.6 | 4.8 | | | |
| Reactivity worth of sodium voids, β | 0.36 | 8.07 | 0.23 | -0.33 | 11 |
| Doppler constant ($T dk/dT$), core and radial blankets | -0.0039 | -0.004 | -0.0094 | -0.0073 | -0.0102 |
| Thermal to electrical conversion efficiency, % | 37.0 | 39.2 | 40.0 | 43.5 | 43.5 |
| Compound core doubling time, years | | | 15.00 | 8.00 | 7.00 |

^aSodium void coefficient.

reactors, and steam-cooled fast reactors were done within the study. In general, the study indicated that the LMFBR is the principal reactor constructed when the advanced oxide and the carbide LMFBR's are employed. Therefore, the target fuel designs are those that have average discharge burnups of the order of 100,000 MWd/metric ton of heavy metal for the core fuel, cladding hot spot temperatures near 700°C, and peak linear rod power of 20 kW/ft for oxide fuels and 33kW/ft for carbide fuel. Assuming penetration of the market by the HTGR, maintenance of a market for LWR's, and some continued construction of fossil fuel plants, the LMFBR market penetration is of the order of that shown in Fig. 6.18. Depending on the particular

assumptions, the end point in the year 2020 varies between 1400 and 2400 GW(e).

6.2.1.2 Fuel Cycle Material Balance and Process Demand

Figure 6.19 shows a typical equilibrium material balance flowsheet.⁵² The reactor contains both core axial blanket fuel elements and radial blanket fuel elements. These must be treated separately in certain of the fuel fabrication operations.

⁵² *Reactor Fuel Cycle Costs for Nuclear Power Evaluation*, WASH-1099 (December 1971).

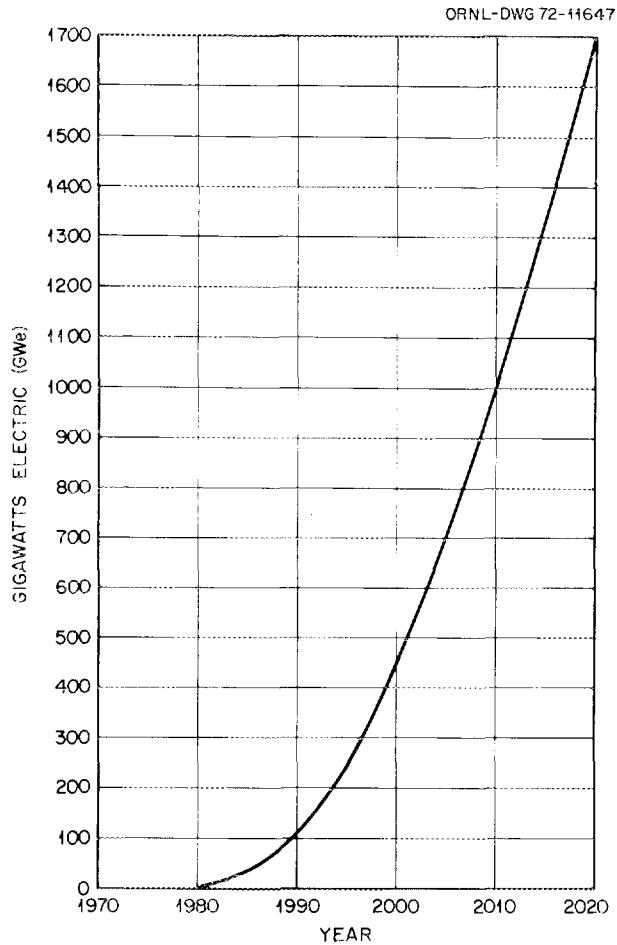


Fig. 6.18. Projected installed electrical capacity of LMFBR's.

The blanket material is fabricated from depleted UF_6 , and the core materials are fabricated from recycled plutonium and depleted UF_6 . Some excess plutonium is produced, and this plutonium is used to start up new fast breeder reactors, or it can be recycled to light-water reactors or HTGR's. In the chemical processing operation, both radial blanket elements and core axial blanket elements are processed for recovery of plutonium.

Calculation of the material balance for the entire LMFBR fuel cycle industrial base is not a simple matter because of the variation in the material balances for the LMFBR's that might exist in the economy. As an example of this, material balances for the several 1000-MW(e) LMFBR's considered by the Systems Analysis Task Force are compared in Table 6.7. As can be seen, the total uranium charged to the LMFBR core can vary from 15.8 to 41.1 metric tons/year and the plutonium can vary from 0.91 to 3.1 metric tons/year. Figure 6.20 shows the full range of the projected fabrication and reprocessing demand for LMFBR fuels as a function of time, as calculated from the installed electrical capacity of Fig. 6.18 and data given in Table 6.7. In 1990 for example, the fabrication demand can vary from 5 to 15 metric tons of heavy metal per day. In Fig. 6.20 the demand for reprocessing service always lags the fabrication service demand significantly because of additional LMFBR's being added to the system.

Table 6.7. Comparison of material balances for several 1000-MW(e) LMFBR's

| | Loading or discharge (metric tons/year) | | | | |
|----------------------|---|--|--|-------------------|------------------|
| | Reference oxide | Advanced oxide (negative) ^a | Advanced oxide (positive) ^a | Reference carbide | Advanced carbide |
| Core fabrication | | | | | |
| Uranium | 6.40 | 4.51 | 5.34 | 7.33 | 5.54 |
| Plutonium | 2.10 | 1.78 | 1.42 | 1.65 | 0.91 |
| Blanket fabrication | | | | | |
| Uranium | 15.00 | 20.55 | 13.38 | 33.79 | 10.26 |
| Total (core-blanket) | | | | | |
| Uranium | 21.40 | 25.06 | 18.72 | 41.12 | 15.80 |
| Plutonium | 2.10 | 1.78 | 1.42 | 1.65 | 0.91 |
| Discharge | | | | | |
| Uranium | 20.31 | 23.99 | 17.70 | 39.78 | 14.57 |
| Plutonium | 2.35 | 2.04 | 1.68 | 2.11 | 1.29 |
| Fission products | 0.83 | 0.81 | 0.77 | 0.87 | 0.85 |

^aSodium void coefficient.

6.2.1.3 Isotopic Composition

The principal source of plutonium for start-up of LMFBR reactors will be plutonium produced primarily in LWR's. This is a very important consideration, since the radioactivity associated with the various plutonium isotopes will affect the design of the fuel fabrication plant. The plutonium isotopes of importance are ^{238}Pu , ^{239}Pu , ^{240}Pu , ^{241}Pu , and ^{242}Pu . The ^{236}Pu is not assessed as being particularly important, since it has not been measured in any quantity greater than 1 ppm. But, as pointed out by Smith et al.,⁵³ should this isotope ever be produced in significant quantities by any reactor, handling of the resultant plutonium will require massive shielding and rapid recycle. Smith et al.,⁵³ Bell and Nichols,⁵⁴ Frankhouser et al.,⁵⁵ and Shuck⁵⁶ have reported on the ranges of plutonium isotope concentrations in various fuels. These data are summarized in Fig. 6.21.

The principal interest among these isotopes is the penetrating radiations associated with the (1) neutrons generated by the spontaneous fission of ^{238}Pu , ^{240}Pu , and ^{242}Pu ; (2) neutrons from the (α, n) reaction with light elements; and (3) gamma radiation from the plutonium isotopes and from the ^{237}U and ^{241}Am that result from the radioactive decay of ^{241}Pu . In addition, residual fission products may exist in the fuel, giving a source of gamma radiation that should also be considered. The radioactivity from plutonium isotopes is summarized in Table 6.8, and that from plutonium decay products and residual fission products in Table 6.9.

6.2.1.4 Transition Period in Developing an LMFBR Fuel Recycle Economy

When LMFBR's commence production of electricity in the mid-1980's, the complexion of the fuel cycle

53. R. C. Smith, H. H. Van Tuyl, and L. G. Faust, "The Effect of Radiation Levels from Plutonium on Fuel Fabrication Process Design," pp. 59-73 in *Symposium on Sol-Gel Processes and Reactor Fuel Cycles*, Gatlinburg, Tenn., May 4-7, 1970, CONF-700502.

54. M. J. Bell and J. P. Nichols, "Penetrating Radiation Dose Rates and Shield Requirements in Fabrication of Fuels Containing ^{233}U and High-Exposure Plutonium," pp. 74-84 in *Symposium on Sol-Gel Processes and Reactor Fuel Cycles*, Gatlinburg, Tenn., May 4-7, 1970, CONF-700502.

55. W. L. Frankhouser, U. Decher, and T. E. Potter, "Fabricating Production Quantities of Higher Burnup Plutonium Fuels," *ibid.*, pp. 85-98.

56. A. B. Shuck, A. L. Lotts, and K. Drumbheller, "The Remote Fabrication of Reactor Fuels," pp. 71-148 in *Reactor Technology - Selected Reviews - 1965*, TID-8541 (January 1966).

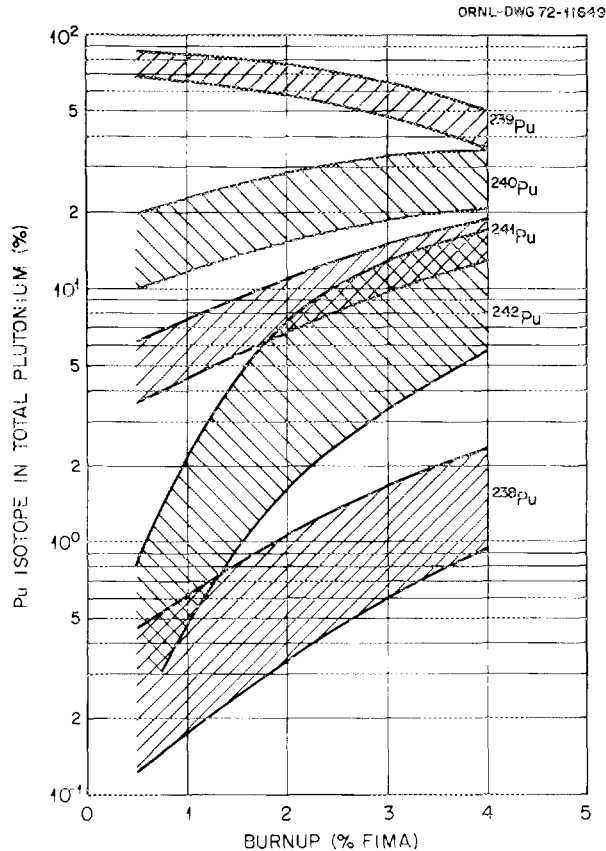


Fig. 6.21. Isotopic distribution in plutonium from LWR's.

industry will be of one that supports light-water reactors. Therefore, the question at hand is how this particular industrial base can be used for the LMFBR fuel cycle industry in the transition period before there is a large enough number of LMFBR's to justify a separate fuel cycle system for the LMFBR. Indeed the question is which of the components of the fuel cycle industry for light-water reactors can be used in the LMFBR system.

Considering the fuel fabrication industry, it is based entirely upon ceramic pellet fabrication with containment in Zircaloy tubes. Recycle of plutonium in light-water reactors is anticipated as an extension of this technology, with the primary difference being that the fabrication will have to be done in glove boxes. Accordingly, both plant and personnel are oriented toward a particular flowsheet and a particular fabrication system. The parts of these systems that involve the fabrication of UO_2 can be directly applied to the fabrication of the radial blankets for LMFBR's, and a substantial part can be applied to the fabrication of pellets for the axial blankets, which are part of the core-axial blanket flue elements. Up to 70 or 75% of

Table 6.8. Radioactivity from plutonium isotopes

| Isotope | Decay modes | Energies (MeV) | Half-life (years) | | Neutron emission ^d (neutrons sec ⁻¹ g ⁻¹) | |
|-------------------|------------------|----------------|--------------------|-----------------------|--|-------------------------------------|
| | | | Alpha | Spontaneous fission | Fission | (α, n) in PuO ₂ |
| ²³⁸ Pu | α | 5.49 | 86.4 | 3.8×10^{10} | 3.4×10^3 | 1.4×10^4 |
| | γ | 0.040 | | | | |
| ²³⁹ Pu | α | 5.15, 5.10 | 2.43×10^4 | 5.5×10^{15} | 0.02 | 45 |
| | γ | 0.035, 0.050 | | | | |
| ²⁴⁰ Pu | α, γ | 5.16 | 6.58×10^3 | 1.22×10^{11} | 1.0×10^3 | 170 |
| ²⁴¹ Pu | α, γ | 4.91 | 5.7×10^5 | | | |
| | β, γ | 0.01 | | | | |
| ²⁴² Pu | α | 4.88 | 3.79×10^5 | 7.1×10^{10} | 1.7×10^3 | 2.7 |
| | γ | 0.044, 0.048 | | | | |

^dFrom Shuck et al., TID-8541, p. 75.

Table 6.9. Radioactivity from plutonium decay products and residual fission products

| Isotope | Decay modes | Energies (MeV) | Half-life |
|-------------------|-------------|---------------------|-----------|
| ²³⁷ U | β | 0.25 | 6.73 days |
| | γ | 0.05, 0.33, 0.371 | |
| ²⁴¹ Am | α | 5.46, 5.433 | 460 years |
| | γ | 0.597, 0.103, 0.041 | |
| ¹⁰⁶ Ru | β | 0.041 | 1.0 year |
| | γ | | |
| ¹⁰³ Ru | β | 0.684, 0.22 | 39.8 days |
| | γ | 0.04, 0.494 | |
| ⁹⁵ Zr | β | 0.39, 1.0 | 65 days |
| | γ | 0.73, 0.23, 0.92 | |
| ⁹⁵ Nb | β | 0.163 | 35 days |
| | γ | 0.771 | |

the volume of uranium handled can be handled in this fashion. Accordingly, there will exist substantial capacity and technology for application to the LMFBR blanket regions. Substantial experience has also been gained in handling plutonium, although the fabrication of LMFBR core fuel is substantially different from recycling plutonium in light-water reactors.

Since there are significant differences that may require new installations for LMFBR core fuel, it would be prudent to consider optional processes that may offer processing or performance advantages. An assessment of the commitment of industry to the particular details of fuel design and fuel fabrication processes must be based on the accumulation of additional data, which should more narrowly define the economic

parameters and performance parameters involved in the various options. In addition, it should be pointed out that initially and substantially through the start-up period for LMFBR's the fuel fabrication industry will be handling recycle fuel from light-water reactors, which in terms of radioactivity places a more stringent requirement on the fuel fabrication plant design than will fuel recycle from LMFBR's. We believe that plant design should be based on the requirements for recycle of plutonium from light-water reactor fuel and thereby enable the handling of almost any contingency that may arise in the future.

6.2.2 Projections for the LMFBR Fuel Fabrication Industry

The questions involving the future of the LMFBR fuel fabrication industry concern (1) fuel fabrication demands and therefore scale of operation, (2) fuel fabrication plant design, (3) probable cost, and (4) probable fuel performance. In addition, an analysis of the type of economies that can be reached through certain improvements is of great interest, since such an assessment would serve as a base line for the cost-benefit analysis of research and development expenditure in the future.

6.2.2.1 Fabrication Demand

The projected fabrication demand based on assumed reactor economy was presented in Fig. 6.20. In addition to this, reports of the system analysis task force⁵⁰ and the fuel recycle task force⁵² show comprehensively the type of demands required for the industry in the future as well as give an indication of the cost of fuel

fabrication. Typically, for a reactor such as the LMFBR advanced oxide system, half-ton core fuel fabrication plants are required in 1990, with the size increasing to approximately 2 tons per day, six plants being required in the year 2000.

6.2.2.2 Plant Design

Bell and Nichols⁵⁴ considered the capabilities of various types of operation classified according to mode of operation, that is, glove boxes, semiremote, or remote operation (operations that have been defined by Shuck et al.⁵⁶). In their analysis, they estimated maximum capacities of fuel fabrication lines preparing $\text{UO}_2\text{-PuO}_2$ as a function of shield thickness. The results are shown in Table 6.10. The calculated shielding requirement for manufacture of LMFBR core fuel at a capacity of 500 kg/day was 22 in. of concrete. That shielding will be required is unquestioned. For the future the problem is to determine the most economical method of incorporating the required shielding and the most economical method for the design of the process to minimize the exposure to the operators. Process designs therefore should emphasize automation and mechanization, close integration of shielding and criticality design, and on-line computerization and instrumentation to minimize holdup of materials.

Frankhouser⁵⁵ concluded that the NUMEC experience with plutonium fuel fabrication does not provide

the basis for design of an oxide fuel rod production facility, but it does allow guidelines to be formulated. He pointed out that other than isotopic composition of plutonium, such practical considerations as age of fuel, concentration of plutonium in fuel, fuel surface-area-to-volume ratio, and fuel mass must be taken into account. Plant design itself can vary all the way from glove-box enclosures with shielding, general enclosure shielding, and shielding on process equipment to completely remote operation. A thorough evaluation of the relationship of capital cost to operating cost must be done to assess the optimum solution to the problem. At this point for large-scale plants, remote operation with automatic equipment appears to be a prudent choice. This would allow for a number of contingencies regarding reduction of permissible operator exposure as well as unexpected increases in radiation associated with the fuels to be fabricated. Operation of the HTGR fuel recycle pilot plant projected for the period 1977-1980 should help define the cost of remotely fabricating nuclear fuels.⁵⁷

6.2.2.3 Process Options for Manufacture of LMFBR Fuel Pins

The principal competing flowsheets for fabrication of LMFBR core-axial blanket fuel elements are the coprecipitation flowsheet, mechanically mixed flowsheet, and the sol-gel pellet and sol-gel Sphere-Pac flowsheets. These are shown in Fig. 6.22. In addition to these indicated routes, vibratory compaction of angular particles or shards has been considered and rejected by most investigators. The material for vibratory compaction can be made by mechanically blending UO_2 and PuO_2 powders or by coprecipitating a mixed powder. The preparation of material in any event involves pressing, sintering, and grinding to obtain the proper sizes for vibratory compaction. In addition, the sol-gel route can be considered for preparation of shards that would follow a route similar to that shown for the preparation of sol-gel-derived pellet material through the calcination and sintering route. It is not necessary to press the sol-gel material to obtain adequate particulate density.

Considering the three principal routes for preparation of pellets shown in Fig. 6.22, almost identical steps are involved in all the routes from the step of pressing pellets to the final inspection of the second weld on the fuel pin. The differences lie in the preparation of the

Table 6.10. Estimated maximum capacities of lines for preparing $\text{UO}_2\text{-PuO}_2$ for LMFBR's^a

| Type of operation | LMFBR core (LWR recycle Pu) $\text{Pu}/(\text{U} + \text{Pu}) = 0.22$ | |
|--------------------------------|--|---|
| | Concrete shield thickness (in.) | Capacity (kg $\text{UO}_2\text{-PuO}_2$ /day) |
| Gloved enclosures ^b | 0 ^c | 7 |
| Semiremote ^b | 12 | 30 |
| Remote ^d | 16 | 100 |
| | 22 | 500 |
| | 24 | 1000 |

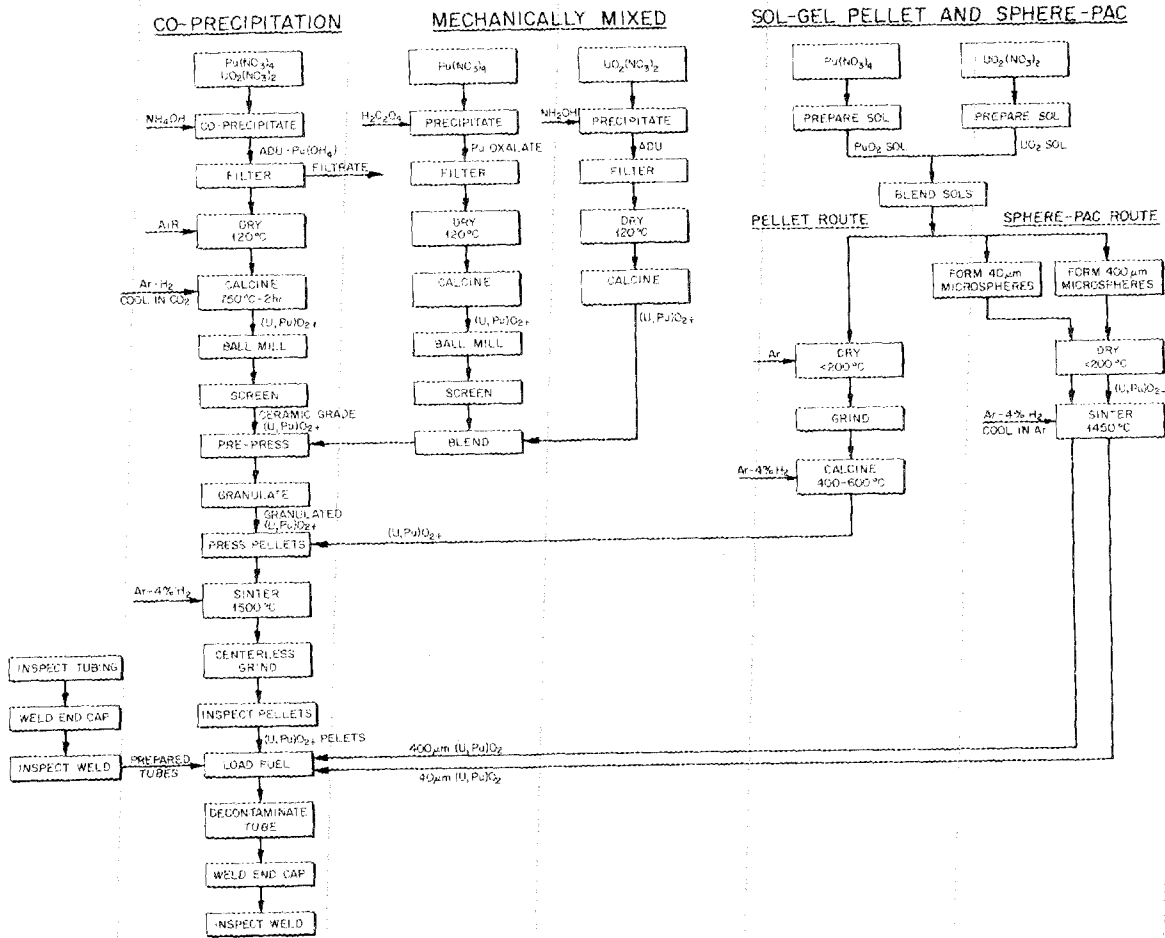
^aAssumes operator dose rate = 40 millirems/week.

^bAssumes process equipment installed 1 ft from inner wall of enclosure.

^cAssumes $1/4$ in. of lead for shielding against soft gamma radiation.

^dAssumes that process vessels (which contain no more than 20% of daily throughput) are installed 2 ft from the inner surface of the shield and that the dose rate at the operating surface is 1.0 millirem/hr.

57. Oak Ridge National Laboratory and Gulf General Atomic, *National HTGR Fuel Recycle Program Plan*, ORNL-4702 (August 1971).

Fig. 6.22. Flowsheet for (U,Pu)O₂ fuel fabrication.

materials. The coprecipitation and mechanically mixed routes are quite similar in that prepressing and granulation are required to prepare a material suitable for pelletizing to the lower stable densities required for LMFBR fuel. In the sol-gel pelletizing route, this step is accomplished by adjustment of the calcination procedure, which is conducted in the range 400 to 700°C on dried gel material. The principal disadvantage of the mechanically mixed route is the need for inspections and qualified procedures to ensure homogeneous mixture of the UO₂ and PuO₂. The principal problem in the coprecipitation route lies in control of the simultaneous precipitation of plutonium and uranium intermediate products. However, as previously noted, a coprecipitation step has been used on very large-scale operations, and it is certainly indicated that the mechanically mixed route will be proven to be satisfactory in the FFTF program.⁵⁸

In the sol-gel pelletizing route, although the preparation of the sol may be a more complicated operation than either precipitation or coprecipitation, the subsequent preparation of a suitable powder for pelletizing is more straightforward than the other two routes. Indeed, the only mechanical operation is a grinding step, which has been accomplished in a fluid energy mill and does not require screening. To summarize the status of the three processes, both coprecipitation and mechanically blended routes involve more mechanical operations, but they have been conducted on a large scale

58. W. E. Roake, C. E. Weber, D. H. Wiese, C. S. Caldwell, I. D. Thomas, J. L. Scott, and A. B. Shuck, "The United States Program for Developing the Manufacture of High-Quality Fast Reactor Fuels," pp. 311-25 in *Peaceful Uses of Atomic Energy, Proc. 4th Int. Conf., Geneva, 1971*, Vol. 8, United Nations, New York, and International Atomic Energy Agency, Vienna, 1972.

and there is a great deal of industrial experience with them, whereas the sol-gel pelletizing route involves more chemical operations and less mechanical handling, but there is experience only on laboratory-scale operations.

The Sphere-Pac technique for sequentially loading two sizes of microspheres into a fuel column, using low-energy vibration, was described in Sect. 3.1. An improvement of this process called the "U-Fines" process, which is a form of Sphere-Pac loading in which all the plutonium is contained in the coarse microspheres, was also described in this report. The principal advantages of the "U-Fines" process stem from the fact that no fine material of plutonium is necessary and from reduction of the quantity of material that must be handled with a high degree of containment and shielding.

Pelletizing and Sphere-Pac comparisons on a qualitative basis are difficult. However, it is our opinion that pellet processes have the advantage of known, industrially applied technology and results, experienced staff, and existing equipment. The process experience with Sphere-Pac is limited, and industrial facilities are almost nonexistent. Pellets processes have such disadvantages as (1) grinding operations, which produce finely divided particulates, which are more subject to process loss and (2) the requirement for finely divided chemically active powder. Sphere-Pac has the advantage of virtually eliminating finely divided plutonium-bearing material in the process and the inherent advantages of liquid chemical processing and fluid methods up to the step of loading fuel pins.

As to differences in the economics of the various preparation procedures, the difference is not substantial and probably lies within the error of the estimates. We⁵⁹ and Colombi and Podo⁶⁰ have assessed the difference in cost between the low-energy Sphere-Pac process and pelletizing routes. We concluded that the cost differential is in the range \$20 to \$25/kg heavy metal in a plant producing 500 kg of core material in finished elements per day. Colombi and Podo in their study saw little economic difference in favor of sol-gel processes. It should be pointed out, however, that more detailed assessment should be made of the alternative processes, with particular attention to any differences

59. J. D. Sease, R. A. Bradley, C. R. Reese, W. H. Pechin, and A. L. Lotts, "Sphere-Pac and Pelletization of (U,Pu)O₂," pp. 323-41 in *Symposium on Sol-Gel Processes and Reactor Fuel Cycles, Gatlinburg, Tenn., May 4-7, 1970*, CONF-700502.

60. G. Colombi and L. Podo, "Conceptual Plant Design and Preliminary Evaluation of Sol-Gel Versus Pellets Production Costs," *Ibid.*, pp. 264-80.

in process losses and the requirement for internal recycling of fuel material. In addition, there may be some differences in the degree of contamination and the relative difficulty expected with it among the different processes.

6.2.2.4 Fuel Element Fabrication Costs

We participated actively in the Fuel Recycle Task Force,⁶¹ developing base cost information for the fabrication of LMFBR fuel elements. Typical results of this work are shown in Fig. 6.23. These costs, which were developed with the FABCOST 9 computer code,^{62,63} contain very low fuel element hardware cost — for example, approximately \$1.25/ft stainless steel tubing. Substantial differences are indicated in the fuel fabrication costs for the various referenced reactors. Most of the differences are attributable to difference in dimensions of the fuel pin. For example, although the preparation of carbide fuels is more expensive, subsequent fabrication in the fuel pins on a weight basis of fuel is less expensive because fewer operations are required per kilogram of fuel. In other words, fuel fabrication cost is proportional to the length of tubing required per kilogram of fuel. The effect of hardware cost, particularly tubing cost, is indicated in Fig. 6.24, which shows the reference case for an LMFBR in the Systems Analysis Task Force study compared with a high cost for tubing representing present-day cost, and an intermediate cost, which represents at least a probable cost for the future. At a production rate of 1000 kg heavy metal/day, escalation of tubing cost from \$1.26/ft to \$6/ft doubles the fuel fabrication cost.

The value of trade-off in terms of final power cost is an important assessment. Figure 6.25, taken from McVey et al.,⁶⁴ is a plot of fuel cycle cost in mils/kWhr against burnup for several fuel cycle costs per kilogram of heavy metal. Applying such data to the worth of various changes for LMFBR core fuel is instructive.

61. *Reactor Fuel Cycle Costs for Nuclear Power Evaluation*, WASH-1099 (December 1971).

62. A. L. Lotts, T. N. Washburn, and F. J. Homan, *FABCOST 9, a Computer Code for Estimating Fabrication Cost for Rod Bundle Fuel Elements*, ORNL-4287 (August 1968).

63. A. L. Lotts and T. N. Washburn, "Use of Computer Codes in Estimating Fuel Element Fabrication Costs," *Nucl. Appl.* 4(5), 307-19 (May 1968).

64. W. H. McVey, N. Haverman, and C. A. Sege, "Fast Reactor Fuel Cycle Economics," pp. 12-29 in *Symposium on Sol-Gel Processes and Reactor Fuel Cycles, Gatlinburg, Tenn., May 4-7, 1970*, CONF-700502.

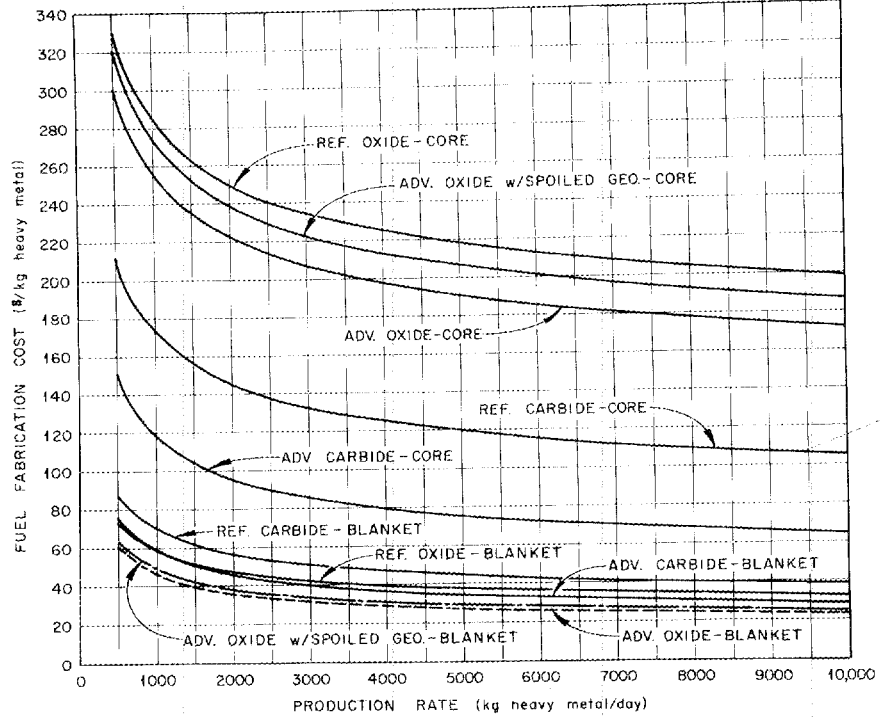


Fig. 6.23. Cost of fabricating LMFBR fuel.

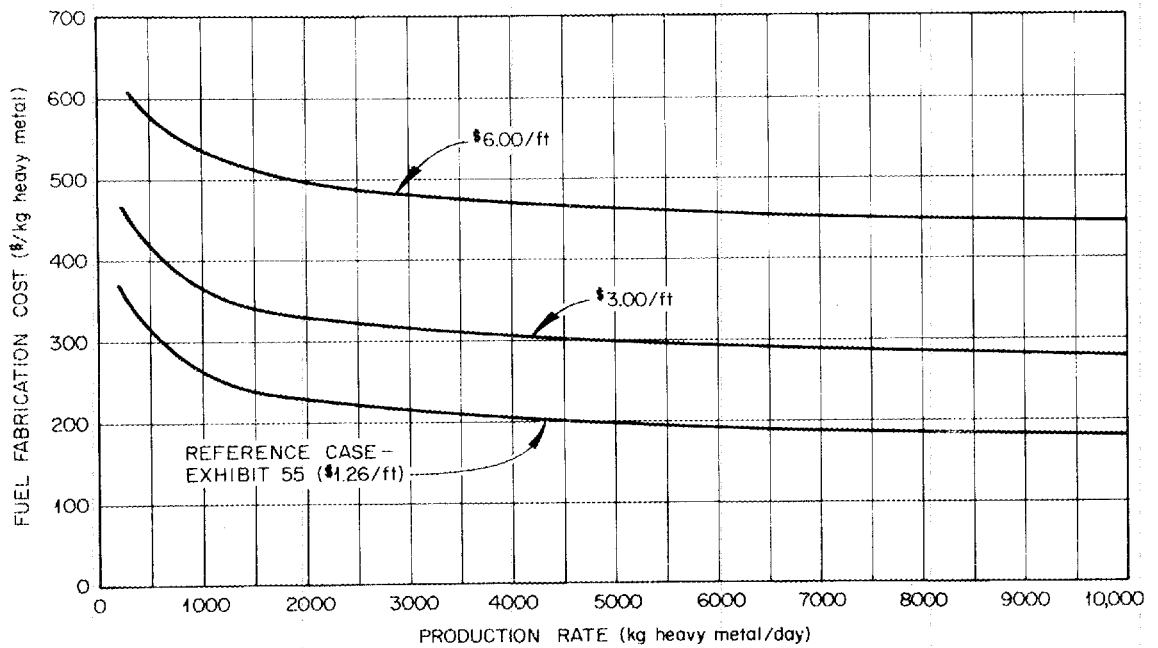


Fig. 6.24. Effect of tubing cost on LMFBR core fuel fabrication cost.

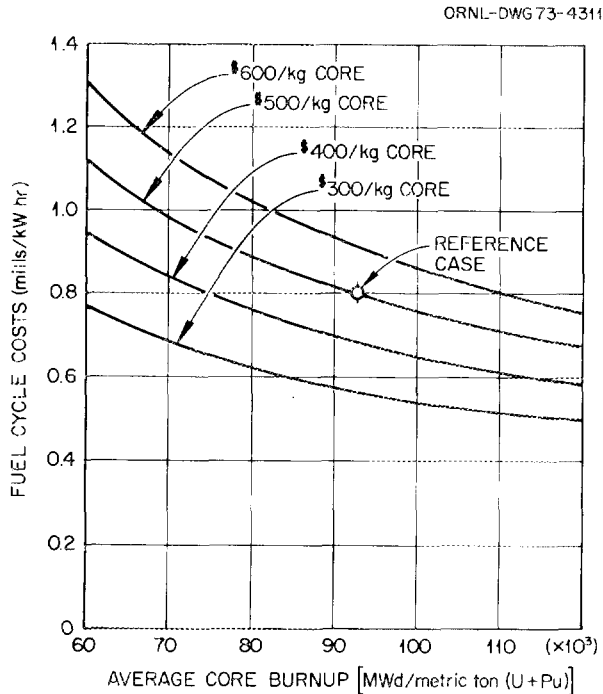


Fig. 6.25. Effect of burnup and out-of-reactor cost on fuel cycle costs. (From McVey et al., CONF-700502, p. 18.)

Table 6.11 shows the worth of several important changes that could be made with respect to scale of operation, process selection, hardware costs, and burnup capability of the fuel. Changes such as doubling the scale of operation, changing the mode of fabrication, and using a different fabrication process when considering only the processing costs result in a decrease of cost at about 5 to 6%. Reduction of tubing costs from the present rate of \$6/ft to \$3/ft gives an improvement of approximately 20%, and a reduction to \$1.25/ft an improvement of approximately 50%. It is notable also

that burnup capability greatly affects the power cost. Therefore one would conclude from these results that significant attention should be given to methods of reducing the cost of fuel element hardware, particularly tubing, and to selection of fuels that will enable the reactors to go to a higher burnup. In this respect, although it has not been reviewed here, there is future potential in a change from the mixed-oxide fuel system to advanced fuels should they prove to have adequate performance and process economics.

6.3 DISCUSSION OF CURRENT STATUS OF FUEL PERFORMANCE, PROCESS, AND ECONOMIC EVALUATIONS

A. L. Lotts

As reported by Nuclear Engineering International,⁶⁵ E. E. Kintner told fast reactor fuel experts at the ANS New Orleans Conference in April 1971 that after 20 years of FBR development in the United States, "We do not yet have the technical understanding necessary to design any fast reactor fuel element with great confidence and will not have that technical understanding necessary to design the fuel elements needed for competitive nuclear breeder industry unless we find ways to make more effective use of applied resources." He related the recent experiences of LMFBR fuel designers to those of Dante, who one day realized that he had strayed from the "true way" into the "dark woods of error." Most of his comments related to understanding fuel and cladding performance, but they also apply to the processes involved in the fabrication of fuel. Indeed, fuel performance is greatly dependent

65. "Fast Reactor Fuel Element Technology," *Nucl. Eng. Intern.* 16(181), 495-99 (June 1971).

Table 6.11. Worth of various changes for LMFBR core fuel^a at 1000-kg/day scale

| | \$/kg | mills/kWhr(e) | % |
|--|-------|---------------|-------|
| Basic reference cost | 530 | 0.830 | |
| Increase scale of operation to 2000 kg/day | -30 | -0.047 | -5.7 |
| Use glove-box facility instead of remote operation | -29 | -0.045 | -5.5 |
| Use Sphere-Pac process instead of mechanically blended powders | -24 | -0.038 | -4.5 |
| Reduce tubing cost from \$6/ft to \$1.25/ft | -268 | -0.420 | -50.6 |
| Reduce tubing cost from \$6/ft to \$3/ft | -98 | -0.153 | -18.5 |
| Decrease average burnup from 10 to 6 at. % | | +0.35 | +42.2 |

^aAverage burnup, 10% FIMA, exhibit 55 - SATF Study, WASH-1098.

upon the fuel form, structure, and composition, as well as similar characteristics of the cladding. It is appropriate, therefore, to review just where the technology stands with regard to processes involved in the fabrication of fuel and in fuel performance. The status of technology must be related or compared then to the original objectives outlined for the competitive reactors considered by the Systems Analysis Task Force and presented previously. It would be instructive also to consider the options that remain for processing technology and fuel design.

6.3.1 Relative Fuel Performance

Murray⁶⁶ has reviewed comprehensively the experience to date with LMFBR ceramic fuels, which are the fuels of primary interest for commercial LMFBR application. In his review he pointed out the substantial involvement of a number of countries, including Russia, the United Kingdom, the United States, France, West Germany, Japan, and Italy, as well as supporting efforts in other countries.

His review may be summarized as follows. Fuel pin irradiations in test reactors have demonstrated the high performance capability of mixed-oxide stainless steel systems. Fission gas release and fuel swelling can be accommodated, and the benefits arising from irradiation-induced effects of swelling and creep in stainless steel cladding give confidence that high-burnup targets for LMFBR fuel can be achieved. Fuel-cladding chemical interaction has emerged as a potential problem that may limit peak cladding temperatures to which mixed-oxide fuel pins are designed and operated. Further detailed results on these limits are needed, particularly in the high-burnup (10% FIMA) range. Reactions caused by fuel-sodium interactions under dynamic cooling conditions do not appear to cause major operating problems. Definition of fuel pin thermal performance models requires additional experimental data to minimize the uncertainties.

Stainless steel swelling and irradiation-induced creep have, in effect, focused attention on the fuel assembly and behavior of the fuel pin spacer system and the flow duct system. These are vital areas in which more precise materials irradiation data and interpretation for design are necessary. Present uncertainties can be overcome by design, giving more reliable irradiation data to the high fluences required for LMFBR application. Accommodation of swelling does, however, introduce an economic

Table 6.12. Oxide irradiations in fast reactors

| Country | Reactor | Number of rods irradiated | Number of rods irradiated |
|----------|------------------|---------------------------|---------------------------|
| U.S.S.R. | BR-5 and BOR-60 | 4600 | 120-150 |
| U.K. | DFR | 800 | 50 |
| France | Rapsodie and DFR | 8000 | 1 |
| U.S.A. | EBR-II and SEFOR | 1500 | 10 |
| Other | Rapsodie and DFR | 200 | 3 |

Note: Abstracted from *Nucl. Eng. Intern.* 16, 496 (June 1971).

penalty that highlights the importance of long-term metallurgical solutions to the swelling problems.

The experience with irradiations of oxide fuels in fast reactors has been summarized⁶⁵ and is given in Table 6.12. In the irradiation program in the United States, in addition to the oxide fuel irradiations, a number of uranium-plutonium carbide and uranium-plutonium nitride irradiations are being performed,⁶⁶ as indicated in Table 6.13.

As previously noted, a large number of mixed-oxide fuel pins have been fabricated and irradiation tested. Most of these have been made by coprecipitation and mechanical blending routes for preparation of fuel pellets. Accordingly, most of the experience being accumulated is for pellets, and this experience generally indicates there may be some problems with respect to maximum temperature of the fuel, primarily due to fuel-cladding chemical interaction. Although most of the experience is being obtained on pellet fuels, the future application of a fuel system to the LMFBR should consider other alternatives; in particular, results from irradiation of Sphere-Pac fuels are encouraging in that they have exhibited better compatibility with cladding and better fuel-cladding thermal conductance, as reported in Chap. 5. However, these results have been obtained on a relatively small number of fuel pins, and any conclusion should await the results of postirradiation examination of the fuel pins that are presently being irradiated in the EBR-II.

6.3.2 Process Options

In addition to the fuel fabrication experience implied by Tables 6.12 and 6.13, primary and essential experience is being obtained through the procurement of fuel for the Fast-Flux Test Facility. The program for

66. P. Murray, "Fast Breeder Fuel," *Reactor Technol.* 15(1), 16-58 (Spring 1972).

Table 6.13. Fuel pins irradiated in EBR-II^a

| Fuel | Up to 5 at. % | | 5 to 10 at. % | | Beyond 10 at. % | | Total | |
|----------------|-------------------|---------------------|-------------------|---------------------|-------------------|---------------------|-------------------|---------------------|
| | Encap- sulated | Unencap- sulated | Encap- sulated | Unencap- sulated | Encap- sulated | Unencap- sulated | Encap- sulated | Unencap- sulated |
| Oxide | 147 | 559 | 127 | 241 | 39 ^b | 0 | 313 | 800 |
| Carbide | 49 | 0 | 71 | 0 | 8 | 0 | 128 | 0 |
| Nitride | 18 | 0 | 0 | 0 | 0 | 0 | 18 | 0 |
| Metal + cermet | 70 | 196 | 4 | 38 | 0 | 0 | 74 | 234 |
| Total | 284 | 755 | 202 | 279 | 47 | 0 | 533 | 1034 |

^aStatus as of December 1971.

^bPeak cladding fluences up to 0.95×10^{23} neutrons/cm² (>0.1 MeV) have been achieved.

development of high-quality fast reactor fuels in support of the FFTF was reported by Roake et al.^{6,7} at the Fourth Geneva Conference. That paper pointed out that strong emphasis is placed on product specifications, process description and control, and quality assurance procedures and practices. The flowsheet for the FFTF fuel is based on mechanically mixed oxides. Substantial experience has been gained with the coprecipitated mixed-oxide material, and, in particular; the coprecipitation process was used by the Kerr-McGee Corporation for the production of mixed oxides for the zero-power reactor fuel rods during 1970 and 1971 at its Cimarron Plutonium Facility. Kerr-McGee produced 13,000 fuel rods with the nominal composition (Pu-85 wt % U)O₂ and 6000 fuel rods with the nominal composition (Pu-70 wt % U)O₂. In addition, Nuclear Fuel Services used the coprecipitation process for the production of SEFOR fuel, and General Electric^{6,8} and NUMEC^{6,9} have also used the coprecipitation process for production of mixed-oxide fuels. Substantial experience in laboratory operation exists on sol-gel processes for preparation and fabrication of mixed-oxide fuels.

67. W. E. Roake, C. E. Weber, D. H. Wiese, C. S. Caldwell, I. D. Thomas, J. L. Scott, and A. B. Shuck, "The United States Program for Developing the Manufacture of High-Quality Fast Reactor Fuels," pp. 311-25 in *Peaceful Uses of Atomic Energy, Proc. 4th Int. Conf., Geneva, 1971*, Vol. 8, United Nations, New York, and International Atomic Energy Agency, Vienna, 1972.

68. W. L. Lyon, C. M. Ryer, and C. N. Craig, "Laboratory-Scale Preparation of Plutonia-Urania Fast Reactor Fuel," pp. 59-63 in *Preparation of Nuclear Fuels, Nucl. Eng. Part 18*, Vol. 63, American Institute of Chemical Engineers (1967).

69. C. S. Caldwell and I. D. Thomas, "Plutonium-Uranium Mixed Oxide Preparation and Fabrication Experience," pp. 147-55 in *Preparation of Nuclear Fuels, Nucl. Eng. Part 18*, Vol. 63, American Institute of Chemical Engineers (1967).

We conclude that the gamma and neutron radiation from plutonium, recycled from both light-water reactors and LMFBR's, will require substantial shielding in commercial-scale operation, and automation should be used.

6.3.3 Fuel Element Hardware

Because of the stringent service conditions expected for the diverse hardware contained in LMFBR fuel elements, it is necessary that detailed attention be given to the metallurgical characteristics of the materials used and to strict quality assurance procedures for the manufacture of such materials. Roake^{5,8} has reported the progress of the FFTF hardware procurement program in obtaining increased levels of quality, and this improvement can be expected to continue as industrial experience is gained. The commercial application of LMFBR's will require the continual assessment of the technology of the structural materials, since developments can be expected leading to cladding materials, for example, with less susceptibility to chemical attack by the fuel and less susceptibility to swelling. It should also be noted that the hardware costs, particularly for tubing, account for a substantial part of the fuel fabrication costs, and, therefore, economies in processing suitable tubing and other hardware must be obtained if the goal of a competitive LMFBR is to be reached. In fact, the fuel element hardware can account for more than 50% of the total costs of manufacturing LMFBR core axial blanket fuel elements.

6.3.4 Recommendations

Optional methods for commercial fabrication and refabrication of fuel must be based on assessment of the

relative performance of alternative fuel structures and the economics of the fabrication processes that produce those structures, taking into consideration that shielded facilities are required. Thus, in the final analysis, irradiation data and process cost for mechanically blended pellets, coprecipitated pellets, and Sphere-Pac materials should be compared. At present there are substantial data on pellet routes, both from the standpoint of processing cost and fuel performance; but the Sphere-Pac process has had only limited application, and the irradiation results on such material, while promising, are not comprehensive. It should be particularly noted that close attention should be given to methods by which process cost can be reduced by selection of different fuel design. In addition, improvements in the economical production of LMFBR fuel tubing would have a substantial impact on future costs, as would develop of fuel structure and design that would allow the attainment of the maximum burnups and heat rates required for competitive LMFBR's.

Refinement and improvement of the tools for evaluation are needed in the areas of fuel performance and

cost analysis. Such improvements must necessarily await the results of experimental work and of products from a larger-scale process system. Nevertheless, a continuous effort to incorporate new models, data, and information into the evaluation activity is essential. Such continuous interaction will assure maximum relevancy of the LMFBR fuel design and development work and help attain the optimum system for fuel design, management, and processing. This approach may appear expensive and redundant now, but it will pay off in the future in better understanding of a complicated system.

Analytical treatment of the important problem of cladding attack cannot reach meaningful conclusions without better thermodynamic data. The question of oxygen potential in an operating fuel pin cannot be answered without knowledge of the oxygen affinity of rare-earth fission products. Work on this topic was initiated, but the program was terminated before meaningful results could be obtained.

7. Summary, Conclusions, and Recommendations

This chapter summarizes the work conducted at ORNL and the conclusions drawn from that work. Recommendations are given at the end of the chapter on future work involving fast breeder reactor fuels in general and specifically certain aspects of the ORNL Fast Breeder Reactor Oxide Fuel Program.

7.1 SUMMARY AND CONCLUSIONS OF RESEARCH AND DEVELOPMENT

Oak Ridge National Laboratory has conducted the Oxide Fuel Development Program for a period of five years with the objectives of: (1) establishing the performance characteristics and limitations of (U,Pu)O₂ fuels fabricated by different processes; (2) obtaining a fundamental understanding of the mechanisms involved in the irradiation behavior of fuel elements incorporating these fuels; (3) developing fabrication techniques that provide both economy and product with optimized fuel performance; and (4) developing analytical models adequate to optimize experimental design and to predict fuel element response to LMFBR conditions. Funding for the program was terminated June 30, 1972, a time when partial progress toward meeting these ultimate objectives had been obtained.

The program has included development for fabrication of fuel with different structures, characterization of these structures by out-of-reactor methods, determination of irradiation performance, and analytical mathematical modeling of fuel behavior to enable prediction of LMFBR fuel performance. A comprehensive effort was made to develop and apply quality assurance procedures to the development work and to the irradiation tests. The facilities and equipment were designed and constructed at the beginning of the program. Critical-path methods were used successfully to schedule and coordinate all aspects of the program.

Sol-gel technology was used to prepare small quantities of (U,Pu)O₂ microspheres and powder for fabrication of fuel pellets. In addition, mechanically blended oxide material was used in certain aspects of the

program. Each fuel form to be irradiated was characterized with complete microstructural, x-ray diffraction, and chemical analyses to assure a better understanding of its irradiation performance. Substantial effort was made to improve fuel characterization procedures and methods. The purpose of the irradiation testing of oxide fuels was to compare the performance of the various fuel forms and to obtain basic information on the effects of the irradiation on (U,Pu)O₂ fuels and fuel-cladding interactions. The irradiation test program used thermal reactors and fast-flux facilities as well as the TREAT facility for transient tests. In the analysis of fuel element performance, the objective was to develop an adequate computer model and to integrate mathematically various aspects of the oxide fuels development program in such a way that fundamental understanding of the behavior of LMFBR fuel elements could be obtained.

By way of summarizing conclusions concerning the program, it may be fairly stated that adequate methods were shown on a laboratory scale for preparation of the appropriate materials for both Sphere-Pac and sol-gel pelletized fuel. Significant contributions were made to the procedures for fabricating high-quality (U,Pu)O₂ fuel, particularly in the areas of control of absorbed gases and control of oxygen-to-metal ratio. The irradiation test program showed that Sphere-Pac and pellet fuels perform similarly in transient situations, and some advantages to the use of Sphere-Pac types of fuel are indicated for steady-state operation. In the description of fuel performance, through mathematical modeling a workable computer code was developed and successfully applied to the analysis of fuel pin behavior under varied conditions.

The following are summaries and conclusions in various functional areas of the work.

7.1.1 Fuel Preparation

Fuel material for the program was prepared by mixing UO₂ sols with PuO₂ sols to give the desired uranium-to-

plutonium ratio. The mixed sol was then either formed into microspheres for use in Sphere-Pac fuel studies or dried to form shards, which were used to prepare powder for use in fuel pellet studies. The UO_2 sols were prepared by the concentrated urania sol preparation (CUSP) process. This is a process for batch preparation of 1 to 1.4 M crystalline urania sol directly by solvent extraction.

The sols prepared by the CUSP process have exhibited better reproducibility and longer shelf life than urania sols prepared by other methods. Plutonia sols were prepared from aqueous $\text{Pu}(\text{NO}_3)_4$ according to the standard ORNL precipitation-peptization flowsheet. Sols prepared in this manner were typically stable over long periods of time. Microspheres were prepared by dispersion of sol into drops and suspension of the sol drops in an organic liquid, usually 2-ethyl-1-hexanol, while water is extracted to cause gellation. Microspheres are then dried and fired at controlled conditions to remove volatiles. Sol-gel powder was prepared by blending UO_2 and PuO_2 sols, drying these at about 100°C to form shards, and then grinding to -325 mesh in a fluid energy mill. Methods were developed for forming an active ceramic-grade powder for preparation of pellets.

The work accomplished to date represents laboratory-scale development and indicates that adequate methods are available for preparation of the fuel materials required for fabrication of Sphere-Pac and sol-gel pelletized fuel.

7.1.2 Fabrication Development

The fabrication development work included methods for packing microspheres of $(\text{U,Pu})\text{O}_2$ and for forming pellets from sol-gel precursor materials. In addition, work was done to control sorbed gases in $(\text{U,Pu})\text{O}_2$ fuels and to adjust oxygen-to-metal ratios. Sequential loading of coarse and then fine fractions of oxide microspheres produced packing densities near 84%. A refinement of the Sphere-Pac process was development of the U-Fines method, which is a method for loading in which all the plutonium is contained in coarse microspheres, and the fine fraction consists of pure UO_2 . We also demonstrated that the U-Fines method can be used in conjunction with pellets in any of the blanket regions or core regions of the fuel pin.

We developed fabrication methods for pelletizing sol-gel precursor materials at controlled densities from 83 to 97% of theoretical. Proper combinations of powder activity, pressing procedure, and sintering conditions were determined to give controlled densities

over this large range. Some work was done to form fuel bodies or pellets through extrusion of sol-gel-derived clays. Although we had experimental difficulties with the method, experience with thorium-base sol-gel extrusions indicates that the process can be made applicable to the fabrication of urania-base reactor fuels.

In our study of oxygen-to-metal ratio (O/M), the kinetic analysis and experimental data show that reduction by carbon monoxide is much quicker than by flowing hydrogen. Also much lower O/M's can be achieved than are practical with hydrogen. Procedures were also developed for reduction of sorbed gas, primarily by controlling the atmosphere during cooling of the fuel after O/M adjustment. Experimental work showed that high sorbed gas contents were due to the reabsorption of hydrogen upon cooling, and that this could be prevented by cooling in pure argon.

We conclude that satisfactory methods have been developed on the laboratory scale for Sphere-Pac in various modes and for preparation of pellets using sol-gel material. Also, good control of sorbed gases and O/M can be obtained through careful selection and control of the sintering atmosphere. The use of the U-Fines method of Sphere-Pac may have advantages by decreasing the amount of fine plutonium-bearing materials in fuel fabrication plants, either through the use of plutonium-bearing coarse microspheres or by elimination of the need for grinding by the use of UO_2 fines in the gap between the fuel pellet and the cladding.

7.1.3 Fuel Characterization

For oxygen-to-metal determinations, a thermal gravimetric method was used, and our statistics show that 80% of the samples follow a normal distribution, whose standard deviation is about 0.003 O/M unit, but the remainder of the samples deviate significantly from this distribution.

Moisture was determined with a commercial instrument using a current integrator on a P_2O_5 electrolytic cell. The standard deviation was 12.6 ppm for samples averaging 33 ppm. By enclosing the instrument and sample bottle in a plastic bag purged with argon, the standard deviation was reduced to 3.2 ppm on samples averaging 18 ppm moisture.

Precision of the absorbed gas analytical technique was significantly improved by reducing the background in the apparatus from approximately $0.25 \text{ cm}^3/\text{g}$ to the range of 0.001 to $0.005 \text{ cm}^3/\text{g}$. Other techniques such as mass spectrographic analyses for determination of isotopic distribution, optical microscopy, replica electron microscopy, electron microprobe analysis, and

alpha autoradiography were used to characterize the fuel.

Our work in determination of the structure of sol-gel-derived $(U,Pu)O_2$ showed that microspheres and pellets prepared by the sol-gel technique are typically single-phased and homogeneous in composition. The grain size is usually in the range of 1 to 5 μm . Typically the coarse microspheres have densities greater than 95% of theoretical. Fine microspheres are essentially theoretically dense. Low-density cold-pressed and sintered pellets have a triplex microstructure consisting of high-density and medium-density islands in a porous matrix. High-density pellets have a more uniform pore distribution.

In conclusion, analytical techniques suitable for characterization of $(U,Pu)O_2$ fuels were developed, and, although improvements are indicated in certain areas, the techniques are believed to be adequate for preirradiation characterization of $(U,Pu)O_2$ fuels.

7.1.4 Irradiation Program

Sol-gel-derived $(U,Pu)O_2$ fuels were tested in steady-state thermal and fast-flux tests and in the TREAT facility. Both pelletized and Sphere-Pac structures were tested. Some of the results of these tests are as follows.

Instrumented tests in the ORR Poolside Facility provided data that indicated that the gap conductance for Sphere-Pac fuel at linear heat rates up to 16 kW/ft and at burnup levels up to 6% FIMA is approximately twice that of pellet fuels under similar conditions. Thus, the thermal performance of Sphere-Pac fuels should permit as much as 110% of the linear heat rate of pellet fuels while maintaining the same fuel center temperature.

Fuel restructuring has an appreciable effect on fuel operating temperature, and the Sphere-Pac fuel tests showed that the primary mode of restructuring at high temperature is a vaporization-condensation mechanism. The kinetics of restructuring was not fully defined, but postirradiation examinations have shown a distinct time dependence. The principal structural changes occurred early in the irradiation experience of the fuel, but some structural changes occurred at higher burnup levels. Another important observation regarding structure is that high-burnup (approx 10% FIMA) fuel columns in a thermal reactor test all decreased in length from 1.2 to 4.2%, with the amount of shrinkage increasing with peak linear heat rate (temperature) and decreasing with the initial fuel smear density, as would be expected for a sintering process.

The movement of actinides and fission products in the fuel has significant effects on the performance

characteristics of the fuel. Our tests showed clear evidence of the preferential movement of uranium down the temperature gradient in the columnar grain growth regions (temperature $> 1650^\circ C$). This caused a concentration of plutonium in the region near the central void, lowering the permissible linear heat rate of $(U,Pu)O_2$ fuels by as much as 2.5 kW/ft. A secondary effect of this change in actinide distribution has been seen in fuel reprocessing studies, where the higher plutonium content fuels are less soluble in nitric acid and may require a secondary dissolution step with a fluoride addition to the solvent. Concurrent with actinide redistribution is a redistribution of oxygen, which can affect the form of fission product inclusion in the fuel structure and also the fuel-cladding chemical interaction. The effect of oxygen potential on the form of the fission product molybdenum was clearly seen in the uninstrumented high-burnup EBR-II tests, where the molybdenum in a metallic inclusion decreased with location from the center of the fuel to the cladding. There was evidence of molybdenum migration down the temperature gradient, but it was incorporated in the oxide at the lower temperatures. We observed distinct accumulations of barium and ruthenium at the higher-temperature fuel regions, and molybdenum, cesium, and tellurium in the fuel adjacent to the cladding.

Electron microscopy of irradiated $(U,Pu)O_2$ gave strong evidence that intergranular pores as large as 0.2 μm in diameter do not disappear during irradiation. There were indications that fission gas bubble migration and coalescence were influenced by movement of columnar grain boundaries perpendicular to the thermal gradient as well as by the presence of subgrains within the equiaxed grain region.

Although several mechanisms of fuel-cladding mechanical interaction can be postulated, experiments to date have not provided any evidence for significant mechanical deformation that can be attributed to such interaction: most of the fuel pins had smear densities less than 85%, and the majority of the burnup levels had been less than 50,000 MWd/ton, a combination of conditions under which General Electric investigators have also reported no significant mechanical interactions. We have also noted two cases where plastic deformation of the cladding occurred. In the transient tests on unirradiated Sphere-Pac fuel, there was metallographic evidence of spheres being forced against the cladding by differential thermal expansion during the rapid power excursion. The second observation, though not clearly defined, occurred in the EBR-II series I pins.

Chemical interactions between the fuel and stainless steel cladding have been repeatedly observed by a

number of experimenters at temperatures as low as 500°C and burnup levels in excess of 3 to 5% FIMA. The only significant fuel-cladding chemical interaction with Sphere-Pac fuels seen in the ORNL irradiation test program was in the high-burnup instrumented thermal flux test, and here the Sphere-Pac fuel showed about half the attack seen in a companion pin with pellet fuel. A similar result with no attack for Sphere-Pac fuel and some attack for pellet fuel was seen in the ORR thermal performance test. Although the improved performance of Sphere-Pac fuel with respect to fuel-cladding chemical interaction has not been proven incontrovertibly, the evidence overwhelmingly supports this conclusion. In every test examined to date, the Sphere-Pac fuel has shown less reaction.

In the chemical interactions between fuel and stainless steel cladding, two types of oxidation have been seen by various observers: (1) a general or matrix oxidation with a buildup of a significant surface oxide layer and more or less uniform reduction in wall thickness, and (2) an intergranular attack, which is often only in localized areas but which proceeds to significant depths. One interesting result in cursory out-of-reactor oxidation studies conducted as an adjunct to the ORNL irradiation program was that both types of attack could be developed in the absence of both fission products and fuel. The type of attack in these tests was related to the morphology of the carbide ($M_{23}C_6$) structure.

Reaction mechanisms to explain the presence of matrix attack and intergranular attack have been postulated. Our conclusion is that oxygen activity is the primary variable in fuel-cladding reactions, that the temperature is important, particularly for the intergranular attack, and finally that the cladding is a very important part of the reaction, with intergranular attack varying from one lot to another, depending on as yet undefined variations in composition and/or fabrication history that can affect carbide morphology.

7.1.5 Fuel Performance, Process, and Economic Evaluations

The performance and economic evaluation studies were conducted primarily to optimize the design of oxide fuel pins for fast breeder reactors. The fuel model computer code, FMODEL, was written to predict the in-reactor performance of a single LMFBR fuel pin consisting of pelletized oxide fuel clad with stainless steel. The basic economic code was for fuel fabrication (FABCOST-9 computer code). In the program, we hoped that the behavior models would be capable of accurately predicting the useful lifetime of a fast

reactor fuel pin. Availability of such predictions would permit trade-off studies to be made to select a fuel pin design that would result in minimum fuel cycle costs consistent with achievement of desired burnup levels.

The FMODEL fuel pin performance code has proven to be a valuable tool for planning and design of irradiation experiments and interpretation of data from the experiments. The code contains models to describe most of the phenomena known to occur in an operating fuel pin. Some of the models are derived from first principles, whereas others are empirical or semi-empirical. The overall calculational framework is logically and efficiently laid out so that individual models can be replaced when more sophisticated analytical models become available. The code has been able to reasonably reproduce experimental measurements without the use of adjustable parameters to force-fit code predictions to experimental observations.

In addition to development of the integrated model, at the termination of the program we were working on thermodynamic considerations and fuel behavior but did not have the opportunity of incorporating in FMODEL a large number of the thermodynamic effects. These studies emphasized kinetics of intergranular attack, type of reaction layers, mechanisms of cladding transport, oxygen buildup in mixed-oxide fuel, and oxygen gradients in mixed-oxide fuels.

In our economic studies we compared the cost of fabricating fuel by three principal routes for preparation of pellets and also compared the cost of Sphere-Pac and pellet flowsheets. We have not observed a substantial difference in the economics of the various preparation procedures; any differences calculated probably lie within the error of the estimates. In addition, we investigated the effect of plant scale, various hardware costs, and other variables on fabrication costs for LMFBR fuel. The conclusion is that hardware costs contribute in large proportion to the total cost for fabricating LMFBR fuel and that significant attention should be given to methods of reducing the cost of fuel element hardware, particularly tubing.

7.2 RECOMMENDATIONS FOR FUTURE WORK

For the future, our recommended approach is to consider LMFBR fuel technology from the standpoint of a complete system consisting of such components as fuel behavior, fuel element design, and fuel cycle processes. The purpose should be to develop comprehensive data and technology to enable optimization of the fuel system from the standpoint of performance and cost variables, with the final decision being based

on cost effectiveness. This requires additional information in specific technological areas, and experience must be gained with larger-scale systems in order to assess economic alternatives. The following are recommendations in specific areas in which we have been involved.

7.2.1 Fuel Preparation

For full assessment of the economic capability of the sol-gel processes, data must be obtained on engineering-scale demonstrations of technology for preparation of $(U,Pu)O_2$ coarse microspheres and $(U,Pu)O_2$ powder for fuel pellets. Whether this should be done depends on results from the continuing irradiation program and a comparison of these results with results obtained with conventional pellet technology. Adequate UO_2 technology exists on an engineering scale to permit an economic assessment of sol-gel UO_2 processes.

If the irradiation program and thermodynamic analyses indicate that additional control of fuel composition or additional buffers or additives are needed to control chemical activity of the fuel, laboratory-scale work will be required to establish the processes and analytical procedures necessary to assure a fuel of sufficient quality. Should derivation of ceramic-grade powder by the sol-gel process be desired, engineering-scale work will be needed to determine the precise flowsheet for preparation of highly reproducible powder. In addition, engineering-scale work will be required to demonstrate suitable equipment and techniques for semiremote or remote operation, which will be required for fabrication of LMFBR fuels using recycle plutonium from light-water reactors or recycle fuel from LMFBR's.

7.2.2 Fuel Fabrication

As previously noted, conduct of additional fabrication work based on sol-gel-derived $(U,Pu)O_2$ materials depends on the outcome of the current irradiation program and the comparison of the results with behavior of more conventional fuels. Should the performance of sol-gel fuels indicate additional interest for the future, work in additional areas will be needed to develop fabrication methods adequately for pilot-plant-scale work or for commercial application. For loading Sphere-Pac fuels we would need to further optimize the particle distributions to accelerate the rate of loading individual fuel pins. In addition, for semiremote or remote application, we would need to design and develop suitable devices for handling and accurately dispensing fuel microspheres. A great amount of the technology being developed in the National HTGR

Recycle Development Program would be applicable to this particular need, since in both cases the problems are handling, dispensing, and control of a microsphere product.

Should an interest develop in sol-gel-derived pellets, additional studies of pressing and sintering phenomena will be needed to determine the optimum procedure for fabricating $(U,Pu)O_2$ pellets. The object of this work would be to optimize such a process from the standpoint of economics and to obtain a microstructure that is stable under normal conditions.

It is highly recommended that in future sintering treatments attention be given to the use of the $CO-CO_2$ system for adjusting the oxygen-to-metal ratios and that an inert atmosphere be used for cooling substoichiometric fuel to ambient temperature.

7.2.3 Fuel Characterization

Although a substantial amount of work was done on fuel characterization, we feel that fuel technology would profit by additional emphasis on methods for analyzing and characterizing fuels. In particular, we were never completely satisfied with the thermogravimetric technique for determination of oxygen-to-metal ratio and would recommend that a galvanic-cell oxygen determination be pursued, as this determination will measure the actual oxygen potential in the fuel and should be rapid and relatively inexpensive. Another analysis that can be very difficult is that for trace elements. The cause of the danger is cross-contamination from other samples. We recommend that halide determinations be performed in an area that is completely isolated from other analyses. We also recommend that in determining metallic impurities, detailed attention be given to sample preparation, since we observed that direct analysis of small solid samples is not satisfactory because metallic impurities can form inclusions, which will cause a wide spread in results. Mass spectrographic analysis of a solution of the sample is recommended.

7.2.4 Irradiation Program

As a minimum, we recommend that the irradiations existing at the termination of this program be continued in the EBR-II for their planned completion and that examinations be conducted. This will allow an assessment of the performance capability of the sol-gel-derived fuels and a comparison of these fuels with more conventional fuel forms. Whether any future program is to be conducted on sol-gel-derived material would

depend to a great extent upon the results of examinations of the EBR-II tests. Should there be continuing or additional interest in sol-gel-derived fuels, it will, of course, be necessary to conduct tests on a more statistical basis in order to obtain confidence with the system.

Recommendations concerning specific experiments are as follows:

1. A thermal cycling experiment should be conducted to determine any mechanical interacting effects that may occur during cycling operations. Center-line and cladding thermocouples are suggested to monitor the kinetics of sintering, restructuring, and gap conductance changes. It would be desirable to compare pellets and Sphere-Pac fuels and to investigate the effect of thermal cycling on a range of initial densities and fabrication techniques.

2. Transient tests should be conducted on selected EBR-II series II pellet and Sphere-Pac pins, as these tests would supplement transient tests of unirradiated pins.

3. EBR-II tests should be conducted with plutonium and natural or depleted uranium, since the amount of oxygen used by oxide-forming fission products is significantly greater in the case of ^{235}U fuel than in the case of plutonium fuel because of the important difference in fission product distribution. Since all EBR-II fuel pins to date have contained enriched $(^{235}\text{U},\text{Pu})\text{O}_2$, the chemical interactions between fuel and cladding could have been substantially less than what could occur when one irradiates natural or depleted uranium-plutonium oxide fuels.

4. Work should be continued on the out-of-reactor chemical interaction studies to investigate the effect of cold work and composition of cladding on such phenomena as general matrix attack and intergranular

attack. This type of experimentation is inexpensive and can provide valuable data for interpretation of irradiation results.

7.2.5 Fuel Performance, Process, and Economic Evaluations

We recommend that one integral group be charged with the task of continuing to refine and improve the tools for evaluation of both fuel performance and fuel economics. A continuous effort to incorporate new models, data, and information concerning fuel performance and process technology is essential, since such continuous interaction will ensure maximum relevancy of the LMFBR fuel design and development work and help obtain the most optimum system for fuel design, management, and processing.

Although many data are needed in other areas and must await the results of ongoing experimental work in other programs, we would like particularly to suggest that better thermodynamic data should be obtained so that the problems associated with compatibility between fuel and cladding can be assessed in a meaningful way. For example, the question of oxygen potential in operating a fuel pin cannot be answered without knowledge of the oxygen activity of the rare-earth fission products. A full set of such data is not now available.

Finally, we recommend that fuel performance and economic models attempt to incorporate statistical variations in the properties of the materials used and in the processes used. Such an approach will yield insight into variations that reduce substantially the maximum performance rating of LMFBR fuels or reduce their economic potential.

8. Publications and Documents

Listed chronologically below are the various topical reports, papers, and publications of the program. Also included is a list of unpublished quality assurance documents used internally at ORNL for conduct of the work.

8.1 TOPICAL REPORTS AND PAPERS

- T. N. Washburn, A. L. Lotts, and F. E. Harrington, *Comparative Evaluation of Sol-Gel Fuel Fabrication Costs*, ORNL-TM-1979 (September 1967).
- R. B. Fitts, A. R. Olsen, and J. Komatsu, "Sphere-Pac Fabrication of Sol-Gel Nuclear Fuels" (Abstract), *Amer. Ceram. Soc. Bull.* **47**(9), 844 (September 1968).
- F. G. Kitts, R. B. Fitts, and A. R. Olsen, "Sol-Gel Urania-Plutonia Microsphere Preparation and Fabrication into Fuel Rods," pp. 195–210 in *Intern. Symp. Plutonium Fuels Technol., Scottsdale, Ariz., 1967*, *Nucl. Met.* **13**, ed. by K. E. Horton, R. E. Macherey, and R. J. Allio, American Institute of Mining, Metallurgical and Petroleum Engineers, New York, 1968.
- A. R. Olsen, J. D. Sease, R. B. Fitts, and A. L. Lotts, "Fabrication and Irradiation Testing of Sol-Gel Fuels at Oak Ridge National Laboratory," pp. 321–67 in *Sol-Gel Processes for the Production of Ceramic Fuels*, Comitato Nazionale Energia Nucleare, Rome, 1968.
- T. N. Washburn, A. L. Lotts, and F. E. Harrington, "Comparative Evaluation of Sol-Gel Fuel Fabrication Costs," pp. 381–426 in *Sol-Gel Processes for the Production of Ceramic Fuels*, Comitato Nazionale Energia Nucleare, Rome, 1968.
- C. M. Cox and F. J. Homan, *PRØFIL – A One-Dimensional FØRTRAN IV Program for Computing Steady-State Temperature Distributions in Cylindrical Ceramic Fuels*, ORNL-TM-2443 (March 1969).
- K. E. Spear, A. R. Olsen, and J. M. Leitnaker, *Thermodynamic Applications to (U,Pu)O_{2+x} Fuel Systems*, ORNL-TM-2494 (April 1969).
- C. M. Cox and F. J. Homan, *PRØFIL – A One-Dimensional FØRTRAN IV Program for Computing Steady-State Temperature Distributions in Cylindrical Ceramic Fuels*, ORNL-TM-2443, Addendum (August 1969).
- C. M. Cox, "The Irradiation Performance of Uranium-Plutonium Mixed Oxide Fuel Pins," *Nucl. Safety* **10**(5), 380–91 (Sept.–Oct. 1969).
- R. A. Bradley and J. D. Sease, "Fabrication of (Pu,U)O₂ Pellets by the Sol-Gel Process" (Abstract), *Amer. Ceram. Soc. Bull.* **48**(9), 884 (September 1969).
- A. R. Olsen, R. B. Fitts, and C. M. Cox, *Analysis of the Validity of Fast Reactor Fuel Tests in Existing Test Reactors*, ORNL-TM-2716 (October 1969).
- C. M. Cox and F. J. Homan, "Analysis of Mixed Oxide Fuel Pin Performance Using the FMØDEL Computer Code" (Summary), *Trans. Amer. Nucl. Soc.* **12**(2), 536–37 (November 1969).
- A. R. Olsen, C. M. Cox, and R. B. Fitts, "Low Burnup Irradiation Tests of Sphere-Pac Sol-Gel (U,Pu)O₂ Fuels" (Summary), *Trans. Amer. Nucl. Soc.* **12**(2), 605–6 (November 1969).

- A. R. Olsen, R. B. Fitts, and C. M. Cox, "Analysis of the Validity of Fast Reactor Fuel Tests in Existing Test Reactors," pp. 127--50 in *National Symposium on Developments in Irradiation Testing Technology held at Sandusky, Ohio, September 9--11, 1969*, CONF-690910.
- F. E. Harrington, R. W. Horton, R. B. Pratt, and J. D. Sease, *Cost Study of Four Alternate Routes for LMFBR Fuel Material Preparation and Element Fabrication*, ORNL-TM-2813 (February 1970).
- A. R. Olsen, *Experiment Description and Hazards Evaluation for the Series I ORNL Oxide Fuels Irradiation in EBR-II*, ORNL-TM-2635 (April 1970).
- C. M. Cox, A. R. Olsen, R. B. Fitts, and A. L. Lotts, "Irradiation Performance of Sol-Gel (U,Pu)O₂ Fuels for Breeder Reactors," pp. 359--73 in *Symposium on Sol-Gel Processes and Reactor Fuel Cycles, Gatlinburg, Tennessee, May 4--7, 1970*, CONF-700502.
- J. D. Sease, R. A. Bradley, C. R. Reese, W. H. Pechin, and A. L. Lotts, "Sphere-Pac and Pelletization of (U,Pu)O₂," pp. 323--41 in *Symposium on Sol-Gel Processes and Reactor Fuel Cycles, Gatlinburg, Tennessee, May 4--7, 1970*, CONF-700502.
- A. R. Olsen and F. J. Homan, *Experiment Description and Hazards Evaluation for the Series I ORNL Oxide Fuels Irradiation in EBR-II*, ORNL-TM-2635 (Supplement) (June 1970).
- A. R. Olsen, "Intermediate-Burnup Irradiation Tests of Sphere-Pac Sol-Gel Fuels" (Summary), *Trans. Amer. Nucl. Soc.* **13**(1), 32--33 (June 1970).
- W. L. Moore, M. K. Preston, and J. D. Sease, *Fabrication of ORNL Series I Irradiation Test Capsules for Experimental Breeder Reactor II*, ORNL-TM-2922 (July 1970).
- C. M. Cox and F. J. Homan, "Performance Analysis of a Mixed-Oxide LMFBR Fuel Pin," *Nucl. Appl. Technol.* **9**(3), 317--25 (September 1970).
- C. M. Cox, E. J. Manthos, and D. R. Cuneo, "Transient Performance of Sol-Gel (U,Pu)O₂ Sphere-Pac and Pellet Fuels" (Summary), *Trans. Amer. Nucl. Soc.* **13**(2), 653--54 (November 1970).
- R. B. Fitts, V. A. DeCarlo, E. L. Long, Jr., and A. R. Olsen, "Thermal Performance and Restructuring of Pellet and Sphere-Pac Fuels" (Summary), *Trans. Amer. Nucl. Soc.* **13**(2), 549--51 (November 1970).
- F. J. Homan, "Fuel-Cladding Mechanical Interaction During Startup" (Summary), *Trans. Amer. Nucl. Soc.* **13**(2), 576--77 (November 1970).
- B. R. Dewey, *Discrete Element Analysis of the Creep of Stainless Steel Tubing for LMFBR Application*, ORNL-TM-3294 (March 1971).
- C. M. Cox, D. R. Cuneo, and E. J. Manthos, "Performance of Sphere-Pac and Pelletized (U,Pu)O₂ During Severe Overpower Transients" (Summary), *Trans. Amer. Nucl. Soc.* **14**, Suppl. 1, 31--33 (April 1971).
- F. J. Homan, W. H. Bridges, W. J. Lackey, and C. M. Cox, "Comparison of FMØDEL Predictions with EBR-II Irradiation Data" (Summary), *Trans. Amer. Nucl. Soc.* **14**, Suppl. 1, 8--10 (April 1971).
- T. B. Lindemer and R. A. Bradley, *Kinetic Models for the Synthesis of (U,Pu)O_{2-y} by Hydrogen-Reduction and Carbothermic Techniques*, ORNL-TM-3358 (April 1971).
- A. R. Olsen, R. B. Fitts, and W. J. Lackey, "In-Reacto Restructuring Temperatures and Kinetics for (U,Pu)O₂" (Summary), *Trans. Amer. Nucl. Soc.* **14**, Suppl. 1, 24--25 (April 1971).
- F. J. Homan, W. J. Lackey, and C. M. Cox, *Comparison Between Predicted and Measured Fuel Pin Performance*, ORNL-TM-3386 (May 1971).
- W. E. Stillman, *TRANS -- A One-Dimensional FØRTRAN IV Program for Computing the Time Response of Fuel Rods to a Loading-Unloading Environment*, ORNL-TM-3293 (May 1971).
- C. M. Cox, A. R. Olsen, R. B. Fitts, and E. L. Long, Jr., "Fuel-Cladding Chemical Interactions in Low-Density (U,Pu)O₂ Fuel Pins" (Summary), *Trans. Amer. Nucl. Soc.* **14**(1), 173--75 (June 1971).
- W. J. Lackey, A. R. Olsen, J. L. Miller, Jr., and D. K. Bates, "Actinide Redistribution in Irradiated (U,Pu)O₂" (Summary), *Trans. Amer. Nucl. Soc.* **14**(1), 180--82 (June 1971).

- W. J. Lackey, R. A. Bradley, W. H. Pechin, and T. L. Hebble, *Statistical Technique for Determining Sources of Variation in (U,Pu)O₂ Oxygen-to-Metal Ratio*, ORNL-TM-3362 (June 1971).
- J. M. Leitnaker, J. P. De Luca, and R. B. Fitts, "Influence of Burnup on Reactivity of Oxide Fuel with Cladding" (Summary), *Trans. Amer. Nucl. Soc.* **14**(1), 177 (June 1971).
- C. M. Cox, D. R. Cuneo, and E. J. Manthos, *Performance of Sphere-Pac and Pelletized (U,Pu)O₂ During Severe Overpower Transients*, ORNL-TM-3384 (July 1971).
- A. R. Olsen, R. B. Fitts, and W. J. Lackey, *In-Reactor Restructuring Temperatures and Kinetics for (U,Pu)O₂*, ORNL-TM-3387 (July 1971).
- F. J. Homan, *Oak Ridge National Laboratory Solutions to a Modeling Round-Robin Exercise*, ORNL-TM-3360 (August 1971).
- F. J. Homan, *A Parametric Analysis of Fuel-Cladding Mechanical Interactions*, ORNL-TM-3508 (August 1971).
- F. J. Homan, "Use of a Fuel Performance Model to Analyze Materials Data" (Summary), *Trans. Amer. Nucl. Soc.* **14**(2), 629 (October 1971).
- A. R. Olsen, "Sol-Gel Sphere-Pac (U,Pu)O₂ Fuel Performance in EBR-II Irradiation Tests" (Summary), *Trans. Amer. Nucl. Soc.* **14**(2), 596-98 (October 1971).
- A. R. Olsen et al., *Preirradiation Data for ORNL Series H and B & W Oxide Fuel Tests in EBR-II*, ORNL-TM-3446 (November 1971).
- C. M. Cox and R. E. Adams, *Safety Analysis and Test Specifications for Transient Tests of Sol-Gel (U,Pu)O₂ Fuel Pins (ORNL Series I)*, ORNL-TM-3574 (December 1971).
- W. J. Lackey and R. A. Bradley, *Microstructure of Sol-Gel-Derived (U,Pu)O₂ Microspheres and Pellets*, ORNL-TM-3588 (December 1971).
- T. B. Lindemer and R. A. Bradley, "Kinetic Models for the Synthesis of (U,Pu)O₂ by Hydrogen-Reduction and Carbothermic Techniques," *J. Nucl. Mater.* **41**(3), 293-302 (December 1971).
- C. M. Cox, D. R. Cuneo, and E. J. Manthos, "Performance of Sphere-Pac and Pelletized (U,Pu)O₂ During Severe Overpower Transients," pp. 701-24 in *Proc. Conf. Fast Reactor Fuel Element Technology*, ed. by Ruth Farmakes, American Nuclear Society, Hinsdale, Illinois, 1971.
- F. J. Homan, C. M. Cox, and W. J. Lackey, "Comparisons Between Predicted and Measured Fuel Pin Performance," pp. 243-58 in *Proc. Conf. Fast Reactor Fuel Element Technology*, ed. by Ruth Farmakes, American Nuclear Society, Hinsdale, Illinois, 1971.
- A. R. Olsen, R. B. Fitts, and W. J. Lackey, "In-Reactor Restructuring Temperatures and Kinetics for (U,Pu)O₂," pp. 579-602 in *Proc. Conf. Fast Reactor Fuel Element Technology*, ed. by Ruth Farmakes, American Nuclear Society, Hinsdale, Illinois, 1971.
- R. B. Fitts, J. L. Miller, Jr., and E. L. Long, Jr., *Observations on Tungsten-Rhenium Thermocouples Used In-Reactor in (U,Pu)O₂ Fuel Pins*, ORNL-TM-3617 (February 1972).
- R. A. Bradley and J. D. Sease, "The Design and Operation of a Plutonium Laboratory," *Nucl. Mater. Manage.* **1**(1), 11-14 (April 1972).
- W. J. Lackey, R. A. Bradley, W. H. Pechin, and T. L. Hebble, "Precision and Source of Variation of Oxygen-to-Metal Determinations for (U,Pu)O₂," *Nucl. Technol.* **13**(4), 105-7 (April 1972).
- R. B. Fitts and F. L. Miller, "Analysis and Performance of Instrumented Fuel Pins" (Summary), *Trans. Amer. Nucl. Soc.* **15**(1), 180 (June 1972).
- F. J. Homan, "Influence of Materials Data Uncertainty on Fuel Pin Performance Predictions" (Summary), *Trans. Amer. Nucl. Soc.* **15**(1), 183-84 (June 1972).
- W. J. Lackey and R. A. Bradley, *Microstructure of Sol-Gel-Derived (U,Pu)O₂ Microspheres and Pellets*, ORNL-TM-3588 (December 1971); also *Nucl. Technol.* **14**(6), 257-68 (June 1972).
- J. M. Leitnaker and K. E. Spear, *Elimination of CO₂ and H₂O as Oxygen Transport Species in Mixed Oxide Fuel Pins*, ORNL-TM-3849 (June 1972).

- A. R. Olsen, "High-Burnup Irradiation Tests of Sphere-Pac Sol-Gel Fuels" (Summary), *Trans. Amer. Nucl. Soc.* **15**(1), 181--82 (June 1972).
- R. L. Senn, J. A. Conlin, and R. B. Fitts, "An Improved Capsule Design for Experimental Measurement of Fuel-Cladding Mechanical Interaction" (Summary), *Trans. Amer. Nucl. Soc.* **15**(1), 218--19 (June 1972).
- W. J. Lackey, F. J. Homan, and A. R. Olsen, *Porosity and Actinide Redistribution During Irradiation of (U,Pu)O₂*, ORNL-TM-3762 (August 1972).
- W. J. Lackey, F. J. Homan, and A. R. Olsen, "Porosity and Actinide Redistribution During Irradiation of (U,Pu)O₂," *Nucl. Technol.* **16**(1), 120--42 (October 1972).
- D. E. Ferguson and A. L. Lotts, "Fast Reactor Fuel Processing" (Summary), *Trans. Amer. Nucl. Soc.* **15**(2), 597 (November 1972).
- R. L. Shepard, R. B. Fitts, H. E. Robertson, and R. F. Hyland, "Thermoelectric, Resistance, and Ultrasonic Centerline Thermometry for a (U,Pu)O₂ Fuel Pin" (Summary), *Trans. Amer. Nucl. Soc.* **15**(2), 766--67 (November 1972).
- F. J. Homan, "A Parametric Analysis of Fuel-Cladding Mechanical Interactions," pp. 209--22 in *Proc. 1st Intern. Conf. Structural Mechanics in Reactor Technology, Berlin, Germany, 20--24 September 1971*, Vol. 2, Part C, Commission of the European Communities, Center for Information and Documentation, Luxembourg.
- W. E. Roake, C. E. Weber, D. H. Wiese, C. S. Caldwell, I. D. Thomas, J. L. Scott, and A. B. Shuck, "The United States Program for Developing the Manufacture of High-Quality Fast Reactor Fuels," pp. 311--25 in *Peaceful Uses of Atomic Energy, Proc. 4th Int. Conf., Geneva, 1971*, Vol. 8, United Nations, New York, and International Atomic Energy Agency, Vienna, 1972.
- P. G. Shewmon, G. W. Cunningham, C. E. Dickerman, D. P. Hines, F. J. Homan, G. A. Last, and P. Murray, "Analytical Methods to Design and Predict Performance of Fast Reactor Fuel Elements," pp. 123--39 in *Peaceful Uses of Atomic Energy, Proc. 4th Int. Conf., Geneva*, Vol. 10, United Nations, New York, and International Atomic Energy Agency, Vienna, 1972.
- W. H. Pechin, R. A. Bradley, W. J. Lackey, and J. D. Sease, "Analysis of (U,Pu)O₂ Fuels at Oak Ridge National Laboratory," pp. 279--94 in *Analytical Methods in the Nuclear Fuel Cycle* (Symp. in Vienna, 29 November--3 December 1971), International Atomic Energy Agency, Vienna, 1972.
- E. A. Evans, E. E. Kintner, E. L. Zebroski, L. A. Neimark, and C. M. Cox, "The Status of Engineering Design and Irradiation Testing of the Stainless-Steel-Clad Mixed Oxide Fuel System for Fast Breeder Reactors," pp. 53--67 in *Peaceful Uses of Atomic Energy, Proc. 4th Intern. Conf., Geneva, 1971*, Vol. 10, United Nations, New York, and International Atomic Energy Agency, Vienna, 1972.
- R. Salmon, J. T. Roberts, A. L. Lotts, T. N. Washburn, and W. H. McVey, "Price Forecasting and Resource Utilization for the Fuel-Cycle Industry of the United States of America," pp. 255--65 in *Peaceful Uses of Atomic Energy, Proc. 4th Intern. Conf., Geneva, 1971*, Vol. 4, United Nations, New York, and International Atomic Energy Agency, Vienna, 1972.
- F. J. Homan, W. J. Lackey, and C. M. Cox, *FMODEL -- A FORTRAN IV Computer Code to Predict In-Reactor Behavior of LMFBR Fuel Pins*, ORNL-4825 (January 1973).

8.2 PROGRESS REPORTS

The FBR oxide fuels development program was also reported as distinct sections in three periodical progress reports. Additional details may be obtained from the Metals and Ceramics Division annual reports, the Fuels and Materials Development Program quarterly progress reports, and the LMFBR Fuel Cycle Studies monthly report. The following is a listing of these reports.

8.2.1 Metals and Ceramics Division Annual Reports

| | |
|-----------|-----------------------------|
| ORNL-4170 | Period Ending June 30, 1967 |
| ORNL-4370 | Period Ending June 30, 1968 |
| ORNL-4470 | Period Ending June 30, 1969 |
| ORNL-4570 | Period Ending June 30, 1970 |
| ORNL-4770 | Period Ending June 30, 1971 |
| ORNL-4820 | Period Ending June 30, 1972 |

8.2.2 Fuels and Materials Development Program Quarterly Progress Reports

| | |
|--------------|----------------------------------|
| ORNL-TM-2090 | Period Ending December 31, 1967 |
| ORNL-TM-2217 | Period Ending March 31, 1968 |
| ORNL-4330 | Period Ending June 30, 1968 |
| ORNL-4350 | Period Ending September 30, 1968 |
| ORNL-4390 | Period Ending December 31, 1968 |
| ORNL-4420 | Period Ending March 31, 1969 |
| ORNL-4440 | Period Ending June 30, 1969 |
| ORNL-4480 | Period Ending September 30, 1969 |
| ORNL-4520 | Period Ending December 31, 1969 |
| ORNL-4560 | Period Ending March 31, 1970 |
| ORNL-4600 | Period Ending June 30, 1970 |
| ORNL-4630 | Period Ending September 30, 1970 |
| ORNL-TM-3300 | Period Ending December 31, 1970 |
| ORNL-TM-3416 | Period Ending March 31, 1971 |
| ORNL-TM-3540 | Period Ending June 30, 1971 |
| ORNL-TM-3550 | Period Ending September 30, 1971 |
| ORNL-TM-3703 | Period Ending December 31, 1971 |
| ORNL-TM-3797 | Period Ending March 31, 1972 |
| ORNL-TM-3969 | Period Ending June 30, 1972 |

8.2.3 LMFBR Fuel Cycle Studies Progress Reports

| | |
|--------------|--------------------|
| ORNL-TM-2710 | For August 1969 |
| ORNL-TM-2748 | For September 1969 |
| ORNL-TM-2764 | For October 1969 |
| ORNL-TM-2795 | For November 1969 |
| ORNL-TM-2819 | For December 1969 |
| ORNL-TM-2871 | For January 1970 |
| ORNL-TM-2918 | For February 1970 |
| ORNL-TM-2949 | For March 1970 |
| ORNL-TM-2996 | For April 1970 |
| ORNL-TM-3018 | For May 1970 |
| ORNL-TM-3072 | For June 1970 |
| ORNL-TM-3095 | For July 1970 |
| ORNL-TM-3127 | For August 1970 |
| ORNL-TM-3180 | For September 1970 |
| ORNL-TM-3217 | For October 1970 |
| ORNL-TM-3250 | For November 1970 |
| ORNL-TM-3281 | For December 1970 |
| ORNL-TM-3312 | For January 1971 |
| ORNL-TM-3345 | For February 1971 |

| | |
|--------------|--------------------|
| ORNL-TM-3375 | For March 1971 |
| ORNL-TM-3412 | For April 1971 |
| ORNL-TM-3456 | For May 1971 |
| ORNL-TM-3487 | For June 1971 |
| ORNL-TM-3534 | For July 1971 |
| ORNL-TM-3571 | For August 1971 |
| ORNL-TM-3614 | For September 1971 |
| ORNL-TM-3624 | For October 1971 |
| ORNL-TM-3663 | For November 1971 |
| ORNL-TM-3698 | For December 1971 |
| ORNL-TM-3724 | For January 1972 |
| ORNL-TM-3759 | For February 1972 |
| ORNL-TM-3807 | For March 1972 |
| ORNL-TM-3823 | For April 1972 |
| ORNL-TM-3888 | For May 1972 |
| ORNL-TM-3924 | For June 1972 |

8.3 QUALITY ASSURANCE DOCUMENTS

The following is a list of unpublished quality assurance and operating procedure documents developed within the program and used to control the development and to assure a high standard of quality in its execution. The quality assurance program evolved over a period of time to a formalized program designed to meet the requirements of RDT Standard F2-2T, "Quality Assurance Program Requirements." Other published codes, standards, and specifications were used, but these will not be enumerated here.

8.3.1 General Operating and Quality Assurance Plans

| | | |
|--------------|---|---------------|
| MET-FCT-GP-1 | Program Management and Planning Procedure | July 15, 1970 |
| MET-FCT-GP-9 | Experimental Data File Contents | Sept. 3, 1970 |

8.3.2 Experimental Plans

| | | |
|---------------|---|----------------|
| MET-FCT-EP-1 | Series II Mixed Oxide Fuel Pins (Unencapsulated) in EBR-II | Oct. 1, 1969 |
| MET-FCT-EP-5 | Fuel-Cladding Mechanical Interaction Tests, Capsule MINT-1 | Sept. 8, 1970 |
| MET-FCT-EP-6 | Irradiation Capsules for LMFBR Fuel Reprocessing Tests | Sept. 18, 1970 |
| MET-FCT-EP-9 | Preparation of Sol-Gel (U,Pu)O ₂ Powder for Cold Dissolution Studies | Feb. 22, 1971 |
| MET-FCT-EP-10 | In-Situ Measurement of Fission Gas Release | March 18, 1971 |
| MET-FCT-EP-13 | Series II Out of Reactor Cladding Oxidation Studies | Dec. 8, 1971 |

8.3.3 Preirradiation Data Summary

| | | |
|--------------|---|----------------|
| MET-FCT-DP-1 | ETR 43-117, -118, and -119 Fuel and Fuel Pin Data Package | April 16, 1971 |
| MET-FCT-DP-2 | MINT-1 Fuel and Fuel Pin Data Package | July 19, 1971 |

8.3.4 Fabrication and Quality Assurance Plan

| | | |
|---------------|--|----------------|
| MET-FCT-FQ-1 | Fabrication and Quality Assurance Plan, Series II Pins (EBR-II) | Sept. 15, 1969 |
| MET-FCT-FQ-6 | Irradiation Capsules for LMFBR Fuel Reprocessing Tests | Sept. 21, 1970 |
| MET-FCT-FQ-10 | In-Situ Measurement of Fission Gas Release | Oct. 20, 1971 |
| MET-FCT-FQ-11 | Fabrication and Quality Assurance Plan, Fission Gas Release Test | June 30, 1971 |

8.3.5 Process Procedures

| | | |
|----------------|---|----------------|
| MET-FCT-PP-1 | Fabrication of Pellets for EBR-II, Series II | Oct. 8, 1969 |
| MET-FCT-PP-2 | Sphere-Pac Fuel Preparation | Nov. 19, 1969 |
| MET-FCT-PP-3 | Preparation of UO ₂ Blanket Pellets for EBR-II, Series II | Oct. 10, 1969 |
| MET-FCT-PP-4 | Preparation of ThO ₂ Insulator Pellets for EBR-II, Series II | Oct. 10, 1969 |
| MET-FCT-PP-5 | Fuel Pin Components | Jan. 30, 1970 |
| MET-FCT-PP-6 | EBR-II Fuel Pin Components Assembly Procedure | Feb. 24, 1970 |
| MET-FCT-PP-7 | General Welding Procedure for EBR-II, Series II | May 19, 1970 |
| MET-FCT-PP-7-1 | Bottom End Plug Weld | May 19, 1970 |
| MET-FCT-PP-7-2 | Capillary to Top Plug Weld | May 20, 1970 |
| MET-FCT-PP-7-3 | Top End Plug to Clad Welding | May 20, 1970 |
| MET-FCT-PP-7-4 | Capillary Edge Weld | May 21, 1970 |
| MET-FCT-PP-7-5 | Top End Cap to Top End Plug Weld | May 21, 1970 |
| MET-FCT-PP-8-1 | Preparation and Cold Loading of EBR-II Pins | March 17, 1970 |
| MET-FCT-PP-8-3 | Preparation and Cold Loading of EBR-II Pins SP85UO | March 17, 1970 |
| MET-FCT-PP-8-4 | Preparation and Cold Loading of EBR-II Sphere-Pac Archive Pins | March 17, 1970 |
| MET-FCT-PP-8-5 | Preparation and Cold Loading of EBR-II Pellet Archive Pins | April 7, 1970 |
| MET-FCT-PP-8-6 | Preparation and Cold Loading of EBR-II Blanket and Insulator Archive Pin | April 7, 1970 |
| MET-FCT-PP-8-7 | Loading of EBR-II Sphere-Pac and Archive Pins | March 17, 1970 |
| MET-FCT-PP-8-8 | Loading of EBR-II Pellet Pins | April 7, 1970 |
| MET-FCT-PP-9 | Fuel Assembly and Inspection | May 19, 1970 |
| MET-FCT-PP-22 | Welding of End Fittings to Capsule Tubes | June 3, 1970 |
| MET-FCT-PP-23 | Helium Leak Testing of Capsules | June 3, 1970 |
| MET-FCT-PP-24 | Dimensional Inspection and Weighing of Completed Capsules | June 9, 1970 |
| MET-FCT-PP-25 | X-Ray Radiography of Capsule Welds and Capsules | June 9, 1970 |
| MET-FCT-PP-26 | Specifications for Inspection of Sodium Bond Quality by Eddy Currents | June 18, 1970 |
| MET-FCT-PP-28 | Loading of Sodium into Irradiation Capsules | May 15, 1970 |
| MET-FCT-PP-29 | Loading of NaK into Irradiation Capsules | Aug. 31, 1970 |
| MET-FCT-PP-31 | Welding Spacers to Fuel Pin | Aug. 17, 1970 |
| MET-FCT-PP-36 | Fuel Pin Loading and Final Inspection -- Fuel Reprocessing Pins | Sept. 18, 1970 |
| MET-FCT-PP-37 | Preparation for ETR 43-117, -118, and -119 Pellets | Sept. 18, 1970 |
| MET-FCT-PP-38 | Procedure for Brazing Thermocouples to Mechanical Interaction Primary Containment Capsules | Nov. 16, 1971 |
| MET-FCT-PP-39 | MINT-1 Fuel Pellet Preparation | Nov. 19, 1971 |
| MET-FCT-PP-40 | Fuel Pin Loading and Final Inspection -- Mechanical Interaction Pins | Nov. 11, 1970 |
| MET-FCT-PP-41 | Welds for Fuel Reprocessing Fuel Pins | |
| MET-FCT-PP-42 | Procedure for Brazing Bulkhead Assembly for Capsule Irradiation Experiments | Sept. 29, 1971 |
| MET-FCT-PP-45 | ETR-II Fuel Pin Component -- Cladding Tube | Feb. 17, 1971 |
| MET-FCT-PP-46 | ETR-II End Plugs or Fittings | Feb. 18, 1971 |
| MET-FCT-PP-47 | ETR-II Neutron Shield Rods | Feb. 18, 1971 |
| MET-FCT-PP-48 | EBR-II Fuel Pin Initial End Plug -- Fuel Tube Assembly Procedure | Feb. 12, 1971 |
| MET-FCT-PP-49 | EBR-II Fuel Pin Final End Plug -- Fuel Tube Assembly and Inspection | Feb. 12, 1971 |
| MET-FCT-PP-51 | Process Procedure for Assembly of EBR-II Fuel Rods | April 19, 1971 |
| MET-FCT-PP-57 | Fuel Preparation for ORNL-43-125 and ORNL-43-126 (In-Situ Measurement of Fission Gas Release) | July 21, 1971 |
| MET-FCT-PP-58 | Fuel Pin Loading and Final Inspection of ETR 43-125 and -126 Instrumented Fuel Pins | Oct. 19, 1971 |

| | | |
|---------------|--|---------------|
| MET-FCT-PP-60 | Fabrication of ETR Instrumented Capsules -- Series II. ORNL-43-124, ORNL-125, and 43-126. In-Situ Measurement of Fission Gas Release | Oct. 14, 1971 |
| MET-FCT-PP-68 | Fuel Preparation for ORNL 43-123 (Fuel Reprocessing Fuel Pin) | Feb. 18, 1972 |

8.3.6 Operator Procedures

| | | |
|------------------|---|----------------|
| MET-FCT-OP-1 | Procedure for Marking Metallic Components by Electro Etching | Jan. 30, 1970 |
| MET-FCT-OP-2 | Cleaning of Fuel Pins and Components | July 1, 1969 |
| MET-FCT-OP-3 | Preservation, Handling, Storage, and Packaging of Metallic Components | Feb. 4, 1970 |
| MET-FCT-OP-4 | Sheathing of Sphere-Pac Fuel Pins | April 7, 1970 |
| MET-FCT-OP-5 | Sheathing Technique for Pellet Fuel Pins | March 18, 1970 |
| MET-FCT-OP-6 | Loading Microspheres by Sphere-Pac | March 17, 1970 |
| MET-FCT-OP-7 | Pellet Loading | April 7, 1970 |
| MET-FCT-OP-8 | Fuel Pin Handling | April 6, 1970 |
| MET-FCT-OP-9 | Fuel Pin Welding | Feb. 27, 1970 |
| MET-FCT-OP-10 | Procedure for Initial Loading of Xenon and Helium into Fuel Rods | May 7, 1970 |
| MET-FCT-OP-10-1 | Procedure for Subsequent Loading of Xenon and Helium into Fuel Rods | May 7, 1970 |
| MET-FCT-OP-11 | Outgassing Fiberfrax | Jan. 10, 1969 |
| MET-FCT-OP-12 | Fuel Pin Decontamination | April 7, 1970 |
| MET-FCT-OP-13 | Preparation of Sol-Gel (U,Pu)O ₂ Powder for Pellets | April 25, 1969 |
| MET-FCT-OP-13-R1 | Preparation of Sol-Gel (U,Pu)O ₂ Powder for Pellets | Jan. 26, 1971 |
| MET-FCT-OP-14 | Operation of Welding Vacuum Chamber | Aug. 26, 1969 |
| MET-FCT-OP-15 | Identification of Fuel Materials | Oct. 15, 1970 |
| MET-FCT-OP-16 | Operation Procedure for Tube Furnace Glove Box 2 | Sept. 30, 1970 |
| MET-FCT-OP-17 | Operation Procedure for Tube Furnace Glove Box 8 | Sept. 30, 1970 |
| MET-FCT-OP-18 | NaK Transfer Procedure -- Irradiation Capsule Welding Box | Oct. 5, 1970 |
| MET-FCT-OP-23 | Procedure for Pressing (U,Pu)O ₂ Pellets | Feb. 18, 1971 |
| MET-FCT-OP-27 | Procedure for Adjusting Oxygen-to-Metal Ratio of (U,Pu)O ₂ | March 24, 1971 |
| MET-FCT-OP-28 | Procedure for Determining Void Volume and Loading Xenon Tag Gas into Fuel Rods | April 12, 1971 |
| MET-FCT-OP-29 | Procedure for Determining the Amount of U and Pu in (U,Pu)O ₂ Powders (for accountability purposes) | April 19, 1971 |
| MET-FCT-OP-30 | Operation of Auto-Arc TIG 50 Welder | May 28, 1971 |
| MET-FCT-OP-33 | Routine Testing of FCAF Glove Box Water Detectors, Furnace Cooling Water Interlocks, Furnace Temperature Limiting Devices | Sept. 21, 1971 |

8.3.7 Material Specifications

| | | |
|---------------|---|----------------|
| MET-FCT-MS-1 | Ceramic Fiber Wool for Use in Fuel Irradiation Tests | Oct. 15, 1969 |
| MET-FCT-MS-3 | Uranium Dioxide Pellets | Oct. 4, 1969 |
| MET-FCT-MS-4 | Thorium Dioxide Pellets | Oct. 4, 1969 |
| MET-FCT-MS-5 | Specification for Uranium-Plutonium Oxide Pellets | Oct. 1, 1969 |
| MET-FCT-MS-6 | Specification for Uranium Dioxide Microspheres | Oct. 1, 1969 |
| MET-FCT-MS-7 | Specification for Uranium-Plutonium Oxide Microspheres | Oct. 1, 1969 |
| MET-FCT-MS-9 | Sodium-Potassium Alloys | Oct. 27, 1970 |
| MET-FCT-MS-12 | Specification for Inconel-X Springs for (U,Pu)O ₂ Fuel Pins -- EBR-II | April 20, 1971 |

8.3.8 Test Specifications

| | | |
|---------------|---|----------------|
| MET-FCT-TS-1 | Micrometer Standardization | Feb. 2, 1970 |
| MET-FCT-TS-2 | Procedure for Balance Standardization | Feb. 2, 1970 |
| MET-FCT-TS-3 | Pellet Inspection | Feb. 15, 1970 |
| MET-FCT-TS-4 | Microsphere Tap Density | Feb. 15, 1970 |
| MET-FCT-TS-5 | Procedure for Visual Inspection of Incoming Metallic Materials | Jan. 30, 1970 |
| MET-FCT-TS-6 | Length Measurement of Finished Fuel Pins | May 28, 1970 |
| MET-FCT-TS-7 | Outside Diameter Measurement of Finished Fuel Pins | May 3, 1970 |
| MET-FCT-TS-8 | Method for Measuring Total Indicated Runout of Finished Fuel Pins | May 3, 1970 |
| MET-FCT-TS-9 | Use of Dermitron with Chart Recorder | May 3, 1970 |
| MET-FCT-TS-10 | Procedure for Ultrasonic Wall Thickness Measurements of Stainless Steel Tubing, 0.250-in. OD × 0.015-in. Wall | Oct. 15, 1970 |
| MET-FCT-TS-11 | Inspection of Inconel-X Springs for EBR-II Fuel Rods | April 20, 1971 |

8.3.9 Fabrication and Quality Assurance Networks

| | | |
|--------------|---|---------------|
| MET-FCT-QP-1 | Fabrication and Quality Assurance Network EBR-II, Series II | |
| MET-FCT-QP-2 | Fabrication and Quality Assurance Network for Preparation of Sol-Gel (U,Pu)O ₂ Powder from WADCO | Feb. 22, 1971 |

INTERNAL DISTRIBUTION

(138 copies)

- (3) Central Research Library
ORNL -- Y-12 Technical Library
Document Reference Section
- (10) Laboratory Records Department
Laboratory Records, ORNL RC
ORNL Patent Office
G. M. Adamson, Jr.
R. E. Blanco
E. E. Bloom
B. Borie
- (5) R. A. Bradley
R. E. Brooksbank
J. V. Cathcart
G. W. Clark
J. A. Conlin
J. H. Coobs
F. L. Culler
J. E. Cunningham
J. H. DeVan
R. G. Donnelly
W. P. Eatherly
D. E. Ferguson
- (5) R. B. Fitts
B. Fleischer (K-25)
M. H. Fontana
R. J. Gray
P. A. Haas
W. O. Harms
R. F. Hibbs
- (5) M. R. Hill
- (10) F. J. Homan
P. R. Kasten
R. T. King
J. D. Jenkins
- (5) W. J. Lackey
J. M. Leitnaker
T. B. Lindemer
- (5) E. L. Long, Jr.
- (10) A. L. Lotts
T. S. Lundy
R. E. MacPherson
W. R. Martin
C. L. Matthews
W. T. McDuffee
D. L. McElroy
C. J. McHargue
F. L. Miller
J. P. Nichols
K. J. Notz
- (5) A. R. Olsen
R. A. Olstad
R. B. Parker
P. Patriarca
- (5) W. H. Pechin
S. Peterson
A. C. Schaffhouser
J. L. Scott
- (5) J. D. Sease
R. L. Senn (K-25)
G. M. Slaughter
G. P. Smith
J. O. Stiegler
D. B. Trauger
W. E. Unger
J. E. Van Cleve
T. N. Washburn
A. M. Weinberg
J. R. Weir, Jr.
F. W. Wiffen
- (5) R. G. Wymer
H. L. Yakel
Leo Brewer (consultant)
Walter Kohn (consultant)
G. V. Smith (consultant)
W. S. Williams (consultant)

EXTERNAL DISTRIBUTION

(247 copies)

USAEC DIVISION OF REACTOR RESEARCH AND DEVELOPMENT, Washington, D.C. 20545

(2) Director

USAEC-RRD SENIOR SITE REPRESENTATIVE, Oak Ridge National Laboratory, Oak Ridge, TN 37830

USAEC OAK RIDGE OPERATIONS OFFICE, P.O. Box E, Oak Ridge, TN 37830

Research and Technical Support Division

USAEC TECHNICAL INFORMATION CENTER, Office of Information Services, P.O. Box 62, Oak Ridge, TN 37830

(243) For distribution as shown in TID-4500 Distribution Category, UC-79b, Fuels and Materials Engineering and Development